TRACE ELEMENT SYSTEMATICS OF MAFIC-ULTRAMAFIC VOLCANIC ROCKS FROM THE ARCHEAN ABITIBI GREENSTONE BELT, CANADA: IMPLICATIONS FOR CHEMICAL EVOLUTION OF THE MANTLE AND ARCHEAN GREENSTONE BELT DEVELOPMENT

A Thesis

Submitted to the College of Graduate Studies and Research in Partial Fulfillment of the

Requirements for the Degree

of

Doctor of Philosophy

in the

Department of Geological Sciences

University of Saskatchewan

Saskatoon

by

Qianli Xie

January 1996

UNIVERSITY OF SASKATCHEWAN

College of Graduate Studies and Research

SUMMARY OF DISSERTATION

Submitted in partial fulfillment

of the requirements for the

DEGREE OF DOCTOR OF PHILOSOPHY

by

Qianli Xie

Department of Geological Sciences
University of Saskatchewan

Spring 1996

Examining Committee:

Dr. D.-Y. Peng	~~Acting Dean~~, Chair, College of Graduate Studies and Research
Dr. M.R. Stauffer	Chair of Advisory Committee, Department of Geological Sciences
Dr. R. Kerrich	Supervisor, Department of Geological Sciences
Dr. K. Ansdell	Department of Geological Sciences
Dr. Y. Pan	Department of Geological Sciences
Dr. J. Merriam	Department of Geological Sciences
Dr. G.T. Sofko,	Physics & Engineering Physics

External Examiner:

Dr. Phil Thurston
Ontario Geological Survey
Chief Geologist
Ministry of Northern Development & Mines
8 th Floor, 933 Ramsey Road
Sudbury, Ontario
P3E 6B5

ABSTRACT

Notwithstanding recent advances in the study of the evolution of earth's mantle and Archean greenstone belt development, many fundamental questions remain unresolved. This study attempts to provide further constraints on (1) the early history of the mantle and (2) the geodynamic evolution of Archean greenstone belts, based on trace element systematics of mafic-ultramafic volcanic rocks from the Archean Abitibi Southern Volcanic Zone (SVZ).

Analysis of trace element contents in Archean mafic-ultramafic rocks presents special challenges to traditional analytical techniques, as many trace elements occur in relatively low abundance in these rocks. Accordingly, the first step of this study was to characterize multiple trace element analysis of low abundance samples by inductively coupled plasma mass spectrometry (ICP-MS). Detailed experiments evaluate quantitatively potential difficulties in ICP-MS analysis, such as possible incomplete sample dissolution and solute instability, potential isobaric and polyatomic interferences, and memory effects. Analytical protocols were developed that either overcome such problems, or demonstrated that the effects were negligible. New data for 28 elements, including all rare earth elements (REEs) and high field strength elements (HFSEs), in some international reference materials have been obtained by ICP-MS, using the new protocols. The new ICP-MS data for these international reference materials indicate that precise and accurate multiple trace element data can be obtained by ICP-MS for Archean komatiites and basalts.

Experiments were also conducted to optimize instrumental operating parameters (IOPs) for isotope ratio measurement by ICP-MS. These IOPs include rf power, dwell time, B lens setting, and nebulizer flow rate. Mass bias, showing preferentially reduced response of light isotopes, has been observed. The mass bias factor is independent of analyte concentration in the range from sub ppb to ppm, and is stable over a period of several hours. Under optimized IOPs, precision of 0.2 to 0.6% relative standard deviation can be achieved for isotope ratio measurement using ICP-MS. Isotope dilution analysis for Zr and Hf in low abundance samples confirms the data obtained by external calibration ICP-MS.

Three komatiite-tholeiite sequences from the Archean Abitibi SVZ, which are separated by major terrane boundaries, show distinct geochemical characteristics. Tisdale komatiites are Al-undepleted, with Al_2O_3/TiO_2=13-17 and CaO/Al_2O_3=1.0-1.3, flat REE patterns [$(La/Yb)_n$=0.7-1.2], and zero HFSE/REE fractionation (Nb/Nb*=0.9-1.1, Zr/Zr*=0.8-1.3, Hf/Hf*=0.8-1.2). Spatially associated Mg-tholeiites share similar geochemical features with komatiites. Munro komatiites are also Al-undepleted, with Al_2O_3/TiO_2=17-20 and CaO/Al_2O_3=1.0-1.2, LREE depleted patterns [$(La/Yb)_n$ =0.2-0.4], and positive HFSE anomalies relative to REEs (Nb/Nb*=0.9-2.0, Zr/Zr*=1.0-1.4, Hf/Hf*=1.1-2.1), whereas spatially associated Mg-tholeiites have flat REE patterns [$(La/Yb)_n$ =0.8-2.1] and zero HFSE/REE fractionation (Nb/Nb*=0.8-1.4, Zr/Zr*=0.8-1.0, Hf/Hf*=0.8-1.2), similar to Tisdale komatiites and Mg-tholeiites. Boston komatiites and tholeiites are distinct in terms of their Al-depletion (Al_2O_3/TiO_2=4-5, CaO/Al_2O_3=1.0-2.5), enriched LREE [$(La/Yb)_n$ =5.6-7.7], fractionated HREE [$(Gd/Yb)_n$=2.0-2.2], and negative Zr and Hf anomalies relative to REEs (Zr/Zr*=0.38, Hf/Hf*=0.40-0.54).

The three komatiite-tholeiite sequences, with distinct geochemical characteristics, are interpreted as having formed in mantle plumes originating from different mantle sources at different depths. Tisdale komatiites may have been generated by a plume originating from an undepleted mantle source at shallow depth (<300 km). Spatially associated Mg-tholeiites

are likely products of low pressure olivine fractional crystallization of the komatiitic magma. Munro komatiites may have formed in a plume originating from a mantle source enriched in Mg-perovskite at great depth (>650 km), that subsequently segregated melt at shallow depths (<300 km). Coexisting Mg-tholeiites may represent either more primitive materials entrained in the plume, or an independent plume source. The Al-depleted Boston komatiites may have formed by partial melting in a plume at mantle depths between 400 to 650 km, where majorite is a liquidus phase. These results suggest that various komatiite-tholeiite sequences in the Abitibi SVZ may represent parts of distinct Archean oceanic plateaus formed from different plumes. In addition, the positive HFSE anomalies relative to REEs in Munro komatiites, and the negative HFSE anomalies in Boston komatiites, are consistent with Mg-perovskite, and majorite signatures, respectively, and may indicate Mg-perovskite and majorite fractionation in earth's early mantle evolution.

The Kinojevis (KJG) and Blake River (BRG) groups are two volcanic sequences with contrasting geochemical characteristics from the central block of the Abitibi SVZ. The KJG consists mainly of tholeiitic basalts, with flat REE patterns [$(La/Yb)_n$=0.8-1.3], and no Nb, Ta or Ti anomalies relative to REEs [$(Nb/La)_n$=0.8-1.2, $(Ta/La)_n$=0.8-1.2, $(TiO2/Sm)_n$ =0.8-1.4]. The KJG tholeiites are geochemically similar to Tisdale and Munro Mg-tholeiites, suggesting common mantle sources and magma evolution, that is having formed in mantle plumes deriving from undepleted mantle source at shallow depths.

In contrast, the BRG is dominantly calc-alkaline andesites, enriched in LILEs and LREEs [$(La/Yb)_n$=3.0-5.0], depleted in Nb, Ta and Ti relative to LILEs and LREEs [$(Nb/La)_n$=0.4-0,6, $(Ta/La)_n$=0.3-0.7, $(TiO2/Sm)_n$=0.4-0.8], and depleted HREEs, Sc and Y. The BRG calc-alkaline andesites have geochemical characteristics closely resembling that of one type of modern oceanic island arc volcanic rocks, namely adakite, where melting of subducted young (<25 Ma) oceanic crust is involved. Crust melting versus crust dehydration is indicated by enrichment of Nb and Ta relative to HREEs.

The temporal and spatial relationships of magmatism in the Abitibi SVZ may be accounted for by a geodynamic model that includes a composite of volcanic sequences of different plumes and oceanic island arc terranes, which were tectonically juxtaposed during terminal accretion of the Abitibi greenstone belt.

In presenting this thesis in partial fulfillment of the requirements for a postgraduate degree from the University of Saskatchewan, I agree that the Libraries of this University may make it freely available for inspection. I further agree that permission for copying of this thesis in any manner, in whole or in part, for scholarly purposes may be granted by the professor or professors who supervised my thesis work or, in their absence, by the Head of the Department or the Dean of the College in which my thesis work was done. It is understood that any copying or publication or use of this thesis or parts thereof for financial gain shall not be allowed without my written permission. It is also understood that due recognition shall be given to me and to the University of Saskatchewan in any scholarly use which may be made of any material in my thesis.

Requests for permission to copy or to make other use of material in this thesis in whole or part should be addressed to:

Head of the Department of Geological Sciences
University of Saskatchewan
Saskatoon, Saskatchewan S7N 5E2

N[illegible] striking
Archean g[illegible] stone belt
study att[illegible] to provi
the geody[illegible] evoluti
of mafic-[illegible]

A [illegible] of ance
challenge[illegible] to [illegible]
abundanc[illegible] ness
multiple [illegible] element
mass sp[illegible] etry (
difficultie[illegible] in [illegible]
instability [illegible] al
protocol[illegible] wer[illegible] develop
effects we[illegible] ne[illegible]igible.
and high [illegible] eld [illegible]
been obt[illegible] ined by [illegible]
internatic[illegible] [illegible] ference
data can [illegible] [illegible]

Ex[illegible]eriments we
(IOPs) for [illegible] ope ratio
B lens set[illegible], and [illegible]
of light [illegible] es, had
concentra[illegible] the ra
Under opt[illegible] ized [illegible]
for isotope [illegible] measure
abundance [illegible] ples

Th[illegible] oma
separated [illegible] ion
komatiite[illegible] and Al-unde
patterns [illegible] Yb)$_n$=0.
Zr/Zr*=0.[illegible] [illegible] Hf/
geochemi[illegible] atures
Al_2O_3/Ti[illegible] -20 and
and pos[illegible] ive [illegible] SE
Hf/Hf*= [illegible] -2 [illegible] ther
[(La/Yb)$_n$ [illegible] -2] and
Hf/Hf*=0.[illegible] -[illegible]), simi
tholeiites [illegible] [illegible] ti
enriched [illegible] [illegible] La/Yb
Zr and H[illegible] and nanes [illegible]

T[illegible] [illegible] oma
interpret[illegible] as having f
different [illegible]. Tisdal
an undepl[illegible] [illegible]

ABSTRACT

Notwithstanding recent advances in the study of the evolution of Earth's mantle and Archean greenstone belt development, many fundamental questions remain unresolved. This study attempts to provide further constraints on (1) the early history of the mantle and (2) the geodynamic evolution of Archean greenstone belts, based on trace element systematics of mafic-ultramafic volcanic rocks from the Archean Abitibi Southern Volcanic Zone (SVZ).

Analysis of trace element contents in Archean mafic-ultramafic rocks presents special challenges to traditional analytical techniques, as many trace elements occur in relatively low abundance in these rocks. Accordingly, the first step of this study was to characterize multiple trace element analysis of low abundance samples by inductively coupled plasma mass spectrometry (ICP-MS). Detailed experiments evaluate quantitatively potential difficulties in ICP-MS analysis, such as possible incomplete sample dissolution and solute instability, potential isobaric and polyatomic interferences, and memory effects. Analytical protocols were developed that either overcome such problems, or demonstrated that the effects were negligible. New data for 28 elements, including all rare earth elements (REEs) and high field strength elements (HFSEs), in some international reference materials have been obtained by ICP-MS, using the new protocols. The new ICP-MS data for these international reference materials indicate that precise and accurate multiple trace element data can be obtained by ICP-MS for Archean komatiites and basalts.

Experiments were also conducted to optimize instrumental operating parameters (IOPs) for isotope ratio measurement by ICP-MS. These IOPs include rf power, dwell time, B lens setting, and nebulizer flow rate. Mass bias, showing preferentially reduced response of light isotopes, has been observed. The mass bias factor is independent of analyte concentration in the range from sub ppb to ppm, and is stable over a period of several hours. Under optimized IOPs, precision of 0.2 to 0.6% relative standard deviation can be achieved for isotope ratio measurement using ICP-MS. Isotope dilution analysis for Zr and Hf in low abundance samples confirms the data obtained by external calibration ICP-MS.

Three komatiite-tholeiite sequences from the Archean Abitibi SVZ, which are separated by major terrane boundaries, show distinct geochemical characteristics. Tisdale komatiites are Al-undepleted, with Al_2O_3/TiO_2=13-17 and CaO/Al_2O_3=1.0-1.3, flat REE patterns [$(La/Yb)_n$=0.7-1.2], and zero HFSE/REE fractionation (Nb/Nb*=0.9-1.1, Zr/Zr*=0.8-1.3, Hf/Hf*=0.8-1.2). Spatially associated Mg-tholeiites share similar geochemical features with komatiites. Munro komatiites are also Al-undepleted, with Al_2O_3/TiO_2=17-20 and CaO/Al_2O_3=1.0-1.2, LREE depleted patterns [$(La/Yb)_n$ =0.2-0.4], and positive HFSE anomalies relative to REEs (Nb/Nb*=0.9-2.0, Zr/Zr*=1.0-1.4, Hf/Hf*=1.1-2.1), whereas spatially associated Mg-tholeiites have flat REE patterns [$(La/Yb)_n$ =0.8-2.1] and zero HFSE/REE fractionation (Nb/Nb*=0.8-1.4, Zr/Zr*=0.8-1.0, Hf/Hf*=0.8-1.2), similar to Tisdale komatiites and Mg-tholeiites. Boston komatiites and tholeiites are distinct in terms of their Al-depletion (Al_2O_3/TiO_2=4-5, CaO/Al_2O_3=1.0-2.5), enriched LREE [$(La/Yb)_n$ =5.6-7.7], fractionated HREE [$(Gd/Yb)_n$=2.0-2.2], and negative Zr and Hf anomalies relative to REEs (Zr/Zr*=0.38, Hf/Hf*=0.40-0.54).

The three komatiite-tholeiite sequences, with distinct geochemical characteristics, are interpreted as having formed in mantle plumes originating from different mantle sources at different depths. Tisdale komatiites may have been generated by a plume originating from an undepleted mantle source at shallow depth (<300 km). Spatially associated Mg-tholeiites

are likely products of low pressure olivine fractional crystallization of the komatiitic magma. Munro komatiites may have formed in a plume originating from a mantle source enriched in Mg-perovskite at great depth (>650 km), that subsequently segregated melt at shallow depths (<300 km). Coexisting Mg-tholeiites may represent either more primitive materials entrained in the plume, or an independent plume source. The Al-depleted Boston komatiites may have formed by partial melting in a plume at mantle depths between 400 to 650 km, where majorite is a liquidus phase. These results suggest that various komatiite-tholeiite sequences in the Abitibi SVZ may represent parts of distinct Archean oceanic plateaus formed from different plumes. In addition, the positive HFSE anomalies relative to REEs in Munro komatiites, and the negative HFSE anomalies in Boston komatiites, are consistent with Mg-perovskite, and majorite signatures, respectively, and may indicate Mg-perovskite and majorite fractionation in Earth's early mantle evolution.

The Kinojevis (KJG) and Blake River (BRG) groups are two volcanic sequences with contrasting geochemical characteristics from the central block of the Abitibi SVZ. The KJG consists mainly of tholeiitic basalts, with flat REE patterns [$(La/Yb)_n$=0.8-1.3], and no Nb, Ta or Ti anomalies relative to REEs [$(Nb/La)_n$=0.8-1.2, $(Ta/La)_n$=0.8-1.2, $(TiO2/Sm)_n$ =0.8-1.4]. The KJG tholeiites are geochemically similar to Tisdale and Munro Mg-tholeiites, suggesting common mantle sources and magma evolution, that is having formed in mantle plumes deriving from undepleted mantle source at shallow depths.

In contrast, the BRG is dominantly calc-alkaline andesites, enriched in LILEs and LREEs [$(La/Yb)_n$=3.0-5.0], depleted in Nb, Ta and Ti relative to LILEs and LREEs [$(Nb/La)_n$=0.4-0,6, $(Ta/La)_n$=0.3-0.7, $(TiO2/Sm)_n$=0.4-0.8], and depleted HREEs, Sc and Y. The BRG calc-alkaline andesites have geochemical characteristics closely resembling that of one type of modern oceanic island arc volcanic rocks, namely adakite, where melting of subducted young (<25 Ma) oceanic crust is involved. Crust melting versus crust dehydration is indicated by enrichment of Nb and Ta relative to HREEs.

The temporal and spatial relationships of magmatism in the Abitibi SVZ may be accounted for by a geodynamic model that includes a composite of volcanic sequences of different plumes and oceanic island arc terranes, which were tectonically juxtaposed during terminal accretion of the Abitibi greenstone belt.

ACKNOWLEDGEMENTS

First of all I would like to thank Rob Kerrich, my supervisor, who introduced me to Abitibi geology and allowed me the freedom to pursue my own interests. His continued guidance, encouragement, and patience through the entire process of my thesis work in Saskatoon are invaluable to me, especially when it comes to difficulties in publishing stemming from different interpretations from 'conventional wisdom'. I would also like to thank Claude Herzberg for helpfull discussion and encouragement during this study. J. Jain, who operated and maintained the ICP-MS used in this research; D. Pezderic, and A. Vuletich are thanked for their assitance in my laboratory work.

Various chapters of this thesis have been greatly improved by incisive critiques and suggestions from C. Herzberg, D. Wyman, L. Coleman, Y. Pan, N.T. Arndt, J. Ludden, P. Potts, C. Riddle, G.E.M. Hall, K. Govindaraju, J. Kane, B. Fryer, S.S. Sun, E. Ohtani, and members of my supervisory committee.

Thanks are extended to fellow graduate students and staff of the Department of Geological Sciences for help and friendship. L. Jensen of Ontario Geological Survey, and geologists from the Resident Geologist Office of Timmins, Kirkland Lake, and Ruoyn-Ronanda, are thanked for logistical support in the field.

I am greatly in debt to my wife and daughter. Without their continuous understanding and support, this thesis could never be completed.

This research was supported by NSERC operating grants to Rob Kerrich, the George McLeod endowment to the Department of Geological Sciences, and a University Graduate Scholarship to the author.

TABLE OF CONTENTS

LIST of FIGURES

LIST of TABLE

LIST of ABBREVIATION

BRG	-- Blake River Group
D	-- Partitioning coefficient
D′	-- 670 km discontinuity
D′′	-- Core-mantle boundary
DM	-- Depleted upper mantle
DPFZ	-- Destor-Porcupine Fault Zone
EMI	-- Enriched mantle I
EMII	-- Enriched mantle II
E-MORB	-- Enriched midocean ridge basalts
GF-AAS	-- Graphite furnace atomic absorption spectrometry
HIMU	-- High $^{208}U/^{204}Pb$ mantle reservoir
HFSE	-- High field strength elements (Nb, Ta, Zr, Hf etc.)
HREE	-- Heavy rare earth elements (Tb to Lu)
IAV	-- Island arc volcanics
ICP-AES	-- Inductively coupled plasma atomic emission spectrometry
ICP-MS	-- Inductively coupled plasma mass spectrometry
ID	-- Isotope dilution
INAA	-- Instrumental neutron activation analysis
IOPs	-- Instrumental operating parameters
KJG	-- Kinojevis Group
KLFZ	-- Kirkland Lake-Larder Lake-Cadillac Fault Zone
LILE	-- Large lithophile elements (Li, Rb, K, Na etc.)
LREE	-- Light rare earth elements (La to Nd)
MORB	-- Midocean ridge basalts
MREE	-- Middle rare earth elements (Sm to Gd)
N-MORB	-- Normal midocean ridge basalts
OIB	-- Ocean island basalts
REE	-- Rare earth elements (La to Lu)
SSMS	-- Spark source mass spectrometry
SVZ	-- The Abitibi Southern Volcanic Zone
TIMS	-- Thermal ionization mass spectrometry
XRF	-- X-ray fluorescence spectrometry

CHAPTER 1. INTRODUCTION

1-1. Archean mantle geochemistry

Geochemical studies of mantle derived rocks have greatly improved understanding of the origin and evolution of the Earth. For example, based on isotope studies of modern oceanic basalts, four endmember mantle source compositions have been identified, that developed their distinct isotopic signatures over billion year time scales; namely depleted upper mantle (DM), enriched mantle sources I and II (EM I and EM II), and a source with high U and Th relative to Pb (HIMU) [Zindler and Hart, 1986; Hart and Zindler, 1989]. Recently, Hart et al. (1992) proposed a fifth mantle endmember reservoir termed FOZO (for focal zone in Sr-Nd-Pb isotope co-ordinate space), that is likely located in the lower mantle and is also characterized by more radiogenic Ar, signifying a less degassed state relative to the other endmembers.

Major and trace element abundances of oceanic basalts and primitive mantle peridotites have been utilized to estimate the chemical composition of so called "primitive mantle", which lays the foundation of our understanding of the chemical evolution of the mantle (Jagoutz et al., 1979; Sun, 1982; Hofmann, 1988; Sun and McDonough, 1989). "Primitive mantle" as used here is the bulk silicate fraction of the Earth, prior to extraction of the crust and the mantle lithosphere that resulted from internal differentiation processes (Anderson, 1989b).

Notwithstanding these advances, fundamental questions regarding the composition,

structure and evolution of the Earth's mantle remain unresolved, especially for the early history of the mantle. These fundamental questions include:

(1). Was the mantle substantially molten in the early stage of Earth formation, hypothesized as a magma ocean stage? (Nisbet and Walker, 1982; Ohtani, 1985; Agee and Walker, 1988; Melosh, 1990)

(2). If a magma ocean existed, did it fractionate and stratify into different layers based on liquid-mineral density contrasts? (Anderson, 1979; Herzberg, 1984; Kato et al., 1988b; Ohtani, 1988; Miller et al., 1991b)

(3). If the mantle fractionated and stratified into different layers at a magma ocean stage, have the layers been preserved in whole or in part due to subsequent convection in separate upper and lower mantle cells, or alternatively has the mineralogical and compositional signatures of early mantle fractionation and stratification been destroyed because of whole mantle convection? (Herzberg and Forsythe, 1983; Anderson, 1989a; Jeanloz and Knittle, 1989; Ringwood, 1991)

(4). Did the modern upper mantle deplete continuously from an initially homogeneous "primitive mantle"? or alternatively was the chemical evolution of the mantle episodic? For example, it has been suggested that there are major geochemical changes in basalt compositions at the Archean-Proterozoic boundary, indicative of chemical changes in mantle sources, or changes in melting conditions (Condie, 1989). Hofmann (1989) suggested that the mantle underwent a two stage evolution, in which the crust was first extracted from part of the mantle, and the mantle subsequently rehomogenized to a uniform Nb/U and Ce/Pb ratio, albeit with isotopically distinct endmember sources. Galer et al. (1989) proposed physically and

compositionally separate upper and lower mantle convection, with steady state 'leakage' of less depleted lower mantle into the upper mantle, to explain disparities between the ratios and isotopic composition of certain trace elements in the depleted upper mantle (the so called Pb paradox). Alternatively, Stein and Hofmann (1994) proposed that the mantle switched between two modes: separate upper and lower mantle convection with intervening episodes of coupled behaviour marked by superplumes originating in the lower mantle. These issues remain unresolved.

(5). What impact would chemical changes in the mantle have on global tectonics? For example, is there a secular change of global tectonics from "plume" dominated tectonics in the Archean to modern ocean floor spreading related plate tectonics? (Fyfe, 1978; Hoffman and Ranalli, 1988; Storey et al., 1991).

One of the theories of Earth formation predicts that the Earth was substantially molten in the Hadean (~4.5 billion years ago), based on considerations of the energies of accretion and core-formation (Abe and Matsui, 1986; Matsui and Abe, 1986; Agee, 1990; Ahrens, 1990). The result of complete melting would plausibly be a global encircling magma ocean (Nisbet and Walker, 1982; Ohtani, 1985; Agee and Walker, 1988; Melosh, 1990). Upon cooling, the magma ocean would have crystallized various phases as the temperature dropped below their liquidus. Experimental studies have demonstrated that the principal liquidus phases are olivine + clinopyroxene + orthopyroxene at pressures below ~ 15 GPa (< ~ 300 km), majorite + magnesiowustite between 15-24 GPa (300-600 km), and Mg-perovskite above 24 GPa (> ~ 700 km) [Ito and Takahashi, 1987; Ohtani and Sawamoto, 1987; Knittle and Jeanloz, 1989; Herzberg et al., 1990; Wei et al., 1990; Zhang and

Herzberg, 1994]. If these liquidus phases crystallized and fractionated in the magma ocean, and stratified from density contrasts between solids and liquid silicate, they would be expected to impart distinct chemical signatures to the composition of mantle, and a chemically layered mantle might have developed (Anderson, 1979; Herzberg, 1984; Agee and Walker, 1988; Ohtani, 1988). That the upper and lower mantle, and perhaps the D' transition zone (670 km discontinuity) may differ in composition today seems to support this theory (Anderson, 1989a; Jeanloz and Knittle, 1989). Neodymium isotope systematics of Archean mantle derived rocks also indicate early mantle differentiation, given the diversity of ξ_{143Nd} values of late-Archean (~ 2.7 Ga) komatiites and basalts that span +1 to +5 (Shirey and Hanson, 1986; Smith and Ludden, 1989; Blichert-Toft and Albarede, 1994; Bowring and Housh, 1995), and positive ϵ_{142Nd} values (+3), a decay product of short-lived ^{146}Sm, in the Archean rocks (Harper and Jacobsen, 1992; Bennett et al., 1993).

It is widely accepted that the initial composition of the primitive mantle resembles chondrites with Fe and siderophile element depletion after core formation (Hofmann, 1988; Anderson, 1989b; Sun and McDonough, 1989). However, whether or not the mantle underwent extensive chemical differentiation upon cooling of a magma ocean remains the subject of active debate. One method for testing possible differentiation of the early mantle is to use phase equilibrium relations and geochemical partitioning data to calculate the chemical mass balance between estimated primitive upper and lower mantle versus estimated bulk primitive mantle (Ito and Takahashi, 1987; Agee and Walker, 1988, 1989; Kato et al., 1988a, b, 1989; Hart and Zindler, 1989; McFarlane and Drake, 1990; Ringwood, 1990). A complementary approach is to investigate the geochemical characteristics of magmas which may have been derived from the deep mantle, thereby providing information on the

composition of deep mantle sources and processes that may have influenced their compositions. Archean komatiites are good examples of the rock types required for this second approach.

Komatiites are high MgO volcanic rocks which occur principally in Archean greenstone belts. There are essentially two types of komatiite: Al-undepleted and Al-depleted komatiites (Nesbitt et al., 1979). Various models have been proposed for the petrogenesis of komatiites. Initially, it was suggested that komatiites formed by high degree (60-80%) partial melting of mantle peridotite at relatively low pressure (Viljoen and Viljoen, 1969; Brooks and Hart, 1972; Arndt, 1977). Subsequently, low degree partial melting at relatively high pressures was advocated, based on the argument of density contrasts between komatiitic liquid and residual mantle crystals (Beswick, 1982; Nisbet, 1982). From recent experimental studies it has been suggested that komatiites may form by low degree partial melting at very high pressure (Herzberg and Ohtani, 1988; Wei et al., 1990; Miller et al., 1991a, b; Herzberg, 1992a). Miller et al. (1991b) suggested that the ultimate sources of komatiitic magmas are solid diapirs which may have originated from great depths in the mantle. This mantle source is thought to have been ~700 °C hotter than the sources of MORBs, thus produces high-Mg liquids during adiabatic decompression. Herzberg (1992) suggested that komatiites of Gorgona, Munro and Barberton types may have formed by < 50% melting at different depths. From considerations of fluid dynamics, Campbell et al. (1989) proposed that Archean komatiites might have formed by melting in the high-temperature axis of a starting plume which originated from the lower mantle or core-mantle boundary (D").

There are at least two implications from these various proposals for high pressure

melting. First, if some komatiitic liquids did form in diapiric plumes originating from the deep mantle, then the geochemical characteristics of these rocks may reflect sources that have undergone majorite or silicate-perovskite fractionation from an early magma ocean. Second, if some hot mantle diapirs melted at great depth to generate komatiitic liquids, rather than solid diapirs melting at shallow depth, the geochemical features of komatiites should provide information on deep mantle processes, such as majorite or silicate-perovskite fractionation during partial melting.

What geochemical features would be generated from majorite or silicate-perovskite fractionation? Experimental partitioning studies indicate that high field strength elements (HFSEs; e.g., Nb, Ta, Zr, Hf) and rare earth elements (REEs) have similar degrees of compatibility at low pressures, where olivine is the main liquidus phase (McCallum and Charette, 1978; Ewart and Hawkesworth, 1987; Kennedy et al., 1993), and accordingly are not fractionated. This behaviour is reflected in the fact that oceanic basalts, such as MORB and OIB that result from melt segregation at depths of < 80 km, show zero HFSE/REE fractionations on primitive mantle normalized diagrams (Sun and McDonough, 1989). However, at high pressure, Nb, Zr and Hf have different partitioning behaviour from REEs, because of the presence of majorite and silicate-perovskite, and consequently HFSEs and REEs may be fractionated during melting or fractional crystallization at high pressures (Kato et al., 1988a, b; Ohtani et al., 1989; Herzberg, 1992b; Yurimoto and Ohtani, 1992). Accordingly, HFSE and REE characteristics of komatiites should provide information on their mantle sources, if the sources have experienced early majorite or perovskite fractionation; and/or on the depths of the source melting, if the komatiites were derived from distinct mantle sources at different depths. As discussed by Herzberg (1992, and references

therein), major element compositions of komatiites may also reflect the depth of partial melting or melt segregation.

Well preserved komatiites of various compositional types have been documented in the 2.7 Ga Archean Abitibi greenstone belt, Canada (Arndt et al., 1977; Beswick, 1982; Ludden and Gelinas, 1982; Jensen and Langford, 1985; Cattell and Arndt, 1987; Stone et al., 1987; Xie et al., 1993). This 2.7 Ga greenstone belt has special significance given that several major geological events are prominently expressed at that time. These include:

(1). Mafic magmatism changed from plume related komatiitic-tholeiitic sequences to subduction related calc-alkalic magmas (Thurston, 1990; Xie and Kerrich, 1993);

(2). The first major occurrence of shoshonitic lamprophyres, analogous to Phanerozoic counterparts normally formed in an accretionary geodynamic settings (Wyman and Kerrich, 1989);

(3). The first major episode of lode gold-silver vein deposits, which are genetically associated with translithospheric structures representing boundaries between distinct tectonostratigraphic terranes (Kerrich and Wyman, 1994, and references therein).

Collectively, these major changes at 2.7 Ga may signify a global trend in the thermal and tectonic evolution of the planet, that in turn may be reflected in the geochemistry of mantle magmas (Condie, 1989; Armstrong, 1991). Accordingly, this thesis addresses specific questions of Abitibi belt volcanic sequences and their geodynamic development, in the much larger context of global problems listed earlier in this section.

1-2. Analytical difficulties

Geochemical analysis of Archean komatiites present special difficulties. The least tractable problem is analysis of trace elements, particularly REE's and HFSE's, as these elements normally occur at sub part per million levels in komatiites, at or below the detection limits of conventional instruments such as X-ray fluorescence spectrometry (XRF), inductively coupled plasma atomic emission spectrometry (ICP-AES), and instrumental neutron activation analysis (INAA). Graphite furnace atomic absorption spectrophotometry (GF-AAS) offers exceptionally low detection limits, but Hf, Nb and Ta cannot be analyzed given their high volatization temperatures.

Conventionally, the analysis of all REEs and HFSEs in rocks generally required some combination of different analytical techniques. For example, XRF is excellent for the determination of Zr to ~ 6 ppm (Potts, 1987), but not for Nb or Hf at the levels at which these elements occur in mafic and ultramafic rocks. INAA yields precise results at low levels for Hf and most REEs, but cannot be used for Zr and Nb, and excessively long counting times (> 1 year) or radiochemical NAA is required for measurement of Ta. Thermal ionization mass spectrometry (TIMS) using isotope dilution (ID) confers superior precision, but is time consuming, and is only optimized when combined with ion exchange separations (Potts, 1987).

Another potential problem stemming from combining different instrumental techniques to obtain all REEs and HFSEs is the different calibration strategies involved: for XRF, a rock reference material calibrated by another technique using separate reference materials for calibration; or for INAA, use of NIST 1633 coal fly ash standard for rocks, with NIST 1633 calibrated by yet another technique. The combination of different calibration

strategies, and reference materials with contrasting matrices, may introduce uncertainties in quantification of REE and HFSE interrelationships, which, as discussed in the previous section, may be important indicators of depths of mantle melting and source mineralogy.

Traditionally, one of the preferred analytical techniques for the determination of all REEs and HFSEs in low abundance samples has been spark source mass spectrometry (SSMS), as it has low detection limits and is capable of analyzing multiple elements using ID techniques (Jochum et al., 1988). A potential difficulty with this methodology is that equilibration between spike and sample, a prerequisite of isotope dilution analysis, may not be achieved, as the elemental spike in aqueous solution is in a very different chemical form to the element in the rock powder-graphite mixture (Fassett and Paulsen, 1989; Kane, 1993, personal communication). For example, Zr and Hf are added to rock powders as spikes in an HNO_3 medium (Jochum et al., 1988), whereas in the rock, Zr and Hf may reside in baddelleyite or pyroxene. Furthermore, a very small quantity of sample is excited and analyzed in ID-SSMS analysis (< 2 mg), thus it may suffer severely from effects of sample heterogeneity. Collectively, these problems may be reflected in the fact that HFSE data for some low abundance international reference materials determined by ID-SSMS have been revised several times in the past 3 years, and accordingly, HFSE/REE relations in unknowns calibrated against the reference materials would also change, as discussed by Xie et al. (1994).

Recent developments in inductively coupled plasma mass spectrometry (ICP-MS) have proven its advantages for low abundance multi-element analysis using a common calibration strategy of pure elements in solution (Hall and Pelchat, 1990; Longerich et al., 1990; Schonberg, 1993; Xie et al., 1994), that in turn circumvents uncertainties in the

contents of some HFSEs in international reference materials (Longerich et al., 1990). Low detection limits, the capability of multi-element determination at low concentrations, potential for isotope dilution analysis, and fast sample throughput, make ICP-MS a method of choice for trace element analysis of Archean komatiites and basalts.

This thesis reports the first high precision, low level, trace element analysis of komatiites by ICP-MS. Notwithstanding the advantages of ICP-MS, there are various potential problems, such as incomplete digestion of refractory minerals, instability of some elements in solution, memory, and interferences, that need to be addressed, before ICP-MS can successfully be used in the analysis of REEs and HFSEs in mafic and ultramafic rocks. As part of this thesis, such problems have been addressed and quantified.

1-3. Sampling strategy

The 2.7 Ga Abitibi greenstone belt, and in particular the Southern Volcanic Zone (SVZ) [Ludden et al., 1986], has been chosen as the study area. The state of mapping in this area is sufficiently far advanced that outcrops, tectonostratigraphic relations, age relations of various geological units, and structures, are known in broad outline. Accordingly, this study draws on existing mapping as a basis for sampling design, rather than setting out to map individual outcrops. Typical and well exposed localities of least altered komatiites, tholeiites, and calc-alkaline basalts have been sampled. Given the lack of systematic trace element data in previous studies of Abitibi komatiites and basalts, that stems from the lack of multielement capability of many instruments as discussed above, this study emphasizes the trace element systematics of komatiites, tholeiites and calc-alkaline basalts, and in particular the interrelationships of REEs and HFSEs.

Eighty samples were collected from four komatiite-tholeiite sequences, which are separated by major terrane boundaries, and represent different types of komatiites and tholeiites. For comparison, another 21 samples of tholeiitic and calc-alkaline basalts from the central Abitibi SVZ were collected, which have been considered to have formed in geodynamic settings that are distinct from those of the three komatiite-tholeiite sequences (Jackson and Fyon, 1992).

Various experiments have been conducted in the laboratory to investigate the potential problems for analysis of REEs and HFSEs in low abundance samples by ICP-MS. The corresponding calibration strategies have been established. In particular, isotope dilution ICP-MS analysis of Zr and Hf has, for the first time, been developed by the author in this laboratory. International reference materials (e.g. BIR-1, BCR-1 etc.) and independent external laboratory cross checks have been employed to ensure the quality of data. Precise and accurate REE and HFSE data for some low abundance international reference materials have also been generated in this laboratory.

1-4. Structure of the thesis

A brief synthesis of the geology of the Abitibi greenstone belt is presented in Chapter 2, as a context for the different volcanic sequences that were sampled. Chapters 3 and 4 describe ICP-MS development studies, aimed at obtaining precise and accurate analysis of REEs and HFSEs in international reference materials and unknowns. New high precision trace element determinations of komatiite-tholeiite sequences in Munro, Tisdale and Boston Townships are reported in Chapter 5, with implications for Archean mantle plume composition and melting depths. In Chapter 6, trace element characteristics of a fourth

komatiite-tholeiite sequence from the central Abitibi SVZ are reported and compared with that of the other three komatiite-tholeiite sequences. Chapter 7 presents the geochemistry of tholeiitic and calc-alkaline volcanic flows from the central Abitibi SVZ, with implications for their petrogenesis and tectonic settings. The final Chapter 8 summarizes the principal results of the thesis, explores the implications of the results, and uses the trace element data to critically evaluate models for Archean greenstone belt development.

This study revealed distinct geochemical characteristics of the three komatiite-tholeiite sequences from the Abitibi SVZ, specifically the REE patterns and HFSE/REE interrelationships. This is the first time that distinct HFSE/REE fractionations have been reported in Archean komatiites and tholeiites. For example, previous data for komatiites determined by ID-SSMS shows essentially zero Zr(Hf)/MREE fractionation in Al-depleted and Al-undepleted variaties (Jochum et al., 1991). Most results of this thesis have been published in seven referred papers (Xie et al., 1993, 1994, 1995; McCuaig et al., 1994; Xie and Kerrich, 1994, 1995a, b). This thesis synthesizes all the results in an attempt to address some of the fundamental questions regarding the petrogenesis of Archean komatiites, early mantle evolution, and tectonic evolution of the Abitibi SVZ.

CHAPTER 2. GEOLOGICAL SETTING OF THE ABITIBI GREENSTONE BELT

2-1. Introduction

The late Archean (~ 2.7 Ga) Abitibi volcanic-plutonic belt is the largest contiguous greenstone belt globally. This chapter summarizes the lithological characteristics of the Abitibi belt, its setting within the larger Superior Province, and current thinking on the geochronological and geodynamic development of this Archean craton.

The Abitibi belt is bounded to the north by the Archean Quetico gneiss belt; to the south by the Archean Pontiac granitoid-gneiss Subprovince and a belt of Proterozoic rocks of the Southern Province; to the southeast by the Proterozoic Grenville front; and to the west by the Kapuskasing gneiss zone (Figure 2-1; Goodwin and Ridler, 1970; Jackson and Fyon, 1992). The Abitibi greenstone belt is one of the east-west trending volcanic-, metasedimentary-, and plutonic-dominated subprovinces, that collectively constitute the Superior Province. The various subprovinces accreted at ~ 2.7 Ga, and are separated by bounding brittle-ductile structures interpreted as terrane boundaries (Wyman and Kerrich, 1988, 1989; Card, 1990; Thurston et al., 1992).

The east-west trending Abitibi belt, which is about 700 km long by 400 km wide, is composed of low-grade metamorphosed volcanic, sedimentary and plutonic rocks. One of the characteristics of the Abitibi greenstone belt is the relatively high proportion of supracrustal versus intrusive rocks. The metamorphic grade of the belt is generally

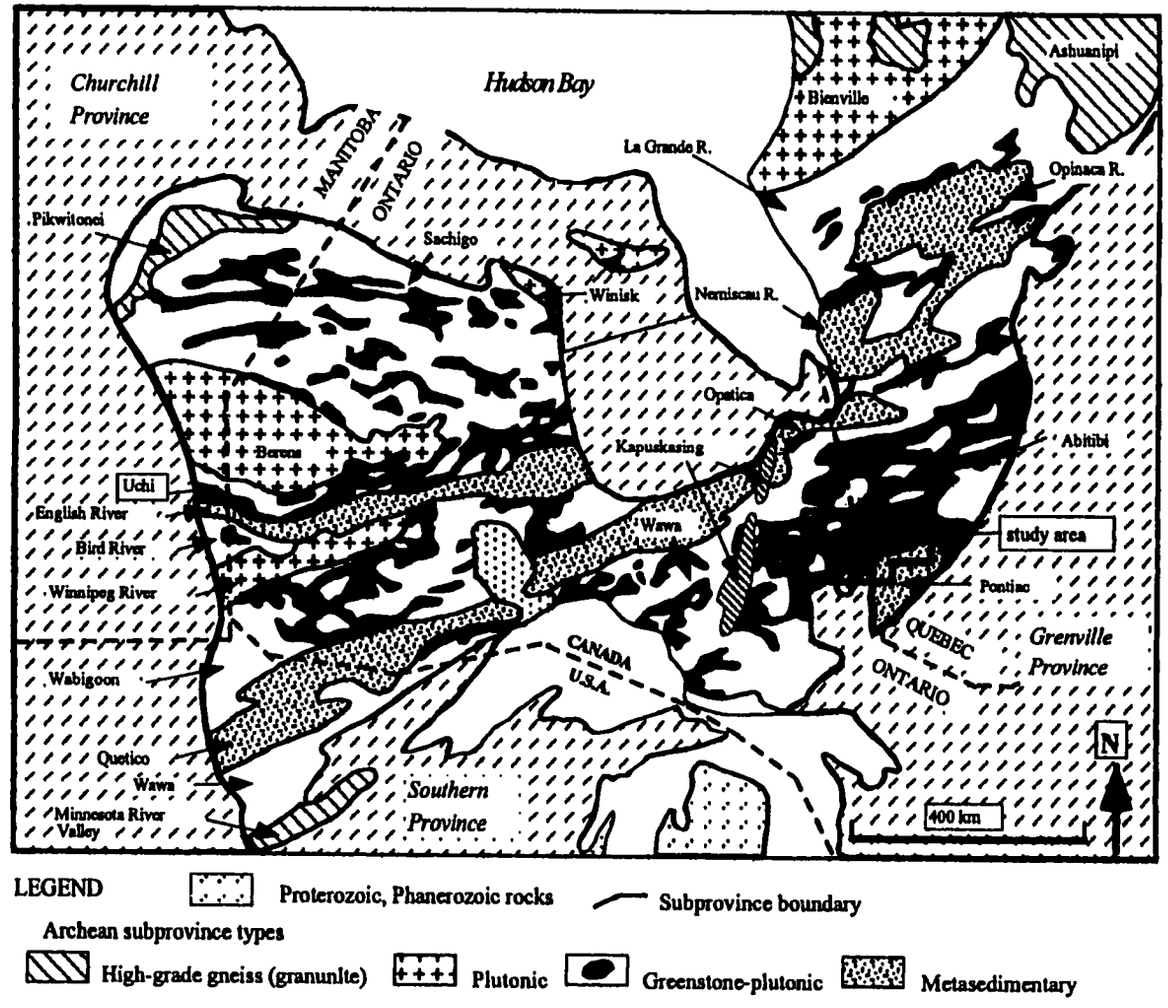

Figure 2-1. General geological map of the Superior Province, showing different subprovince types (modified after Thurston et al., 1991)

greenschist facies, with locally subgreenschist domains, or amphibolite or higher grade proximal to batholiths (Jolly, 1978).

Numerous studies have addressed various aspects of the Abitibi greenstone belt, including ***regional geology and evolution*** (Dimroth et al., 1982, 1983a, b; Pyke, 1982; Ayres and Thurston, 1985; Jensen and Langford, 1985; Ludden et al., 1986; Card, 1990; Kerrich and Feng, 1992; Thurston et al., 1992); ***metallogeny*** (Colvine et al., 1988; Kerrich, 1989); ***metamorphism*** (Jolly, 1978; Dimroth et al., 1983b; Feng et al., 1993b); ***temporal framework*** (Corfu et al., 1989a, 1991; Kerrich, 1991; Mortensen, 1993a, b, c); ***volcanic characteristics*** (Arndt et al., 1977; Arndt and Nesbitt, 1982; Cattell and Arndt, 1987; Lafleche et al., 1992; Desrochers et al., 1993); ***alteration and mineralization characteristics*** (Kerrich and Fryer, 1979; Ludden and Gelinas, 1982; Ludden et al., 1982; Kishida and Kerrich, 1987; Kerrich, 1989; Feng et al., 1993a); ***granitoid magmatism*** (Feng and Kerrich, 1992); ***sedimentary rocks*** (Feng and Kerrich, 1990b; Feng et al., 1993a); and ***PTt evolution*** (Feng and Kerrich, 1990a; Feng et al., 1993b).

2-2. Lithotectonic divisions

Based on the differences in volcanic stratigraphy and sedimentology, and on the volume of pre-kinematic plutons, two zones were defined by Dimroth et al. (1982): a northern internal zone and a southern external zone. The internal zone consists of two volcanic cycles, and the external zone of four cycles. In this interpretation, all cycles are characterized by a basal komatiitic unit overlain by: (1) tholeiitic basalt and minor tholeiitic andesite and rhyolite; (2) variable tholeiitic to calc-alkaline basalt to rhyolite, and in places (3) alkaline volcanic units (Ayres and Thurston, 1985; Jensen and Langford, 1985; Colvine

et al., 1988). Alternatively, Ludden et al (1986) divided the Abitibi belt into three domains, the Northern Volcanic Zone (NVZ), the Southern Volcanic Zone (SVZ), and an intervening granite-gneiss terrane (Figures 2-2, 2-3). The SVZ broadly corresponds to the external zone of Dimroth et al. (1982), and is bounded to the north and south by major east-west trending brittle-ductile shear zones, namely the Destor Porcupine Fault Zone (DPFZ) and Kirkland Lake-Larder Lake-Cadillac Fault Zone (KLFZ), respectively (Figures 2-2 and 2-3). This study focuses on komatiite-tholeiite, tholeiitic and calc-alkaline volcanic sequences in the western SVZ.

2-3. The Southern Volcanic Zone

Six major distinctive lithotectonic associations of supracrustal rocks, also termed assemblages, have been recognized in the SVZ (Ludden et al., 1982; Jensen and Langford, 1985; Thurston, 1990; Jackson and Fyon, 1992). These include three volcanic assemblages and three sedimentary assemblages. The former comprise: (1) komatiitic and tholeiitic rocks (e.g. Tisdale and Munro Group); (2) dominant tholeiitic basalts (e.g. Kinojevis Group); (3) calc-alkaline basalts with minor rhyolite interbeds and synvolcanic mafic to felsic intrusions (e.g. Blake River Group). The latter comprise: (4) quartz-rich turbidites with local interbeds of banded iron formation (BIF), and komatiitic basalts and trachytes (e.g. Pontiac and Kewagama Groups; Lajoie and Ludden, 1984); (5) synvolcanic greywacke (e.g. Hoyle assemblage); and (6) post-metamorphic fluviatile sandstone, with polymictic conglomerates and minor turbidites (e.g. Timiskaming Group).

A summary of the stratigraphy of the supracrustal sequences in the SVZ is given in Figure 2-4. According to Hodgson and Hamilton (1989), these assemblages reflect four

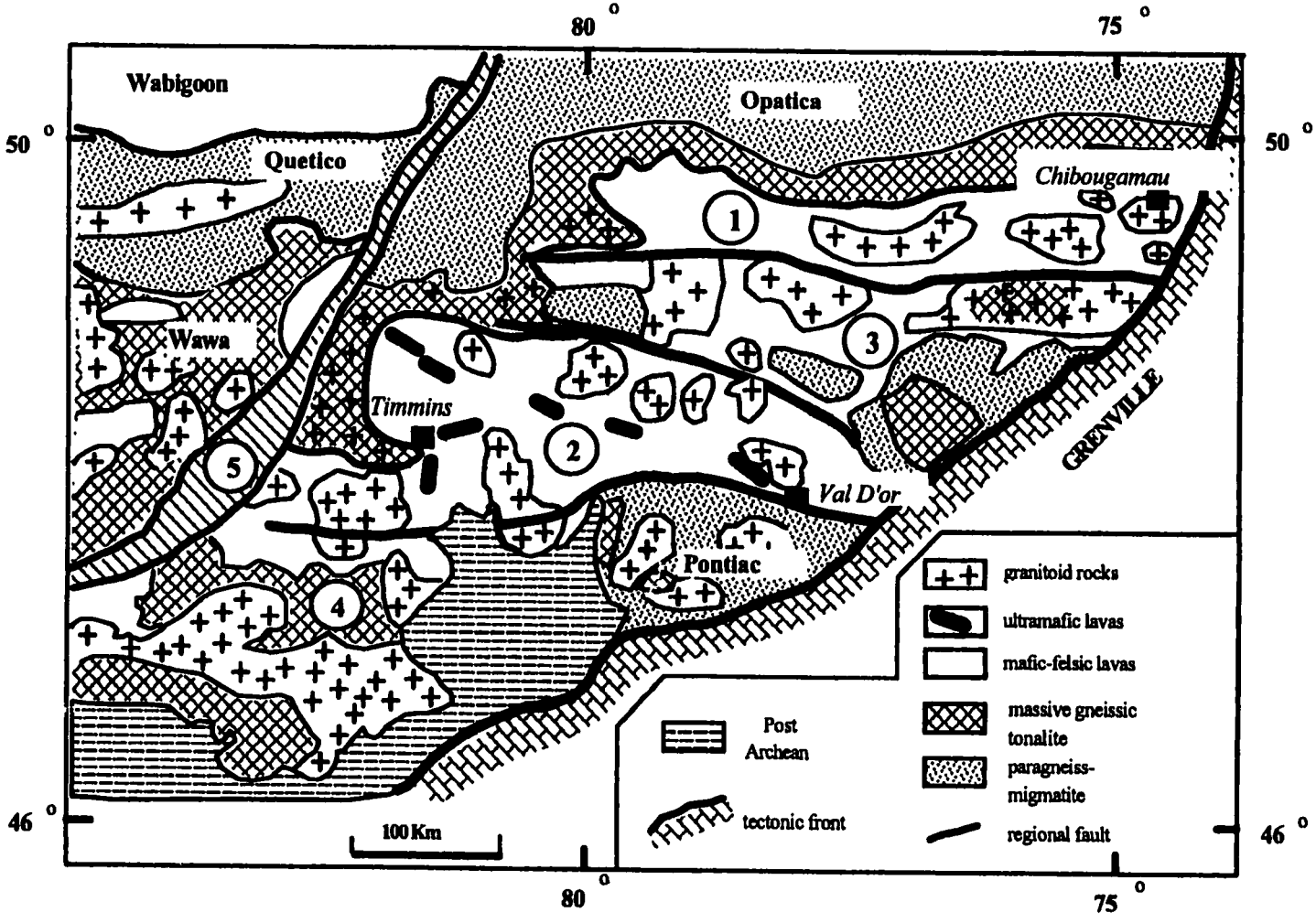

Figure 2-2. Schematic map of the Abitibi greenstone belt showing internal subdivisions after Ludden et al. (1986). ① Northern Volcanic Zone (NVZ); ② Southern Volcanic Zone (SVZ); ③ Intervening Granite-Gneiss Zone; ④ Southern Granite-Gneiss Zone, which includes the Pontiac Subprovince; ⑤ Kapuskasing Structural Zone (KSZ). ■ Locations of large towns.

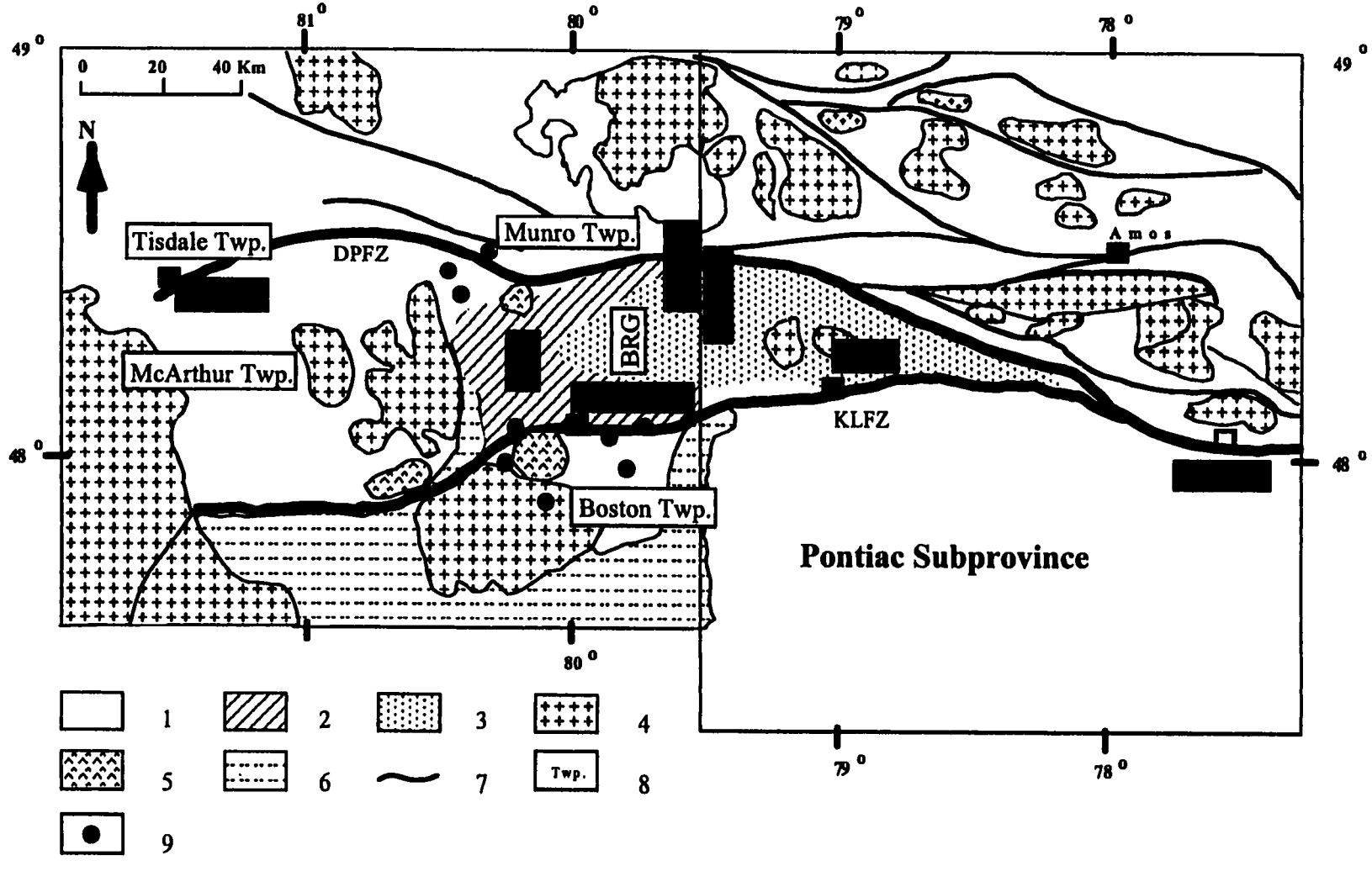

Figure 2-3. Simplified geological map of the Abitibi Southern Volcanic Zone (Jensen and Langford, 1985; Wyman and Kerrih, 1990; Feng and Kerrich, 1992). Note 1. komatiite-tholeiite; 2. Kinojevis tholeiitic basalt (KJG); 3. Blake River calc-alkaline basalt (BRG); 4. syn-volcanic and syn-tectonic TTG and TGGM; 5. post-tectonic alkaline granitoids; 6. Proterozoic; 7. major fault zone; 8. sampling areas in specified Townships; 9. lamprophyre dykes.

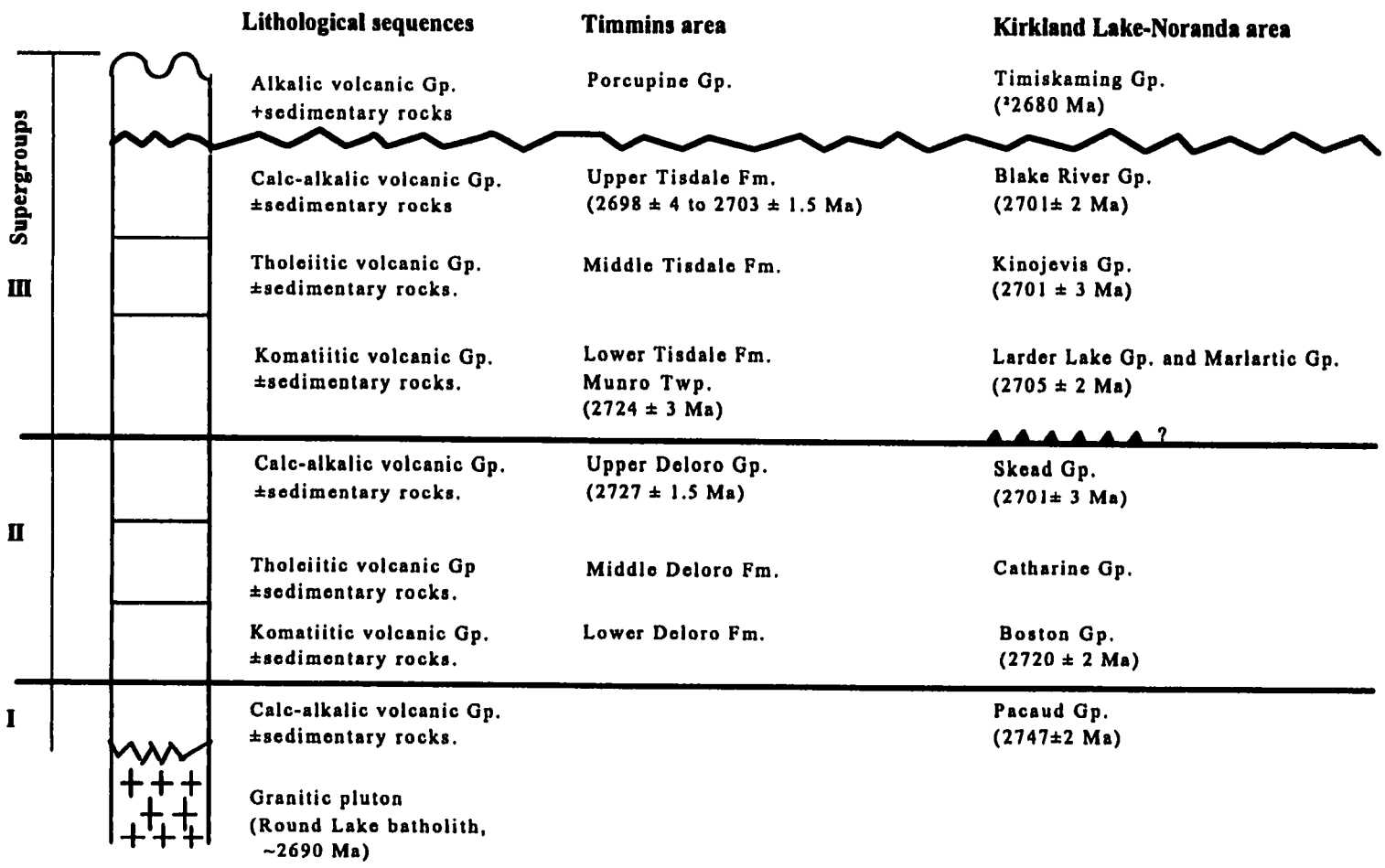

Figure 2-4. Stratigraphic subdivision, lithological sequences, and U-Pb zircon ages of the Abitibi SVZ and the Pontiac Sbprovince from MERQ-OGS (1983), Jensen (1985) and Corfu et al. (1989, 1993). Formations (Fm.) as defined by Pyke (1982) for the Timmins area correspond to Groups (Gp.) in the other area. Note that there may be an apparent age reversal between the Larder Lake group Gp. and Skead Gp., indicating thrusting and tectonic thickening in the Archean (Corfu et al., 1989).

distinctive tectonic settings as below:

(1) komatiitic and tholeiitic assemblages formed in an oceanic extensional environment;

(2) calc-alkalic volcanic and associated sedimentary rocks formed in an island-arc environment;

(3) an assemblage of craton derived quartzose sedimentary units with komatiitic basalt interbeds formed on a passive continental margin; and

(4) molasse-type sedimentary assemblages with alkalic volcanic rocks and felsic intrusions formed in pull-apart basins.

General characteristics of individual volcanic assemblages sampled for this study are further described in Chapters 5 and 6.

2-4. Structural geology

Tectonic fabrics and mesoscopic structures are domainal in distribution and type within the Abitibi SVZ. In general, fabrics and structures are parallel, and best developed adjacent to regional faults, large batholiths and many of the exposed assemblage boundaries.

In general, structures within the Abitibi SVZ can be assigned to one of the following classes: (1) "pre-cleavage" folds which are the earliest recognized structures; (2) structures related to batholith emplacement at ~ 2700 to 2690 Ma; and (3) syn- to post-Timiskaming structures (Jackson and Fyon, 1992). "Pre-cleavage" folds, some thrust faults, emplacement of large granitoid complexes and formation of related structures predated deposition of the 2685 to 2675 Ma Timiskaming-like assemblages. Prominent regional shear zones and fold sets developed coeval with or postdate deposition of the Timiskaming-like molasse assemblages. They include a northwest- to west-northwest-striking set, notably the Desto-

Pocupine Fault Zone (DPFZ) and the Kirkland Lake-Lard Lake Fault Zone (KLFZ), that predates a northeast-to east-northeast-striking set. Thrust faulting and/or high angle reverse faulting also occurred at this time. These structures can be interpreted to have formed during late-Archean, protracted north-south subhorizontal compression (Dimroth et al., 1983a, b; Green et al., 1990).

The above structures are overprinted by north-east-, northwest- and north-northeast-striking brittle faults related to the development of Proterozoic and Phanerozoic rifts (Jackson and Fyon, 1992).

2-5. Metamorphism

The metamorphic grade of the Abitibi SVZ varies from subgreenschist facies in the area of the Blake River assemblage to greenschist facies to the north, south and west of the Blake River assemblage (Jolly, 1978). Amphibolite facies contact aureoles are well developed near most of the large syn-tectonic tonalite-granodiorite batholiths (2695-2685 Ma; e.g., Lake Abitibi batholith) and near the late-tectonic granodiorite to monzonite intrusions (~ 2680 Ma; e.g., Watabeag batholith; Jolly, 1978; Feng et al., 1993b). The greenschist and amphibolite facies assemblages spatially associated with granitoid intrusions apparently overprint and postdate prehnite-pumpellyite facies assemblages (Jolly, 1978; Dimroth et al., 1982).

The following observations bear on the timing of regional metamorphism:

(1) Many of the metavolcanic rocks are ~ 2700 Ma. Thus, regional metamorphism postdates 2700 Ma;

(2) Metamorphic grade increases towards large batholiths (e.g. Lake Abitibi Batholith).

Most of these bodies were emplaced between 2690 and 2685 Ma. Thus, if regional metamorphism is associated in time and space to these intrusions, it must have predated or shortly followed 2690 Ma (Corfu, 1993).

(3) The Timiskaming assemblage and related rocks in the Abitibi SVZ are not metamorphosed, and have been dated at 2681-2672 Ma (Corfu, 1993).

(4) $^{40}Ar/^{39}Ar$ mineral age spectra of granitic and metamorphic rocks, in conjunction with existing conventional zircon geochronology, indicate that there were at least two thermal events in the eastern Abitibi SVZ. Earlier thermal activity (2690-2680 Ma) throughout the SVZ was accompanied by the intrusion of syntectonic plutons and caused low-pressure, greenschist facies metamorphism. In the eastern SVZ, and Pontiac Subprovince, a second thermal event (2660-2630 Ma) was coeval with the emplacement of syncollisional S-type granite, and reset the K-Ar systems in preexisting rocks (Figure 2-5; Feng et al., 1993b).

2-6. Geochronology

Precise dating of lithological units in the Abitibi greenstone belt has provided important constraints on the temporal relationship of magmatism, metamorphism, deformation, and mineralization. A recent compilation of isotopic ages, obtained using different dating methods (e.g. U-Pb, K-Ar, Rb-Sr, and Sm-Nd dating) on different geological samples, is shown in Figure 2-5. In general, concordant U-Pb ages on zircons give primary magmatic ages, whereas other systems may record secondary resetting events. Contributions on zircon U-Pb ages have been given by numerous workers (e.g., Nunes and Pyke, 1981; Frarey and Krogh, 1986; Corfu et al., 1989b, 1991; Barrie and Davis, 1990; Claoue-Long

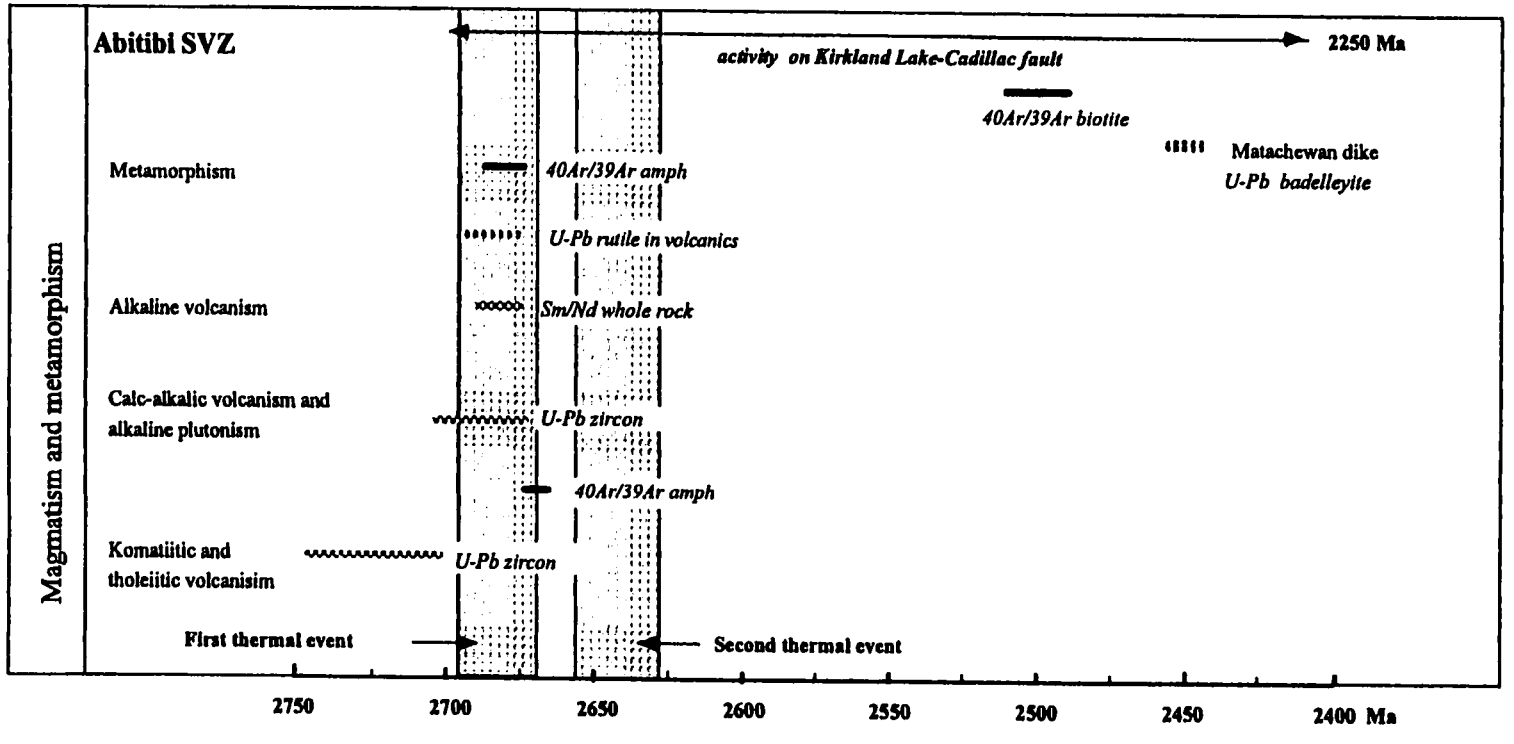

Figure 2-5. Ages of magmatism. metamorphism, resetting events in the Abitibi SVZ, based on different radiometric methods. Data sources: $^{40}Ar/^{39}Ar$ ages from Feng et al. (1993b). For other data sources, see Kerrich and Cassidy (1994).

et al., 1990; Feng and Kerrich, 1991; Corfu, 1993; Mortensen, 1993a, b, c).

Corfu (1993) summarized U-Pb zircon ages for the southern Abitibi greenstone belt and integrated them into a general framework for the evolution of the region. These results suggest that the Abitibi SVZ developed between 2750 and 2670 Ma. The earliest ages are generally restricted to remnants of volcanic belts at the periphery of the belt. Major preorogenic volcanic activity was mainly confined to the period of 2720-2700 Ma, and dominated by komatiites and tholeiites. The extensional volcanic regime was followed by a period of compression that caused folding and thrusting, emplacement of calc-alkaline plutons and deposition of turbidites between 2700 and 2688 Ma. The magmatism became predominantly alkaline during the main Timiskaming period between 2681 and 2672 Ma, accompanied by deposition of alluvial-fluvial sequences, followed by renewed compression that resulted in polyphase folding and thrusting, probably between 2676 and 2670 Ma. Lamprophyre dikes formed during the final stages of deformation (Corfu, 1993; Wyman and Kerrich, 1993).

2-6. Geodynamic development

Previously, the Abitibi greenstone belt, and at a larger scale the entire Superior Province, had been viewed as forming in-place, in a "static" geodynamic framework. The Abitibi greenstone belt was interpreted as a series of contemporaneous volcanic-plutonic centres that developed adjacent to one another, with intervening belts of volcanoclastic and chemical sedimentary rocks (Goodwin and Ridler, 1970). Regional stratigraphic correlations were drawn between volcanic sequences, such as at Timmins, and Kirkland Lake, ~ 100 km to the southeast (Jensen and Langford, 1985). The continuity of these regional stratigraphic

correlations between geographically separated supracrustal sequences has been challenged by the recognition of major strike-slip and thrust faults within the belt (Ludden et al., 1986; Green et al., 1990; Thurston et al., 1992).

The Superior Province has now been reinterpreted as a series of allochthonous subprovinces, or tectonostratigraphic terranes formed at different times in distinct areas, that were accreted from north to south, diachronously over 2720 to 2680 Ma. Similarly, the Abitibi SVZ is viewed as a collage of tectonostratigraphic terranes that accreted at 2720-2680 Ma (Wyman and Kerrich, 1988; Thurston et al., 1992; Desrochers et al., 1993; Jackson et al., 1994). Feng and Kerrich (1992) and Xie et al (1993) suggested a model based on the geochronology and geochemistry of volcanic-plutonic rocks, whereby the belt developed in space and time through evolving geodynamic settings from plume, to arc, to arc-continent collision.

Geochronological and structural data demonstrate that the distribution of regional scale deformation zones within the Superior Province can best be accounted for by accretionary tectonics (Card, 1990), a trend of younging towards the southern part of the Superior Province, from ~ 2710 Ma at Uchi-English River Subprovince boundary, to 2692-2681 Ma at Quetico subprovince boundary, to 2680-2670 Ma at the Abitibi-Pontiac Subprovince boundary (Stott et al., 1987; Wyman and Kerrich, 1989; Feng and Kerrich, 1990a; Kerrich and Feng, 1992). The earliest komatiite-tholeiite sequences formed from mantle plumes in an oceanic environment. Subsequently, oceanic suprasubduction zone volcanic-plutonic associations developed, some of which evolved into oceanic magmatic arcs with granitoid batholiths. Recently, Fan (1995) reported evidence for the eruption of some komatiites in the Timmins district through continental crust, from the conjunction of light

rare earth element (LREE) enrichment with negative Nb, P, and Ti anomalies.

At ~ 2680 Ma, the plume, suprasubduction zone, and magmatic arc terranes were accreted, followed by the development of the Timiskaming shoshonite-molasse assemblage in transtensional jogs along collisional terrane boundaries. The entire collage was then thrust over an older continental fragment - the Pontiac Subprovince, leading to intracrustal melting reflected in extensive S-type granitoids, at 2645-2611 Ma. Finally, differential uplift exposed some inliers of high grade Pontiac Subprovince within the low grade Abitibi thrust sheets (Feng and Kerrich, 1990a, 1992; Feng et al., 1993b; Xie et al., 1993).

CHAPTER 3 MULTI-ELEMENT ANALYSIS OF THE INTERNATIONAL REFERENCE MATERIAL BIR-1: RESULTS BY ICP-MS

3-1. Introduction

International rock reference samples have been introduced to analysts and geochemists for three principal reasons: (1) to optimize precision by calibration of analytical techniques; (2) to validate analytical results by characterizing the accuracy of the technique; and (3) to compare interlaboratory analytical data (Potts et al., 1992). The availability of reliable rock reference material data is, therefore, vital to the analyst involved in the calibration and the routine operation of an analytical technique, and to the geochemist who needs to demonstrate the quality of results prior to interpretation. In order to demonstrate the accuracy of the data, one can only use reference materials with concentration ranges of the elements of interest similar to that in unknown samples. The reference materials have sometimes been termed standards. However, this is an inappropriate term, inasmuch as the materials have to be calibrated against 'primary standards', and errors in published values for some elements, in 'standards' such as BIR-1, MRG-1 and BHVO-1, have recently come to light (Jenner et al., 1990; Jochum et al., 1990a, b; Potts et al., 1990; Xie et al., 1994).

For precise and accurate analysis of trace elements in komatiites, BIR-1 serves as a good reference material, as most trace element concentrations in BIR-1 are in the same range as in typical komatiites, mantle peridotites and picrites. However, there appear to be some discrepancies in existing data for BIR-1 in the literature, specifically for HFSEs, but not for

REEs (Govindaraju, 1989; Jenner et al., 1990; Jochum et al., 1990b; Potts et al., 1992). These discrepancies exacerbate difficulties in intercomparisons of different datasets from independent laboratories, specifically for quantifying HFSE/REE fractionations, which is essential for recognizing majorite or Mg-perovskite in mantle sources (Xie et al., 1993), or HFSE/REE signatures of depleted mantle sources (Salters and Shimizu, 1988). Consequently, additional data for BIR-1 acquired by different instrumental techniques is necessary to establish it with sufficient confidence as a low-abundance reference material.

This chapter reports the results of 30 new analyses of BIR-1 conducted by ICP-MS over the last 2 years at the University of Saskatchewan by the author. In addition, the ICP-MS results for Sm and Hf in BIR-1 and some low-abundance komatiites were checked using INAA. ICP-MS results for Zr in the standards and unknowns were checked using ICP-AES. Also reported are new data for the international reference materials SY-2, MRG-1, BCR-1 and BHVO-1. This study was designed to characterize BIR-1 as a reference material for the analysis of samples with low trace element abundances. Potential analytical problems in ICP-MS, stemming from sample dissolution, solution instability, bias at low levels, isobaric interferences, memory effects and inhomogeneity in different batches of BIR-1 are systematically explained. This chapter has been expanded, and reformatted from, a paper by the author (Xie et al., 1994).

One advantage of ICP-MS is the capability of using pure elemental standards in solution, such that the standards and unknowns are in the same dilute acid matrix. As a result, the concentrations in unknowns can be determined with reference to pure elemental standards, and values in international reference materials checked.

3-2. Analytical techniques

3-2-1. Sample preparation —— ICP-MS

About 100 mg of powdered sample was digested in a screw-top Teflon bomb (Savillex®) at 150°C for 48 hours, using 2 ml 8N HNO_3 and 1 ml HF. The HF-HNO_3 mixture was then evaporated to dryness, and the residue taken into solution in concentrated HNO_3. A second evaporation to dryness was performed to ensure conversion of residual fluorides to nitrates, as the former are relatively insoluble. The residue was taken up in 2 ml 8N HNO_3, transferred to a 125 ml bottle, and diluted with distilled deionized water (DDIW) to about 100 g. The entire procedure of sample preparation was conducted gravimetrically under clean-lab conditions, and all reagents were triply distilled. Analysis of acids, DDIW, and procedural blanks yield total levels of between 1 ppb (e.g., Hf, Tb) and 10 ppb (e.g., Sr, Zr,) for all 28 elements determined, when recalculated to the sample weight.

3-2-2. Instrumentation

—— ICP-MS

A Perkin Elmer Sciex Elan 5000 ICP-MS was used in this study. The instrument was operated at a power setting of 1000 W. The spray chamber was cooled by means of a refrigerated chiller Model HX - 150 (Neslab Instruments, Portsmouth, NH, USA) to minimize internal temperature fluctuations and backfeed. The argon plasma gas flow was set at 15 l/min. Auxiliary gas flow and nebulizer gas flow were 0.8 L/min. A sample delivery rate of 1.0 ml/min was used. Platinum tipped sampler and skimmer cones with orifice diameters of 1.1 mm and 0.89 mm, respectively, were employed.

Instrumental conditions were as follows: B, P, E1 and S2 ion lens settings were 45,

45, 25 and 45 digipots respectively. Peak hopping mode was used for measurement, with 3 counts/per mass. Total counting time was 10 s/per mass, and dwell time was 50 ms/per mass. Sample equilibration time was 150 s, and intersample wash was 180 s. Isotopes measured were as follows; ^{45}Sc, ^{51}V, ^{85}Rb, ^{86}Sr, ^{89}Y, ^{90}Zr, ^{93}Nb, ^{133}Cs, ^{137}Ba, ^{139}La, ^{140}Ce, ^{141}Pr, ^{145}Nd, ^{147}Sm, ^{151}Eu, ^{157}Gd, ^{159}Tb, ^{163}Dy, ^{165}Ho, ^{167}Er, ^{169}Tm, ^{173}Yb, ^{175}Lu, ^{177}Hf, ^{181}Ta, ^{206}Pb, ^{232}Th and ^{238}U (cf. Jenner et al., 1990; Longerich et al., 1990).

The ICP-MS calibration protocol involves external calibration and standard additions. Pure elemental standards in solution (from Inorganic Ventures Inc.) were employed for external calibration and standard additions. Standard addition was used to overcome possible matrix effects; each unknown was run unspiked and spiked. Data reduction followed the procedure of Jenner et al. (1990). Detection limits, defined as 3σ of procedural blanks, for most elements were between several ppb (e.g. Zr, Hf, Ce) and 100 ppb (e.g. Rb, Sr, Ba) relative to the rock.

---- INAA

BIR-1, MRG-1, BHVO-1 and 8 unknown komatiites were analyzed in duplicate for Sm and Hf by INAA at the University of Michigan, and Activation Labs., Canada, using NIST 1633a coal fly ash as a calibration standard. 0.5 g aliquots of whole rock powder were exposed to a neutron flux (approximately 1×10^{13} n/cm^2/s) for 45 minutes; allowed to "cool" for 7 days; and then counted for 2000 seconds each. Pure elemental standard solutions of Sm and Hf, as used for external calibration and spiking unknowns in the ICP-MS protocol, were analyzed along with the powders. Detection limits are 0.01 ppm for Sm and 0.05 ppm for Hf.

—— ICP-AES

The international reference materials BIR-1, MRG-1, BHVO-1, and two low level unknowns were analyzed for Zr by ICP-AES at Saskatchewan Research Council on solutions prepared by the author. 0.5 g aliquots of whole rock powder were digested using the same procedure as for ICP-MS. A Thermo Jarrell Ash Atom Scan 25 was used with the following instrumental parameters: RF power ~ 1150 W; analysis pump rate = 100 RPM; nebulizer pressure = 28 PSI (~ 0.2 MPa); observation height = 19 mm. High torch gas flow and medium (1.0 L/min) auxiliary gas flow were used. The wavelength used for Zr was 349.621 nm. The detection limit for Zr is 1 ppm referenced to the rock.

3-3. Results

Averages, standard deviations and relative standard deviations for 28 elements in the well-established international reference materials SY-2, MRG-1, BCR-1 and BHVO-1 are presented in Table 3-1, together with comparisons with compiled values (Potts et al., 1992). In general, there is good agreement between the U. of S. ICP-MS data and compiled values for these four reference materials. The mean deviations of the ICP-MS data from compiled values for 28 elements range from 3% to 7%, excepting Ta (Table 3-1 and Figure 3-1). There is also good agreement between the new ICP-MS results for these reference materials and results by ID-SSMS (Jochum et al., 1990b).

For the low-abundance reference material BIR-1, REE data by ICP-MS are consistent with both compiled values (Potts et al., 1992), and ID-SSMS data (Jochum et al., 1990b), whereas there are inconsistencies for other elements. Of the latter, Nb, Zr, Hf and Ta are of particular interest, as interrelationships between REEs and HFSEs are significant

Table 3-1. Multielement analysis of specified trace elements in international reference materials by ICP-MS

	SY-2				MRG-1					BCR-1				
No. analysis	$\overline{X}$ [a] 32	STD	RSD(%)	Compiled values	$\overline{X}$ 16	STD	RSD(%)	Compiled values	ID-SSMS	$\overline{X}$ 9	STD	RSD(%)	Compiled values	ID-SSMS
Sc	7.79	0.8	10.3	7 [b]	58.5	2.49	4.3	55		34.7	1.1	3.2	32.6	
V	48.9	3.8	7.8	50	562	16	2.8	526		421	27	6.4	407	
Rb	218	16	7.3	217	7.33	0.2	2.7	8.5?	7.4? [c]	47.1	1.5	3.2	47	47
Sr	272	19	7	271	283	5	1.8	266	264	332	11	3.3	330	327
Y	119	9	7.6	128	12.2	0.1	0.8	14	17	29	2.5	8.6	38	38
Zr	303	24	7.9	280	103	2	1.9	108	107	201	12	6	190	186
Nb	33.8	2.6	7.7	29?	24.9	1.7	6.8	20?	18.4	14.6	0.7	4.8	14	13.6
Cs	2.77	0.2	7.6	2.4	0.627	0.02	3.2	.57?	.32?	0.967	0.07	7.2	0.96	0.91
Ba	443	32	7.2	460	47.6	0.7	1.5	61?	51	680	36	5.3	681	653
La	70.3	5.4	7.7	75	9.42	0.48	5.1	9.8	9.5	26	0.8	3.1	24.9	24.7
Ce	164	12	7.3	175	26.8	0.7	2.6	26	25.4	54.6	2.1	3.8	53.7	54
Pr	20.2	1.5	7.4	18.8	3.89	0.09	2.3	3.4	3.87	6.95	0.33	4.7	6.8	6.79
Nd	78.5	5.6	7.1	73	18.9	0.4	2.1	19.2	17.8	28.4	1.1	3.9	28.8	29.1
Sm	16	1.1	6.9	16.1	4.55	0.19	4.2	4.5	4.05	6.47	0.4	6.2	6.59	6.63
Eu	2.44	0.2	7	2.42	1.44	0.02	1.4	1.39	1.26	1.95	0.11	5.6	1.95	1.96
Gd	17	0.9	5.3	17	4.3	0.14	3.3	4	3.52	6.84	0.39	5.7	6.68	6.56
Tb	2.8	0.2	6.4	2.5?	0.548	0.01	1.8	0.51	0.443	1	0.04	4	1.05	1.07
Dy	20.2	1.3	6.4	18	3.04	0.06	2	*2.76*	2.61	6.38	0.21	3.3	6.34	6.35
Ho	4.49	0.3	6.7	3.8	0.504	0.01	2	0.49	0.463	1.26	0.05	4	1.26	1.24
Er	15	0.9	6	12.4	1.21	0.04	3.3	1.12	1.15	3.67	0.14	3.8	3.63	3.77
Tm	2.48	0.2	7.3	2.1	0.149	0.01	6.7	.11?		0.54	0.02	3.7	0.56	0.617
Yb	17.8	1.1	6.2	17?	0.848	0.03	3.5	.6?	0.81	3.4	0.12	3.5	3.38	3.43
Lu	2.96	0.2	6.8	2.7	0.114	0.01	8.8	*0.13*	0.121	0.502	0.02	4	0.51	0.525
Hf	8.86	0.7	7.3	7.7	3.87	0.14	3.6	3.76	3.51	5.87	0.49	8.3	4.95	4.9
Ta	2.04	0.3	14.2	2.01	1.19	0.19	16	0.8		1.03	0.16	15.5	0.81	
Pb	94.4	7.3	7.7	85	5.17	0.39	7.5	10?	4.41	13.9	0.72	5.2	13.6	15.9
Th	390	31	7.9	379	0.793	0.03	3.8	0.93	0.83	6.7	0.52	7.8	5.98	6.02
U	288	23	8	284	0.251	0.02	8	0.24	0.248	1.75	0.1	5.7	1.75	1.73

a $\overline{X}$: average of the analysis; STD: standard deviation; RSD%: relative standard deviation (this work);

b compiled values from Potts et al. (1992); confidence limits distinquished as: underline -- precision better than 10%; plain typeface -- other compiled data; ? -- additional uncertainty; *italic* -- from individual analysis;

c ID-SSMS data from Jochum et al. (1990).

(Table 3-1 continue)

	BHVO-1					BIR-1(HF-HNO3)			BIR-1(Laser)			
No. analysis	$\overline{X}$ 8	STD	RSD(%)	Compiled values	ID-SSMS	$\overline{X}$ 30	STD	RSD(%)	$\overline{X}$ 5	STD	RSD(%)	Compiled values
Sc	32.7	0.8	2.4	31.8		46.1	1.4	3				44
V	334	14	4.2	317		346	11	3.2				313
Rb	9.38	0.17	1.8	11	11	0.172	0.03	17.4	0.3	0.1	33.3	*0.27*
Sr	407	5	1.2	403	394	112	2.07	1.8	119	7	5.9	108
Y	22.2	0.1	0.5	28	30	14.6	0.25	1.7	14.3	1.2	8.4	16
Zr	178	2	1.1	179	182	15.7	0.5	3.2	13.2	1.3	9.8	22
Nb	21.2	0.2	0.9	19	19.8	0.738	0.07	9.5	0.6	0.04	6.7	2
Cs	0.093	0.002	2.2	0.13	0.11	0.007	0.001	14.3				0.45
Ba	131	1	0.8	139	143	6.47	0.15	2.3	7.2	0.64	8.9	7.7?
La	16	0.2	1.3	15.8	14.5	0.614	0.02	3.3	0.8	0.06	7.5	.88?
Ce	39.3	0.2	0.5	39	36.3	1.93	0.05	2.6	2.3	0.8	34.8	2.5?
Pr	5.6	0.03	0.5	5.7	5.36	0.382	0.01	2.6	0.4	0.04	10	.5?
Nd	24.6	0.3	1.2	25.2	23.6	2.47	0.07	2.8	2.6	0.7	26.9	2.5
Sm	6.01	0.12	2	6.2	5.68	1.14	0.06	5.3	1.3	0.21	16.2	1.08
Eu	2.14	0.11	5.1	2.06	1.85	0.524	0.03	5.7	0.5	0.07	14	0.54
Gd	6.55	0.47	7.2	6.4	5.96	1.91	0.06	3.1	1.6	0.28	17.5	1.9
Tb	0.895	0.03	3.4	0.96	0.864	0.351	0.01	2.8	0.3	0.06	20	0.41
Dy	5.37	0.06	1.1	5.2	5.17	2.63	0.08	3	2.7	0.23	8.5	2.4
Ho	0.958	0.02	2.1	0.99	1	0.567	0.02	3.5	0.5	0.1	20	0.5
Er	2.56	0.06	2.3	2.4	2.63	1.72	0.04	2.3	1.8	0.18	10	1.8
Tm	0.331	0.01	3	0.33		0.26	0.01	3.8	0.2	0.02	10	0.27
Yb	2.01	0.05	2.5	2.02	1.93	1.71	0.05	2.9	1.6	0.26	16.3	1.7
Lu	0.288	0.02	6.9	0.291	0.311	0.259	0.01	3.9	0.2	0.02	10	0.26
Hf	4.39	0.54	12.3	4.38	4.6	0.639	0.04	6.3	0.6	0.08	13.3	0.58
Ta	1.35	0.15	11.1	1.23		0.213	0.08	37.6	0.3	0.1	33.3	.062?
Pb	2.11	0.05	2.4	2.6	2.12	3.13	0.14	4.5	8.8	7.2	81.8	3.2
Th	1.4	0.23	16.4	1.08	1.43	0.06	0.01	16.7				*0.031*
U	0.424	0.02	4.7	0.42	0.422	0.011	0.002	18.2				*0.01*

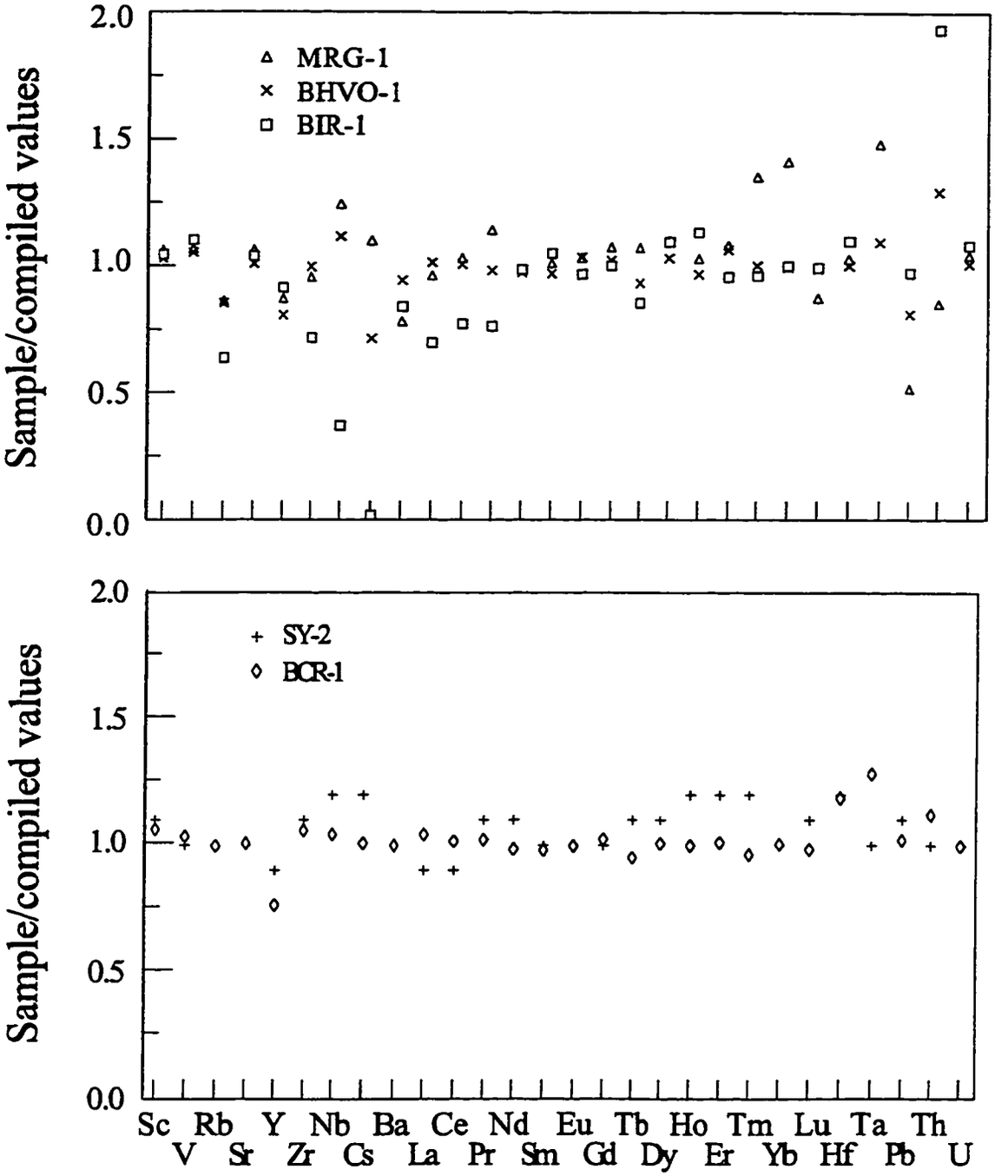

Figure 3-1. Comparison of ICP-MS data with compiled values for international reference materials. The compiled values are from Potts et al., 1992.

for geochemical studies of mafic and ultramafic rocks (Pearce and Cann, 1973; Hall and Pelchat, 1990a; Hawkesworth et al., 1991; Jochum et al., 1991; Hall and Plant, 1992; Xie et al., 1993).

The new results for Nb, Zr and Hf are systematically higher than those by ID-SSMS by 44%, 29% and 72%, respectively, or different by 18%, -28% and 10% relative to the values compiled by Potts et al. (1992). To evaluate the ICP-MS data for these elements, a comparison with data obtained by other techniques was compiled, abstracted from the literature (Table 3-2). Data generated by ICP-MS at the University of Saskatchewan are in good agreement with other ICP-MS data, as well as the median values of data by various techniques, excepting Ta, for which our data is much higher than those obtained by other laboratories. The high Ta value may be due to some unresolved interferences, and is the subject of on-going study.

Results for Sm and Hf in BIR-1, MRG-1, BHVO-1, and low-level unknowns by INAA are commensurate with ICP-MS data for these elements. Samarium is within 10% of the ICP-MS data over the concentration range of 0.1 to 1 ppm, whereas Hf is within 15% of the ICP-MS results over the range 0.2 to 1 ppm (Figure 3-2). Analyses of the pure elemental solutions of Sm and Hf, used for external calibration and standard additions, are within error of their certified and gravimetrically determined values. Similarly, the values for Zr in BIR-1, MRG-1, BHVO-1 and unknowns by ICP-AES are within 15% of the ICP-MS data, over the concentration range of 9 to 170 ppm (Figure 3-3).

3-4. Discussion

Several authors have drawn attention to problems with the analysis of REEs and

Table 3-2. Comparison of data for Hf, Nb, Ta and Zr

	Technique	Hf	Nb	Ta	Zr
Flanagan (1984) U.S.G.S. Bulletin, 1623	Compilation	0.64 ± 0.078	2.26 ± 0.42	0.07	18.4 ± 1.19
Gladney et al. (1988) Geostandards Newsletter, 12, 63-118	Compilation	0.58±0.06	2.0±0.5	0.062±0.036	22±7
Jochum and Seufert(1984) quoted in Gladney et al. (1988)	SSMS	0.48	0.78		18
Jochum et al. (1988) Fresenius Z. Anal. Chem., 81, 104-110	ID-SSMS		0.508		14
Jochum et al. (1990) Geostandards Newsletter, 14, 3, 469-473	ID-SSMS	0.36	0.49		12.1
Jochum et al. (1994) Geostandards Newsletter, 18, 1, 43-51	ID-SSMS	0.51	0.5	0.03	15.4
Potts et al. (1981) Chem. Geol., 34, 331-352	INAA	0.61		0.03	
Potts et al. (1990) Geostandards Newsletter, 14, 127-136	ED-XRF				20
Webb et al. (1990) Geostandards Newsletter, 14, 361-372	ED-XRF		2		26
Watkins and Nolan (1990) Geostandards Newsletter, 14, 11-20	ICP-AES	0.4			
Garbe-Schonberg (1993) Geostandards Newsletter, 17, 81-97	ICP-MS	0.61	2.11		13.8
Poitrisson et al. (1993) Geostandards Newsletter, 17, 209-215	ICP-MS		0.60	0.09	
Jenner et al. (1990) Chem. Geol., 83, 133-148	ICP-MS	0.60±0.03	0.59±0.05	0.09±0.01	16.3±0.4
Hall and Pelchat (1990) Geostandards Newsletter, 14, 197-206	ICP-MS Fusion	0.64±0.02	1.5±0.07	0.05	18±0.36
Univ. of Sask. (this work)	ICP-MS	0.64±0.04	0.74±0.08		15.7±0.51
MEDIAN of analysed data		**0.60**	**0.78**	**[0.03]**	**18**

All data in ppm.

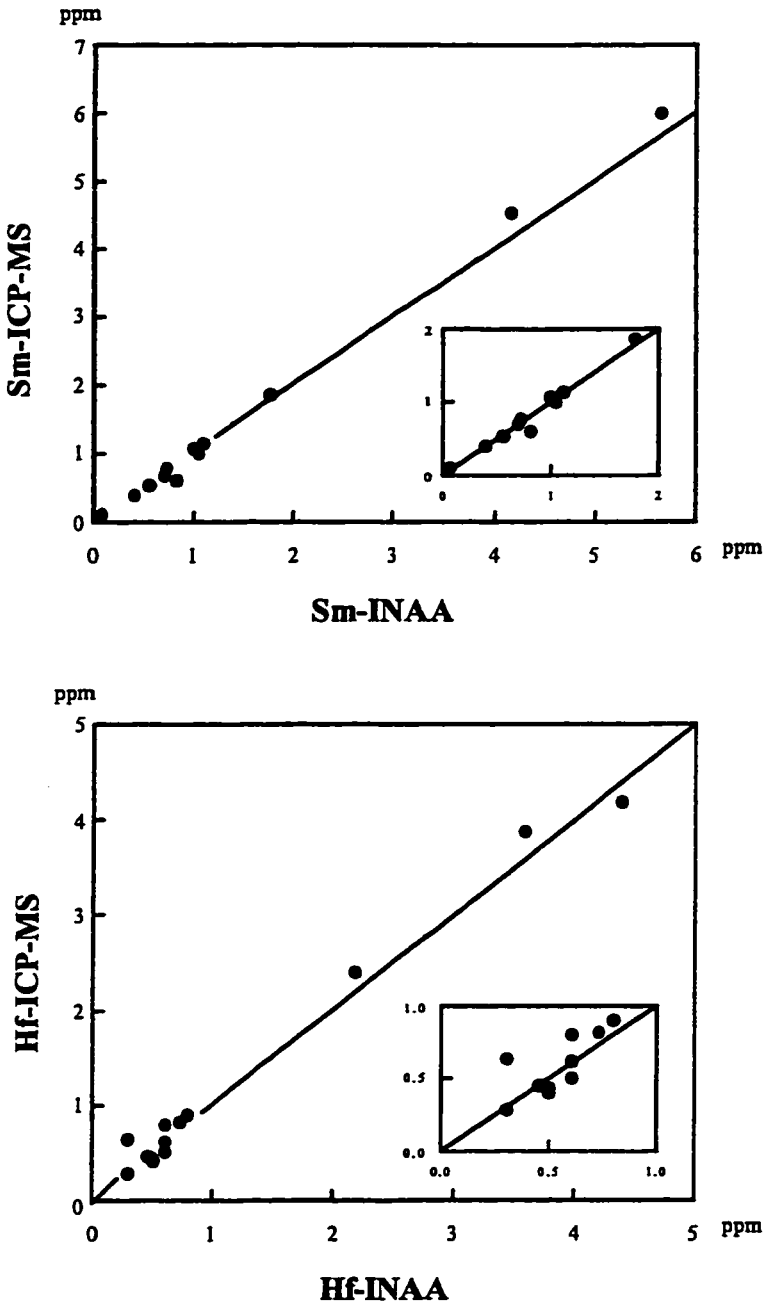

Figure 3-2. Comparison of Sm and Hf determined by ICP-MS and INAA (U. of Michigan) for BIR-1, MRG-1, BHVO-1 and 9 unknown komatiites

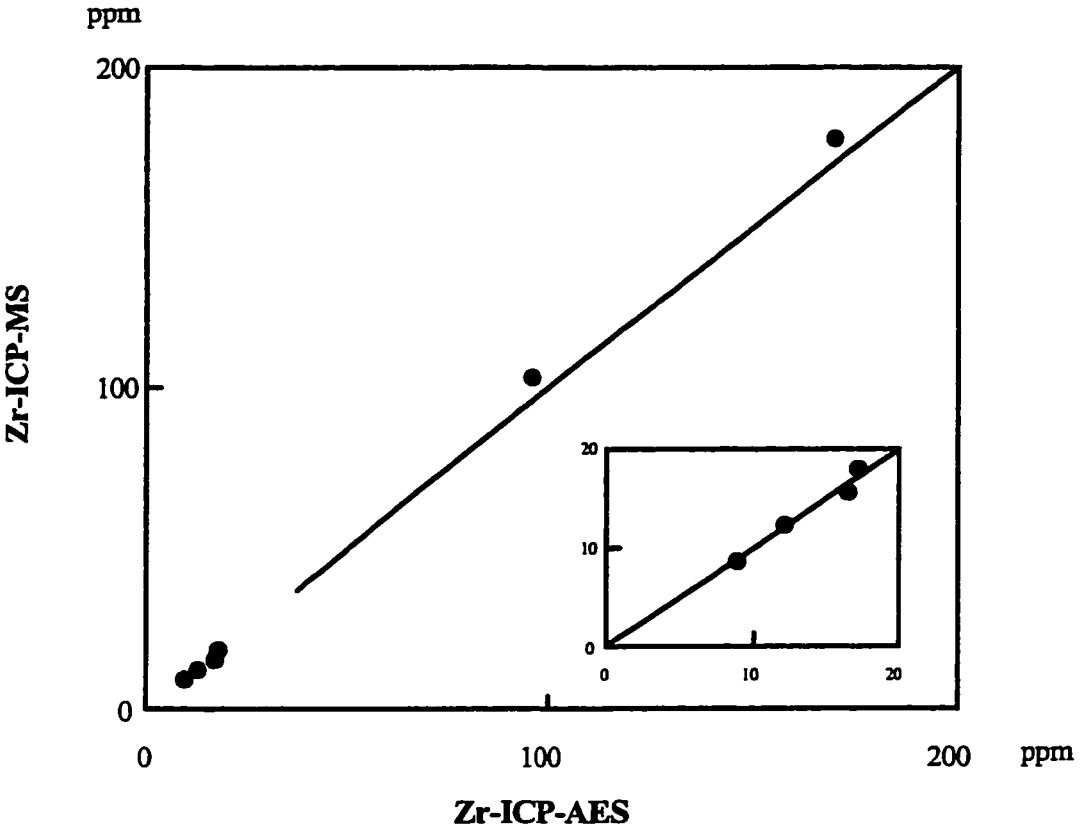

Figure 3-3. Comparison of Zr determined by ICP-MS and ICP-AES for BIR-1, MRG-1, BHVO-1 and 3 unknown komatiites.

Table 3-3. Results of experiment to test possible isobaric interferences [a]

elements	mass	Stda	Stdb	flush(1 N HNO3)	Procedural blank	synthetic rock solution
Zr	90	170698 [b]	1482	450	21	168
Nb	93	241	121	87	41	74
Hf	177	485	26941	24	19	18
Ta	181	861	36	45	24	34
Th	232	112736	143227	201	17	36

a Samples were analyzed in the sequence from left to rght;

b Counts/s; values are the average of three counts/mass.

HFSEs in rocks (Hall and Pelchat, 1990b; Hall and Plant, 1990; Potts et al., 1990; Longerich, 1993, personal communication). These problems include incomplete dissolution of refractory minerals, formation of insoluble Zr, Hf fluorides during digestion (Boer et al., 1993), and other instabilities of HFSEs in solution. Singly or collectively, these effects yield erratically low results over the long term. Memory effects and/or unresolved isobaric interferences may yield aberrantly high values.

3-4-1. Incomplete digestion and solution instability

Incomplete digestion of refractory minerals and solution instability is not considered to be a problem in this study, given the compliance of the results for REEs and HFSEs with compiled values for these elements (Potts et al., 1992), and the agreement with results based on techniques that do not require dissolution (e. g. REEs and Hf by INAA; Xie et al., 1993). Moreover, chondrite normalized REE patterns of the mafic rock reference materials are smooth and flat. Most refractory minerals, such as zircon or baddeleyite, are characterized by strongly fractionated REEs, such that their incomplete digestion would be reflected in sloping whole rock REE patterns.

As a further test of HFSE stability in solution, compositionally uniform glasses were made from whole rock powders of reference materials and unknowns at the University of Saskatchewan, using a Mo-strip heater and 275 KPa Ar atmosphere. No flux was employed. Results for REEs and HFSEs in BIR-1 and other reference materials are in agreement with solution mode ICP-MS and recommended values for these elements (Table 3-1; Fedorowich et al., 1993). Thus these effects are considered to be insignificant.

3-4-2. Systematic bias towards high values at low-levels

Jochum et al. (1990) noted that data for Nb, Zr and Hf in the literature, by various techniques, were systematically biased to higher values compared with data by ID-SSMS for low abundance samples (Jochum et al., 1990b). To address this possibility for ICP-MS, a dilution experiment was conducted. Using BCR-1, MRG-1, BHVO-1 and BIR-1, a series of dilutions were made to give the concentrations of Nb, Zr, Hf, Ta, Dy, Sm, Yb between ≤ 10 ng/L to 100 ng/L.

Results of the experiment are presented in Figure 3-4. For Nb, Ta, Dy and Sm, systematic bias was not observed when samples were diluted 100 times, equivalent to a few ppb to 10 ppb in rock samples; a bias was evident only after 500 times dilution, equivalent to concentrations much less than in low-level rocks. A bias was present for Th after 10 times dilution of MRG-1, equivalent to ~ 0.08 ppm. For Zr and Hf, a systematic bias towards high values occurred after MRG-1 was diluted 100 and 25 times, respectively, equivalent to 1 ppm Zr and 0.1 ppm Hf in rock samples. Corresponding figures for Zr and Hf in BIR-1 are biased at 25 and 10 times dilution, again equivalent to ~ 1 ppm Zr and 0.1 ppm Hf in rock samples. The bias at high dilutions may be due to the increased uncertainty in the measurement, owing to counting statistics, and/or memory. Collectively, the results imply that there is no systematic bias towards high values by ICP-MS for REEs, Zr, Nb, Hf and Ta at the concentration levels present in BIR-1 .

3-4-3. Isobaric interferences

Isobaric interferences are one of the possible causes of a systematic bias towards high values. Among the elements analyzed, the most serious isobaric interferences are REE oxide

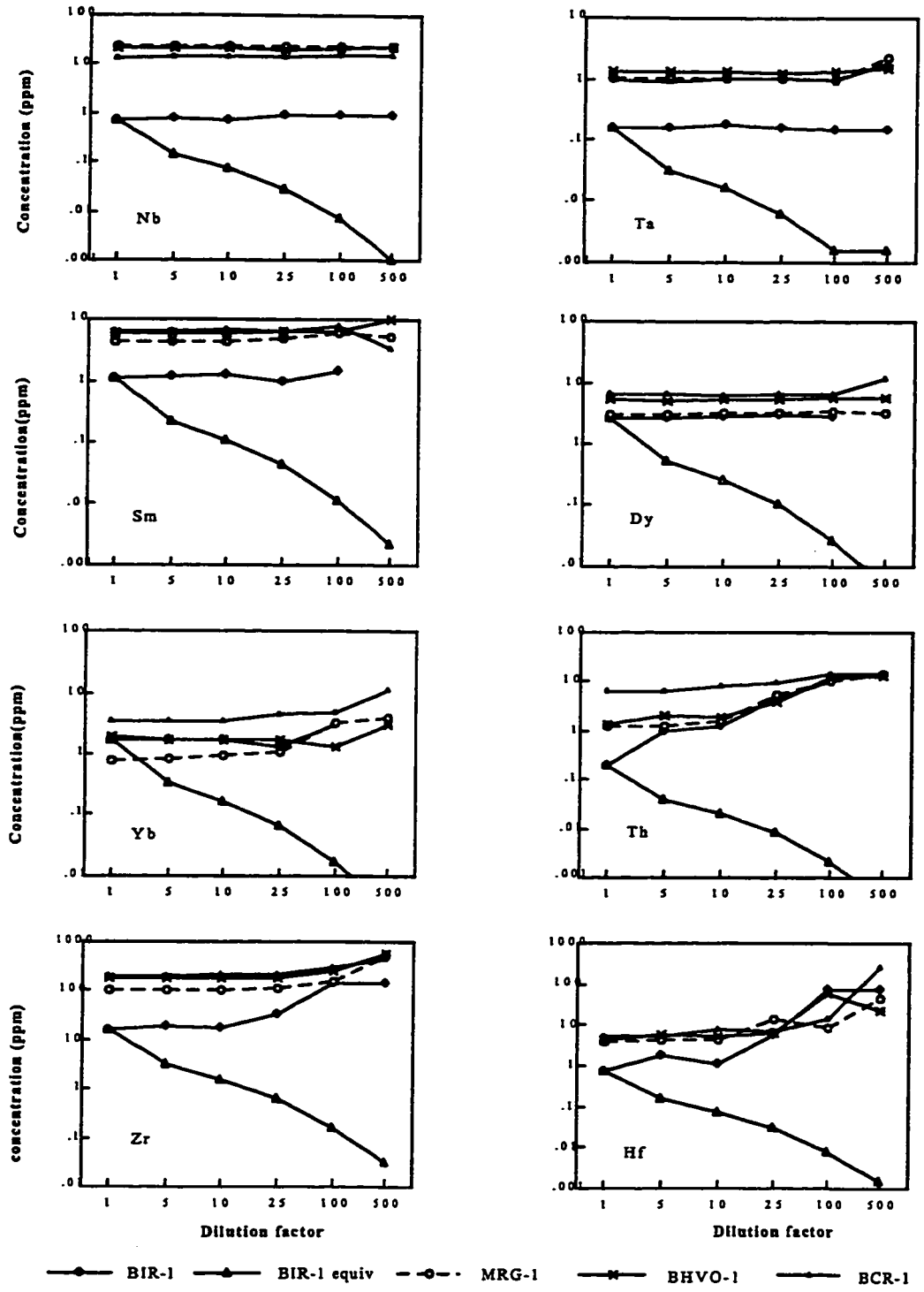

Figure 3-4. Results of dilution experiments. Measured concentrations are multiplied by the dilution factor. BIR-1 equiv expresses the concentration in the rock taking into account the dilution factor. The specified international reference materials were run at the standard dilution of 100 mg rock powder in 1000 g 0.2 HNO_3 (dilution 1), and at further dilutions 5 and up to 500 of the standard dilution. Bias to high values, possibly due to counting statistics and/or memory, are only apparent at concentrations of elements at levels much below their concentrations in BIR-1 or komatiites.

species, e.g. $^{141}Pr^{16}O$ on ^{157}Gd and $^{161}Dy^{16}O$ on ^{177}Hf etc. (Lichte et al., 1987; Jenner et al., 1990). Thus, oxide correction factors were determined using two external standards (stdA and stdB), and these were factored into the data reduction programme as described by Jenner et al. (1990).

The formation of oxide polyatomic species is dependent on instrumental operating conditions and analyte composition (Lichte et al., 1987; Jenner et al., 1990). An experiment was designed to test for unresolved polyatomic interferences that might cause anomalously high measured values of Nb, Zr and Hf, under the operating conditions for ICP-MS at the University of Saskatchewan lab. For example, $^{53}Cr + ^{40}Ar$ and $^{89}Y + ^{4}He$ could potentially interfere on ^{93}Nb, but the magnitude of these isobaric interferences had not formerly been evaluated. Pure elemental standard solutions were employed to make up a synthetic rock solution with all major and trace elements in the concentration range of BIR-1, except Nb, Zr, Hf, Ta and Th. Therefore, any signal detected at masses 90, 93, 177, 181 and 232 in this synthetic sample should arise from polyatomic species, mainly oxide ions such as $^{161}Dy^{16}O$.

Results of the experiment are presented in Table 3-3. Standard A (stdA) contains 192 ppb Zr and 109 ppb Th, whereas standard B (stdB) contains 98 ppb Hf and 141 ppb Th. The signals at mass 90, 93, 177 and 232 in the synthetic sample are close to those in the procedural blank. This indicates that isobaric interferences from polyatomic species are not significant for Nb, Zr and Hf under the ICP-MS operating conditions in the University of Saskatchewan lab.

3-4-4. Memory effects

One of the potential difficulties for analyzing HFSEs by ICP-MS is memory effects,

stemming from deposition of analyte on the sampler and skimmer. The memory effect is concentration dependant. In the routine analytical protocol, approximately 200 ppb Zr and 100 ppb Hf were used in standards for external calibration. Niobium and Ta were not used for external calibration, because of the experience of memory problems for these elements. Rather, surrogate calibration is employed (Jenner et al., 1990). Concentrations of Zr and Hf in external standards (200 ppb) are relatively high compared to their levels in analyte solutions of BIR-1 (~ 15 and 0.6 ppb respectively), and other low level samples. This factor may impose memory effects on unknowns run immediately after external standards.

Experiments to test possible memory effects from external standards were conducted. Results of the experiments are presented in Figure 3-5. Samples were analyzed in the following sequence; stdA; stdB; flush (1 N HNO_3); reagent blank (0.2 N HNO_3); BIR-1-1 unspiked; BIR-1-1 spiked; .....; BIR-1-10 unspiked; BIR-1-10 spiked, stdA, stdB. Niobium and Ta do not show memory effects, as they are not used in external standards. Zr and Hf show a memory effect, although not as serious for Zr as for Hf. Memory signal enhancement, however, affects only the first sample after the external standards. Remaining unknowns give results within error of the long-term averages (e.g. Zr: 15.4±0.3 ppm and Hf: 0.62±0.01 ppm; Table 3-1). It appears that the flush and reagent blank employed prior to the first unknown did not entirely eliminate memory for Zr and Hf arising from external standards, whereas an unknown rock solution did eliminate memory effects. This is attributed to chemical differences between rock solutions and pure acid solutions, possiblv from trace F in the former. Based on this observation, a BIR-1 solution diluted 1000 times was applied as a flush every time after external standards were run. This rock solution effectively flushes off memory arrising from external standards, yet will not impose serious memory on

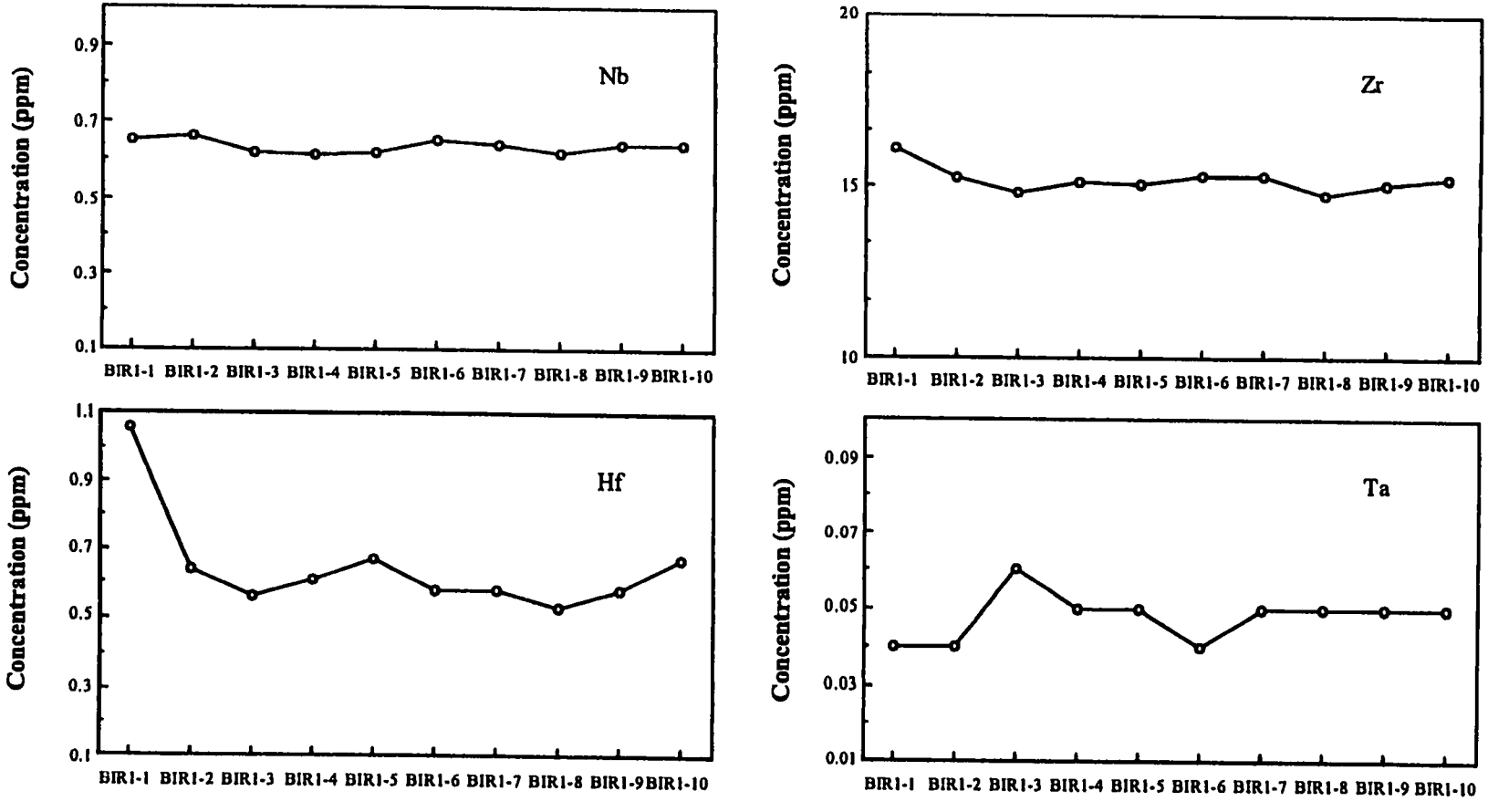

Figure 3-5. Memory effects on Nb, Zr, Hf and Ta from external standards and their decay during ICP-MS analysis. Samples were analyzed in the following sequence: StdA, StdB, flush, acid blank, BIR-1-1 unspiked, and BIR-1-1 spiked up to BIR-1-10 unspiked and BIR-1-10 spiked.

following samples, as Zr and Hf in the BIR-1 diluted solution are low (~ 15 ppb and 0.6 ppb respectively), compared with external standards (~200 ppb).

3-4-5. Inhomogeneity in BIR-1

Jochum et al. (1990) have pointed out possible compositional inhomogeneity amongst different aliquots of BIR-1 (e.g. for Zr). At the U. of S., the long term average for all elements in BIR-1 is from analysis of powders from two different bottles, yet the results of the analyses do not indicate any inhomogeneity between these batches. Moreover, three independent ICP-MS labs., using different instruments and separate aliquots of BIR-1, all yield the same results within error for REEs, Zr and Hf in BIR-1 (Table 3-2).

It is possible that inhomogeneities in separate batches of BIR-1 could stem from non-uniform distribution of plagioclase in the original rock, that arose in turn from plagioclase cumulus. If this was the case, then heterogeneous distribution of plagioclase would be reflected in variations of Sr and Eu between aliquots of BIR-1, but this is not observed. Similarly, an anomalously high proportion of plagioclase in a batch of BIR-1 could act to dilute the HFSE relative to other batches, but this would commensurately dilute the HREE, Y etc. -- an affect that is also not observed.

In mafic rocks, Zr and Hf are likely to be sited in baddeleyite, whereas Nb substitutes in Ti-bearing phases such as titanite or rutile. However, BIR-1 is unlikely to have such accessary phases, as it is a basalt. Furthermore, inhomogeneous distribution of baddeleyite would show up in differences of REE patterns between batches, yet all labs report similar REE contents for BIR-1. Finally, it is noted that the partitioning coefficients (Ds) for REEs and HFSEs between pyroxene and melt are all low (Kennedy et al., 1993), such that erratic

distribution of pyroxene should not result in differences of REEs and HFSEs between aliquots of BIR-1.

3-5. Conclusions

New data for 28 elements, including REEs, Zr, Nb, and Hf, in BIR-1 have been obtained by ICP-MS. This reference material is useful for conducting analysis of samples such as peridotites, komatiites and depleted basalts, where REEs and HFSEs are present at low concentrations. Having quantitatively evaluated solution stability, isobaric interferences, and memory effects for REEs and HFSEs by ICP-MS, studies to determine Zr and Hf by ID-ICP-MS in BIR-1 and low abundance unknowns, with a view to refining characterization of HFSE/REE fractionations in komatiites and basalts, are reported in Chapter 4. Further work and lower detection limits are needed to solve possible interferences on Th and Ta at low concentrations.

CHAPTER 4 ISOTOPE DILUTION ANALYSIS OF ZR AND HF IN LOW ABUNDANCE REFERENCE MATERIALS AND KOMATIITES

4-1. Introduction

Previous studies have addressed the special difficulties and corresponding analytical strategies for determination of HFSEs in geological samples (Hall and Pelchat, 1990b; Xie et al., 1994), as discussed in Chapter 3. Most ICP-MS data to date were obtained using external calibration, which may not achieve precisions as good as that obtainable by isotope dilution (ID). Thus, it is important to check ICP-MS data based on external calibration with isotope dilution, particularly for low abundance samples.

The development of ICP-MS has documented its suitability for relatively precise trace element measurement using isotope dilution (Heuzen et al., 1989; Longerich, 1989), albeit at precisions inferior to that attained with thermal ionization magnetic sector instruments (TIMS). The advantages of ID-ICP-MS are:

(1) The spike is added before sample decomposition, such that isotope equilibration between sample and spike is achieved;

(2) ID-ICP-MS is more tolerant of solutions with appreciable total dissolved solid (TDS) concentrations (> 1% TDS) than external calibration. Accordingly, lower dilution factors can be applied in ID analysis in order to obtain maximum signal intensities in analyte solutions, which is crucial for low abundance samples;

(3) 500 mg aliquots of sample powders are digested, thus ID-ICP-MS is less subject to

possible effects of sample heterogeneity than ID-SSMS, for which 50 mg of powders is mixed with 50 mg of graphite, and only ≤ 1% of the total is sparked and analyzed.

To obtain the desired precision in ID-ICP-MS analysis, a systematic evaluation of the instrumental operating parameters (IOPs) is required in order to sufficiently understand their effects on the measurement of isotope ratios (Longerich et al., 1987a; Ting and Janghorbani, 1988). For example, previous studies have explored the optimized IOPs for enhanced precision in determination of Pb isotopes in geological materials (Longerich et al., 1987a).

In this chapter, an evaluation of selected IOPs for improving the precision in measurement of the stable isotopes of Zr and Hf is first presented. Then, the results of ID-ICP-MS analyses for Zr and Hf in low level international reference materials and samples, acquired under optimum IOPs, are discussed. The objectives of this study were (1) to evaluate the data obtained by routine external calibration ICP-MS; (2) to provide more precise data for low abundance international reference materials, especially for BIR-1, as Zr and Hf in most komatiites, other peridotites, and picrites, are of similar abundance levels as in BIR-1; and (3) to investigate factors which may affect ID-ICP-MS analysis for measurement of other elements with low concentrations, such as Th and Ta in these reference materials, or unknowns. This chapter has been expanded, and reformatted from, two papers by the author (Xie and Kerrich, 1995a, b).

4-2. Optimization of IOPs

4-2-1. Experiments

a. Instrumentation: The ICP-MS employed in this study was an Elan Model 5000 system

(Perkin-Elmer-Sciex, Rexdale, Ontario, Canada), operated under conditions as reported in Chapter 3, with exception as described below. The argon coolant flow-rate 15 L/ min. Auxiliary flow-rate was adjusted at 0.8 L/min. Nebulizer gas (Ar) flow was controlled using a mass flow controller, and was adjusted at 0.8 L/min for isotope ratio measurements, but was varied to investigate oxide formation effects. Plasma power was a variable parameter. Ion-lens settings were varied. Liquid analyte was aspirated into the argon plasma using an autosampler (Gilson, 212B Liquid Handler) and a cross flow nebulizer, and sample flow-rates were controlled at 1 ml/min with a peristaltic pump (Gilson, Middleton, WI, USA).

b. Reagents: Pure elemental standard solutions (from Inorganic Ventures Inc., Lakewood, NJ, USA) were used to prepare the analyte solutions used for all experiments in this investigation. Standard solutions of Zr and Hf were diluted to various concentrations with 0.2 M nitric acid (prepared from triply distilled concentrated HNO_3), and de-ionized distilled water (obtained from a Barnstead NANO pure II system; Sybron-Barnstead, Boston, MA, USA).

Enriched isotope spike materials ^{91}Zr and ^{179}Hf (oxide) were purchased from Oak Ridge National Laboratory. The ZrO_2 and HfO_2 spikes were accurately weighted (±0.00001 g) and dissolved in 25 M HF, and fumed with a few drops of concentrated $HClO_4$. After evaporation of HF, the solution was diluted with 2.5 M HCl. The concentrations of spikes in solution were calculated from accurately weighted quantities of spike materials and reagents. No further calibration was performed. The precision of the spike concentrations was estimated to be better than 0.01%. All chemical preparations were conducted under clean-lab conditions.

c. Data acquisition: The isotopes of interest are ^{90}Zr, ^{91}Zr, ^{92}Zr, ^{94}Zr, ^{177}Hf, ^{178}Hf, ^{179}Hf, and ^{180}Hf. Data acquisition was in the peak-hopping isotope ratio mode, with 1 point per mass peak. The dwell time was varied. Isotope ratios are the mean of a set of 80 intensity ratios. The whole procedure was controlled via Elan software provided by the manufacturer. All isotope ratios presented are background corrected using counting rates on the reagent blank (0.2 M HNO_3).

In evaluating the overall performance of isotope ratio measurement by ICP-MS, two parameters are of fundamental concern: precision of isotope ratios measured and their deviation from the "true values". The precision of measured isotope ratios is expressed in relative standard deviation (RSD%) of 80 intensity ratios, whereas the deviation from the true values is calculated using

$$\Delta\% = (\text{measured ratio} - \text{natural ratio})/\text{natural ratio} * 100 \qquad (4\text{-}1)$$

The natural stable isotope ratios of Zr and Hf are from De Laeter et al. (1991). The deviation of measured isotope ratios from the true values stems from mass bias in the mass spectrometer. For ICP-MS, mass bias is the composite of several different processes, including mass fractionation in the ion lens, and mass discrimination in the quadrupole mass filter, and may be positive or negative (Russ III, 1989; Jarvis et al., 1992). For the Elan 5000 instrument and specified operating conditions, preferential reduction in response of light masses was always observed.

4-2-2. Variations of RSD% and Δ% with RF power

Previous studies have shown the effects of RF power on ion signal, and hence measured isotope ratios in ICP-MS (Longerich et al., 1987a; Ting and Janghorbani, 1988).

Solutions with 0.1 ppm Zr and Hf, prepared from pure elemental solution, were used to investigate the effects of RF power in this study. The results are shown in Figure 4-1.

The precision of measured isotope ratios are between 0.2 to 0.6 RSD%. There is no apparent increase or decrease of RSD% with respect to RF power changes (Figure 4-1a, 4-1b). Mass bias was observed for all measured isotope ratios, with consistent preferential loss of counts for light isotopes of a given element (Figure 4-1c, 4-1d). Similarly, there is no obvious correlation between Δ% and RF power, especially for ratios of neighbouring masses (i.e. $^{91}Zr/^{90}Zr$ and $^{179}Hf/^{180}Hf$). Accordingly, 1000 watts RF power was chosen in subsequent experiments.

4-2-3. Variations of RSD% and Δ% with dwell time

Dwell time (DT) is another important IOP which may affect the precision and accuracy of isotope ratio measurements (Ting and Janghorbani, 1988; Begley and Sharp, 1994). The same pure elemental solutions with 0.1 ppm Zr and Hf were employed in this experiment. Dwell time varied from 5 to 60 ms. The counting statistics remained essentially constant, as the integration time per isotope was held constant (Figure 4-2). It can be seen that RSD% tends to decrease with increasing DT (Figure 4-2a, 4-2b). At DT = 30 milliseconds (ms), RSD% of measured isotope ratios are between 0.2 to 0.6%, which is the overall precision for Zr and Hf isotope ratio measurement for the U. of S. instrument. With further increase of DT, the precision of measurement is apparently limited by counting statistics. Similarly, the Δ% of isotope ratio measurement was improved with increasing DT, especially from 5 to 30 ms, with the degree of mass bias decreasing significantly at larger DT (Figure 4-2c, 4-2d). Considering the overall measurement time and reasonable sample

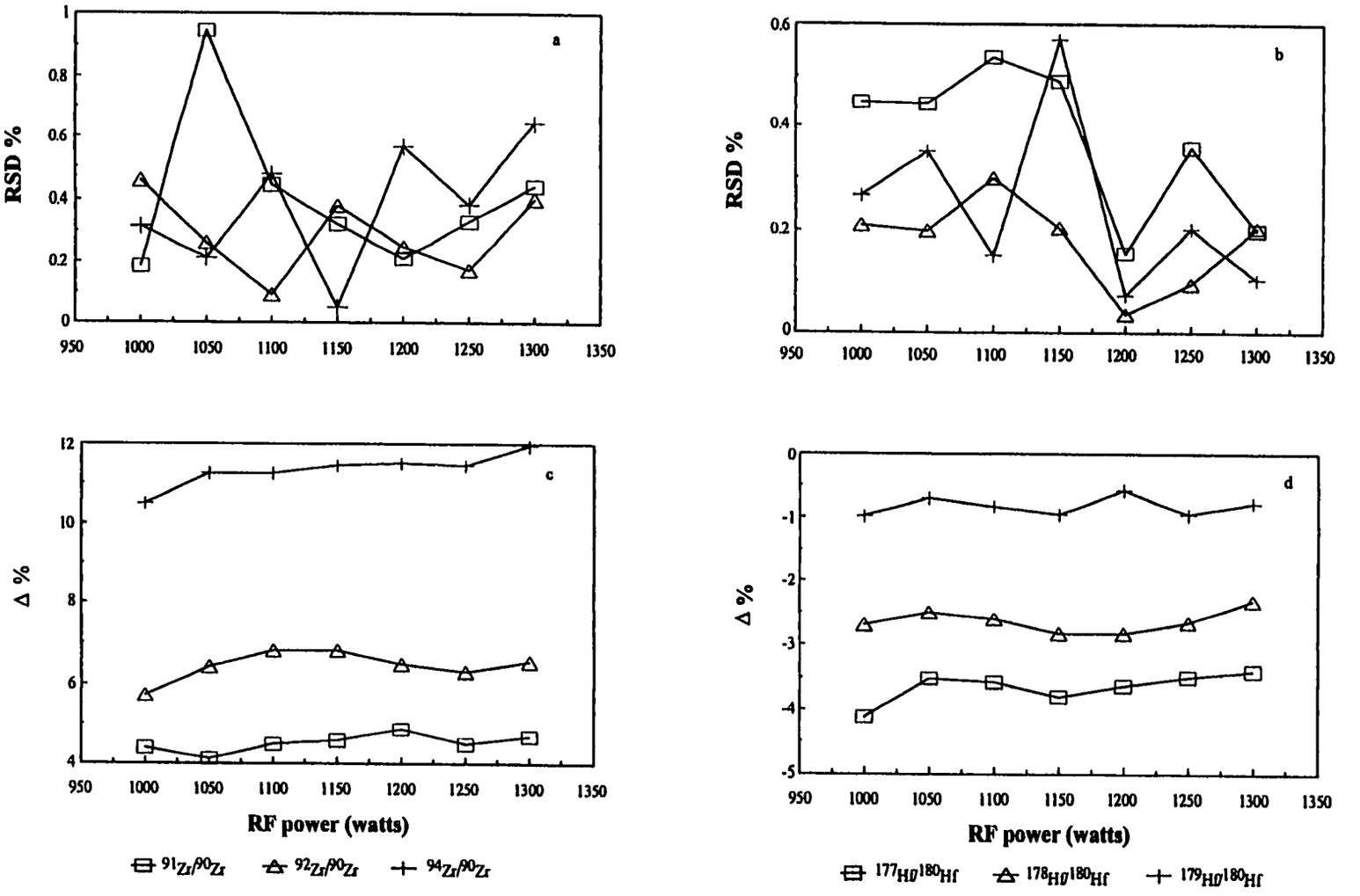

Figure 4-1. RSD% and Δ% versus RF power. Measured in solutions of 0.1 ppm pure Zr and Hf.

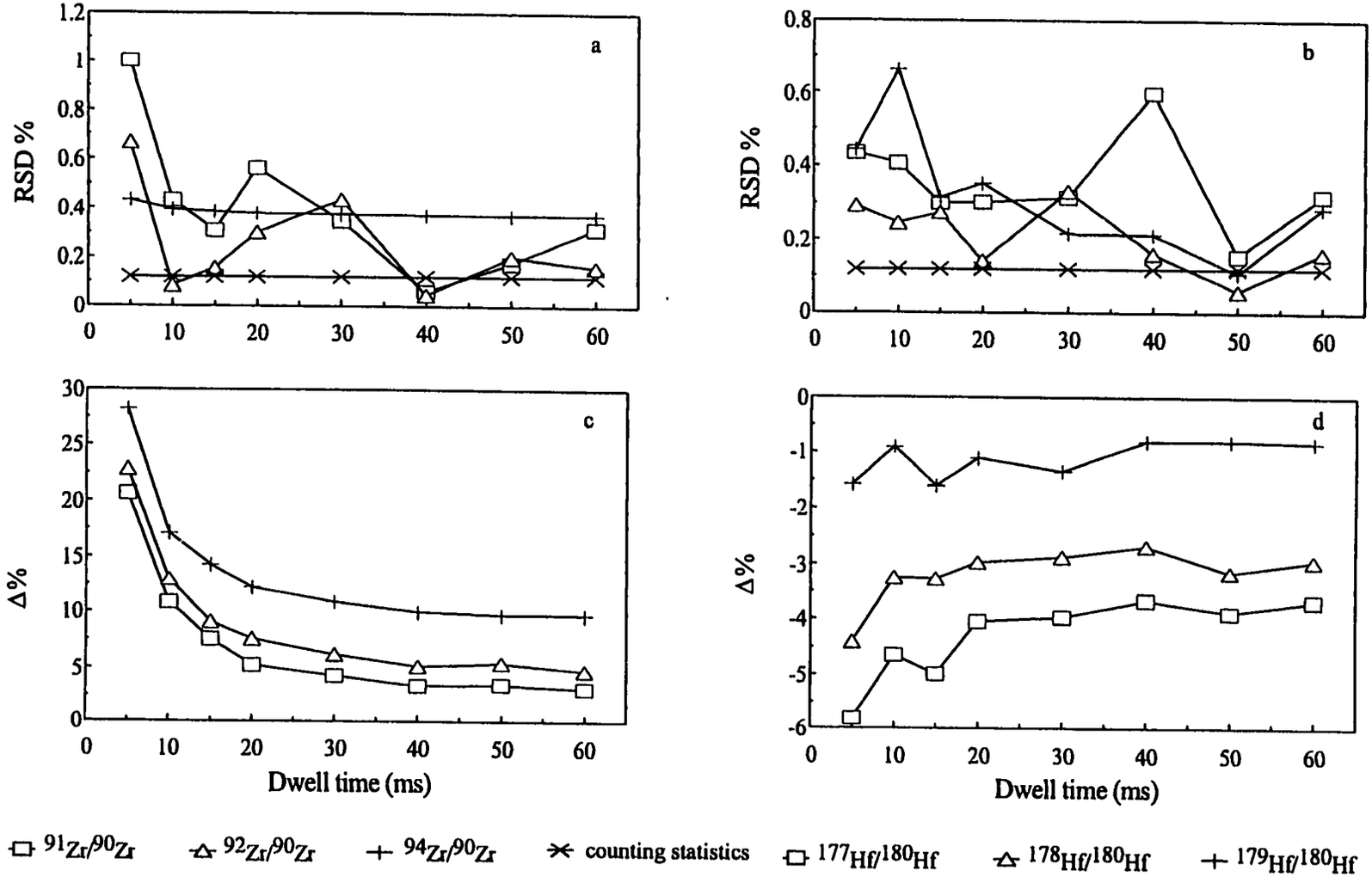

Figure 4-2. RSD% and Δ% versus dwell time. Measured in solutions of 0.1 ppm pure Zr and Hf.

consumption of 5 ml for ~ 5 minutes total sample aspiration time, 30 ms was selected as the optimum DT for Zr and Hf isotope ratio measurement.

4-2-4. Effects of B lens settings on Δ%

Longerich et al. (1987) found that significant variations in measured isotope ratios occurred as a function of the B lens settings. Similar variations for Zr and Hf isotope ratios were also observed in this study. Figure 4-3 presents the deviation of measured Zr and Hf isotope ratios from their true values, with respect to varying B lens setting. The degree of mass bias is not unidirectionally correlated with B lens settings. Increasing the B lens setting from 40 to 80 digipots, the degree of mass bias first decreases, then increases after a minimum at 60 digipots. This may due to the fact that ions of different m/z (m=mass; z=charge) have different kinetic energies and thus have different paths through the ion lens. For a given element, increasing B lens voltage enhances the sensitivity of heavy isotopes (Longerich et al., 1987a). Accordingly, it is essential to find an optimum setting to minimize mass bias. For Zr and Hf isotope measurements, a B lens setting of 60 digipots gave the least mass bias for both Zr and Hf isotope ratios, results similar to those for Pb isotope ratios observed by Longerich et al. (1987) on a different instrument. Thus, the optimum B lens setting for Zr and Hf isotope ratio measurement is 60 digipots.

4-2-5. Concentration dependence of measured isotope ratios

Measured isotope ratios by ICP-MS may be concentration dependent, due to the limitation of counting statistics for low-abundance isotopes, and background noise from different matrices (Janghorbani and Ting, 1989). Variations in isotope ratio may also occur

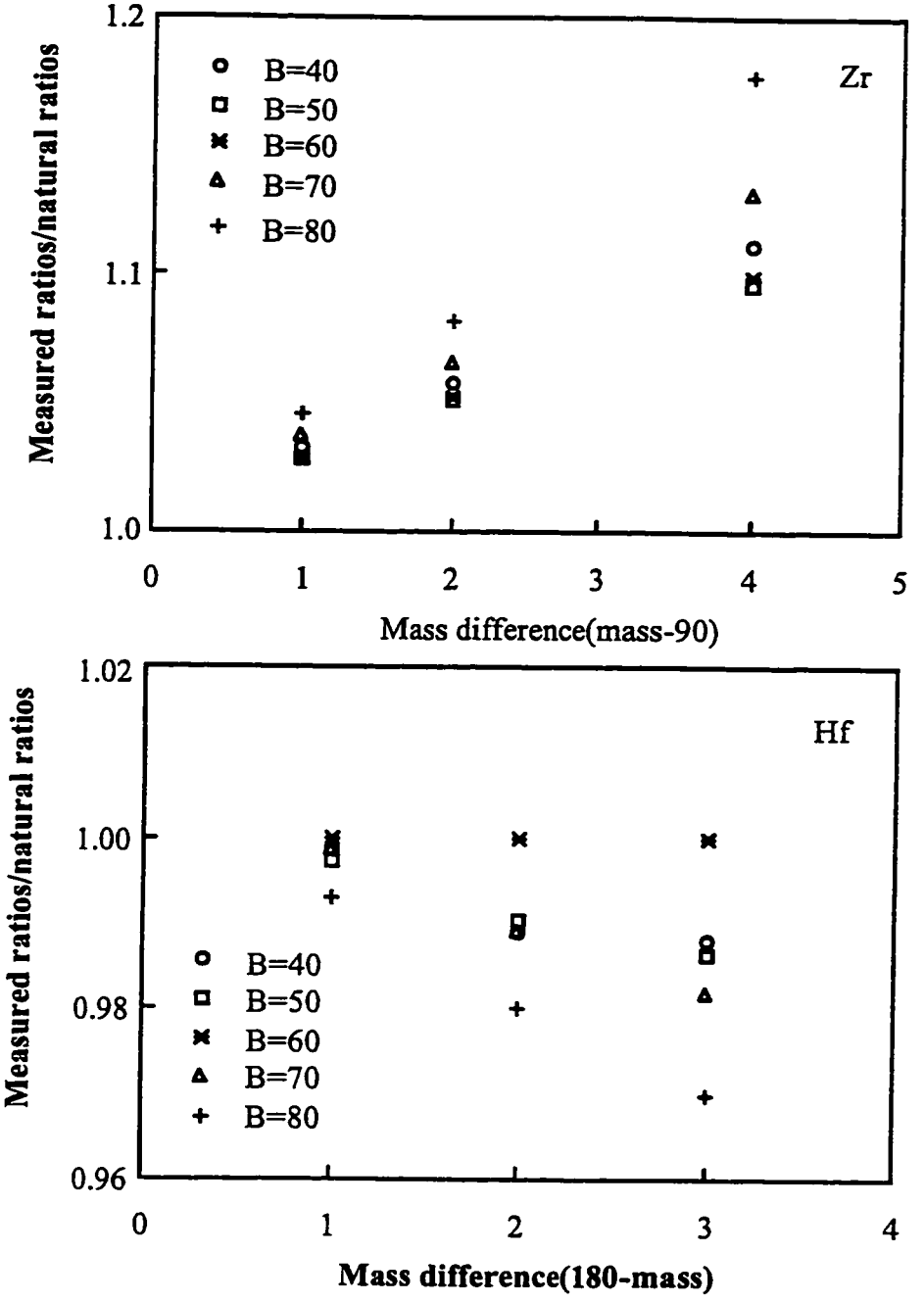

Figure 4-3. Mass bias of measured Zr and Hf isotope ratios at different B lens settings. Measured in a solution of 0.1 ppm pure Zr and Hf. The unit of B lens setting is digipots.

at high analyte concentrations, which may be due to non-linearity in the detector at high count rates or due to inaccuracies in dead-time corrections (Russ III and Bazan, 1987). An example of this effect has been reported by Janghorbani and Ting (1989). They found that a systematic variation of measured $^{6}Li/^{7}Li$ ratios occurred at Li concentrations < 100 ng g^{-1}. However, at analyte concentrations of 100 to 1000 ng g^{-1}, measured $^{6}Li/^{7}Li$ ratios were consistent within error.

Only $^{91}Zr/^{90}Zr$ and $^{179}Hf/^{178}Hf$ ratios were measured in this experiment, in relation to possible use for future isotope dilution analysis. Actual rock sample solutions with different Zr and Hf concentrations were measured, in order to test the effects of concentration dependence and matrices. The results are presented in Table 4-1. The concentration range selected represents typical Zr and Hf abundances for mafic and ultramafic rocks.

There are no apparent systematic variations of RSD% or Δ% with respect to concentration (Figure 4-4). The intersample variation of measured $^{91}Zr/^{90}Zr$ and $^{179}Hf/^{178}Hf$ is, however, larger than intrasample variation (Table 4-1). An F-test conducted to compare inter- and intra-sample precision, with 95% confidence, suggests that the intersample precision is significantly better than that of intrasample. This may due to the different sample matrices. Accordingly, using an unspiked sample to correct mass bias for a spiked equivalent may improve the precision of ID-ICP-MS analysis.

4-2-6. Interferences by polyatomic species

When measuring Zr and Hf isotopes by ICP-MS without pre-separation of analyte elements from matrices, potential interferences of isobaric and polyatomic species must be taken into account in order to obtain optimal precision and accuracy. Based on the

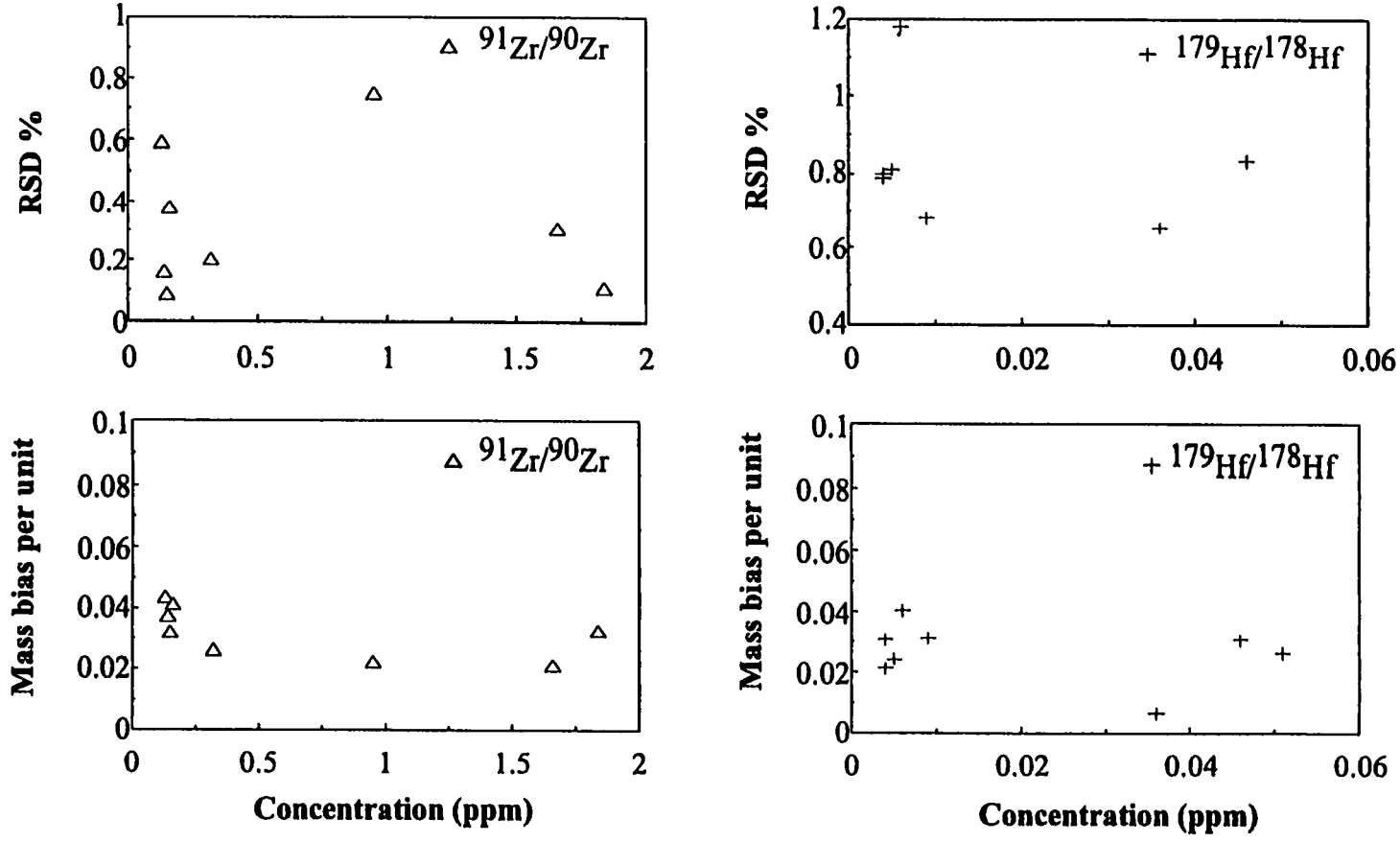

Figure 4-4. RSD% and mass bias of measured $^{91}Zr/^{90}Zr$ and $^{179}Hf/^{178}Hf$ ratios versus concentrations. The concentration range represents the abundance of Zr and Hf characteristic of mafic and ultramafic rocks, after dilution into solution for ICP-MS analysis.

Table 4-1. RSD% and mass bias of measured Zr and Hf isotope ratios in solutions with specified Zr and Hf concentrations

C_{Zr} [a]	$^{91}Zr/^{90}Zr$	RSD%	bias per mass unit	C_{Hf} [a]	$^{179}Hf/^{178}Hf$	RSD%	bias per mass unit
0.08	0.2289	0.55	0.050	0.003	0.5177	0.57	0.037
0.13	0.2276	0.59	0.044	0.004	0.5099	0.8	0.021
0.14	0.2262	0.16	0.038	0.006	0.5194	1.18	0.041
0.15	0.2250	0.08	0.032	0.004	0.5146	0.79	0.031
0.16	0.2270	0.38	0.041	0.005	0.5114	0.81	0.024
0.17	0.2258	0.38	0.036	0.006	0.5147	2.12	0.031
0.32	0.2237	0.20	0.026	0.009	0.5148	0.68	0.031
0.95	0.2229	0.75	0.022	0.036	0.5026	0.65	0.007
1.66	0.2227	0.30	0.021	0.046	0.5146	0.83	0.031
1.84	0.2251	0.10	0.033	0.051	0.5124	1.90	0.027
RSD%	0.9			RSD%	0.9		
natural ratio:[b]	0.2180 ± 0.006			natural ratio:[b]	0.4998 ± 0.006		

[a] Concentration in final analyte solution; ppm.

[b] From De Laeter et al., 1991.

Table 4-2. Instrumental operating parameters(IOP's) for isotope ratio analysis by ICP-MS

ICP		
	RF power	1000 watts
	Ar coolant flow rate	10 L/min
	auxiliary flow rate	0.8 L/min
	nebulizer flow rate	0.8 L/min
	sample uptake rate	1 ml/min
Mass Spectrometer		
	sampler (platinum tipped nickel)	1.1 mm orifice
	skimmer (platinum tipped nickel)	0.89 mm orifice
	resolution	normal
Lens Setting		
	photon stop (S2)	45 digipots
	Bessel box barrel (B)	60
	einzel lenses land 3 (E1)	25
	Bessel box end lenses (P)	45
Data Acquisition		
	dwell time	30 ms
	scanning mode	peak hop
	point/per peak	1 point

experimental results presented in previous sections, the optimal isotope pairs for Zr and Hf ID analysis in rocks would be $^{91}Zr/^{90}Zr$ and $^{179}Hf/^{178}Hf$. These isotopes are free of isobaric interferences. $^{179}Hf/^{178}Hf$, however, may suffer potential interferences from polyatomic species, i.e. $^{138}Ba^{40}Ar$ and $^{139}La^{40}Ar$. Similarly, the REE oxides $^{162}Dy^{16}O$ and $^{163}Dy^{16}O$ may interfere on ^{178}Hf and ^{179}Hf. $^{146}Nd^{16}O$ and $^{147}Sm^{16}O$ interfere with ^{162}Dy and ^{163}Dy.

Formation of polyatomic species with Ar is not a problem with the Elan 5000 instrument and operating conditions, and is normally at background counts of < 30 counts/s, excepting $^{40}Ar^{16}O$ on ^{56}Fe, and the Ar diamer on Se. The extent of REE oxidation, however, is a function of IOPs, especially the nebulizer gas flow rate (Horlick et al., 1985; Lichte et al., 1987; Longerich et al., 1987b). Figure 4-5 presents the results of an experiment testing the degree of oxide formation for Nd, Sm and Dy as a function of nebulizer gas flow rate. The intensity of Nd, Sm and Dy are highest, but M^+O/M^+ lowest, at a nebulizer flow rate of 0.8 l min^{-1} (Figure 4-5a, 4-5b). M O/M does not change with respect to concentrations of the analyte isotope (Figure 4-6), and DyO/Dy is constant between 0.3 to 0.5%. Without correction for oxides, the effects of $^{162}Dy^{16}O$ and $^{163}Dy^{16}O$ polyatomic interferences translate into uncertainties in measured $^{179}Hf/^{178}Hf$ ratios of about 0.02%, well within the error. Thus, it is not necessary to correct for Dy oxide, and more time can be devoted to measuring $^{179}Hf/^{178}Hf$ with reasonable counting times and sample consumption, without laborious chromatographic separations.

4-2-7. Long term stability of measured isotope ratios

The stability of measured isotope ratios is an important issue in ID analysis, when mass bias correction is necessary. Previous studies have shown that whereas ion beam

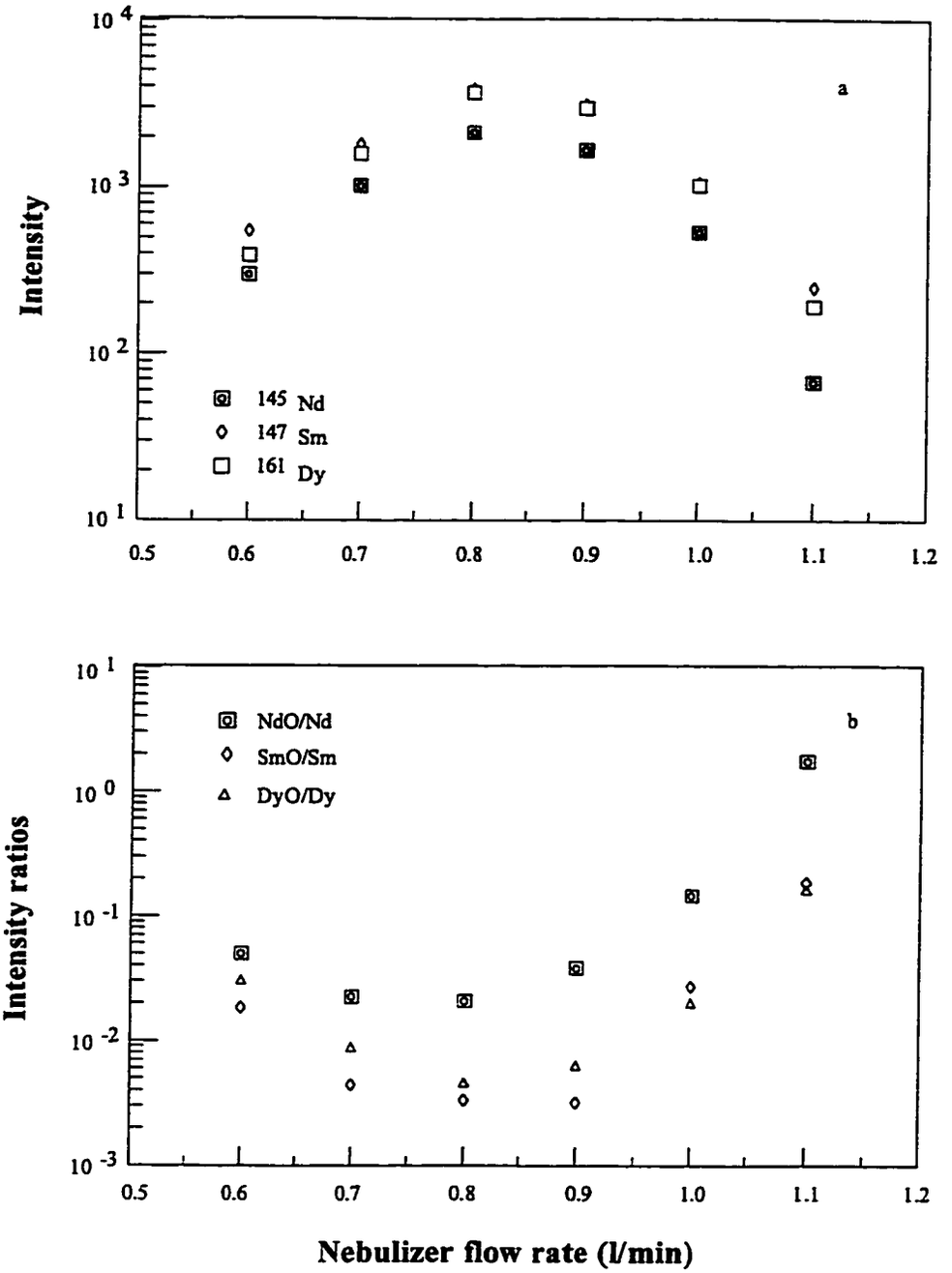

Figure 4-5. Relations between nebulizer flow rate and oxide formation of Nd, Sm and Dy. The concentration of specified analytes in solution is 0.1 ppm.

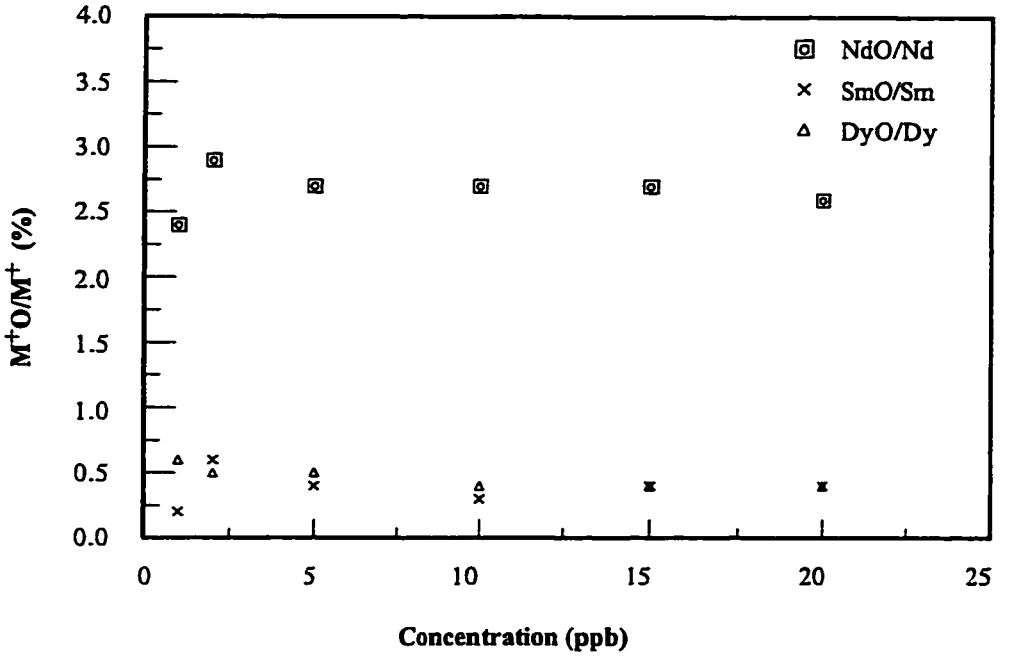

Figure 4-6. M^+O/M^+ versus concentration for spesified analytes

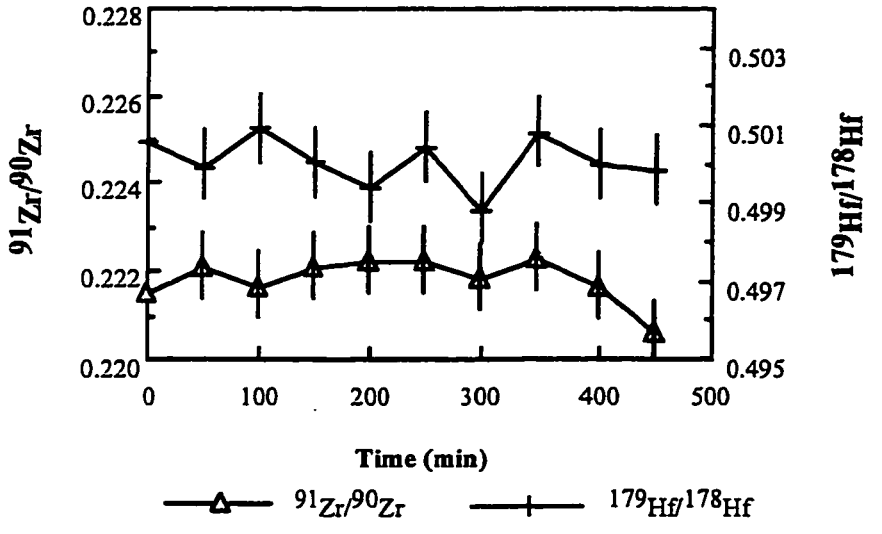

Figure 4-7. Measured $^{91}Zr/^{90}Zr$ and $^{179}Hf/^{178}Hf$ versus time, showing consistency within error. Other Zr and Hf isotopes are also consistent within error. Measured in a solution of 0.012 ppm pure Zr and Hf. Precision (1σ) is shown by error bars.

intensity drift could be significant, measured ratios are generally stable to within the precision of measurement (Sun et al., 1987; Ting and Janghorbani, 1988; Janghorbani and Ting, 1989). Under the optimum IOPs (Table 4-2), stability of measured Zr and Hf isotope ratios were tested for up to 7.5 hours. The test was conducted on solutions with only 0.012 ppm pure Zr and Hf. All measured ratios are consistent within the analytical error (Table 4-3, Figure 4-7).

4-2-8. Optimized IOPs for improved precision in measurement of Zr and Hf isotope ratios by ICP-MS

This study shows that a number of IOPs are important in determination of the precision and accuracy of measurement of Zr and Hf isotope ratios in the aqueous matrices of rock solutions. The results are in general agreement with previous observations for other elements (Longerich et al., 1987a; Russ III and Bazan, 1987; Sun et al., 1987; Ting and Janghorbani, 1988). Although previous studies indicated that increasing RF power gave maximum ion intensity, and improved precision for isotope measurement, the precision and accuracy of Zr and Hf isotope ratio measurements were not significantly affected by RF power varying from 1000 to 1300 watts. Increasing DT significantly improved the precision and accuracy, as high frequency noise is reduced by signal averaging with longer DT (Begley and Sharp, 1994). Mass bias is a strong function of the B lens setting. For the Elan 5000 instrument, a B lens setting of 60 digipots gives the least mass bias for Zr and Hf isotope ratio measurement.

The optimized IOPs are listed in Table 4-2. With optimized IOPs, precisions of 0.2 to 0.6 RSD% can be achieved for Zr and Hf isotope ratio measurement at concentrations

Table 4-3. Measured Zr and Hf isotope ratios with time [a]

Time (min)	$^{91}Zr/^{90}Zr$	$^{92}Zr/^{90}Zr$	$^{94}Zr/^{90}Zr$	$^{176}Hf/^{180}Hf$	$^{177}Hf/^{180}Hf$	$^{178}Hf/^{180}Hf$	$^{179}Hf/^{180}Hf$
0	0.2215 ± 17	0.3472 ± 25	0.3698 ± 31	0.1461 ± 14	0.5203 ± 35	0.7691 ± 59	0.3850 ± 29
50	0.2221 ± 19	0.3479 ± 38	0.3693 ± 29	0.1460 ± 15	0.5205 ± 41	0.7703 ± 44	0.3851 ± 30
100	0.2216 ± 24	0.3471 ± 29	0.3677 ± 28	0.1463 ± 15	0.5222 ± 44	0.7702 ± 64	0.3858 ± 33
150	0.2221 ± 19	0.3481 ± 36	0.3707 ± 32	0.1469 ± 15	0.5235 ± 39	0.7715 ± 62	0.3858 ± 30
200	0.2222 ± 21	0.3471 ± 27	0.3690 ± 37	0.1475 ± 14	0.5227 ± 33	0.7727 ± 44	0.3859 ± 32
250	0.2222 ± 17	0.3473 ± 38	0.3684 ± 34	0.1469 ± 15	0.5236 ± 35	0.7734 ± 53	0.3870 ± 33
300	0.2218 ± 15	0.3471 ± 32	0.3674 ± 24	0.1476 ± 19	0.5245 ± 35	0.7735 ± 44	0.3858 ± 19
350	0.2223 ± 21	0.3465 ± 25	0.3678 ± 35	0.1470 ± 15	0.5234 ± 36	0.7712 ± 43	0.3862 ± 29
400	0.2216 ± 21	0.3469 ± 34	0.3686 ± 34	0.1472 ± 15	0.5241 ± 44	0.7736 ± 55	0.3868 ± 30
450	0.2206 ± 20	0.3459 ± 25	0.3666 ± 31	0.1466 ± 12	0.5231 ± 37	0.7729 ± 61	0.3863 ± 32

[a] Measured in solutions with 0.012 ppm pure Zr and Hf.

ranging from sub ppb to ppm, and can be maintained over 7 hour durations, without pre-separation and preconcentration of analyte elements. $^{91}Zr/^{90}Zr$ and $^{179}Hf/^{178}Hf$ are the best pairs for ID analysis, as they have the least mass bias effects and are essentially free of isobaric interferences. By optimizing IOPs, it is not necessary to correct for potential interferences from REE oxides, without sacrificing precision and accuracy. Mass bias, always showing preferential reduced response of light isotopes, occurs for both Zr and Hf isotope ratio measurement, though the bias for Hf is not as serious as for Zr, in keeping with the greater atomic mass of Hf nuclides, and the smaller percentage mass difference between the Hf isotopes relative to Zr. Accordingly, correction for mass bias is necessary. This study indicates that using an unspiked sample to correct mass bias for a spiked counterpart, may slightly improve the precision of ID analysis.

4-3. ID-ICP-MS analysis of Zr and Hf

4-3-1. Sample preparation

After evaluation of selective IOPs in isotope ratio measurement, it is then possible to apply the optimized IOPs in ID-ICP-MS analysis for Zr and Hf in international reference materials and unknown samples.

Zr and Hf are normally present in minerals such as zircon which are resistant to attack by mineral acids (Mukherji, 1970). Thus, any dissolution procedure must ensure complete breakdown of these phases. In the samples analyzed in this study, i.e. komatiites and basalts, zircon is unlikely to be present, given the attributes of low Zr abundance ($\leq$ 15 ppm) and Si undersaturation. However, the following method, somewhat different from the standard HF-HNO_3 digestion as described in Chapter 3, was adopted in an attempt to ensure

that all Zr and Hf were taken into solution (Patchett and Tatsumoto, 1980; Jarvis, 1990).

500 mg powdered sample was weighed into a 20 ml screw-top Teflon bomb, along with enriched isotope spike solutions. 0.5 ml 16 M HNO_3 and 8 ml 29 M HF were then added, and the bomb left to stand cold for 2-3 hours. The bomb was then opened and warmed for 2-3 hours, during which time the major silicate minerals in the sample were attacked by acids, and most of the Si evaporated as SiF_4. 8 ml 29 M HF and 5 ml 12 M $HClO_4$ were then added to the sample, and the bomb sealed and placed on the hotplate at 200 °C for 4 days; HF thus had the opportunity to attack any residual refractory minerals without being depleted by reaction with the major silicate phases. The advantage of adding $HClO_4$ is more efficient attack of refractory phases by improving the efficiency of HF, due to the increased boiling temperature of the reaction mixture (Jarvis et al., 1992).

After evaporation of HF, 10 ml 16 M HNO_3 was added and the bomb heated until dry; 2 to 3 such treatments normally removed sufficient HF from the residue. The sample was then taken up in 2 ml 8 M HNO_3, and diluted to 50 g with DDIW. For international reference materials with relatively higher Zr contents than BIR-1 (i.e., MRG-1, BHVO-1 and BCR-1), 100 mg powdered sample was used, and diluted to 100 g. After this acid attack protocol, no residue was observed in the final solutions.

One of the potential problems of analyzing HFSEs in solution is the possible instability of these elements in aqueous solution, owing to their tendency for hydrolysis (Mukherji, 1970). In order to avoid this problem, freshly prepared sample solutions were used in the routine external calibration ICP-MS analysis, which gave results consistent with that by laser ablation ICP-MS (Fedorowich et al., 1993; see Chapter 3 for discussion). Isotope dilution techniques circumvent any sporadic loss of Zr and Hf by precipitation, as

the spike is added before dissolution. After isotope equilibration is achieved, any chemical change due to solution instability would not affect the isotope ratios, nor the ID results.

4-3-2. Isotope ratio measurements

$^{91}Zr/^{90}Zr$ and $^{179}Hf/^{178}Hf$ ratios were measured for both unspiked and spiked samples. The intensity data for isotope ratio determinations were acquired in the peak-hopping isotope ratio mode, with 1 point per mass peak, under optimized IOPs (Table 4-2). The quadrupole mass spectrometer was adjusted to normal resolution. Isotope ratios are the mean of a set of 80 intensity ratios, and are background corrected using counting rates on the reagent blank (0.2 M HNO_3). The total measurement time is about 8 min per sample. Entire data acquisition was controlled through computer software provided by the manufacturer.

4-3-3. Mass bias correction

Measured $^{91}Zr/^{90}Zr$ and $^{179}Hf/^{178}Hf$ ratios for unspiked samples are reported in Table 4-1. The natural isotope ratios are from De Laeter et al. (1991). Measured $^{91}Zr/^{90}Zr$ and $^{179}Hf/^{178}Hf$ ratios are consistent within error for all samples, and are significantly higher than their natural ratios, which is evidently due to mass bias. Mass bias has been observed in isotope ratio measurement by ICP-MS in previous studies (Longerich et al., 1987a; Russ III, 1989). For the U. of S. instrument and operating conditions, a reduced response for light masses was always observed (Xie and Kerrich, 1995b). Space charge effects within the plasma region, and supersonic gaseous expansion between the cones, may be responsible for the preferential reduction of response for light masses (Walder et al., 1993); however mass bias is also apparently a function of the B lens setting (Longerich et al., 1987a; Xie and

Kerrich, 1995b), which would influence ion trajectories

The following equation has been shown to predict the mass bias

$$R_{true} = R_{meas} (1 + a)^n \qquad (4\text{-}2)$$

where R_{true} = true isotope ratio, R_{meas} = measured isotope, a = bias per mass unit, and n = mass difference (Russ III and Bazan, 1987). Comparison of measured ratios with the true ratios can thus be used to determine the magnitude of the correction factor $(1 + a)^n$, where n = 1 for the Zr and Hf isotopes in question.

As shown in section 4-2, for analyte solutions with a wide range of Zr and Hf concentrations, the $^{91}Zr/^{90}Zr$ and $^{179}Hf/^{178}Hf$ ratios are consistent within error, indicating that the mass bias effect is independent of concentration, in the concentration range investigated (Table 4-1). The mass bias effect is also stable over a duration of several hours (Table 4-3, Figure 4-7; Xie and Kerrich, 1995b). Similar results have also been reported for other isotope ratios in previous studies (Russ III and Bazan, 1987; Ting and Janghorbani, 1988). Accordingly, it is possible to correct for mass bias using unspiked samples, under optimized IOPs.

4-3-4. Results of isotope dilution analysis

Samples were analyzed in the following sequence: flush (1 M HNO_3), blank (0.2 M HNO_3), unspiked sample, flush, blank, spiked sample. All measured $^{91}Zr/^{90}Zr$ and $^{179}Hf/^{178}Hf$ ratios were corrected for background noise, using the average counting rates for the relevant masses in the blank. Mass bias correction factors were determined with reference to unspiked samples.

Zr and Hf concentrations in the samples were calculated from the formula

$$C = M_s K (A_s R - B_s) / W (B - R A) \quad (4-3)$$

where C is concentration in $\mu g\ g^{-1}$, M_s is the mass of the spike (μg), A is the natural abundance of the reference isotope (^{90}Zr and ^{178}Hf), B is the natural abundance of the spike isotope (^{91}Zr and ^{179}Hf), A_s is the abundance of reference isotope in the spike, B_s is the abundance of the spike isotope in the spike, K is the ratio of the natural and spike atomic weights, W is the sample weight (g), and R is the measured isotope ratio of spiked samples after correction for mass bias. For enriched isotope spikes, certified values furnished by the supplier were used.

The results of ID-ICP-MS analysis of Zr and Hf in some komatiites and international reference materials are reported in Table 4-4. The results for all samples analyzed are in good agreement with data previously obtained by the routine external calibration ICP-MS procedure. ID-ICP-MS data for international reference materials BIR-1, MRG-1, BHVO-1 and BCR-1 are also consistent within error with compiled values (Potts et al., 1992), excepting Zr in BIR-1, for which the compiled value is much higher (22 ppm), whereas ID-ICP-MS gives 14.5 ppm. The only standard for which Zr and Hf data determined by ID-TIMS are available is BCR-1 (Owen and Faure, 1974; Patchett and Tatsumoto, 1980). Zirconium and Hf data for BCR-1 by ID-ICP-MS (Zr: 186.86 ± 0.01 ppm, Hf: 5.3 ± 0.2 ppm) agree well with results from ID-TIMS (Zr: 182 ± 3.5 ppm, Hf: 4.95 ppm; Owen and Faure, 1974; Patchett and Tatsumoto, 1980)).

Compared with external calibration, ID significantly improved the precision of Zr and Hf measurement (< 1% RSD for Zr and < 4% RSD for Hf). Precision for Zr in BCR-1 (184 ppm) by ID-ICP-MS (0.005% RSD) is comparable with that by ID-TIMS (0.001% RSD). Precision comparable with ID-TIMS has also been obtained for Pb concentrations in some

Table 4-4. Results for Zr and Hf abundances in some international reference materials and komatiites by ID-ICP-MS

Samples	ID-ICP-MS			ICP-MS			LA-ICP-MS [a]			ID-TIMS			ID-SSMS			Compiled [b]		Chondrite [c]
	Zr	Hf	Zr/Hf	Zr	Hf	Zr/Hf	Zr	Hf	Zr/Hf	Zr	Hf	Zr/Hf	Zr	Hf	Zr/Hf	Zr	Hf	Zr/Hf
Munro komatiite	12.9 ± 0.2	0.45 ± 0.03	28	12.1	0.43	28												
Munro komatiite	8.73 ± 0.04	0.30 ± 0.01	29	8.79	0.29	30												
Munro komatiite	16.2 ± 0.1	0.54 ± 0.02	30	17.9	0.8	22												
Munro komatiite	18.1 ± 0.3	0.58 ± 0.02	31	20.6	0.67	30							16.8	0.44	38			
Boston komatiite	15.9 ± 0.2	0.41 ± 0.01	38	12.2	0.35	34												
Boston komatiite	32.6 ± 0.3	0.93 ± 0.07	35	32.5	0.91	35												
BIR-1	14.5 ± 0.3	0.63 ± 0.03	23	15.7 ± 0.5	0.64 ± 0.04	24	13 ± 1	0.60 ± 0.08	22				15.4 [e]	0.51 [e]	30	22	0.58	
MRG-1	96 ± 1	3.8 ± 0.1	25	103 ± 2	3.8 ± 0.1	27	99 ± 9	3.7 ± 0.4	26		4.938 [d]		107	3.51	30	108	3.76	
BHVO-1	167 ± 1	4.7 ± 0.2	35	178 ± 2	4.4 ± 0.5	40					4.983 [d]		182	4.6	39	179	4.38	
BCR-1	184.86 ± 0.01	5.3 ± 0.2	34	201 ±12	5.8 ± 0.4	34				182 ± 3.5	4.62 ± 0.04	36	186	4.9	37	190	4.95	36

a Data from Fedorowich et al., 1993;

b Compiled values are from Potts et al., 1993;

c From Sun and McDonough, 1989;

d Hf data for BCR-1 from Patchett and Tatsumoto, 1980;

e The most recent ID-SSMS results from Jochum et al., 1994.

international reference materials using ID-ICP-MS (Campbell et al., 1991), indicating that ID-ICP-MS is a powerful tool for trace element determination when high precision is required. ID-ICP-MS gives a better sample throughput rate, and requires considerably less sample pretreatment than ID-TIMS, where ion chromatographic separations are required.

4-4. Conclusions and implications

This study demonstrates that various IOPs are important in determination of the precision and accuracy of isotope ratio measurement by ICP-MS. These include RF power, dwell time, B lens setting, and nebulizer flow rate. Mass bias, showing preferentially reduced response of light isotopes, has been observed. The mass bias factor is independent of analyte concentrations in the range of sub ppb to ppm, and is stable over a period of several hours. Thus, it is possible to apply mass bias correction by reference to a "true isotope ratio". Under optimized IOPs, precisions of 0.2 to 0.6% RSD can be achieved for isotope ratio measurement by ICP-MS.

With optimized IOPs, ID-ICP-MS analysis of Zr and Hf in low abundance international reference materials and Archean komatiites has been conducted. The results confirm the accuracy of data obtained by routine external calibration ICP-MS, but with significantly improved precision. ID-ICP-MS is proven as a preferred choice of methods for high precision trace element determinations, when high precision at low concentration is required, such as the certification of international reference materials, and trace element analysis of mantle peridotites.

Some of the salient problems of mantle geochemistry concern the chemical composition of different mantle reservoirs, the formation and evolution of the mantle, the

nature of the continental mantle lithosphere, and the trace element characteristics of peridotites. Recent high pressure experimental studies suggest that the dominant mineral phases in the mantle change from olivine+cpx+opx, to majorite + magnesiowustite, to silicate-perovskite + magnesiowustite with increasing pressure (Miller et al., 1991a; Zhang and Herzberg, 1994, and references therein). Given that mineral-melt Kd's for these phases fractionate REEs and HFSEs in distinct ways (Kato et al., 1988b; Yurimoto and Ohtani, 1992; Kennedy et al., 1993), it is clear that precise analysis of REEs and HFSEs in mantle rocks can provide information on the depth of melting, and mantle composition at that depth.

Based on ICP-MS analyses of HFSEs and REEs for three komatiite-tholeiite sequences from Ontario, Canada, Xie et al. (1993) reported positive, zero, and negative normalized anomalies of Zr and Hf relative to REEs in the three komatiite sequences, and interpreted the HFSE/REE fractionations in the context of different mantle sources, residual mineralogies, and source depths. However, the analyses of various komatiites by ID-SSMS show negligible fractionation of HFSEs from REEs, leading to an entirely different geological interpretation (Jochum et al., 1991).

Using ion probe analysis, Salters and Shimizu (1988) found that both clinopyroxenes and whole-rock samples of peridotites from continental, oceanic, and island-arc environments show strong depletions of Zr, Hf and Ti relative to REEs. They suggested that high pressure phases, such as majorite and silicate-perovskite may play a role in the creation of the HFSE depletion in these mantle peridotites. On the contrary, Jochum et al. (1989) analyzed peridotite xenoliths from continental lithospheric mantle by ID-SSMS, and found no HFSE/REE fractionations. Accordingly, they argued that continental lithospheric mantle cannot be related to a subduction environment, but rather may reflect the residue after

extraction of ocean island and/or ocean ridge basalts. These examples underscore the importance of accurate and precise analysis of HFSEs and REEs in mantle derived rocks.

The Zr/Hf ratio of mantle rocks is also an important geochemical parameter. Magmas generated in the upper mantle normally have near chondritic Zr/Hf ratios (Zr/Hf ~ 36), as most solid phases in the upper mantle do not fractionate Zr and Hf. However, non-chondritic Zr/Hf ratios have been reported for some alkaline intraplate basalts (Dupuy et al., 1992). From Table 4-5, Zr/Hf ratios of the rock standards BCR-1 and BHVO-1 are near chondritic, whereas MRG-1 and BIR-1 are apparently non-chondritic. In contrast, Jochum et al. (1990) reported near chondritic Zr/Hf ratios for BIR-1. Accordingly, from this study, some non-alkaline, as well as alkaline mafic rocks may have non-chondritic Zr/Hf, and hence non-chondritic Zr/Sm and Hf/Nd ratios.

In the Archean Abitibi greenstone belt, one komatiite sequence (Boston) has near chondritic Zr/Hf ratios, whereas another komatiite sequence (Munro) has non-chondritic ratios. These results not only have implications of distinct komatiite sequences formed from different plumes having characteristic compositions and melting depths, but also that the greenstone belt must be a tectonic collage of diverse volcanic belts (For an extended discussion see Chapters 5 and 8; Xie et al., 1993; Xie and Kerrich, 1994). Given that high pressure phases (i.e. majorite and silicate-perovskite) may incorporate Zr and Hf in different ways (Kato et al., 1988b; Yurimoto and Ohtani, 1992), the Zr/Hf ratio in some mantle derived rocks may not necessarily be chondritic. Accordingly, it may be inappropriate to judge the quality of analytical data based on the assumption that certain elemental ratios should be chondritic in mantle derived rocks.

CHAPTER 5 REE AND HFSE SYSTEMATICS OF THREE KOMATIITE-THOLEIITE SEQUENCES FROM THE ARCHEAN ABITIBI GREENSTONE BELT: IMPLICATIONS FOR SOURCE COMPOSITION, MANTLE MELTING DEPTHS, AND EARLY MANTLE DIFFERENTIATION

5-1 Introduction

As discussed in Section 1-1, the trace element systematics of Archean komatiites and tholeiites, particularly the interrelationships between REEs and HFSEs, may provide information on the source compositions and the melting depths of the Archean mantle, which in turn can be used to constrain the history of early mantle differentiation and stratification.

There have been numerous geochemical studies of Archean komatiites from the Abitibi greenstone belt, and other greenstone belts worldwide (Nesbitt and Sun, 1976; Nesbitt et al., 1979; Sun and Nesbitt, 1979; Jahn et al., 1980, 1982; Cattell, 1987; Cattell and Arndt, 1987; Jochum et al., 1991; Arndt and Lesher, 1992; McDonough and Ireland, 1993). The question could then be posed as to why reanalysis of intensively studied rocks is warranted?

Interpretation of the origin of komatiites and related problems such as the depth of mantle plume melting, or early mantle stratification, requires accurate and precise analysis of all REEs and HFSEs. Many of the earlier papers report Hf and Sm but not Zr or Nd; or Zr but not Hf, Sm and Nd; accordingly it is not possible to quantify HFSE/REE fractionations (Nesbitt and Sun, 1976; Nesbitt et al., 1979; Sun and Nesbitt, 1979; Arndt and

Nesbitt, 1982). Similarly many early papers do not report Nb and REE; consequently it is not possible to screen samples using the criterion of La/Nb <1 for absence of crustal contamination that could introduce negative HFSE anomalies relative to REEs (Sun and McDonough, 1989; Jochum et al., 1991).

There are also some uncertainties in the existing trace element data of komatiites, especially for analyses conducted during the 1970's and early 1980's. This is mainly due to the following three reasons:

(1) Poor detection limits: For example, Zr and Nb are present at levels in komatiites close to detection limits by XRF. Similarly, Hf and HREE possess abundances in komatiites at the detection limits of INAA. These problems are manifested in extremely scattered Zr/Hf, Zr/Sm and Hf/Nd ratios in early studies, where systematic behaviour should be expected (Beswick, 1982; Barnes et al., 1985), and has subsequently been demonstrated using ICP-MS, with improved detection limits (see chapters 3 and 4).

(2) Calibration strategies: Prior to the advent of ICP-MS, the analysis of all HFSE and REE required some combination of analytical instruments, including XRF, INAA and TIMS. Unknowns analyzed by XRF are calibrated against an international reference material of similar composition and therefore matrix, and the reference material calibrated against yet another primary standard, that may or may not have a comparable matrix. Similarly, unknowns run by INAA are calibrated against reference materials that may in turn have been calibrated against a standard with a different matrix, such as NIST 1633 fly coal ash. Hence ratios of elements such as Nb/La, Zr/Sm and Zr/Hf analyzed by different techniques may be in error.

(3) Uncertainties in international reference materials: Precise and accurate analysis of trace elements in unknowns presupposes that concentrations of the elements in question are known in the reference material used for calibration. For analysis by ICP-MS, pure elemental standards in solution, e.g. 99.9999% Zr, can be used for calibration, such that elemental standards, unknowns and reference materials are all in the same dilute aqueous matrix. As a corollary, pure elemental standards cannot be used to calibrate XRF or INAA, because the standard and unknown present such contrasting matrices to the incident X-rays or neutrons. Jenner et al. (1990), using ICP-MS and pure elemental standards for calibration, showed that the accepted values for several elements in international rock reference materials, including BIR-1, were in error. This observation raises questions as to the quality of data obtained by calibration against the reference materials.

Some of these problems have been discussed in more detail in Chapters 3 and 4. For these, and other, reasons, high precision trace element re-analysis of komatiites from the Abitibi greenstone belt was considered warranted.

Having completed the characterization of ICP-MS and ID-ICP-MS (see Chapters 3 and 4), it is now possible to obtain high quality trace element data, including all REEs and HFSEs, for komatiites and associated basalts. In this chapter, trace element characteristics of three Archean komatiite-tholeiite sequences from the Abitibi greenstone belt are presented. The distinct geochemical features, e.g. REE patterns and HFSE/REE interrelationships, in the three komatiite-tholeiite sequences are interpreted in the context of different mantle source compositions and the depths of melting. Alternative processes, such

as crustal contamination and hydrothermal alteration which may generate various HFSE/REE fractionations in igneous rocks, are also examined. Finally, implications for komatiite petrogenesis and eariy mantle evolution are discussed.

5-2 A brief review of Archean komatiites and tholeiitic basalts

5-2-1 Komatiites

The term komatiite was first used to describe ultramafic lavas from the Barberton greenstone belt of South Africa (Viljoen and Viljoen, 1969). They described field observations such as chilled flow tops, pillow-like structures, spinifex-textures, and the systematic stratigraphy of the ultramafic units when compared with associated mafic lava flows.

Since first introduced, the name komatiite has been applied to suites of rocks with compositions ranging from ultramafic to mafic, including basalts which are commonly spatially associated with ultramafic lavas (Brooks and Hart, 1972; Jensen and Langford, 1985). However, subsequent studies, particularly trace element studies, have revealed that some komatiites and spatially associated basalts may not be genetically related (Nesbitt et al., 1979; Sun and Nesbitt, 1979; Arndt and Nesbitt, 1982). Arndt and Nisbet (1982) reviewed and discussed the development of komatiite terminology, and proposed that the name komatiite be restricted to ultramafic volcanic rocks. They suggested two criteria as diagnostic features of komatiite, including:

(1) features indicating a volcanic origin: such as chilled flow tops, polyhedral jointing, well developed spinifex textures, pillows and rapid-cooling textures;

(2) features indicating ultramafic compositions: such as a predominance of olivine and

pyroxene, MgO > 18% (anhydrous basis). This value corresponds roughly to 20-35 % modal olivine.

In this study, the term "komatiite" is used for volcanic rocks with greater than 18% MgO (calculated anhydrous), derived from a liquid with greater than 18% MgO; the latter caveat is added in order to exclude basaltic cumulate (Arndt and Nisbet, 1982; Cattell and Taylor, 1990). Due to the factor that Mg may be relatively mobile during hydrothermal alteration and metamorphism, other geochemical features, such as Ni and Cr contents, REE patterns and HFSE contents, are also considered, when samples are referred to as komatiite.

Komatiites occurr principally in Archean greenstone belts. The only well characterized Phanerozoic komatiite is of Cretaceous age on Gorgona island, Columbia (Echeverria, 1982). Typical komatiitic lavas commonly form layered flows, with an olivine-phyric basal zone, spinifex-textured zone, and polyhedral jointed flow tops. The presence of olivine spinifex textures in komatiitic flows has been interpreted as an indication of rapid-cooling of high Mg liquids (Arndt, 1977a).

It is generally accepted that spinifex textured komatiite represents the composition of the parental liquid from which komatiite flows originated (Arndt and Nisbet, 1982). Several authors have used olivine spinifex textured komatiites to estimate the compositions of magmas, and given Mg contents of the liquids between 18 to 32% MgO (Arndt, 1986a; Cattell and Arndt, 1987; McKenzie and Bickle, 1988; Nisbet et al., 1993). The high Mg content of komatiitic liquids is indicative of its high temperature origin (Nisbet, 1982; Nisbet et al., 1993). In a recent review of constraints on the thermal structure of the Archean mantle, Nisbet et al. (1993) concluded that an eruption temperature of 1580 °C is required

for komatiitic liquid with 29 wt% MgO, corresponding to a mantle potential temperature of 1900 °C at a pressure of 18 GPa. The potential temperature of the mantle is the temperature at which a mantle-derived domain of solid material would reach at Earth's surface: in other word, it is the temperature of the solid mantle adiabat, projected to surface pressures (McKenzie and Bickle, 1988).

There are essentially two types of komatiite: Al-undepleted and Al-depleted varieties (Nesbitt et al., 1979). Al-undepleted komatiites are characterized by near chondritic CaO/Al_2O_3 (0.8-1.0) and Al_2O_3/TiO_2 (18-22) ratios, LREE depletion and flat HREE patterns, whereas Al-depleted komatiites have $CaO/Al_2O_3 \geq 1$, $Al_2O_3/TiO_2 \leq 14$, enriched LREE, but fractionated and depleted HREE (Nesbitt et al., 1979; Cattell and Taylor, 1990). Originally, it was considered that Al-depleted komatiites are restricted to sequences older than 3.0 Ga, whereas most komatiites younger than 3.0 Ga are Al-undepleted (Nesbitt et al., 1982; Cattell and Taylor, 1990). This observation led in turn to the suggestion that there was a secular change of komatiite compositions from the early towards the late Archean (Nesbitt et al., 1979; Ohtani, 1984). Subsequent studies, however, have demonstrated that Al-depleted komatiites are not uncommon in late Archean greenstone belt, such as the 2.7 Ga Abitibi, Canada and Norseman, Western Australia, greenstone belts (Cattell and Arndt, 1987; Stone et al., 1987; Xie et al., 1993; Barley and Kerrich, 1995). Specifically, Cattell and Arndt (1987) identified coexisting Al-undepleted and Al-depleted komatiites in Newton Township, southwestern Abitibi greenstone belt, suggesting that it is unlikely that there is a general change of komatiite compositions or their sources during the Archean (Cattell and Taylor, 1990).

Trace element and radiogenic isotope studies of komatiites all point to incompatible

element depleted mantle sources. Various Archean komatiites typically have ϵ_{Nd} ranging from +1 to +5 with reference to a chondritic primitive mantle, suggesting long-term depletion of incompatible elements in the mantle sources of komatiites (Sun and Nesbitt, 1978; Nesbitt et al., 1979; Jahn et al., 1982; Zindler, 1982; Machado et al., 1986; Gruau et al., 1988, 1990a, b; Bowring and Housh, 1995).

Various models have been advocated to account for komatiite petrogenesis, such as high degree (>50%) partial melting of a depleted upper mantle (Viljoen and Viljoen, 1969; Brooks and Hart, 1972; Arndt, 1977b), and multistage melting of a primitive mantle (Arndt, 1977b; Weaver and Tarney, 1979). Alternatively, several authors proposed models invoking low degree (<50%) partial melting at high pressures, based on the experimental observation that low percentage mantle melts become increasingly magnesian with increasing pressure (Herzberg and O'Hara, 1985; Takahashi and Scarfe, 1985; Herzberg and Ohtani, 1988; Herzberg et al., 1990; Wei et al., 1990). Specifically, a mantle plume model has recently been put forward, which suggests that komatiitic liquid is formed by an upwelling mantle diapir originating from anomalously hot mantle materials at great depth (Fyfe, 1978; Campbell et al., 1989; Miller et al., 1991b; Herzberg, 1992a; Nisbet et al., 1993). The petrogenesis of komatiites will be further discussed later in this chapter.

5-2-2 Archean basalts

The basalts discussed here are restricted to those in close spatial association with komatiites. They are, sometimes, also referred to as komatiitic basalts, or basaltic komatiites, although the name does not necessarily imply any genetic link between the two types of Archean volcanic flows (Arndt and Nisbet, 1982; Cattell and Taylor, 1990).

The basalts spatially associated with komatiites are essentially tholeiites, consisting mainly of plagioclase and augite microphenocrysts, with occasional olivine phenocrysts (Arndt and Nesbitt, 1982; Dimroth et al., 1982, 1983a; Pyke, 1982; Jensen and Langford, 1985). They occur most typically as pillowed and massive lava flows, although weakly layered flows are not uncommon (Cattell and Taylor, 1990).

Archean tholeiites can be divided into Mg-tholeiite and Fe-tholeiite (Jensen, 1976; Condie, 1990). Some of the Fe-tholeiites are apparently the products of pronounced fractional crystallization of Mg-tholeiites or even komatiites. Others, however, cannot simply be related to either Mg-tholeiites or komatiites; rather they may have formed from a different mantle source (Naldrett and Turner, 1977; Sun and Nesbitt, 1979; Arndt and Nesbitt, 1982).

Archean Mg-tholeiites normally have higher incompatible element contents than komatiites, and are characterized by flat REE and other incompatible element patterns (Sun and Nesbitt, 1979; Arndt and Nisbet, 1982; Cattell and Taylor, 1990). Due to the close spatial association with komatiites, Archean Mg-tholeiites were originally considered to be the fractional crystallization products of komatiitic liquid (Viljoen and Viljoen, 1969; Dimroth, 1982, 1983; Jensen and Langford, 1985). Subsequent trace element studies have suggested that Mg-tholeiites and komatiites cannot be linked by simple fractional crystallization. Some models propose Mg-rich basalts being derived from mantle sources distinct to that of komatiites (Sun and Nesbitt, 1979; Nisbet, 1982; Arndt and Nesbitt, 1982), whereas other models advocate crustal contamination of a komatiitic liquid (Arndt and Jenner, 1986; Barnes et al., 1988; Gruau et al., 1990b). In the mantle plume model, tholeiites associated with komatiites are interpreted as representative of relatively cooler upper mantle material which has been entrained in the hot ascending plume (Campbell et al., 1989).

5-3 Geology and petrology of the three komatiite-tholeiite sequences from the Abitibi greenstone belt

The Abitibi greenstone belt, Canada, can be divided into three tectonostratigraphic zones--the Northern and Southern Volcanic zones, and an intervening granite-gneiss zone (Figure 2-2). The Southern Volcanic Zone (SVZ) extends ~600 km east-west and ~200 km north-south, and consists mainly of komatiitic-tholeiitic volcanic flows and intrusive granitoid batholiths, which are not extensively altered or deformed, except proximal to faults (Figure 2-3). The three komatiite-tholeiite sequences in this study are located in Tisdale, Munro and Boston Townships respectively within the SVZ (Figure 2-3). They are separated by major terrane boundary structures, and have ages of about 2725-2710 Ma (Figure 2-4).

Conventionally, the Abitibi greenstone belt was considered to be a series of contemporaneous volcanic-plutonic centres, with intervening belts of sedimentary rocks (Goodwin, 1977). It is now recognized that this greenstone belt represents a collage of volcanic belts representing different types of plumes, and of different arc volcanic-plutonic belts, that formed separately in different geodynamic environments and were tectonically juxtaposed over 2700-2670 Ma (Wyman and Kerrich, 1989; Thurston, 1990; Kerrich and Feng, 1992; Desrochers et al., 1993; Xie and Kerrich, 1993; Xie et al., 1993). The general geology and petrography of the three komatiite-tholeiite sequences are briefly summarized as follows.

5-3-1 Komatiites and tholeiites from Tisdale Township

Tisdale Township is located in the Timmins area, north of the DPFZ (Figures 2-3 and

5-1). Komatiites and tholeiites form the lower part of the Tisdale Group, that formerly was termed the Lower Tisdale Formation (Figure 2-4). Komatiites have typical polysuturing and spinifex textures, while pillow lavas occur only occasionally (Pyke, 1982). The primary minerals are olivine and pyroxene, which are largely altered to serpentine, lesser amounts of tremolite and chlorite, and carbonate. Up to 20% relict olivine, however, may be present in some massive flows (Pyke, 1982).

Tholeiitic basalts in Tisdale Township can be further divided into two groups; Mg-rich tholeiite and Fe-rich tholeiite. They are confined to the base and middle of the Tisdale Group (Figure 2-4; Pyke, 1982; Jensen and Langford, 1985). Mg-tholeiites are commonly interlayered with komatiites (Pyke, 1982). Thin section examination reveals that Mg-tholeiites consist of 15-50% plagioclase, 40-80% pyroxene, and 2-5% quartz. Plagioclase is virtually completely saussuritized, whereas pyroxene is totally altered to actinolite and tremolite. Fe-tholeiites generally form distinct flow sequences, and comprise 10-40% plagioclase, and 30-80% hornblende. Alteration, such as saussuritization and chloritization, is pervasive.

5-3-2 Komatiites and tholeiites from Munro Township

Munro Township is located about 80 km east of Timmins, and north of the DPFZ (Figures 2-3). The general geology of Munro Township is illustrated in Figure 5-2. Komatiites and tholeiites were sampled from the "classical" Pyke Hill locality, which has an age of 2725 Ma (Walker et al., 1988).

Komatiitic flows in Pyke Hill have been accepted as a type example of Archean ultramafic lavas, with well preserved complete succession of komatiitic flows, including

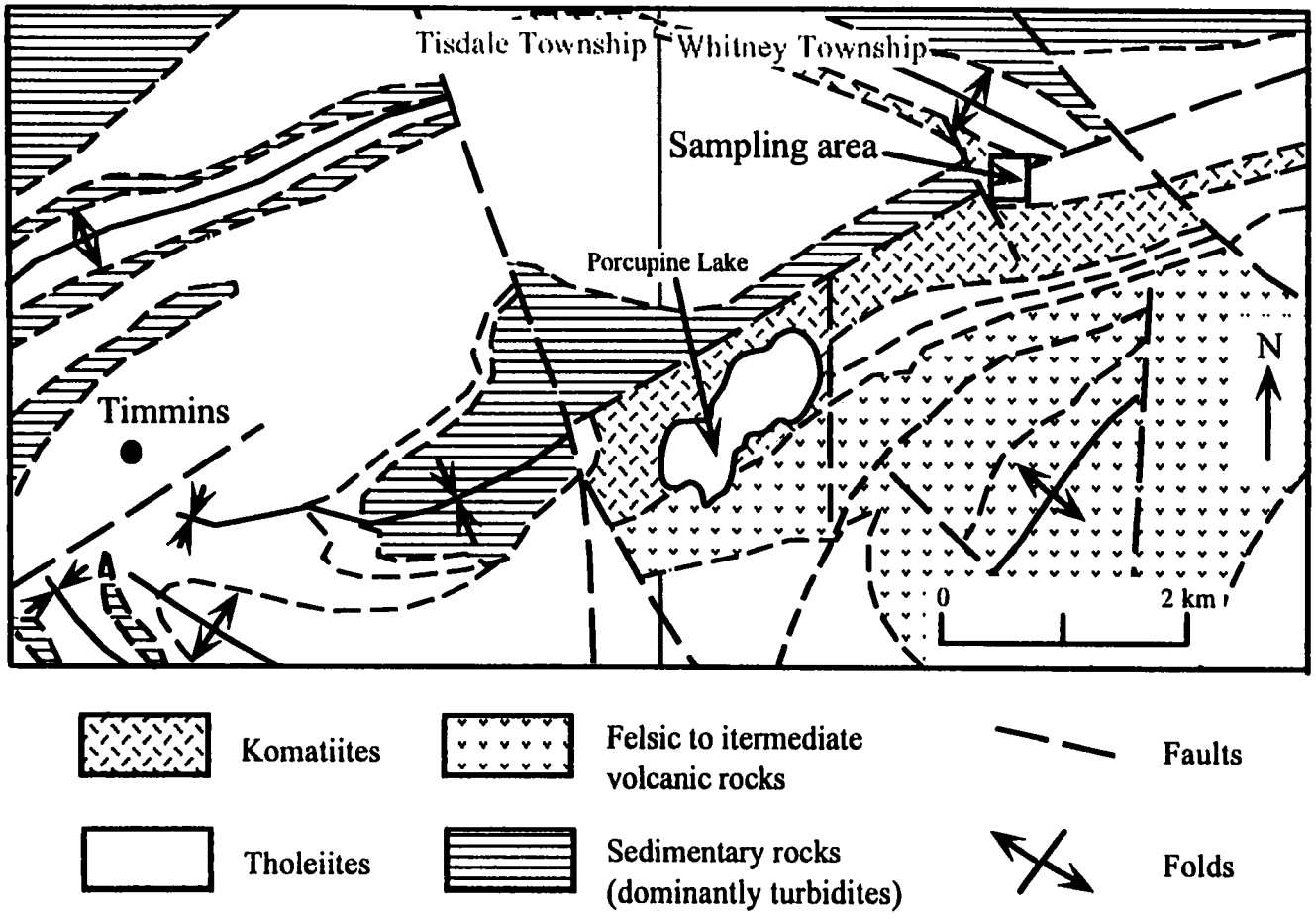

Figure 5-1. Simplified geological map of the Timmins area, showing the distribution of various types of volcanic rocks in the Tisdale Group (modified from Pyke, 1982).

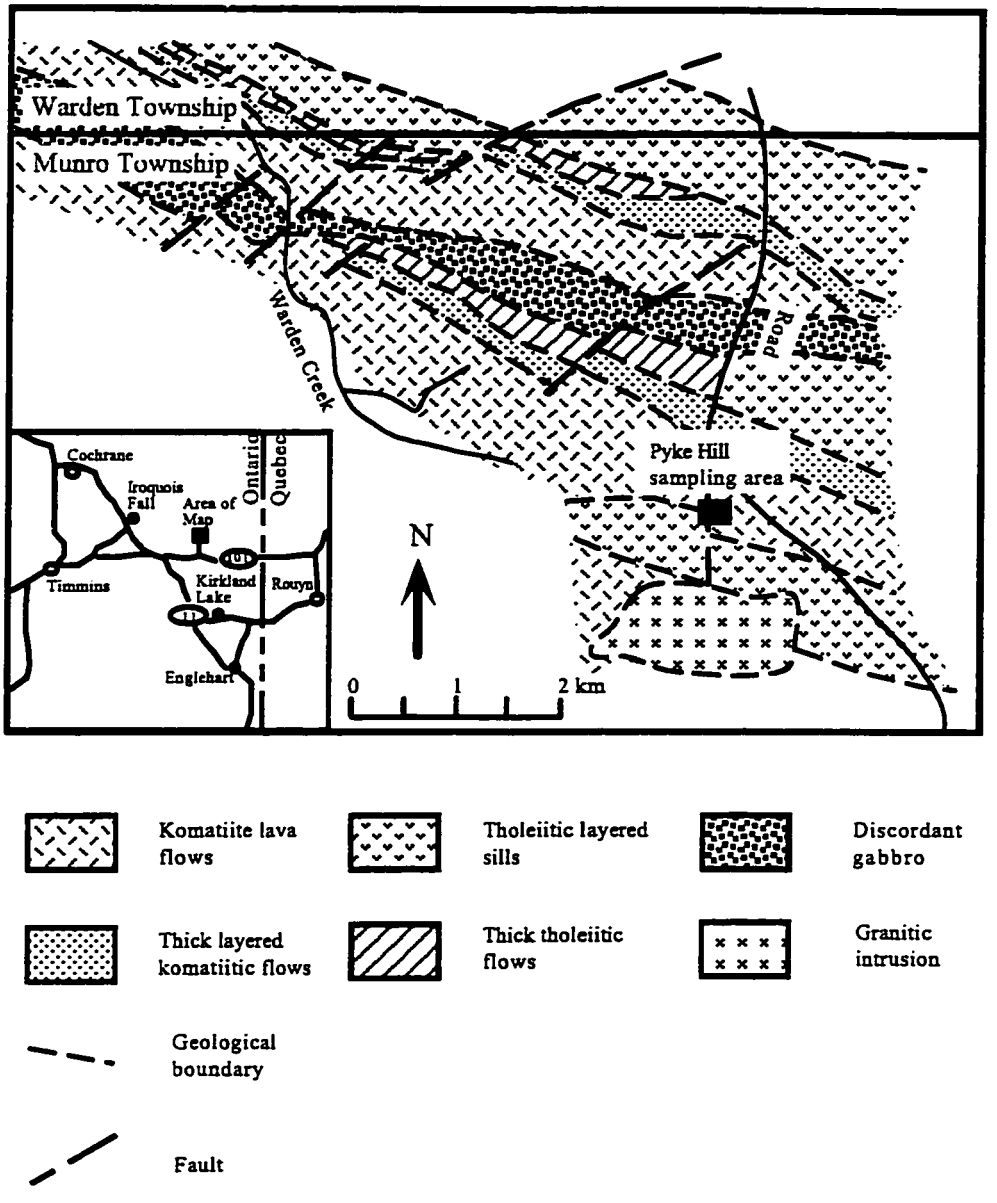

Figure 5-2. Simplified geological map of Munro Township. The Pyke Hill sampling area is highlighted (Modified from Pyke et al., 1978)

olivine cumulate zone, spinifex textured zone, and polysutured flow tops (Pyke et al., 1973; Arndt et al., 1977; Pyke, 1982). Komatiites consist mainly of olivine (Fo_{89} to Fo_{93}) and pyroxene (augite) [Pyke et al., 1973]. The primary minerals are completely serpentinized, although volcanic textures (i.e., spinifex texture and chilled flow top) are well preserved.

Mg-tholeiite is dominant in Munro Township (Figure 5-2). It occurs chiefly as massive flows, and is characterized by microporphyric pyroxene and plagioclase (Pyke et al., 1973; Arndt et al., 1977; Pyke, 1982). Fe-tholeiite is less abundant, and underlies Mg-tholeiite flows; the former is distinguished from Mg-tholeiite by pronounced high Fe and Ti contents (Pyke et al., 1973; Arndt et al., 1977). Two representative tholeiitic flows in Munro Township, i.e. Fred's flow (Mg-tholeiite) and Theo's flow (Fe-tholeiite) have been comprehensively discussed by Arndt (1977) and Arndt and Nesbitt (1982).

5-3-3 Komatiites and tholeiites from Boston Township

Boston Township is situated about 16 km south of Kirkland Lake, and is on the south side of the KLFZ (Figure 2-3 and 5-3). According to Jensen and Langford (1985), Boston komatiitic flows occur in the lower part of Cycle II of the "conventional" three volcanic cycles within the Abitibi SVZ (Figure 2-4). Subsequent dating, however, suggests that the volcanic sequence in Boston Township has a similar age as komatiite flows in Munro and Tisdale Townships (Figure 2-4; Corfu, 1993).

Boston komatiitic flows can be divided into 3 layers, or units from the base to top: (a) peridotite; (b) pyroxenite; and (c) spinifex textured lava flow (Stone et al., 1987, 1992). The komatiitic flow is underlain, as well as overlain, by Mg-tholeiites, which have distinct geochemical characteristics from komatiitic flows (Figure 5-3; see section 5-4).

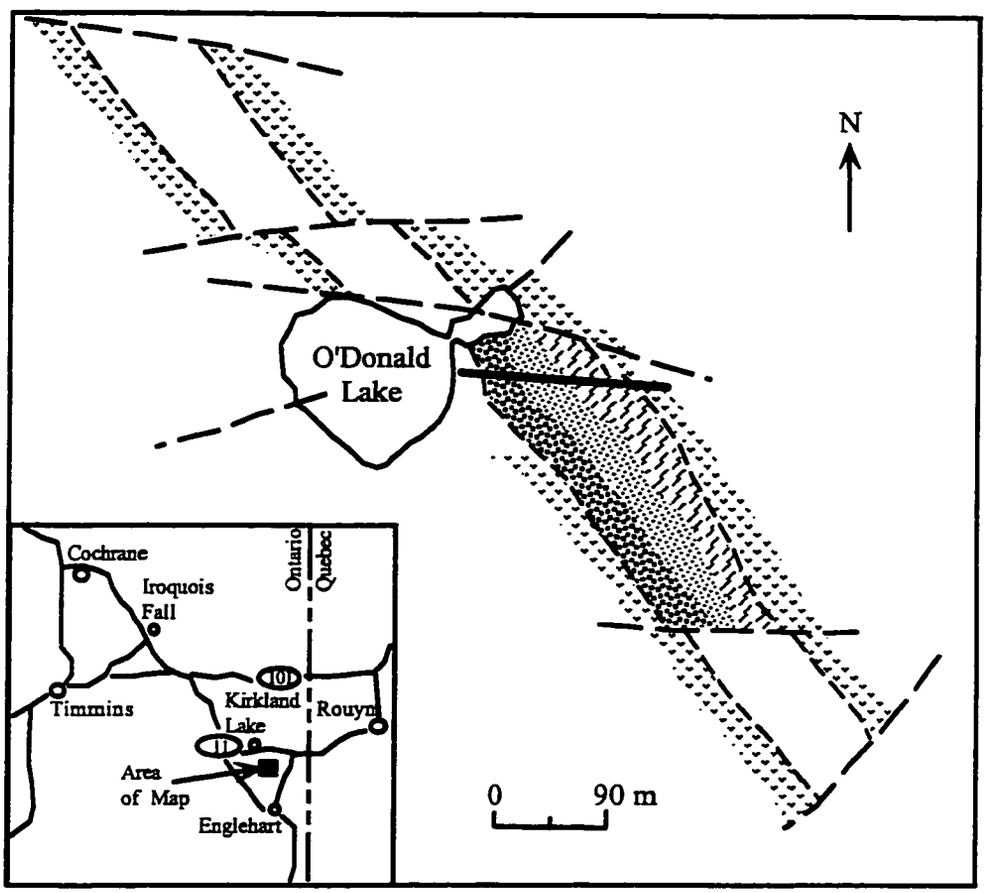

Olivine cumulate zone

Pyroxenite

Mg-tholeiite

Geological boundary

Spinifex textured flow tops

Inferred komatiitic flows

Sampling transect

Fault

Figure 5-3. Simplified geological map of Boston komatiite-tholeiite sequence (from Stone and Fleet, 1992)

Olivine and pyroxene are primary minerals in various zones of the komatiitic flows. Olivines are completely replaced by serpentine and magnetite, whereas pyroxenes are only partly altered to tremolite and chlorite. Well preserved pyroxene is widely present in peridotite and pyroxenite. The petrography and detailed mineralogical studies of Boston komatiites have been reported by Stone et al. (1987, 1992).

5-4 Geochemistry of the three komatiite-tholeiite sequences

Major elements were determined by XRF. REEs and HFSEs were analyzed using ICP-MS at the U. of Saskatchewan, following the techniques described by Jenner et al. (1990) and Longerich et al. (1990). All samples were hand crushed and comminuted to a powder using an agate mill. Details of the analytical techniques are presented in Chapters 3 and 4. The detection limits (in ppm), defined as 3σ of the procedural blank, for some critical elements, are as follows: Th (0.01), Nb (0.006), Hf (0.008), Zr (0.004), La (0.01), Ce (0.009), Nd (0.04), and Sm (0.03). Precision for most elements at the concentrations present in BIR-1 and unknowns is between 2-4% RSD, excepting Nb (RSD 6%). Five komatiite samples and one duplicate have been analyzed by INAA at the U. of Michigan and the Activition Labs., Ontario. The results are within error of the ICP-MS data (Table 5-1).

The new trace element data for Munro komatiites differ from previous results on the same komatiites (2 samples) for Nb, Zr, and Hf (Jochum et al., 1991), in which trace elements were determined by isotope dilution spark-source mass spectrometry (ID-SSMS), whereas there is excellent agreement for REEs. Nb, Zr, and Hf data for BIR-1 by ID-SSMS are apparently lower than preferred working values, as well as ICP-MS values of three different laboratories (Table 5-1), and this may also result in the absence of positive HFSE

Table 5-1. Comparison of the analysis of international reference material BIR-1 and replicate analyses of unknowns by instrumental neutron activation analysis

	BIR-1							komatiites				
	University of Saskatchewan			Jenner et al.(1990)	Hall and	Working values	Jochum et	Mp-1	Mp-4	Mp-6	B-1	B-2
	ICP-MS [a] HF-HNO3	ICP-MS [b] Laser Ablation	INAA [c]	ICP-MS HF-HNO3	Pelchat (1990) [d]	(Govindaraju, 1989)[e]	al. (1990) ID-SSMS	INAA	INAA	INAA	INAA	INAA
Th	0.05±0.01			0.036±0.005		(0.89	0.031					
Nb	0.71±0.16	0.6±0.04		0.59±0.05	1.5±0.07	2±0.5[f]	0.49					
Hf	0.62±0.02	0.6±0.08	0.6	0.60±0.03	0.64±0.02	0.58	0.36	0.5(0.43)[g]	0.3(0.29)	0.6(0.8)	0.5(0.35)	0.8(0.9)
Zr	15.6±0.3	13.2±1.39		16.3±0.4	18±0.36	22±7	12.1					
La	0.61±0.01	0.8±0.06	0.7	0.6±0.02		0.88	0.594	0.4(0.39)	0.2(0.17)	0.5(0.45)	4.4(3.6)	8.2(7.1)
Ce	1.93±0.03	2.3±0.8		1.87±0.05		(2.5	1.83					
Pr	0.38±0.02	0.4±0.04		0.36±0.01		(0.5	0.341					
Nd	2.53±0.03	2.6±0.7		2.3±0.1		2.5	2.19					
Sm	1.14±0.04	1.3±0.21	1.11	1.06±0.04		1.08[f]	1.07	0.55 (0.55)	0.39 (0.4)	0.72 (0.77)	1.04 (1.01)	1.78 (1.8)
Eu	0.53±0.02	0.5±0.07	0.56	0.56±0.04		0.54[f]	0.457					
Gd	1.92±0.07	1.6±0.28		1.73±0.06		1.9	1.52					
Tb	0.35±0.01	0.3±0.06	0.5	0.36±0.01		0.41	0.3					
Dy	2.65±0.06	2.7±0.23		2.69±0.05		2.4[f]	2.25					
Ho	0.57±0.01	0.5±0.1		0.61±0.01		0.5	0.55					
Er	1.74±0.03	1.8±0.18		1.70±0.05		1.8	1.5					
Tm	0.26±0.01	0.2±0.02		0.24±0.01		0.27	0.227					
Yb	1.70±0.04	1.6±0.26	1.64	1.63±0.05		1.7[f]	1.36	0.82 (0.74)	0.58 (0.56)	1.01 (1.05)	0.36 (0.38)	0.65 (0.68)
Lu	0.26±0.01	0.2±0.02	0.25	0.25±0.01		0.26[f]	0.227	0.13 (0.11)	0.09 (0.08)	0.19 (0.15)	0.06 (0.05)	0.09 (0.1)

All data are in ppm.

a Data are the average of 15 analyses during the course of this study, with ± 1σ (Xie et al., 1993, Xie and Kerrich, 1995b).

b Fedorowich et al., 1992.

c Calibrated against NBS 1633a coal fly ash.

d Analyzed by ICP-MS with LIBO2 fusion.

e Proposed values except those preceded by a parenthesis, which are information values.

f Recommended values.

g Numbers in parentheses are ICP-MS data.

anomalies relative to REEs for Munro komatiites in their data. Jochum et al. (1994) reported new trace element data for BIR-1 by ID-SSMS, which are close to ICP-MS data, but significantly higher than their original data (Jochum et al., 1994; see Chapters 3 and 4 for detailed discussion).

5-4-1 Major elements

Major element compositions, and Ni and Cr contents, of the three komatiite-tholeiite sequences are presented in Table 5-2. Komatiites from the Tisdale area are mainly Al-undepleted, with MgO=12-24 wt%, Al_2O_3/TiO_2=13-17, CaO/Al_2O_3=1.0-1.3, and high Ni (722-1275 ppm) and Cr (1875-2820 ppm) contents (Table 5-2; Figure 5-4). Two types of tholeiites, Mg- and Fe-tholeiites, are associated with komatiites, and have distinct trace element characteristics, as further discussed in Section 5-4-2.

At the Pyke Hill location in Munro Township (Figure 5-2), komatiites have relatively higher MgO contents (22-30 wt%), and are Al-undepleted, with Al_2O_3/TiO_2=17-20, CaO/Al_2O_3=1.0-1.2, Ni=831-1590 ppm, and Cr=1250-2760 ppm (Table 5-2; Figure 5-4). There are Mg-tholeiites and Fe-tholeiites associated with komatiites (Table 5-2; Figure 5-5). Arndt and Nesbitt (1982) described the distinct features of the two types of tholeiites.

Komatiites from Boston Township are different from those at the previous two localities, in that they are Al-depleted varieties, with MgO=11-29 wt%, Al_2O_3/TiO_2=4-5, CaO/Al_2O_3=1.4-2.5, high Ni (203-3420 ppm) and Cr (194-1965 ppm) [Table 5-2; Figure 5-4]. These features are similar to early Archean komatiites found in the Barberton greenstone belt, south Africa, and Newton Township, Abitibi SVZ. Another distinctive characteristic of Boston komatiites is the Fe enrichment, as indicated by higher Fe_2O_3 at similar MgO level

Table 5-2. Major element compositions of komatiites and tholeiites from the three volcanic sequences

	Tisdale Township														Munro Township		
	komatiites							tholeiites							komatiites		
	T1	T9	T10	T11	T2	T3	T12	T4	T5	T13	T14	T15	T7	T8	mp-1	mp-3	mp-4
	c	m	m	m	m	c	m	m	m	m	m	m	m	m	m	m	c
SiO2	46.2	49.5	48.7	49.1	46.8	38.0	45.9	54.7	55.9	49.6	54.6	51.3	50.7	45.7	43.2	43.8	42.1
TiO2	0.533	0.53	0.54	0.53	0.49	0.42	0.485	1.410	1.230	0.941	1.301	0.622	0.642	0.53	0.31	0.333	0.213
Al2O3	7.07	8.86	8.26	8.82	8.04	6.77	6.87	15.20	13.60	12.90	14.20	15.63	15.40	14.80	5.75	5.75	3.95
Fe2O3 *	13.3	11.2	12.2	10.5	12.7	11.9	12.4	10.9	10.7	13.7	9.9	13.1	13.6	12.7	10.7	10.4	9.92
MgO	19.2	13.0	16.4	12.3	15.1	23.8	20.5	4.63	5.50	7.55	5.41	5.71	5.8	6.1	28.7	28.3	30
CaO	8.84	9.45	8.30	10.75	9.81	8.35	8.28	6.74	5.34	7.32	6.88	7.58	7.40	11.40	5.77	5.84	4.64
Na2O	0.21	2.72	1.46	2.66	1.52	0.11	0.01	3.61	4.27	2.04	4.17	2.39	2.58	1.87	0.29	0.24	0.01
K2O	0.07	0.02	0.02	0.03	0.01	0.01	0.01	0.23	0.11	0.74	0.16	0.04	0.06	0.05	0.07	0.1	0.01
P2O5	0.05	0.05	0.04	0.04	0.05	0.04	0.04	0.13	0.11	0.08	0.13	0.06	0.07	0.06	0.03	0.03	0.03
MnO	0.29	0.21	0.22	0.21	0.27	0.21	0.21	0.21	0.26	0.18	0.25	0.29	0.30	0.40	0.18	0.17	0.21
LOI	4.47	4.39	3.90	5.17	5.08	10.00	5.45	2.70	2.65	3.30	2.99	3.30	3.70	6.93	4.65	5.3	8.95
Sum	100.2	99.9	100.0	100.0	99.9	99.6	100.2	100.5	99.7	98.4	100.0	100.0	100.3	100.6	99.7	100.3	100.0
Mg #	85	82	84	82	82	89	87	63	67	69	68	63	63	65	91	92	92
Al2O3/TiO2	13.3	16.6	15.2	16.8	16.3	16.0	14.2	10.8	11.1	13.7	10.9	25.1	24.0	27.7	18.3	17.3	18.5
CaO/Al2O3	1.3	1.1	1.0	1.2	1.2	1.2	1.2	0.4	0.4	0.6	0.5	0.5	0.5	0.8	1.0	1.0	1.2
Ni	847	838	589	801	890	1275	722	100	225	120	354	108	102	160	1295	1375	1590
Cr	2590	2820	1875	2450	2430	2220	2290	50	121	293	39	38	27	136	1250	1515	1850

(Table 5-2 continued)

	Munro Township										Boston Township						
	komatiites		tholeiites								komatiites			tholeiites			
	mp-6	mp-7	mp-13	mp-14	mp-15	mp-17	mp-18	mp-20	mp-22	mp-23	B-8	B-1	B-2	B-4	B-5	B-6	B-7
	s	s	m	m	m	m	m	m	m	m	s	c	s	m	m	m	m
SiO2	44.4	44.5	42	49.5	56.6	52.1	54.1	49.9	47.7	46.1	47.1	37.1	42	44.7	44.2	51.2	49.5
TiO2	0.397	0.39	0.376	0.886	1.5	1.91	1.62	1.41	1.84	1.61	1.05	0.385	0.755	1.39	1.93	0.795	0.872
Al2O3	7.59	7.62	6.07	7.08	12.1	13	12	11.7	12	13.6	5.67	1.7	3.37	6.9	6.45	15.4	14.3
Fe2O3*	11.9	11.9	10.7	13.5	12.5	18.5	15	15.9	16.1	16.3	14.8	17.8	17.1	18.7	22.7	16.7	20.7
MgO	23.2	22.3	27.1	12.6	3.03	2.25	2.55	6.05	6.78	6.74	11.2	29.4	22.7	9.8	7.88	2.17	2.55
CaO	7.55	8.1	5.61	11.4	5.45	5.97	7.02	8.84	8.11	10	14.3	2.43	6.67	12.2	11.8	6.04	5.37
Na2O	0.73	0.58	0.14	1.28	5.04	4.27	5.08	3.15	1.49	1.25	0.65	0.01	0.07	1.29	1.35	5.28	5.06
K2O	0.19	0.17	0.09	0.12	0.17	0.32	0.16	0.57	0.89	0.06	0.52	0.01	0.03	0.37	0.6	0.41	0.44
P2O5	0.04	0.04	0.04	0.08	0.03	0.22	0.2	0.14	0.14	0.11	0.08	0.04	0.06	0.09	0.08	0.2	0.21
MnO	0.19	0.19	0.17	0.24	0.21	0.26	0.26	0.28	0.19	0.2	0.23	0.27	0.24	0.25	0.27	0.27	0.28
LOI	3.95	4.4	6.75	1.8	1.9	1.05	0.9	1.75	3.5	4.1	2.7	9.2	5.6	2.95	2.7	1.1	0.65
Sum	100.1	100.2	99.0	98.5	98.5	99.9	98.9	99.7	98.7	100.1	98.3	98.35	98.6	98.6	100	99.57	99.93
Mg #	89	88	91	79	49	33	40	60	63	62	75	87	84	67	58	34	33
Al2O3/TiO2	19.1	19.5	16.1	8.0	8.1	6.8	7.4	8.3	6.5	8.4	5.4	4.4	4.5	5.0	3.3	19.4	16.4
CaO/Al2O3	1.0	1.1	0.9	1.6	0.5	0.5	0.6	0.8	0.7	0.7	2.5	1.4	2.0	1.8	1.8	0.4	0.4
Ni	904	831	1190	362	41	10	3	61	35	68	203	3420	2730	508	127	8	8
Cr	2360	2760	1125	922	44	17	9	28	92	100	194	1965	1520	262	27	3	5

Major elements in wt%; Ni and Cr in ppm. Rock type, elements, and structures (c, cumulate; m, massive; s, spinifex textured zone) are given for each location. LOI, loss on ignition.

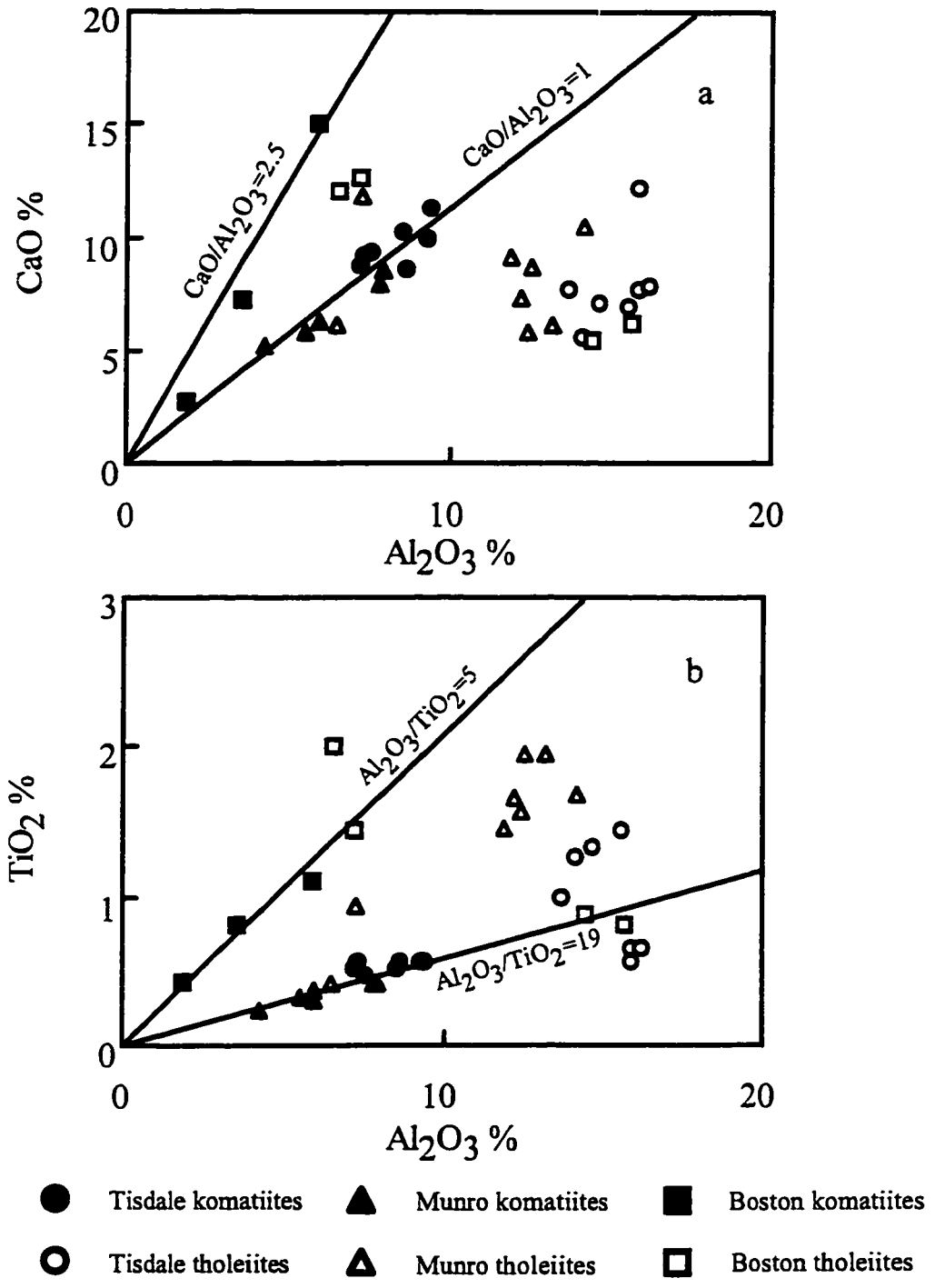

Figure 5-4. CaO-Al_2O_3 (a) and TiO_2-Al_2O_3 (b) plots for the three komatiite-tholeiite sequences, clearly showing Al-depletion, as reflected in high CaO/Al_2O_3 but low Al_2O_3/TiO_2 ratios, in Boston komatiites and Fe-tholeiites. Chondritic CaO/Al_2O_3 (1) and Al_2O_3/TiO_2 (19) lines indicated.

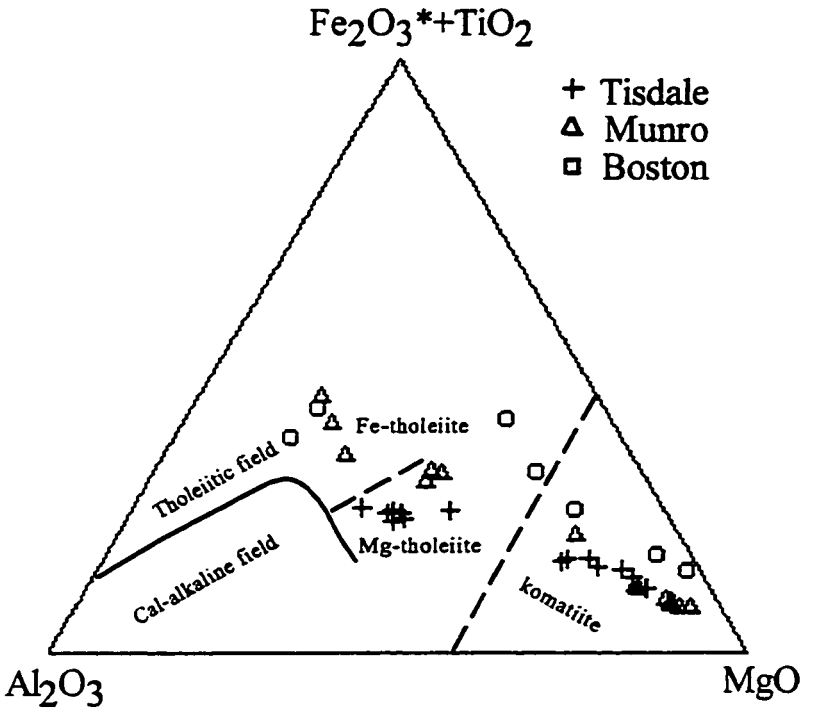

Figure 5-5. Cation triangular plot of komatiites and tholeiites from the three volcanic sequences in the Abitibi SVZ. Field of rock types is from Jensen (1976). Modified from Jensen (1976) using komatiite terminology of Arndt and Nisbet (1982).

(Table 5-2; Figure 5-5).

Plots of oxides versus MgO show that komatiite samples approximately define a negative correlation of SiO_2-, CaO- and Al_2O_3- with MgO, stemming from olivine fractional crystallization (Figures 5-6a, b, c). The positive correlation between Fe_2O_3-MgO and Cr-MgO in Boston komatiite samples also suggest that chromite may have crystallized along with olivine at an early stage, apparently due to high-Fe concentrations in Boston komatiites, whereas chromite seems to have precipitated after olivine in Tisdale and Munro komatiites, as indicated by the weak negative Fe_2O_3-MgO and Cr-MgO correlation (Figures 5-6d, f).

Some samples listed in Table 5-2 have MgO < 18 wt%, yet are inferred to be komatiite on the basis of spinifex textures and independent geochemical criteria of less mobile elements. For example, sample T9 has an MgO content of only 13 wt%, yet high Ni (838 ppm) and Cr (2820 ppm) contents, and low abundances of REEs (see Section 5-4-2), with a pattern coherent with other high MgO and Ni and Cr abundance samples from the same locality (Table 5-3).

5-4-2 Trace elements

All trace element data for the three komatiite-tholeiite sequences, including REEs and HFSEs, are listed in Table 5-3, along with some geochemically significant interelement ratios.

Al-undepleted komatiites from Tisdale area have flat REE patterns with $(La/Yb)_n$=0.5-1.2 and $\sum$REE=9-23 (Table 5-3; Figure 5-7a). Mg-tholeiites have similar REE patterns as the komatiites, but are enriched overall (Table 5-3; Figure 5-7a), whereas Fe-tholeiites have slight LREE depletion [$(La/Yb)_n$=0.3-0.5; Figure 5-7a].

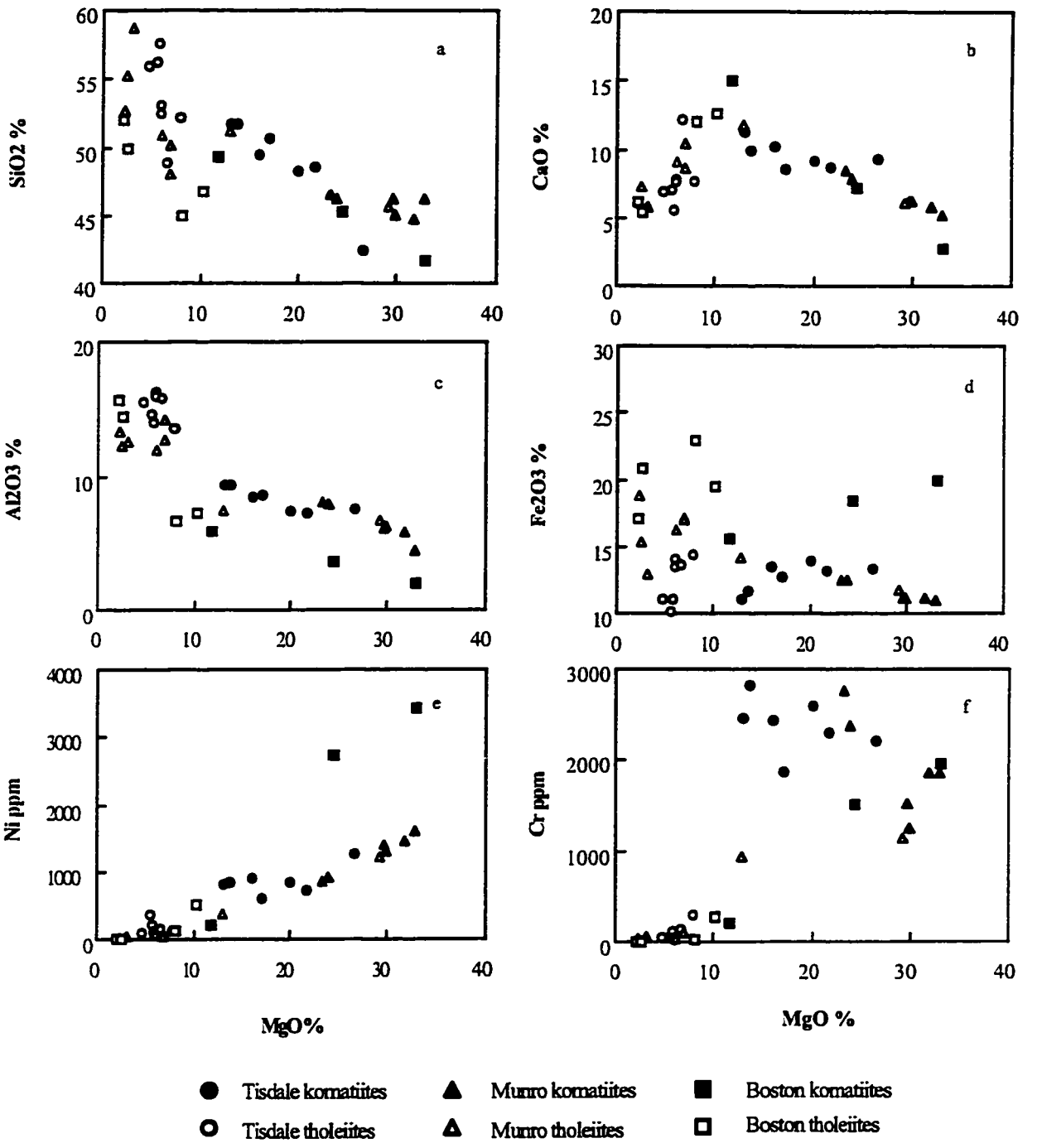

Figure 5-6. Selected oxide compositions of komatiites and tholeiites from the three sequences in Abitibi greenstone belt, plotted versus MgO

Table 5-3. Trace element compositions of komatiites and tholeiites from the three volcanic sequences [a]

Location	Tisdale Township															
Rock type	Komatiites								tholeiites							
Elements	T1	T9	T10	T11	T2	T3	T12	T16	T4	T5	T13	T14	T16	T15	T7	T8
Sc	34.10	26.25	34.24	34.10	33.34	21.13	27.78	37.12	50.59	46.60	45.36	45.35	43.38	71.74	75.20	47.88
V	217	217	209	210	212	163	172	239	426	346	305	355	343	293	297	240
Y	9.89	11.1	10.6	10.6	10.3	5.44	8.15	14.3	36.6	31	23.5	34.5	31.2	23.2	25.9	23.4
Zr	30.3	27.5	26.8	28.2	28.8	13.8	24.4	29.6	89.5	68.2	47.9	79.8	71.1	39.4	39.4	25.3
Nb	1.59	0.99	1.05	1.09	0.93	0.79	1.14	1.5	4.20	3.26	2.33	3.67	3.07	1.8	1.90	1.75
Hf	0.80	0.77	0.91	0.78	0.82	0.45	0.72	1	2.44	1.87	1.39	2.45	2.36	1.1	1.02	0.66
Th	0.72	0.13	0.12	0.1	0.31	0.11	0.12	0.13	0.69	0.39	0.24	0.43	0.38	0.28	0.36	0.26
La	1.66	0.96	1.04	1.18	0.94	0.65	1.07	1.55	4.28	3.89	2.8	3.95	4.66	2.32	2.29	1.54
Ce	4.07	3.10	3.19	3.16	2.81	1.89	2.98	4.64	11.4	10.8	7.61	11.5	12.2	6.39	6.25	4.72
Pr	0.62	0.54	0.54	0.5	0.5	0.33	0.52	0.82	1.87	1.65	1.24	1.85	1.89	0.95	0.94	0.78
Nd	3.62	3.30	3	2.56	2.61	1.97	2.9	4.58	9.97	9.25	7.08	9.72	9.51	4.6	5.27	3.85
Sm	1.20	1.01	1.05	0.92	1.08	0.61	1.02	1.54	3.36	3.02	2.28	3.29	3.09	1.4	1.57	1.28
Eu	0.44	0.47	0.41	0.43	0.43	0.15	0.36	0.7	1.01	0.88	0.88	1	1.1	0.47	0.49	0.43
Gd	1.64	1.65	1.65	1.6	1.53	0.82	1.37	2.3	3.77	4.2	3.32	4.6	4.42	2.04	2.17	1.97
Tb	0.28	0.31	0.28	0.27	0.27	0.14	0.23	0.37	0.77	0.7	0.54	0.8	0.77	0.41	0.43	0.40
Dy	1.81	2.05	1.97	1.99	1.73	1.09	1.6	2.74	5.59	5.44	3.93	6.06	5.52	3.54	3.65	3.22
Ho	0.39	0.44	0.43	0.44	0.35	0.20	0.32	0.53	1.30	1.17	0.87	1.32	1.21	0.87	0.91	0.87
Er	1.11	1.21	1.25	1.32	1.04	0.57	0.89	1.57	3.87	3.5	2.65	4.16	3.78	3.05	3.17	2.91
Tm	0.15	0.17	0.19	0.19	0.15	0.09	0.15	0.25	0.63	0.55	0.4	0.65	0.57	0.51	0.50	0.5
Yb	0.97	1.22	1.14	1.2	1.02	0.59	0.82	1.51	4.04	3.58	2.72	4.38	3.87	3.8	3.40	3.43
Lu	0.15	0.13	0.19	0.17	0.15	0.10	0.12	0.24	0.59	0.55	0.4	0.66	0.6	0.59	0.48	0.54
ΣREE	18.1	16.6	16.3	15.9	14.6	9.2	14.4	23.3	52.5	49.1	36.7	53.9	53.2	30.9	31.5	26.4
(La/Sm)n	0.87	0.60	0.62	0.81	0.55	0.67	0.66	0.63	0.80	0.81	0.77	0.76	0.95	1.04	0.92	0.76
(Gd/Yb)n	1.37	1.10	1.17	1.08	1.22	1.13	1.35	1.23	0.76	0.95	0.99	0.85	0.93	0.44	0.52	0.47
(La/Yb)n	1.2	0.5	0.6	0.7	0.6	0.7	0.9	0.7	0.7	0.7	0.7	0.6	0.8	0.4	0.5	0.3
Eu/Eu*	1.0	1.1	0.9	1.1	1.0	0.6	0.9	1.1	0.9	0.8	1.0	0.8	0.9	0.8	0.8	0.8
Nb/Nb*	0.98	0.91	0.92	0.91	0.92	1.14	1.02	0.90	0.96	0.81	0.81	0.87	0.65	0.75	0.81	1.04
Zr/Zr*	1.02	1.05	1.05	1.28	1.19	0.87	0.99	0.78	1.08	0.90	0.83	0.98	0.92	1.08	0.98	0.80
Hf/Hf*	0.97	1.07	1.30	1.29	1.23	1.04	1.06	0.95	1.07	0.90	0.88	1.10	1.10	1.10	0.92	0.75

a All elements are in ppm.

(Table 5-3 continued)

Location	Munro Township																			
Rock type	Komatiites												Tholeiites							
Elements	mp-1	mp-3	mp-4	mp-5	mp-6	mp-7	mp-2	mp-8	mp-9	mp-10	mp-11	mp-12	mp-13	mp-14	mp-15	mp-17	mp-18	mp-20	mp-22	mp-23
Sc	21.56	22.69	15.58	20.25	27.64	27.65	28.38	23.22	14.87	15.31	27.27	27.81	21.09	28.13	18.26	18.17	17.61	25.16	49.43	44.66
V	127	128	83	114	179	170	122	120	69	78	152	153	121	198	89	68	88	251	413	397
Y	6.28	6.26	5.18	5.68	8.07	8.28	5.77	5.97	3.54	3.63	7.73	7.83	7.74	13.8	34.3	41.4	33.8	25.9	37.6	29
Zr	12.2	13.1	8.8	12.1	18.0	17.1	11.6	12.2	6.1	7.7	16.0	15.7	21.9	57.3	126	169	158	116	116	82.5
Nb	0.50	0.47	0.36	0.34	0.47	0.44	0.61	0.47	0.29	0.33	0.51	0.47	0.90	3.20	9.01	11.6	10.6	7.18	5.83	4.72
Hf	0.43	0.61	0.29	0.40	0.80	0.63	0.39	0.39	0.28	0.2	0.42	0.56	0.69	1.88	3.74	4.7	4.33	3.22	3.22	2.57
Th	0.10	0.17	0.07	0.07	0.16	0.09	0.05	0.05	0.05	0.06	0.05	0.08	0.16	0.43	0.61	1.04	0.93	0.72	0.49	0.39
La	0.39	0.33	0.17	0.30	0.45	0.42	0.26	0.26	0.1	0.16	0.32	0.32	1.15	3.57	5.18	12.3	7.73	7.99	6.48	4.55
Ce	1.12	1.02	0.50	0.86	1.39	1.32	0.86	0.86	0.37	0.58	1.08	1.13	2.99	9.87	19	34.4	23.5	21.4	17.2	12.6
Pr	0.20	0.19	0.10	0.17	0.25	0.23	0.16	0.16	0.08	0.1	0.19	0.23	0.47	1.57	3.49	5.36	3.8	3.25	2.64	2
Nd	1.22	1.08	0.71	1.02	1.67	1.53	0.94	0.89	0.48	0.65	1.12	1.32	2.45	8.41	19.9	26.7	20.3	16.6	14	10.4
Sm	0.55	0.47	0.40	0.47	0.77	0.69	0.46	0.42	0.27	0.28	0.56	0.6	0.84	2.41	5.96	7.39	5.74	4.49	4.44	3.41
Eu	0.21	0.20	0.11	0.20	0.30	0.28	0.19	0.19	0.12	0.1	0.22	0.23	0.28	0.75	1.71	2.1	2.23	1.47	1.39	1.2
Gd	0.88	1.12	0.68	0.76	1.24	1.15	0.72	0.73	0.47	0.45	0.87	1.02	1.19	2.93	6.93	8.29	6.65	5.09	5.63	4.69
Tb	0.16	0.15	0.13	0.14	0.22	0.21	0.14	0.13	0.08	0.09	0.17	0.18	0.20	0.44	1.08	1.26	1.01	0.79	0.97	0.79
Dy	1.14	1.11	0.96	1.02	1.63	1.62	0.95	0.99	0.62	0.69	1.24	1.3	1.43	3.01	6.98	8.15	6.59	5.17	6.97	5.52
Ho	0.24	0.24	0.20	0.21	0.35	0.35	0.21	0.22	0.13	0.15	0.27	0.27	0.30	0.57	1.33	1.58	1.29	1.01	1.45	1.15
Er	0.80	0.74	0.59	0.68	1.08	1.00	0.64	0.67	0.36	0.45	0.82	0.8	0.99	1.68	3.73	4.53	3.69	2.86	4.43	3.56
Tm	0.11	0.11	0.09	0.10	0.16	0.16	0.1	0.11	0.06	0.06	0.12	0.13	0.15	0.23	0.53	0.65	0.55	0.43	0.66	0.53
Yb	0.74	0.72	0.56	0.65	1.05	1.04	0.61	0.63	0.39	0.41	0.73	0.85	0.98	1.54	3.31	4.05	3.53	2.77	4.26	3.41
Lu	0.11	0.10	0.08	0.10	0.15	0.16	0.1	0.1	0.06	0.07	0.12	0.13	0.15	0.22	0.51	0.6	0.53	0.41	0.64	0.51
Σ REE	7.9	7.6	5.3	6.7	10.7	10.2	6.3	6.4	3.6	4.2	7.8	8.5	13.6	37.2	79.6	117	87.1	73.6	71.2	54.3
(La/Sm)n	0.45	0.44	0.27	0.40	0.37	0.38	0.36	0.39	0.23	0.36	0.36	0.34	0.86	0.93	0.55	1.05	0.85	1.12	0.92	0.84
(Gd/Yb)n	0.96	1.26	0.98	0.95	0.96	0.90	0.96	0.94	0.98	0.89	0.97	0.97	0.98	1.54	1.70	1.66	1.53	1.49	1.07	1.11
(La/Yb)n	0.4	0.3	0.2	0.3	0.3	0.3	0.3	0.3	0.2	0.3	0.3	0.3	0.8	1.6	1.1	2.1	1.5	1.9	1.0	0.9
Eu/Eu*	0.9	0.8	0.6	1.0	0.9	1.0	1.0	1.0	1.0	0.9	1.0	0.9	0.9	0.9	0.8	0.8	1.1	0.9	0.8	0.9
Nb/Nb*	1.21	1.30	1.98	1.07	0.95	0.94	2.06	1.58	2.38	1.72	1.38	1.24	0.78	0.87	1.44	0.90	1.26	0.88	0.89	1.00
Zr/Zr*	1.02	1.27	1.11	1.20	1.09	1.15	1.21	1.37	1.13	1.25	1.38	1.22	1.07	0.89	0.81	0.84	1.02	0.93	1.02	0.97
Hf/Hf*	1.31	2.15	1.33	1.44	1.76	1.53	1.47	1.59	1.90	1.18	1.31	1.57	1.22	1.06	0.87	0.84	1.01	0.94	1.03	1.09

(Table 5-3 continued)

Location	Boston Township																	
Rock type	Komatiites					Tholeiites												
Elements	B-8	B-9	B-1	B-2	B-10	B-4	B-5	B-6	B-7	B-11	B-12	B-13	B-14	B-15	B-16	B-17	B-18	B-19
Sc	57.17	11.22	12.22	18.80	14.82	35.62	30.12	6.02	4.24	40.17	52.65	42.96	42.87	41.38	40.75	39.97	77.21	41.12
V	243	72	72	133	77	264	331	12	18	286	305	280	360	366	358	350	343	300
Y	13.4	3.71	3.55	6.45	4.31	14.7	13.1	30.1	25.2	15.1	12.2	14.9	21.6	24.8	23.1	22.4	20.9	21.2
Zr	52.0	14.9	12.2	32.5	16.4	64.5	57.3	141	121	68.3	51.1	60.1	28.5	79.3	80.6	53	41.3	45
Nb	9.46	3.48	3.14	6.29	3.61	11.6	10.2	26.1	22.5	12	8.53	11.5	2.73	4.2	4.2	3.77	2.75	2.65
Hf	1.49	0.46	0.35	0.91	0.49	1.77	1.62	3.5	3.05	1.87	1.63	1.88	1.23	2.2	2.49	1.75	1.22	1.41
Th	0.78	0.29	0.36	0.69	0.33	1.01	0.76	2.6	2.06	0.99	0.76	0.99	0.34	0.54	0.49	0.55	0.2	0.22
La	11	4.08	3.61	7.14	3.85	12.7	10	31.3	19.8	13.8	9.96	9.26	3.09	4.6	4.04	5.07	2.8	2.77
Ce	24.3	8.88	8.05	15.6	8.46	28	23	69.1	44.4	31.5	22.6	23	8.77	12.5	10.6	12.9	7.93	8.03
Pr	3.32	1.15	1.07	2.04	1.15	3.8	3.15	8.9	5.9	4.22	3.13	3.46	1.45	1.99	1.68	1.92	1.27	1.31
Nd	14.7	4.73	4.76	9.20	5.08	17	14.3	37.4	25.5	17.7	13.7	15.4	7.93	9.65	8.19	9.25	6.93	6.85
Sm	3.21	1.09	1.01	1.86	1.07	3.63	3.11	7.41	5.38	4.08	3.23	3.92	2.61	2.98	2.65	2.93	2.5	2.33
Eu	1.24	0.25	0.27	0.48	0.31	1.18	0.98	2.31	1.71	1.31	0.91	1.28	0.78	1.12	1.13	0.85	0.86	0.83
Gd	3.33	1	0.94	1.80	1.06	3.54	3.06	6.97	5.35	3.74	3.27	3.81	3.66	3.87	3.7	3.54	3.3	3.35
Tb	0.46	0.14	0.13	0.24	0.16	0.5	0.44	1	0.8	0.51	0.45	0.51	0.6	0.63	0.62	0.62	0.56	0.56
Dy	2.97	0.85	0.79	1.51	0.94	3.06	2.72	6.36	5.11	3.19	2.73	3.35	4.43	4.75	4.5	4.44	4.02	3.93
Ho	0.55	0.16	0.14	0.27	0.18	0.58	0.52	1.21	1.01	0.62	0.52	0.6	0.89	1.01	0.97	0.92	0.81	0.84
Er	1.53	0.44	0.42	0.79	0.5	1.62	1.39	3.41	2.91	1.77	1.49	1.72	2.72	2.95	2.85	2.83	2.47	2.47
Tm	0.22	0.07	0.06	0.11	0.07	0.22	0.2	0.5	0.42	0.26	0.2	0.23	0.39	0.45	0.45	0.4	0.37	0.39
Yb	1.32	0.36	0.38	0.68	0.43	1.39	1.24	3.03	2.62	1.56	1.27	1.51	2.49	2.99	2.84	2.75	2.39	2.52
Lu	0.2	0.06	0.05	0.10	0.07	0.21	0.19	0.45	0.4	0.23	0.2	0.23	0.35	0.46	0.44	0.39	0.33	0.34
Σ REE	68.4	23.3	21.7	41.8	23.3	77.5	64.2	179	121	84.5	63.6	68.3	40.2	50	44.7	48.9	36.5	36.5
(La/Sm)n	2.16	2.36	2.25	2.42	2.26	2.20	2.03	2.66	2.31	2.13	1.94	1.49	0.75	0.97	0.96	1.09	0.70	0.75
(Gd/Yb)n	2.04	2.25	2.00	2.15	2.00	2.06	2.00	1.86	1.65	1.94	2.09	2.04	1.19	1.05	1.06	1.04	1.12	1.08
(La/Yb)n	5.6	7.7	6.4	7.1	6.1	6.2	5.5	7.0	5.1	6.0	5.3	4.1	0.89	1.1	1.02	1.32	0.84	0.79
Eu/Eu*	1.2	0.7	0.8	0.8	0.9	1.0	1.0	1.0	1.0	1.0	0.8	1.0	0.77	1.01	1.1	1.14	0.91	0.91
Nb/Nb*	0.93	0.92	0.93	0.95	1.01	0.98	1.08	0.90	1.21	0.92	0.91	1.26	0.84	0.88	1.03	0.75	0.93	0.9
Zr/Zr*	0.52	0.45	0.38	0.53	0.48	0.56	0.59	0.57	0.70	0.55	0.53	0.54	0.44	1.03	1.02	0.71	0.7	0.8
Hf/Hf*	0.54	0.51	0.40	0.54	0.52	0.56	0.60	0.52	0.64	0.55	0.61	0.61	0.68	1.03	1.05	0.85	0.75	0.9

Al-undepleted komatiites from Pyke Hill are characterized by pronounced LREE depletions, with $(La/Yb)_n$=0.2-0.4 (Table 5-3; Figure 5-7b). Associated Mg-tholeiites are characterized by flat or slightly LREE enriched patterns, where $(La/Yb)_n$=1-2. Arndt and Nesbitt (1982) reported similar REE features for these komatiites and tholeiites.

Komatiites in Boston Township feature characteristic HREE depletions where $(La/Yb)_n$=6-8 (Table 5-3; Figure 5-7c). Spatially associated tholeiites share similar patterns with the komatiites but are relatively enriched (Figure 5-7c). In contrast, Mg-tholeiites underlying and overlying komatiitic flows have flat REE patterns, with $(La/Yb)_n$=0.8-1.1 (Table 5-3; Figure 5-7c), similar to that of Tisdale komatiites and Mg-tholeiites.

The interrelationships between HFSEs and REEs for the three komatiite-tholeiite sequences are also distinct, as illustrated in Figures 5-8 and 5-9. Fractionations between Nb, Zr, Hf, and REE are expressed as normalized values (Nb/Nb*, Zr/Zr*, and Hf/Hf*), defined as $2 \times Nb_n/(La+Ce)_n$, $2 \times Zr_n/(Nd+Sm)_n$ and $2 \times Hf_n/(Nd+Sm)_n$, calculated using the primitive mantle normalized values of neighbouring REEs in the incompatibility sequence of elements in MORB (Salters and Shimizu, 1988). Considering the possible mobility of Th during hydrothermal alteration, the Nb anomaly is defined relative to La and Ce, instead of Th and La. Although Ce may be mobile during alteration, the REE patterns of all samples studied are smooth between La and Pr, signifying little or no redistribution of Ce.

Komatiites and Mg-tholeiites from the Tisdale area have $(La/Yb)_n$=0.6-1.2, and Nb/Nb*, Zr/Zr*, and Hf/Hf* all $\approx$ 1, and accordingly there are no normalized fractionations of Nb, Zr, and Hf relative to neighbouring REEs in these Mg-rich volcanic rocks (Table 5-3; Figures 5-8 and 5-9). Three Fe-tholeiite samples that show slight LREE and Hf depletions are exceptions (Figures 5-7a and 5-8a). Consequently, komatiites and Mg-tholeiites could

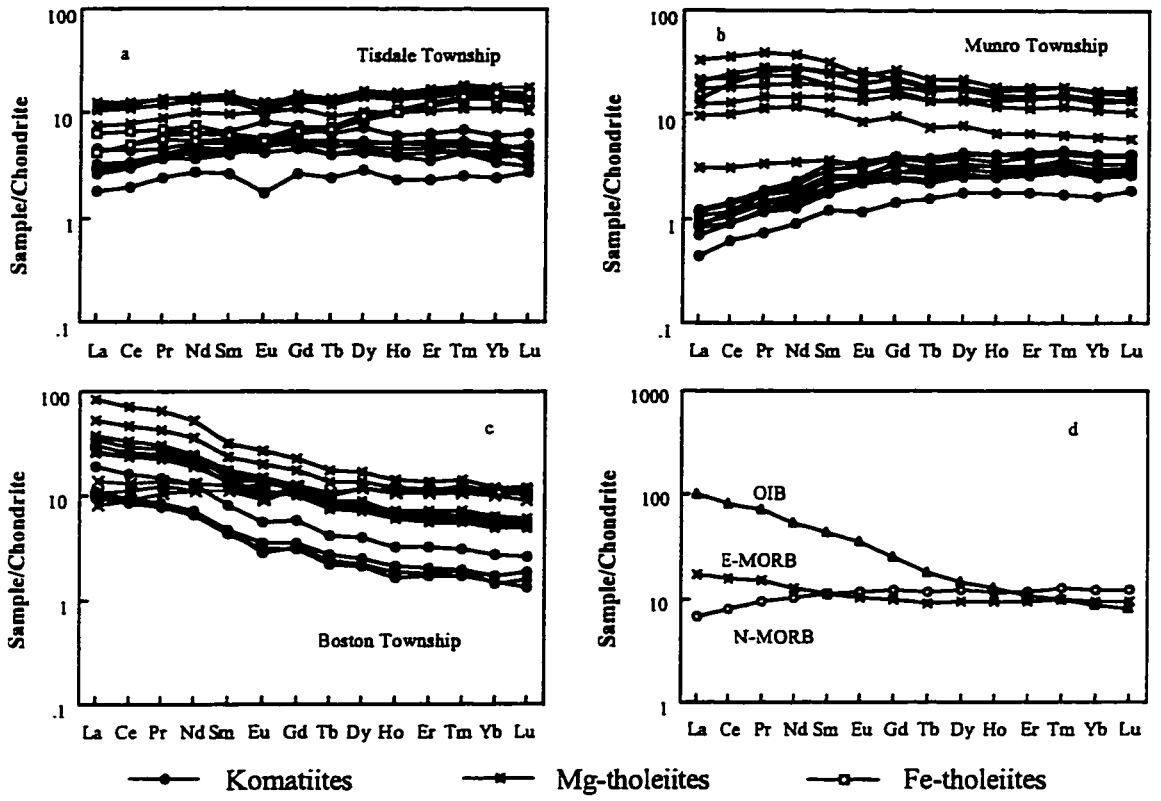

Figure 5-7. REE patterns of komatiites and tholeiites from the three locations in the Abitibi Southern Volcanic Zone. (a) Tisdale Township; (b) Munro Township; (c) Boston Township. (d) The REE patterns of normal mid-ocean ridge basalt (N-MORB), enriched mid-ocean ridge basalt (E-MORB) and oceanic island basalt (OIB) are also shown for comparison (from Sun and McDonough, 1989).

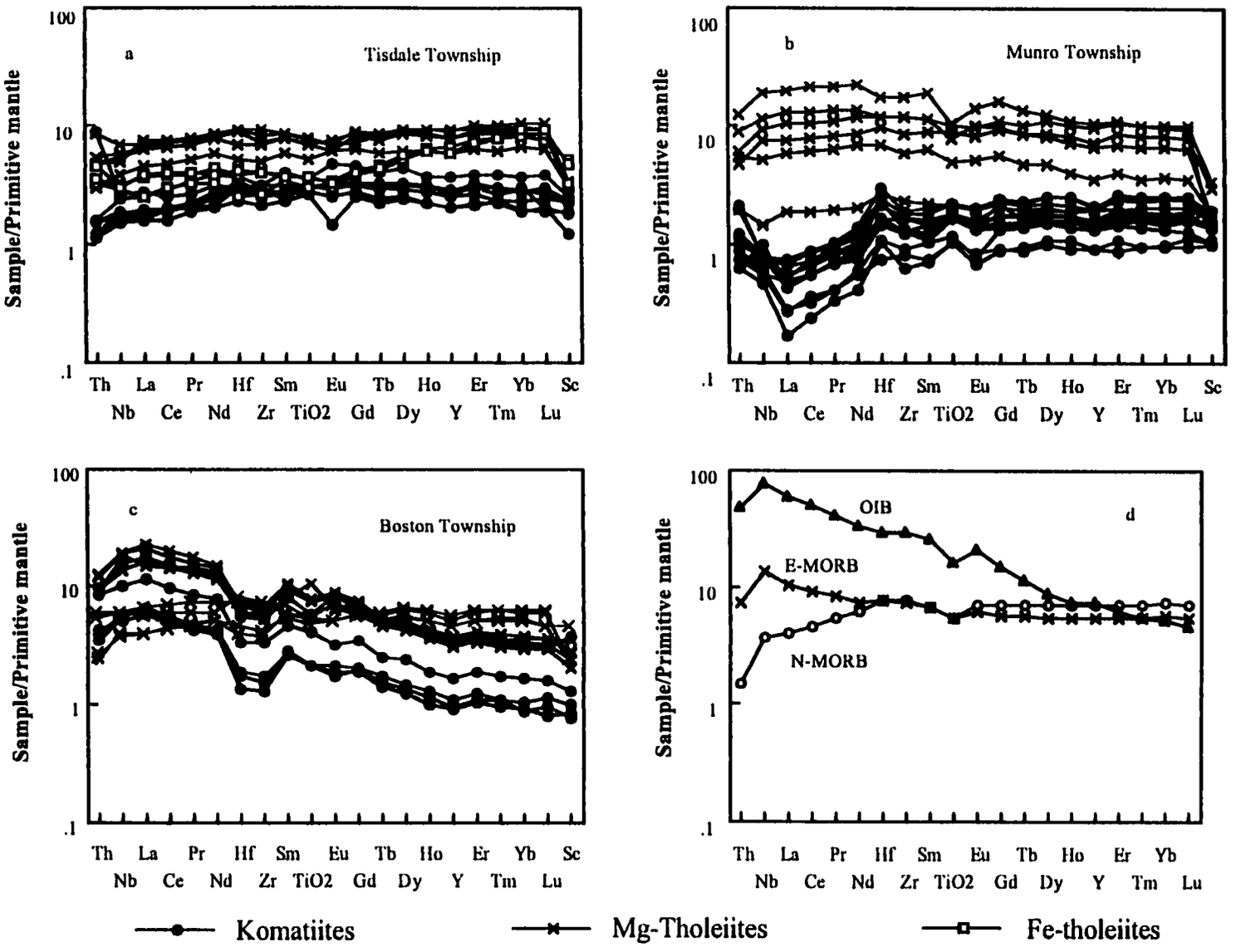

Figure 5-8. Primitive mantle normalized diagrams for the three komatiite-basalt sequences. Primitive mantle values are from Sun and McDonough (1989). (a) Tisdale Township; (b) Munro Township; (c) Boston Township; (d) N-MORB, E-MORB and OIB.

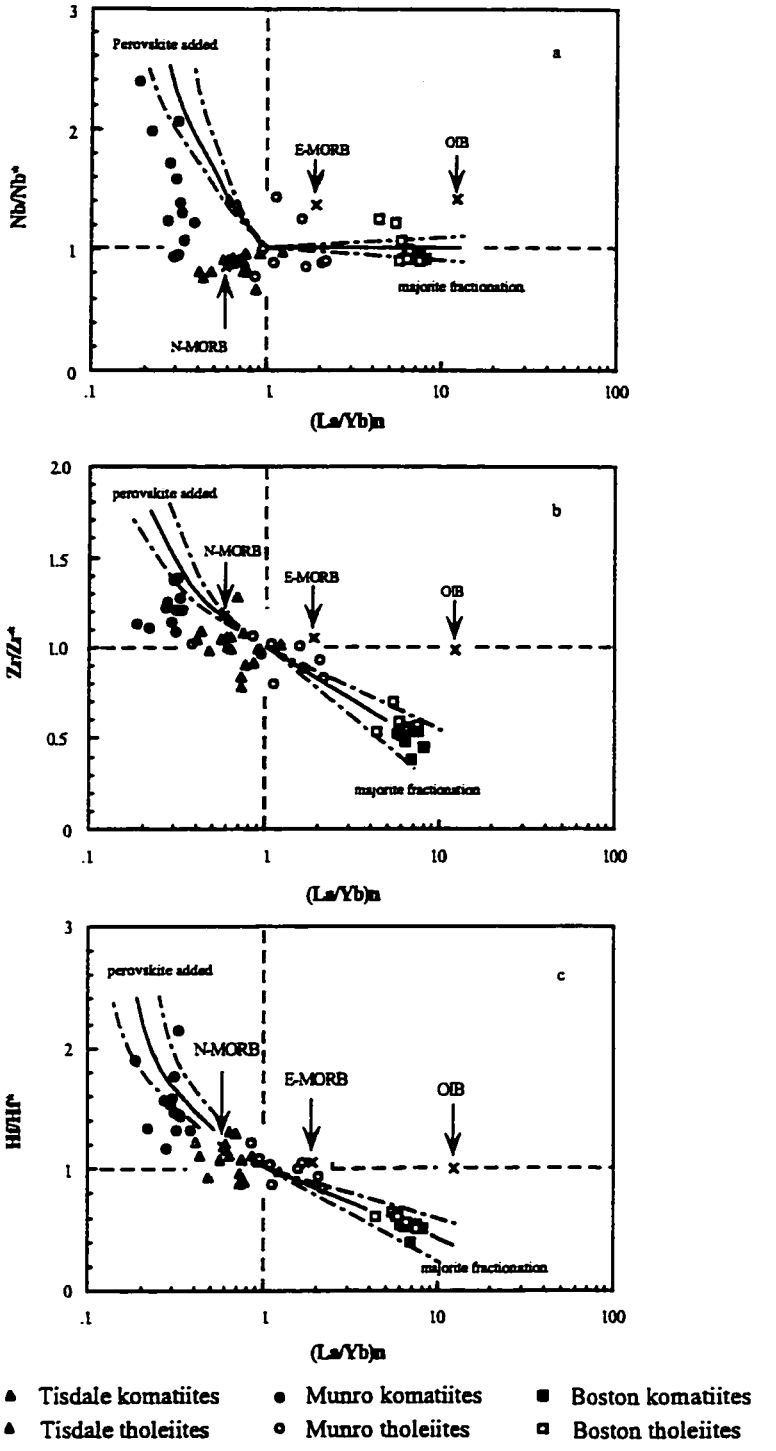

Figure 5-9. Interrelationships between Nb (a), Zr (b), Hf (c) and REE for komatiites and tholeiites from the three locations. Also shown are model calculations of Mg-perovskite addition and majorite fractionation, based on a simple equilibrium melting model. The partition coefficients used in model calculations are from Kato et al. (1988a, b) and Ohtani et al. (1989); interpolated values from neighbouring REEs were employed for Nd and Ce, for which experimental data are lacking. The solid and dashed lines represent the mean and range of D values, respectively. Given the uncertainties in D and the exact melting regime, the model is approximate. Data of N-MORB, E-MORB, and OIB are from Sun and McDonough (1989).

be related by low-pressure olivine fractional crystallization, whereas Fe-tholeiites may have a distinct mantle source.

Komatiites at Pyke Hill in Munro Township are strongly LREE depleted [$(La/Yb)_n$=0.2-0.4], with Nb/Nb*, Zr/Zr*, and Hf/Hf* > 1, implying HFSE enrichment relative to REEs (Table 5-3; Figures 5-8b and 5-9). In contrast, Mg-tholeiites have flat REE patterns and Nb/Nb*, Zr/Zr*, and Hf/Hf* ≈ 1, indicating no HFSE/REE fractionations, excepting small negative Ti anomalies in some of the less mafic rocks (MgO=2.25-3.03 wt%; Table 5-2; Figure 5-8b). It is worth noting that the negative Ti anomalies in less mafic samples are distinct in origin from Nb, Zr, and Hf anomalies in komatiites, as Ti depletion in the former may stem from fractional crystallization of accessory minerals (e.g., titanite), whereas such fractional crystallization of accessory phases are unlikely to occur in komatiites where temperatures are much higher. These results indicate that the komatiites and Mg-tholeiites cannot be related by low-pressure olivine fractionation but rather were derived from distinct mantle sources. Arndt and Nesbitt (1982) also concluded that komatiites and tholeiites from Munro Township had different mantle sources based on their distinct REE distributions, but had not reported HFSE/REE fractionations. REE patterns and HFSE contents of komatiites suggest they were derived from an LREE-depleted, but relatively HFSE-enriched source.

Komatiites and associated tholeiites in Boston Township are distinct in terms of HREE depletion, and pronounced normalized Zr and Hf depletions relative to neighbouring REEs, reflected in values of Zr/Zr* and Hf/Hf* < 1 (Table 5-3; Figures 5-8c and 5-9). Collectively, the data show that each of the three komatiite-tholeiite sequences are geochemically coherent but show systematic differences between volcanic sequences in terms

of major element compositions, REE characteristics, and HFSE/REE interrelationships.

5-5 Fractionation of HFSEs and REEs in the mantle

In this section, the fractionation of HFSE and REE between olivine, majorite and silicate-perovskite and melt, based on both experimental data and crystal chemistry, is first discussed, followed by how the HFSE/REE fractionations in these principal mantle phases may bear on the trace element systematics of the three komatitie sequences is then discussed. Other processes are also examined, including pyroxene fractionation, mantle metasomatism, crustal contamination, and alteration as possible alternative explanations for the observed trace element systematics.

5-5-1 Experimental data on HFSE and REE fractionation

The three komatiite-tholeiite sequences show distinct interrelationships between HFSEs and REEs, as well as distinct major element compositions and REE patterns. The systematic differences of HFSE/REE fractionation may indicate different mantle sources, and the depths of source melting or magma segregation.

The principal liquidus phases in the mantle change from olivine, through majorite, to silicate-perovskite (Ca- and Mg-perovskite) as pressure increases (Figure 5-10; Ito and Takahashi, 1987; Ohtani and Sawamoto, 1987; Knittle and Jeanloz, 1989; Herzberg et al., 1990; Wei et al., 1990; Zhang and Herzberg, 1994). Consequently, the partitioning behaviour of HFSEs and REEs between melt and residual or fractionated phases are expected to vary at different pressures, or depths.

At low pressure, olivine, orthopyroxene and clinopyroxene are the principal liquidus

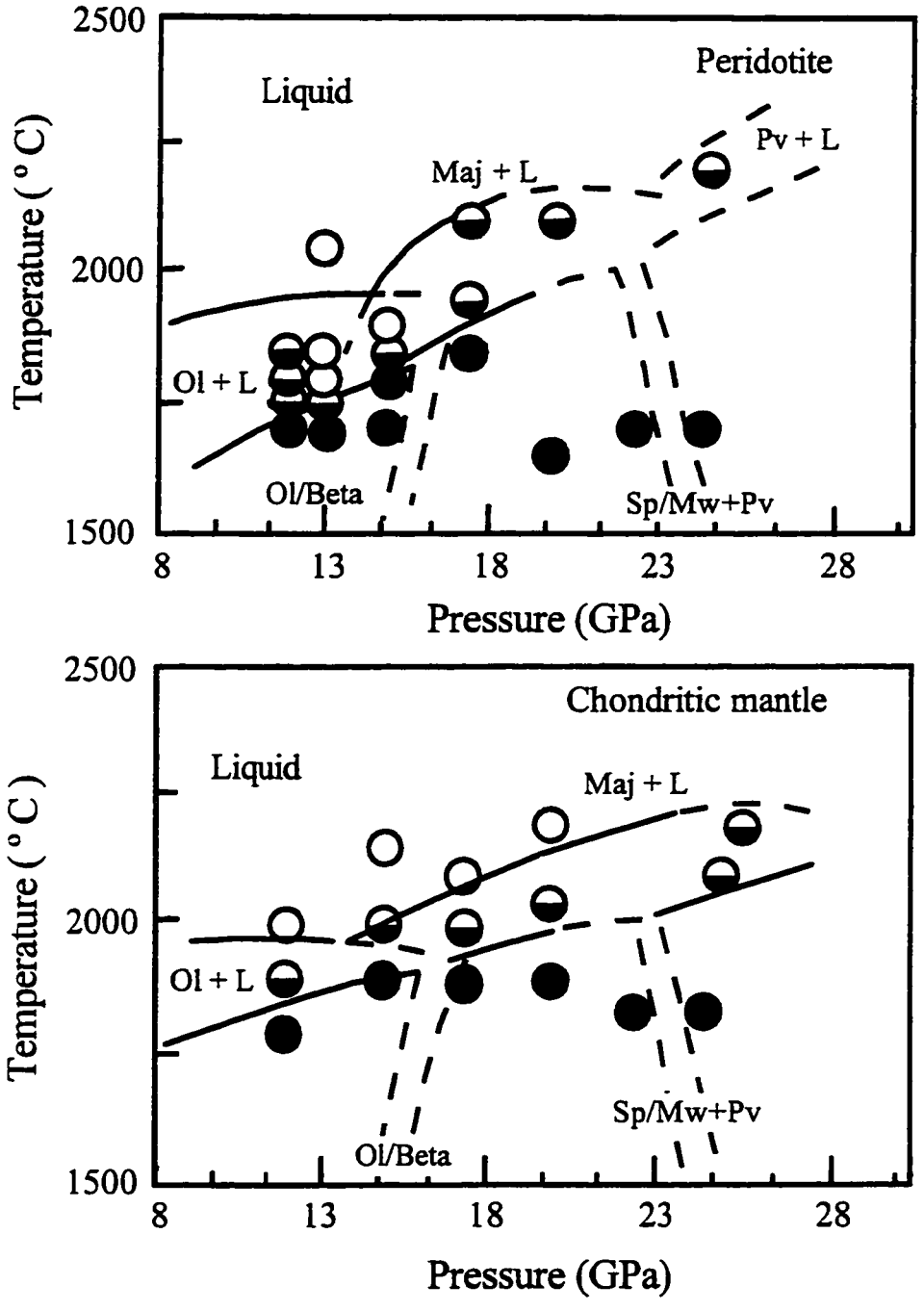

Figure 5-10. Melting relations for peridotite and chondrite compositions in the Na2O-MgO-FeO-Al2O3-SiO2 system at high pressure (after Ohtani, 1990). The experimental data shown as: ○ , liquid; ◒ , liquid + solid; ● , solid. Ol: olivine; Maj: majorite; Sp: spinel; Mw: magnesianwustite; Pv: silicate-perovskite; L: liquid.

phases. HFSEs and REEs are all highly incompatible in these mantle phases (Table 5-4 and Figure 5-11; Ewart and Hawkesworth, 1987; Kennedy et al., 1993), and consequently will be concentrated in the melt. Accordingly, HFSEs and REEs are not mutually fractionated during partial melting or fractional crystallization above depths of 300 km in the upper mantle. This experimental result is confirmed by the observation that for modern MORBs and oceanic plateau basalts HFSE and REE are characterized by smooth patterns on a primitive mantle normalized diagram (Figures 5-8d and 5-9; Sun and McDonough, 1989; Floyd, 1991).

At pressures between 15 to 24 GPa, majorite is the main liquidus phase (Figure 5-10; Ito and Takahashi, 1987; Ohtani and Sawamoto, 1987; Herzberg et al., 1990; Wei et al., 1990; Zhang and Herzberg, 1994). High-pressure experimental partitioning studies indicate that Hf, Zr, and HREEs are more compatible than LREEs and MREEs (Table 5-4 and Figure 5-11; Kato et al., 1988a, b; Ohtani et al., 1989; Herzberg, 1992b; Yurimoto and Ohtani, 1992). Consequently, partial melting with a majorite residue, or majorite fractionation, will generate melts with LREE enrichment and Hf, Zr, and HREE depletions, whereas the residue will have complementary enrichment of these elements. Other well established features arising from garnet or majorite fractionation are Al, Y and Sc depletion of melts (Nesbitt et al., 1979).

At pressures > 24 GPa, silicate-perovskite (Mg- and Ca-perovskite) becomes the main liquidus phases. Here Mg-perovskite is discussed first. The unlikelihood of Ca-perovskite involvement in the processes which may have generated the trace element systematics in the komatiites is examined later. Although there are still some ambiguities on the D for REEs and HFSEs between Mg-perovskite and coexisting melts, the Ds for Nb, Zr,

Table 5-4. Selected partition coefficients for mantle phases

Element	Mg-perovskite[1]	pyrope[2]	majorite	Clinopyroxene[2]	Olivine[2]	Orthopyroxene[2]	Spinel[2]
La	0.1	0.01	0.09	0.054	0.005	0.002	0.01
Ce	0.12 *	0.02	0.095 *	0.098	0.005	0.003	0.01
Nb	1	0.005[3]	0.1	0.05	0.01	0.01[3]	0.01[3]
P	0.55	0.15 [3]	0.53	0.5	0.03	0.01	0.11
Nd	0.2 *	0.08	0.16 *	0.21	0.005	0.007[3]	0.01
Hf	14	0.23	0.69	0.233	0.01	0.01	0.05 #
Zr	9	0.25[3]	0.46	0.2	0.005[3]	0.03[3]	0.05[3]
Sm	0.3	0.22	0.2	0.26	0.005	0.01	0.01
Eu	0.4 *	0.32	0.2	0.31	0.007	0.013	0.01
Ti	3	0.1	0.4	0.1	0.006	0.1	0.15
Gd	0.6*	0.5	0.26	0.3	0.006	0.016	0.01
Yb	2	4	1.4	0.28	0.002	0.049	0.01

* D value logarithmatically interpolated from neighbouring REE; # assumed equal to Zr D;
All D's are compiled from folloing sources:

1 Kato et al., 1988; Ohtani et al., 1989; Yurimo and Ohtani, 1992;

2 McKenzie and O'Nions, 1991;

3 Hawkesworth et al., 1993; Kennedy et al., 1993;

4 Ringwood et al., 1992.

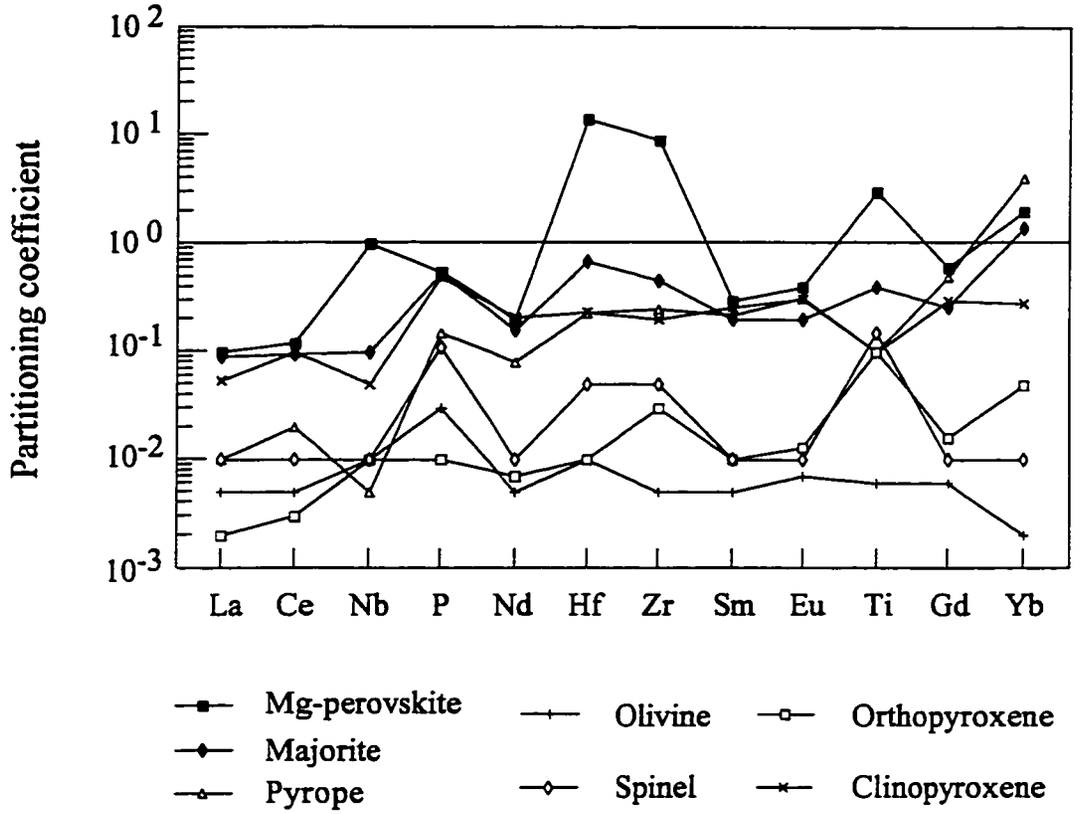

Figure 5-11. Partitioning coefficients of some HFSE and REE for major mantle phases (see Table 5-4 for sources)

and Hf are variably greater than unity (usage of D for distribution coefficients after Beattie et al., 1993), indicating that they are compatible in Mg-perovskite, whereas D for neighbouring REEs (e.g., La, Ce, Nd, and Sm) are all much less than unity, implying high degrees of incompatibility in Mg-perovskite (Table 5-4 and Figure 5-11; Kato et al., 1988a, b; Agee and Walker, 1989; McFarlane and Drake, 1990; Drake et al., 1993). Therefore melts generated at pressures >24 GPa would be enriched in LREEs but relatively depleted in Nb, Zr and Hf, whereas the Mg-perovskite residue or accumulation would show complementary trends. Magmas generated by partial melting of Mg-perovskite enriched sources would have LREE deletion and HFSE depletion or enrichment depending on the depth of melting or melt segregation.

It is emphasized that although there are small differences in measured Ds for the mantle phases in question from independent experimental studies, the relevant Ds all have the same sign and accordingly would influence the magnitude, but not the direction of HFSE/REE fractionations.

The compatibility changes of HFSEs and REEs with increasing pressure are also in accordance with predictions based on the crystal chemistry of mantle minerals. Partitioning of trace elements in minerals is chiefly controlled by atomic properties, such as ionic radius and charge (Goldschmidt, 1937). Figure 5-12 is a plot of valence versus ionic radius for HFSEs, REEs and major cations of mantle minerals. The structural formulae of the principal mantle phases, and coordination number of major cations, are also shown on Figure 5-12. This kind of plot can be used to qualitatively predict trace element partitioning in these minerals, provided that the major cations with which trace elements will substitute are known (McKay, 1989). Trace elements with the same valence and similar ionic size as the major

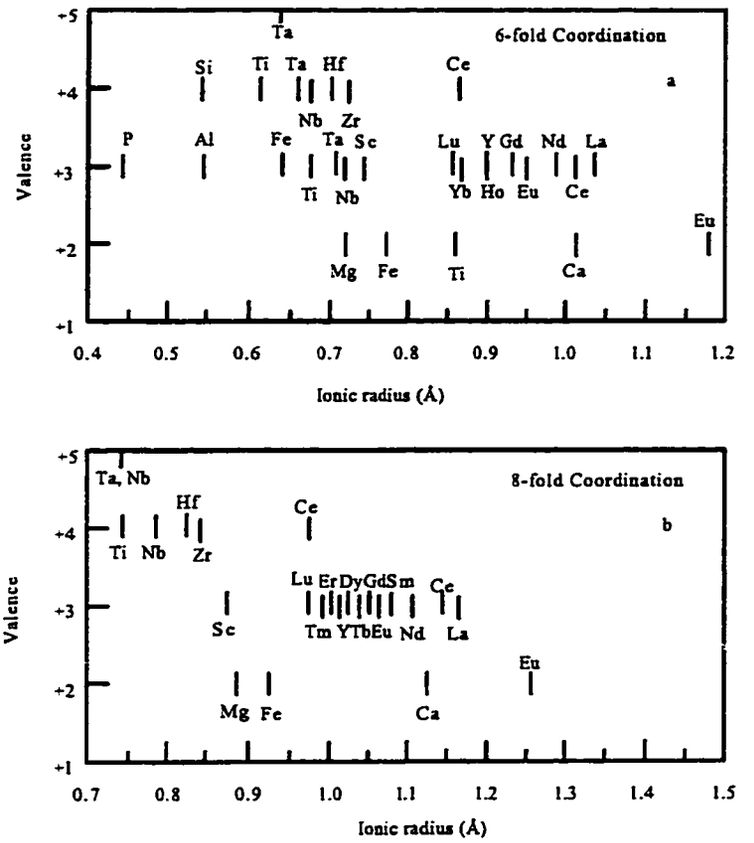

Olivine: $(Mg^{2+}, Fe^{2+})^{VI}[Si^{IV}O_4]$

Pyroxene: $M_1M_2[Si^{IV}O_3]_2$

M_1: $(Mg^{2+}, Fe^{2+})^{VI}$

M_2: $(Ca^{2+}, Mg^{2+}, Fe^{2+})^{VIII}$

Pyrope garnet: $(Mg^{2+})_3^{VIII}(Al^{3+})_2^{VI}[Si^{IV}O_4]_3$

Majorite garnet: $(Mg^{2+})_3^{VIII}(Fe^{3+}, Si^{4+}, Al^{3+})_2^{VI}[Si^{IV}O_4]_3$

Mg-perovskite: $(Mg^{2+})^{XII}(Si^{4+})^{VI}O_3$

Figure 5-12. Plots of valence versus ionic radius in VI-fold (a) and VIII-fold (b) coordination for HFSE, REE and major contituents of mantle minerals (modified from McKay, 1989). The structural formulae and coordination of major cations of the mantle minerals are also shown. Ionic radii are from Shanon (1976)

cation will have a higher D than elements with different valences and ionic size.

Inspection of Figure 5-12 suggests that all HFSEs and REEs would have very small Ds in olivine and pyroxene, as they have very different valence and ionic radii compared with those of Mg^{2+} and Fe^{2+} in VI-fold sites, the major constituents for which HFSEs and REEs are likely to substitute. For pyrope ($Mg_3Al_2Si_3O_{12}$ with 22-24% Al_2O_3; Herzberg, 1992), P^{3+}, Sc^{3+}, Y^{3+} and HREE are likely to have high Ds, given that Sc^{+3}, Y^{+3} and HREE are close in size to Mg^{2+} in VIII-fold coordination sites, whereas P^{+3} has same valence and ionic size as Al^{3+}. LREE, Zr and Hf, however, would remain incompatible. When garnet composition changes from pyrope to majorite, Al concentration decreases ($MgSiO_3$ with 4-8% Al_2O_3; Herzberg, 1992), but Mg and Fe increase, with a significant amount of Si^{+4} entering VI-fold coordination (Herzberg and Gasparik, 1991; Sautter et al., 1991). Accordingly, Zr and Hf, as well as P, Sc, Y and HREE, would have higher Ds than LREE and MREE, as Zr^{4+} and Hf^{4+} are similar in charge and ionic size to Si^{4+} in VI-fold coordination, whereas Sc, Y, and HREE replace Mg^{2+} in VIII-fold coordination sites, a prediction incommensurate with experimental results (Table 5-4).

In a standard Mg-perovskite structure, Mg^{2+} occupies large XII-fold coordination sites, whereas Si^{4+} occupies sites with VI-fold coordination (Hemley and Cohen, 1992). HFSE and HREE would have higher Ds either by substituting for Mg^{2+} in XII coordination (Kesson et al., 1983; Solomah et al., 1987), or replacing Si^{4+} at VI coordination, as +4 ions tend to enter VI-fold coordination sites in silicate melt (Farges, 1991). However, LREE and MREE would have low Ds, due to their very different valence and ionic size. This result is in accord with the experimental data (Table 5-4). It is noteworthy that Nb, Ta and Ti, also often referred as HFSE, may have different Ds in the mantle phases compared to Zr and Hf,

when Nb, Ta and Ti have charges other than 4+ (Figure 5-12). In Figure 5-11, it appears that Mg-perovskite may also fractionate HREE. This slope, however, may be an artifact, as only Ds for La, Sm, Y, Zr, and Hf are experimentally determined, whereas Ds for Ce, Nd, Eu, and Yb are extrapolated from experimental data. Considering that ionic radius decreases progressively from La to Lu, it is reasonable to assume that LREE and HREE may have quite different Ds in Mg-perovskite, but HREE as a group may have similar Ds. Thus, one may expect fractionation between LREE and HREE in Mg-perovskite, but not among HREEs.

Model calculations were performed for partial melting of a mantle source with peridotite composition and with Mg-perovskite as residue. The results show that $(La/Yb)_n$ decreases, but Hf/Hf*, Zr/Zr*, and Nb/Nb* all increase in the residual solids with progressive melting (Figure 5-9). From these calculations, the Munro-area komatiite compositions are consistent with partial melting of an Mg-perovskite enriched source formed either by previous partial melting with Mg-perovskite residue or Mg-perovskite accumulation. Munro-area komatiites have anomalously low Zr/Hf ratios (22-30) relative to chondritic ratios of 36 seen in most modern non-alkaline MORBs and OIBs. For Mg-perovskite-melt, the D for Hf may be greater than for Zr (Kato et al., 1988b). Notwithstanding the uncertainties in most experimental Ds, these results predict larger anomalies for Hf than Zr, relative to neighbouring REEs, and consequently, low Zr/Hf ratios in the Mg-perovskite residue as possibly reflected in the Munro-area komatiites.

The major element compositions of the Munro komatiites, such as MgO content, are consistent with partial melting or magma segregation at pressures of 5-7 GPa, or 160-250 km (cf. Herzberg, 1992). Collectively, the LREE-depletion, systematic positive Nb, Zr, and

Hf anomalies, and low Zr/Hf ratios are all consistent with experimental Mg-perovskite-melt Ds. These results can be interpreted in terms of Munro komatiites having been generated in a mantle plume which may have originated from deep mantle sources enriched in Mg-perovskite, that subsequently melted in the upper mantle. This interpretation is consistent with ϵ_{Nd} values of +2 to +3 for the komatiites, signifying long-term LREE depletion of the source (Walker et al., 1988). Ca-perovskite could not have been involved in generation of the Munro komatiites, inasmuch as the Ds predict LREE enrichment in the residue (Kato et al., 1988a, b).

According to Ohtani et al. (1989), Mg-perovskite is stable at pressures of > 24 GPa, corresponding to depths of > 650 km. If this interpretation is correct, LREE depletion and HFSE enrichment in Munro komatiites suggest that there were some Mg-perovskite enriched reservoirs in the deep mantle, signifying Mg-perovskite fractionation in the deep mantle during early mantle differentiation.

Similar model calculations have been conducted for majorite fractionation (Figure 5-9). For the Boston-area Al-depleted komatiites and tholeiites, LREE enrichment, combined with Al, Y, Sc depletion, and normalized Hf and Zr depletions relative to MREEs, are collectively consistent with either the partial melting of a majorite-depleted mantle source or majorite fractional crystallization in the parent magma under deep mantle conditions. The Ds for REEs and HFSEs for pyrope are such that pyrope fractionation would not generate Zr, Hf/REE fractionations such as observed in Boston-area komatiites(c.f. McKenzie and O'Nions, 1991; Ringwood, 1991; Xie et al., 1995). Majorite has previously been invoked to explain the petrogenesis of Al-depleted komatiites, specifically the 3.5 Ga Barberton examples (Green, 1975; Nesbitt et al., 1979; Herzberg and Ohtani, 1988; Herzberg et al.,

1988; Wei et al., 1990; Herzberg, 1992a). According to Herzberg (1992b), liquidus garnet are: "pyropic" ($Mg_3Al_2Si_3O_{12}$; 22-24% Al_2O_3 and 3% CaO) in the low pressure range (10 GPa); "majorite" ($MgSiO_4$; 4-8% Al_2O_3) in the highest pressure range (20-26 GPa); pyrope-majorite (e.g., 16% Al_2O_3) at intermediate pressures. The most recent high pressure experimental study suggests that majorite is stable at 14-24 GPa, or 400-650 km (Zhang and Herzberg, 1994).

If Boston-area komatiites and tholeiites represent a majorite-depleted mantle source, this may imply that majorite fractionation occurred sometime during early mantle differentiation. Alternatively, majorite fractionation may have occurred during magma formation, and in this case the geochemical features may not necessarily indicate majorite fractionation during early mantle evolution. Thus trace element geochemistry alone cannot discriminate between the two possibilities, and further Sm-Nd and Lu-Hf isotope studies are necessary to address this question. If Al-depleted komatiites represent a long term majorite depleted mantle source, they should have negative ϵ_{Nd} and ϵ_{Hf}. On the other hand, if majorite fractionation occurs during magma formation, the komatiites should have positive or zero ϵ_{Nd} and ϵ_{Hf}, depending on whether they are from a depleted or a primitive mantle source. Another implication of the HFSE/REE fractionation induced by majorite is the decoupling of Sm-Nd and Lu-Hf isotope systematics. It has been suggested that Nd and Hf isotopes are well correlated in modern MORBs, indicating a compatibility sequence of Lu > Sm > Hf > Nd (Patchett and Tatsumoto, 1980; White and Patchett, 1984). However, decoupled Sm-Nd and Lu-Hf isotope systematics have recently been reported for sub-oceanic mantle peridotites, which have extremely radiogenic Hf isotope compositions and are attributed to the involvement of garnet in the formation of the mantle peridotites (Salters and Zindler,

1995).

The existing Sm-Nd isotopic data for the Al-depleted komatiites from Barberton seem to favour majorite fractionation during melting processes (Jahn et al., 1982; Gruau et al., 1990a), whereas other Sm-Nd data for the same komatiites show negative ϵ_{Nd} values, that have been attributed to crustal contamination (Gruau et al., 1990b). Similarly, Lu-Hf isotopic data from Barberton volcanic sequences seem to support majorite fractionation during melting, although all Hf isotope data are from basaltic rocks, which may not be cogenetic with Al-depleted komatiites (Gruau et al., 1990a).

In summary, the REE distributions and HFSE/REE fractionations of the three komatiite-tholeiite sequences are distinct, implying that the three ultramafic volcanic sequences may have formed from different mantle sources at different depths. It is emphasized that the Tisdale-area komatiites and Mg-tholeiites have zero fractionation between Nb, Zr, and Hf/REEs, whereas the Munro-area komatiites as a group all have positive Nb, Zr, and Hf anomalies, and separately, the Boston-area komatiites and associated tholeiites all have negative Zr and Hf anomalies, relative to neighbouring REEs. It is unlikely that these results could concurrently be generated by analytical bias.

Unfractionated REEs and zero HFSE/REE fractionation of Tisdale-area komatiites and Mg-tholeiites are consistent with olivine fractionation. LREE depletion and HFSE enrichment of Munro komatiites are in accord with Mg-perovskite-rich sources, whereas the conjuction of LREE enrichment with HREE and HFSE depletion of Boston-area komatiites and tholeiites are consistent with majorite fractionation. Departure of the data from model vectors could reflect the exact composition and proportion of fractionating phases, uncertainties in Ds, simplified modelling, or some combination of these factors (Figure 5-9).

For example, the model calculation is simplified by using majorite or Mg-perovskite as the only liquidus phase. It has been suggested, however, that magnesiowüstite is an important minor phase in the deep mantle (Ito and Takahashi, 1987; Ohtani and Sawamoto, 1987; Jeanloz and Knittle, 1989; Agee, 1990; Zhang and Herzberg, 1994). In addition, Ds used are for a temperature about 2000 K (Kato et al., 1988a, b). Murthy (1991) pointed out that Ds for incompatible elements may increase with increasing temperature, whereas the reverse effect may occur for compatible elements. If his inference is correct, the model vector for Mg-perovskite fractionation (Figure 5-9) would be shifted towards unity at higher temperatures, closer to the data trend of Munro-area komatiites. The significance here is the noncoherent behaviour of HFSEs and REEs in the generation of two of the three komatiite sequences.

5-5-2 Alternative processes for HFSE and REE fractionation

Pyroxene fractionation, mantle metasomatism, crustal contamination, and secondary hydrothermal alteration may also generate various types of HFSE/REE interrelationships. These possibilities are considered in turn below.

Some upper mantle peridotites and harzburgites may have negative Zr and Ti anomalies relative to REE, which have been attributed to fractionation of orthopyroxene and clinopyroxene (Salters and Shimizu, 1988; Rampone et al., 1991). This is, however, considere dunlikely for Munro and Boston komatiites, for the following reasons:

(1) If komatiites form in the upper mantle, the high degree of partial melting required to generate komatiitic liquids would leave orthopyroxene and clinopyroxene completely dissolved in the melt, and hence there could be no effect of these minerals on trace

element partitioning behaviour during partial melting of mantle peridotite;

(2) Komatiite samples from Munro and Boston areas include spinifex textured zones, massive flows, and cumulate zones which have different contents of pyroxene, yet they share similar REE patterns and HFSE/REE fractionation within each group (Figures 5-7 and 5-8);

The shape of the REE patterns of Munro-area rocks have some superficial resemblance to the patterns for N-MORB. However, careful inspection of the compilation of N-MORB data by Sun and McDonough (1989) shows no HFSE/REE fractionation (i.e., Nb/Nb*, Zr/Zr*, Hf/Hf* ≈ 1), and chondritic La/Nb, Hf/Sm, and Zr/Hf ratios. In contrast, the Munro-area komatiites have much lower absolute REE contents, Nb/Nb*, Zr/Zr*, and Hf/Hf* are all > 1, and La/Nb, Hf/Sm, and Zr/Hf ratios are nonchondritic, collectively consistent with Mg-perovskite-melt Ds.

Recent studies have shown that Zr/REE and Zr/Hf fractionation may occur in intraplate alkali basalts (Dupuy et al., 1992; Hart and Dunn, 1993), and that the metasomatization of depleted mantle peridotite by "enriched magmas" may produce Zr/REE and Ti/REE fractionations in arc basalts (Kelemen et al., 1990, 1992). It is unlikely that the HFSE/REE fractionations observed in any of the komatiites studied arise in the same way, because the geochemistry of komatiites and residual, or fractionating phases, are distinct from those of alkali basalts and island arc basalts.

It is also unlikely that different REE patterns and HFSE/REE interrelationships of the three komatiite-tholeiite sequences could be generated by crustal contamination, as this process would cause unidirectional LREE enrichment and negative Nb, P and Ti anomalies relative to REEs (Sun and McDonough, 1989), which are not seen in any of the Abitibi SVZ

komatiites (Table 5-3; Figures 5-7 and 5-8), or other komatiites reported in the literature (Jochum et al., 1991).

Most of the komatiites and tholeiites analyzed in this study have negative Eu anomalies varying from 1.0 to 0.7. This feature is not unusual in Archean mafic and ultramafic rocks that have experienced hydrothermal alteration and low-grade regional metamorphism. Several studies have suggested that hydrothermal alteration may mobilize Ce, Eu, and Th but does not affect other REEs and HFSEs (Sun and Nesbitt, 1979; Ludden and Gelinas, 1982; Lesher et al., 1991). The systematic REE patterns for each group of komatiites and tholeiites, the smooth distributions from La to Gd, and uniform La/Nb, Sm/Zr, and Zr/Hf ratios within each group of komatiites collectively signify that the REE patterns and HFSE contents have not been significantly disturbed by alteration, excepting Eu.

It is emphasized here that pyroxene fractionation, mantle metasomatism crustal contamination, and hydrothermal alteration are generally heterogeneous processes that exert a corresponding spread of secondary geochemical trends on the primary geochemical characteristics of a suite of volcanic rocks (i.e., variable negative Eu anomalies from 1.0 to 0.7; Table 5-3). In contrast, the three komatiites sequences show coherence of both REE patterns and HFSE/REE systematics within each sequence, albeit with consistent differences of these geochemical characteristics between the sequences. Accordingly, these secondary processes can probably be ruled out as a cause of the observed trace element characteristics.

5-6 Implications

5-6-1 Komatiite petrogenesis

Models for komatiite petrogenesis have all focused on the explanation of high Mg contents in these ultramafic liquids. There is a simple "recipe" for generating komatiites: induce > 50% melting of mantle peridotite and then extract and erupt the resultant liquid (Arndt, 1977b). This interpretation, however, is neither unique nor without difficulties. For example, melt will tend to escape from the source long before 50% melt is produced, and commonly before even 5% melt is reached under upper mantle P-T conditions (Arndt, 1977b; McKenzie, 1985).

The MgO content of the erupted liquid is directly related to the minimum temperature of the liquid arriving at the surface. Although MgO contents of komatiites may have been augmented after eruption by olivine accumulation or alteration, leading to overestimates of eruption temperatures (Beswick, 1982; Barnes et al., 1985; Arndt and Lesher, 1992), there are strong lines of evidence that argue for the existence of komatiitic liquids with 24 to 30 % MgO (Nisbet et al., 1977, 1993; Bickle, 1982; Arndt, 1986a; Cattell and Arndt, 1987). Several authors have proposed a linear relationship between MgO and the eruption temperature of ultramafic liquid (Nisbet, 1982; Smith and Erlank, 1982; Beattie et al., 1991; Renner et al., 1994). Specifically, Nisbet (1982) gave, for komatiitic liquids:

$$T_{liquids}=1400 + [(MgO\%-20)x20]°C \qquad (5-1)$$

Based on this equation, Nisbet et al (1993) estimated an eruption temperature of 1580°C for Munro komatiites. Such an eruption temperature would require a mantle source with much higher (>1900°C) potential temperature (T_p). Miller et al. (1991a, b) gave an even higher T_p (~2200°C) for the mantle sources of komatiitic liquids, based on the equation of state of a molten komatiite. Such high T_p cannot be sustained in the upper mantle, considering the

thermal state of the mantle (Bickle, 1990).

The thermal constraints on komatiites discussed above have led to suggestions that komatiitic liquids may have been generated by hot mantle diapirs derived from deep in the mantle (Nisbet and Walker, 1982; Arndt, 1986b; Miller et al., 1991b; Herzberg, 1992a). Figure 5-13 shows the P-T conditions under which komatiites could have been extracted from their source regions, according to Miller et al.(1991b).

This high pressure origin of komatiites has received considerable support from high pressure experimental data (Herzberg and O'Hara, 1985; Takahashi, 1986; Herzberg et al., 1990; Wei et al., 1990; Zhang and Herzberg, 1994). Herzberg et al. (1990) showed that melts become progressively more magnesian with increasing pressure, and initial melting at high pressure could generate single stage komatiites. Based on recent high pressure experimental studies, Herzberg (1992) discussed the depth and degree of melting of various komatiites, and concluded that komatiites from Barberton, Munro and Gorgona may have formed by < 50% degree of partial melting at different depths. Specifically, Campbell et al. (1989) suggested that komatiites formed by melting of the hot axis of a "starting plume" originating at the core-lower mantle boundary, whereas spatially associated tholeiites formed by melting of cooler upper mantle entrained by the upwelling plume.

The distinct geochemical features of the three komatiite-tholeiite sequences that formed in the Abitibi SVZ between 2725-2710 Ma may be explained in terms of plumes originating from different mantle sources at different depths. A speculative model is illustrated in Figure 5-14. Komatiites in the Tisdale area may have formed in a plume starting at a relatively shallow depth (< 300 km) in undepleted mantle. Spatially associated Mg-tholeiites are likely the products of low pressure olivine fractionation of the komatiitic

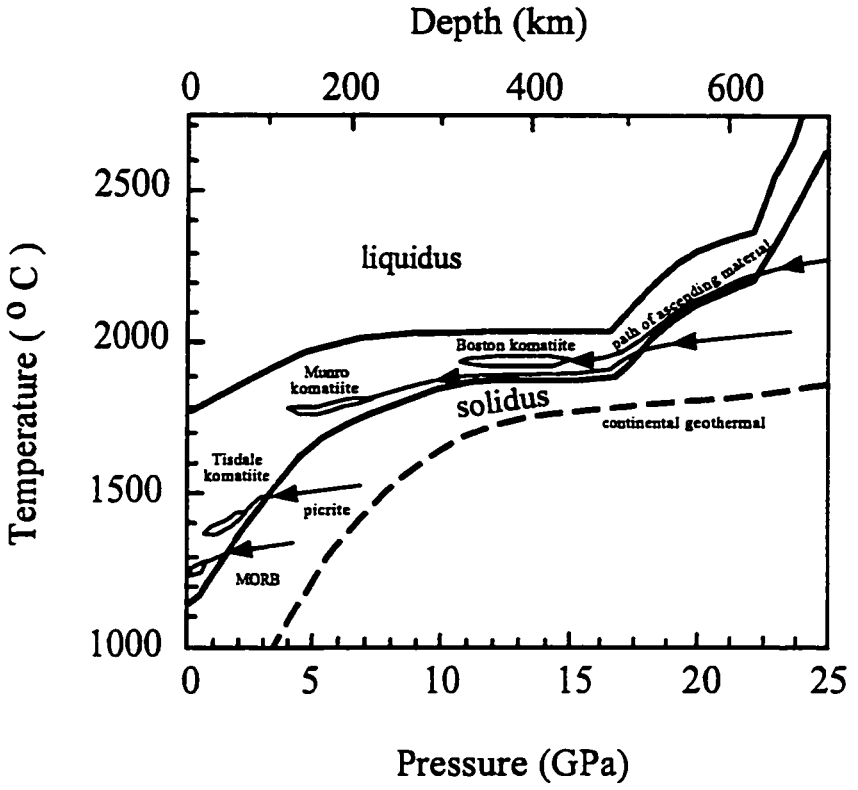

Figure 5-13. Phase diagram for KLB-1 with fields showing conditions under which various komatiites, MORB, and picrite could have been extracted from their source regions (modified from Miller et al., 1991b)

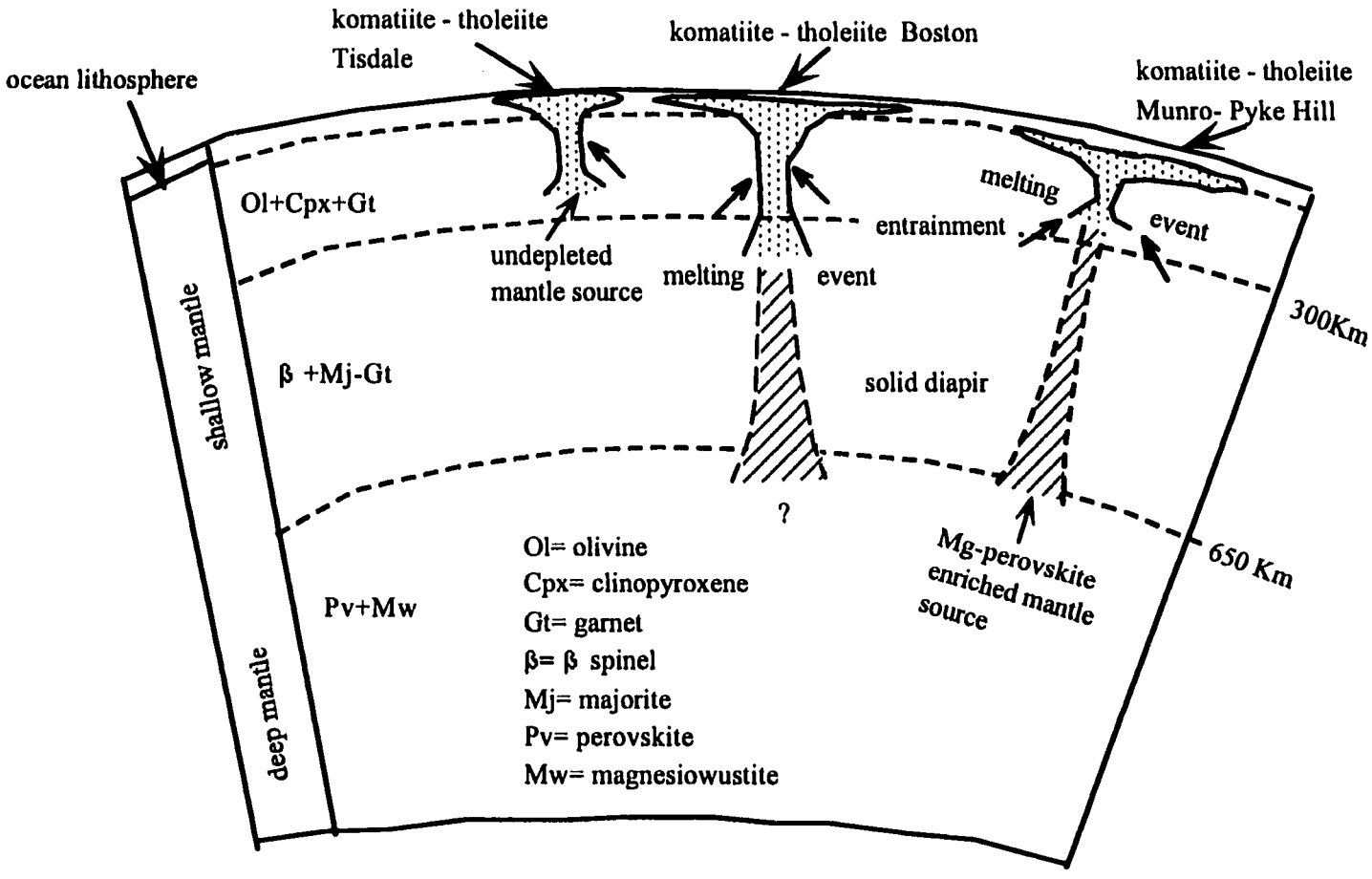

Figure 5-14. A speculative model of multiple plumes for komatiite-tholeiite sequences in the Abitibi Southern Volcanic Zone (cf. Miller et al., 1991; Xie et al., 1993)

magma. In contrast, the LREE depleted Fe-tholeiites probably represent MORB-like upper mantle entrained by the ascending plume, or an independent plume from a depleted mantle source.

At Munro Township, different sources are required for komatiites and tholeiites. The komatiites may have been derived from partial melting of a diapiric plume which originated from a mantle source enriched in Mg-perovskite at pressures > 24 GPa, corresponding to depths of > 650 km. Initial melting of the plume may have occurred in the deep mantle. However, the positive HFSE/REE anomalies in komatiites suggest that final melting or melt segregation may have happened at shallow depth (< 300 km) in equilibrium with olivine, Opx and Cpx. Coexisting Mg-tholeiites may represent either more primitive mantle material that was entrained in the ascending plume, or an independent plume source.

Al-depleted komatiites from Boston Township may have been generated by partial melting of a plume at pressures between 14-24 GPa, corresponding to depths of 400-650 km, where majorite is a liquidus phase. According to the phase diagram of mantle peridotite (Figure 5-13), the plume which may have produced Boston Al-depleted komatiites should have higher T_p, hence deeper origin, than that of Munro komatiites. Herzberg (1992) also suggested that Barberton Al-depleted komatiites should come from a deeper mantle source than Al-undepleted komatiites in Munro and Gorgona, based on major element compositions and experimental data. A deep melt segregation for Boston komatiites is endorsed by negative HFSE anomalies and HREE depletion, arising from melting with a majorite residue.

This overall scheme is consistent with the scenario of Miller et al. (1991a, b), who suggested that more fertile mantle sources will have lower solidi temperatures, thereby allowing greater degrees of partial melting for a given T_p, implying a shallow depth (e.g.,

Tisdale area), whereas depleted sources will have higher solidi temperatures, signifying greater depth (e.g., Munro and Boston areas). Trace element geochemistry, particularly the interrelationships between HFSE and REE, of the three komatiite-tholeiite sequences from Abitibi greenstone belt seems to support the hypothesis that komatiites may be generated by mantle plumes originating from mantle sources with different compositions at different depths. If this is valid, then trace element characteristics of komatiites, especially the HFSE and REE interrelationships, will be mainly controlled by source compositions and depths of source melting. Accordingly, there cannot be a single komatiite trend in the La-Th-Nb multielement space, as proposed by Jochum et al. (1991).

5-6-2 Early mantle evolution

The three komatiite-tholeiite sequences from the Archean Abitibi SVZ show systematic differences in compositions, REE patterns, and HFSE/REE fractionation, possibly signifying different mantle sources at different depths. These results may indicate a stratified mantle beneath the Archean Abitibi belt and may impose some constraints on early mantle evolution.

One model of early mantle evolution suggests that the primitive mantle had an Fe-depleted chondritic composition and differentiated into olivine-, majorite-, and silicate-perovskite-rich layers in a magma ocean stage (Herzberg, 1984; Agee and Walker, 1988; Ohtani, 1988; Miller et al., 1991b). Agee and Walker (1988) further suggested possible redistribution of original C1 bulk composition, following earliest Earth differentiation, into upper mantle peridotite, basal silicate-perovskite cumulates, and a komatiitic residuum between these two layers, from calculations of major element mass balance between the

modern upper mantle and chondritic bulk Earth composition. They argued that majorite fractionation could occur during the formation of some Archean komatiites after the upper mantle's composition has already been established.

That Munro-area komatiites may have formed in a plume, originating from deep mantle sources enriched in Mg-perovskite based on the trace element data of this study, provides independent evidence for possible Mg-perovskite fractionation during early mantle evolution. Furthermore, if HFSE and HREE depletion of Boston komatiites and tholeiites reflect a majorite depleted mantle source, this in turn may imply majorite fractionation during early mantle evolution. However, if these features were derived from majorite fractionation during magma formation, as inferred by Agee and Walker (1988), then they do not necessarily indicate majorite fractionation during early mantle evolution. Data for the three komatiite-tholeiite sequences in the Archean Abitibi SVZ seem to support possible Mg-perovskite, and maybe majorite, fractionation during early mantle differentiation, a stratified mantle model and possible mass transport across the upper and lower mantle boundary transition zone, e.g., 650 km discontinuity.

Kato et al. (1988a, b; 1989) and Ringwood (1990) argued, however, that little silicate-perovskite fractionation could have been involved in the generation of the upper mantle, because most refractory element ratios observed in this reservoir are near-chondritic. They suggested that the amount of Mg-perovskite fractionation required to generate the observed Mg/Si ratio of the modern upper mantle would have driven some element ratios (e.g., Sm/Hf, Sc/Sm) far from chondritic ratios. Moreover, the Tisdale-area komatiites represent a relatively primitive, undepleted mantle source at shallow depth, formed contemporaneously with Boston- and Munro-area komatiites, yet the interrelationships

between HFSEs and REEs of the Tisdale komatiites show no complementary signatures of majorite or Mg-perovskite extraction. These results seem inconsistent with widespread majorite and Mg-perovskite fractionation during early mantle evolution.

This apperent inconsistency disappears if the composition of primordial upper mantle peridotite is different from C1 chondrite, a type of chondrite currently regarded as representative of the primitive mantle. For example, Herzberg (1992) argued that the composition of modern upper mantle peridotite can successfully be explained by 35% majorite fractionation from a CV chondrite like Allende in the 20 to 26 GPa range. The inconsistency will also vanish, using a boundary layer fractionation model to describe possible differentiation of a cooling magma ocean, involving olivine, majorite, and silicate-perovskite crystallization and stratification (Miller et al., 1991b). Miller et al. (1991b) argued that a silicate-perovskite-rich layer could be created in the vicinity of the perovskite neutral buoyancy horizon due to crystal settling and flotation. Hence the magma from which the upper mantle would ultimately have crystallized might have become initially enriched in silicate-perovskite components when the boundary layer was deeper than 70 GPa, and would later become depleted in these same components as crystallization continued in the 24-70 GPa interval. If their arguments are valid, there would be no incommensurability between evidence for possible Mg-perovskite fractionation in the magma ocean stage and the chondritic interelement ratios observed in the Tisdale-area komatiites, other Archean high-Mg lavas and modern upper mantle peridotite.

It appears that whether or not the mantle has undergone extensive early differentiation remains in question. Further constraints on fractionation mechanisms of the magma ocean, high pressure experimental studies of D, chemical composition of truly

primordial samples of upper mantle peridotite (e.g., analysis of mantle xenoliths), and trace element systematics of magmas which may have been derived from great depths, are necessary. The compositionally diverse Archean komatiites provide possible good samples for the investigation of deep mantle processes, and early mantle evolution.

5-7 Summary

The three komatiite-tholeiite sequences from the Archean Abitibi SVZ show distinct geochemical characteristics. Tisdale komatiites are Al-undepleted, with Al_2O_3/TiO_2=13-17 and CaO/Al_2O_3=1.0-1.3, flat REE patterns, and zero HFSE/REE fractionation. Spatially associated Mg-tholeiites share similar geochemical features with komatiites, whereas Fe-tholeiites show zero HFSE/REE fractionation but LREE depletion. Munro komatiites are also Al-undepleted, with Al_2O_3/TiO_2=17-20 and CaO/Al_2O_3=1.0-1.2, LREE depleted patterns, and positive HFSE anomalies relative to REEs, whereas spatially associated Mg-tholeiites have flat REE patterns and zero HFSE/REE fractionation, similar to Tisdale komatiites and Mg-tholeiites. Boston komatiites and tholeiites are distinct in terms of their Al-depletion (Al_2O_3/TiO_2=4-5 and CaO/Al_2O_3=1.0-2.5), fractionated HREE, and negative Zr and Hf anomalies relative to REEs. Mg-tholeiites underlying and overlying komatiitic flows, however, have flat REE and zero HFSE/REE fractionation, similar to the komatiites and Mg-tholeiites in Tisdale Township, as well as the Mg-tholeiites in Munro Township.

The distinct geochemistry of the three komatiite-tholeiite sequences may be explained in terms of mantle plumes originating from different sources at different depths. Tisdale komatiites may have been generated by a plume originating from an undepleted mantle source at shallow depth (< 300 km). Spatially associated Mg-tholeiites are likely products

of low pressure olivine fractionation of the komatiitic magma, whereas Fe-tholeiites may represent an independent plume from a depleted source. Different sources are required to account for the geochemistry of Munro komatiites and Mg-tholeiites. The komatiites may be generated in a plume originating from a mantle source enriched in Mg-perovskite at great depth (> 650 km), that subsequently segregated or melt at shallow depths (< 300 km). Coexisting Mg-tholeiites may represent either more primitive materials entrained in the plume, or an independent plume source. The Al-depleted Boston komatiites may have formed by partial melting in a plume at mantle depths between 400 to 650 km, where majorite is a liquidus phase. Associated tholeiites could be related to the komatiites either by different degrees of partial melting or fractional crystallization of majorite.

If these interpretations are valid, then the various komatiite-tholeiite sequences in the Abitibi SVZ could represent parts of distinct Archean ocean plateaus formed from different plumes, rather than mid-ocean ridge or arc, that may have been preferentially obducted and juxtaposed along major terrane boundary structures during late accretionary tectonics (see Chapter 8 for further discussion). Similar terrane structures are present demarking the Gorgona komatiite-tholeiite sequences from adjacent arc volcanic and sedimentary terranes (Storey et al., 1991).

HFSE enrichment relative to REEs in Munro Al-undepleted komatiites, and perhaps HFSE depletion relative to REEs in Boston Al-depleted komatiites, may provide independent evidence of silicate-perovskite and majorite fractionation during early mantle differentiation, although more work is required for resolving outstanding problems of this early stage of planetary evolution.

CHAPTER 6 GEOCHEMISTRY OF KOMATIITES AND THOLEIITES FROM MCARTHUR TOWNSHIP, SOUTHERN ABITIBI BELT

6-1. Introduction

The Abitibi SVZ is transected by two large fault zones, the Destor-Porcupine Fault Zone (DPFZ) to the north and the Kirkland Lake-Larder Lake Fault Zone (KLFZ) to the south (Figure 2-3). The three komatiite-tholeiite sequences discussed in Chapter 5 are respectively to the north of the DPFZ (Tisdale and Munro Townships), and to the south of the KLFZ (Boston Township). The Tisdale and Munro volcanic sequences may also be separated by the Pipestone fault, subparallel to and likely a splay of the DPFZ, but lack of outcrop leaves this question unresolved (Figure 2-3). The geochemistry of the three ultramafic-mafic volcanic suites, particularly the REE and HFSE systematics, show distinct characteristics implying different mantle sources and melting depths. Accordingly, a study of another komatiite-tholeiite sequence from the central block of the Abitibi SVZ was considered warranted, for comparison with the three sequences, specifically to establish if the positive HFSE/REE anomalies of the Munro Al-undepleted komatiites occur consistently in other komatiites if this type. Komatiitiic and tholeiitic flows from McArthur Township are good candidates.

McArthur Township is located about 40 km south of Timmins in the central block of the Abitibi SVZ, bounded to the north by the DPFZ, and to the south by the KLFZ (Figure 2-3). Metavolcanic rocks, ranging from ultramafic to felsic in composition, occur in

the area (Pyke, 1978). The petrology and geochemistry of komatiites and tholeiites in McArthur Township have been described in previous studies (Pyke, 1978; Barnes, 1985; Lahaye et al., 1995). However, these studies focused mainly on samples from drill core in a zone of mineralization, namely the Texmont nickel mine, which show intensive serpentinization and carbonatization (Barnes, 1985). Specifically, in a recent study, Lahaye et al. (1995) found that some komatiite samples from the Texmont mine show pronounced depletion of Zr and Hf relative to MREE. They attributed the negative HFSE anomalies to intense carbonate alteration, and suggested that HFSEs are mobile during this secondary hydrothermal alteration (Lahaye et al., 1995). In order to investigate the primary petrogenesis of komatiites and tholeiites from McArthur Township, and to draw comparison with those from the other three localities, it is necessary to examine the freshest samples distal from the zone of mineralization with its associated intense hydrothermal alteration. Recent logging activity has revealed large areas of surface outcrop in the southeast part of McArthur Township. Samples in this study are all from newly revealed surface outcrop.

The objectives of this chapter are: (1) to discuss the possible influence of hydrothermal alteration on REE and HFSE systematics of komatiites; (2) to examine the possible effects of olivine fractional crystallization on REE and HFSE characteristics of komatiites; (3) to discuss the mantle sources of komatiites and tholeiites from the central block of the Abitibi SVZ, and (4) to compare their geochemistry with that of the other three komatiite-tholeiite sequences.

6-2. General geology of McArthur Township

A simplified geological map of part of McArthur Township is presented in Figure 6-

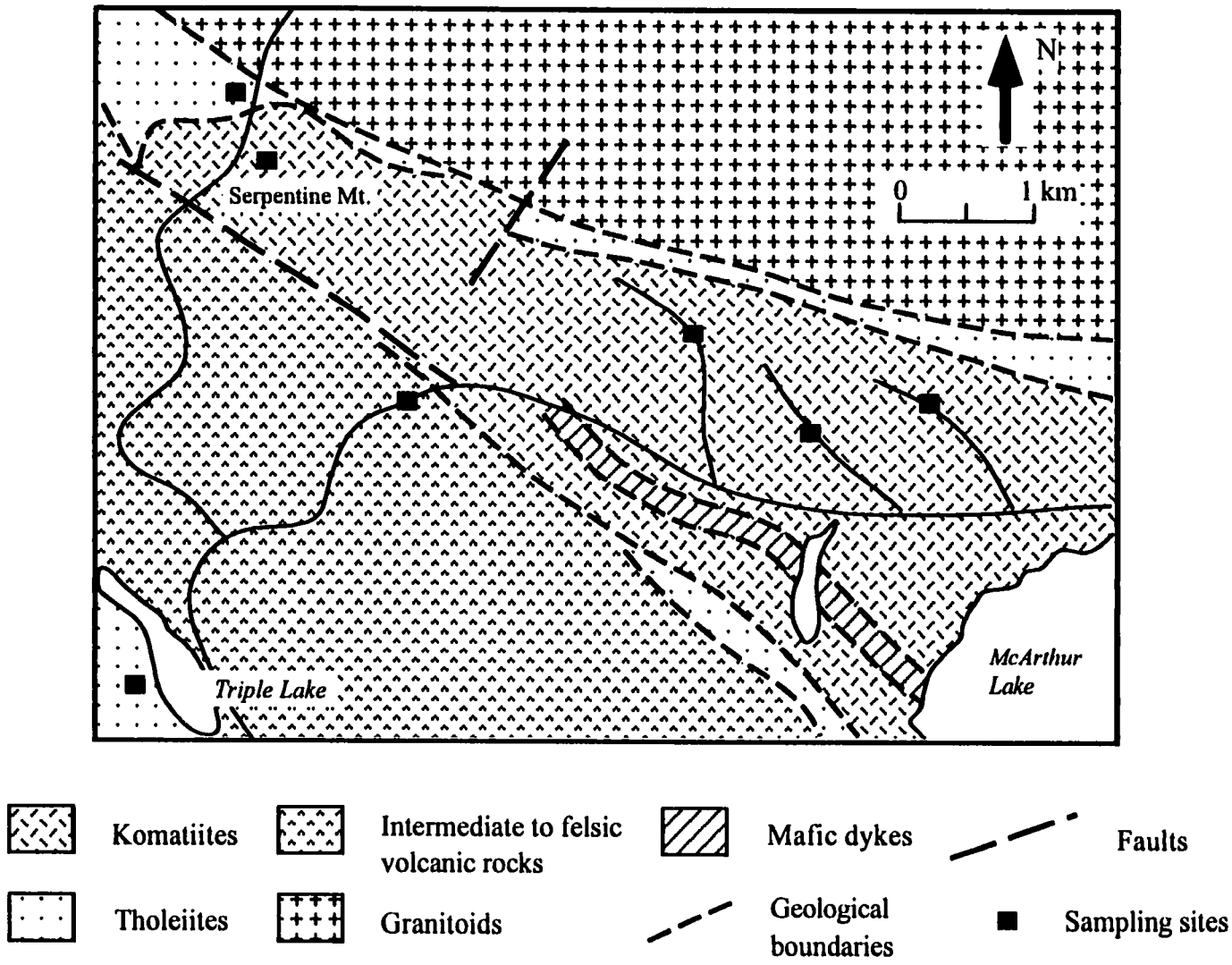

Figure 6-1. Simplified geological map of part of McArthur Township (after Pyke, 1978)

1. Volcanic rocks, ranging from ultramafic to felsic in composition, occur in this area. The Texmont nickel mine is located to the southeast of McArthur Lake, and has been interpreted to lie in the same stratigraphic units as volcanic flows shown in the map area (Pyke, 1978). There are no age data available for mafic and ultramafic volcanic rocks in this area. It has been suggested, however, that mafic and ultramafic flows in McArthur Township are the same age as those in Tisdale and Munro Townships, based on stratigraphic correlations (Pyke, 1978; Jensen, 1985).

Komatiitic flows have typical textural flow differentiation sections, namely an olivine cumulate zone, spinifex textured zone, and chilled and fractured flow top (Pyke, 1978; Barnes, 1985). Metamorphic grade is generally lower greenschist facies, similar to that of volcanic rocks elsewhere in the Timmins district. Microscopically, komatiitic flows are altered largely to serpentine, chlorite, and tremolite, and minor carbonate. Some komatiitic flows contain up to 35% relict olivine, compositionally Fo_{90-94}; grain size is generally 0.5 to 1.0 mm. In spinifex zones, blades of olivine are largely altered to serpentine and chlorite, whereas the interblade areas, originally composed mainly of clinopyroxene and glass, are largely altered to tremolite and lesser chlorite. Extensive carbonatization occurs adjacent to the late granitic intrusive rocks south of McArthur Lake, as well as in the mine area.

Mafic volcanic rocks predominate in the northeast and southwest of the area. They are all tholeiitic in composition (Table 6-1). Tholeiitic basalts are fine to coarse grained, and generally massive to weakly foliated. Variolitic pillow lavas are abundant. In thin section, the original plagioclase is altered to aggregates of sodic plagioclase, epidote-clinozoisite, and minor chlorite. Sericite and lesser calcite are also common alteration products. In some samples, relict andesine was observed.

Table 6-1. Major and trace element compositions of komatiites and tholeiites from McArthur Township

	komatiites (spinifex)											komatiites		
Sample No.	93-18	93-22a	93-25	93-26	93-32	93-48	93-50	93-232	93-236	93-238	93-243	93-29	93-30	93-31
Na2O	0.31	0.77	0.68	0.93	0.77	0.35	1.64	0.59	1.10	0.89	0.27	0.47	0.65	0.54
MgO	25.2	20.9	23.9	21.2	23.4	27.7	18.9	24.5	21.0	22.5	26.8	27.5	25.0	26.9
Al2O3	4.43	8.09	6.67	8.04	7.01	5.63	9.59	6.85	7.90	7.28	5.20	5.60	6.56	5.69
SiO2	42.3	42.8	43.6	43.7	44.1	41.9	41.7	43.2	45.4	43.4	40.6	41.8	43.3	41.8
P2O5	0.03	0.05	0.03	0.04	0.03	0.03	0.05	0.03	0.04	0.04	0.03	0.03	0.04	0.03
K2O	0.01	0.01	0.01	0.02	0.02	0.01	0.04	0.01	0.02	0.01	0.01	0.01	0.01	0.01
CaO	9.40	7.45	6.81	7.28	7.01	5.32	8.76	6.64	8.77	7.16	4.62	4.96	6.41	5.03
TiO2	0.235	0.429	0.335	0.427	0.361	0.318	0.555	0.350	0.375	0.373	0.270	0.296	0.352	0.312
Cr2O3	0.23	0.39	0.36	0.40	0.36	0.29	0.30	0.35	0.56	0.37	0.31	0.36	0.32	0.32
MnO	0.19	0.18	0.16	0.17	0.20	0.17	0.12	0.16	0.16	0.20	0.19	0.16	0.17	0.18
Fe2O3	8.65	12.00	10.90	11.80	11.70	11.00	13.90	10.70	11.00	12.00	12.10	10.70	10.10	11.60
LOI	8.20	4.45	4.90	4.65	4.90	6.85	2.85	5.55	3.90	4.40	8.05	7.05	5.85	6.90
SUM	99.2	97.5	98.3	98.7	99.9	99.6	98.4	98.9	100.2	98.6	98.4	98.9	98.8	99.3
La	0.64	0.42	0.40	0.42	0.48	0.50	1.35	0.50	0.63	0.59	0.54	0.38	0.56	0.52
Ce	1.50	1.48	1.26	1.37	1.39	1.56	3.56	1.58	2.01	1.68	1.43	0.97	1.72	1.27
Pr	0.24	0.29	0.23	0.26	0.26	0.28	0.55	0.28	0.37	0.28	0.23	0.18	0.28	0.21
Nd	1.22	1.65	1.25	1.56	1.44	1.50	2.71	1.52	2.04	1.64	1.33	1.04	1.63	1.17
Sm	0.50	0.79	0.59	0.65	0.61	0.61	1.12	0.66	0.87	0.67	0.50	0.52	0.67	0.52
Eu	0.21	0.32	0.25	0.28	0.23	0.25	0.56	0.23	0.42	0.28	0.21	0.23	0.25	0.23
Gd	0.80	1.30	1.12	1.07	1.14	0.95	1.99	1.03	1.27	1.11	0.89	0.86	1.08	0.86
Tb	0.15	0.23	0.20	0.22	0.20	0.18	0.35	0.19	0.22	0.20	0.14	0.16	0.19	0.15
Dy	1.06	1.73	1.41	1.57	1.56	1.27	2.52	1.39	1.59	1.39	1.08	1.11	1.38	1.06
Ho	0.22	0.35	0.28	0.35	0.34	0.29	0.56	0.31	0.33	0.30	0.23	0.25	0.30	0.24
Er	0.66	1.04	0.85	1.05	1.06	0.85	1.57	0.87	0.99	0.95	0.67	0.73	0.87	0.71
Tm	0.10	0.15	0.13	0.14	0.15	0.12	0.22	0.14	0.15	0.14	0.10	0.11	0.12	0.10
Yb	0.64	0.92	0.80	1.03	0.94	0.77	1.47	0.89	0.97	0.91	0.63	0.77	0.94	0.67
Lu	0.10	0.16	0.13	0.15	0.15	0.12	0.23	0.13	0.16	0.14	0.09	0.10	0.13	0.10
∑REE	8.0	10.8	8.9	10.1	10.0	9.3	18.8	9.7	12.0	10.3	8.1	7.4	10.1	7.8
(La/Sm)n	0.8	0.3	0.4	0.4	0.5	0.5	0.8	0.5	0.5	0.6	0.7	0.5	0.5	0.6
(Gd/Yb)n	1.0	1.2	1.2	0.9	1.0	1.0	1.1	1.0	1.1	1.0	1.2	0.9	1.0	1.1
(La/Yb)n	0.7	0.3	0.4	0.3	0.4	0.5	0.7	0.4	0.5	0.5	0.6	0.4	0.4	0.6
Li	2.68	10.17	14.70	14.48	8.94	21.92	17.89	22.58	4.18	3.43	6.32	7.52	6.25	5.31
Sc	19.70	32.95	27.20	33.18	29.59	22.00	39.01	29.32	28.37	29.13	20.66	30.20	32.41	31.35
V	115.6	203.2	175.1	212.0	199.7	156.3	257.2	175.7	176.9	169.7	121.5	168.4	187.8	179.7
Rb	0.36	0.36	0.70	0.57	1.18	0.64	0.51	0.33	0.82	0.51	1.14	1.21	1.38	0.74
Sr	120.35	15.48	13.55	14.36	16.85	9.84	21.50	17.39	20.10	20.53	36.57	15.08	18.49	22.79
Y	5.49	8.54	7.24	7.57	7.78	6.43	11.64	7.05	8.52	8.18	6.28	7.53	8.66	7.68
Zr	15.68	16.80	13.44	16.80	16.80	14.56	34.72	14.56	21.28	16.80	12.32	13.44	17.47	13.44
Nb	0.61	0.58	0.50	0.58	0.55	0.69	0.99	0.66	0.54	0.61	0.42	0.83	1.01	0.81
Ba	4.67	3.60	6.25	6.53	6.37	3.35	7.77	3.66	10.14	11.54	4.06	4.64	3.47	15.32
Hf	0.47	0.49	0.42	0.55	0.51	0.41	1.02	0.42	0.63	0.51	0.37	0.42	0.51	0.41
Pb	0.53	0.33	0.63	0.48	0.82	2.45	0.74	0.74	0.67	0.62	0.43	0.50	0.83	0.24
Th	0.13	0.12	0.10	0.10	0.09	0.09	0.14	0.12	0.05	0.08	0.04	0.07	0.09	0.07
U	0.10	0.09	0.04	0.11	0.09	0.36	0.61	0.08	0.07	0.08	0.08	0.37	0.85	0.06
Th/La	0.20	0.29	0.25	0.24	0.19	0.18	0.10	0.24	0.08	0.14	0.07	0.18	0.16	0.13
Nb/La	0.95	1.38	1.25	1.38	1.15	1.38	0.73	1.32	0.86	1.03	0.78	2.18	1.80	1.56
Zr/Sm	31.4	21.3	22.8	25.8	27.5	23.9	31.0	22.1	24.5	25.1	24.6	25.8	26.1	25.8
Hf/Sm	0.94	0.62	0.71	0.85	0.84	0.67	0.91	0.64	0.72	0.76	0.74	0.81	0.76	0.79
Nb/Nb*	1.0	1.1	1.1	1.2	1.0	1.2	0.7	1.1	0.7	0.9	0.7	2.1	1.6	1.5
Zr/Zr*	1.4	1.0	1.1	1.1	1.2	1.0	1.4	1.0	1.1	1.1	1.0	1.2	1.2	1.2
Hf/Hf*	1.5	1.1	1.2	1.4	1.4	1.1	1.5	1.0	1.2	1.2	1.1	1.4	1.2	1.3

Note: major elements in wt%, trace elements in ppm.

(Table 6-1 continue)

(cumulate)					tholeiites						
93-37	93-46	93-248	93-250	93-249	93-262	93-263	93-264	93-266	93-268	93-40	93-43
0.13	0.28	0.05	0.05	0.06	2.21	1.60	4.62	0.22	2.78	3.48	2.82
33.4	29.0	33.6	37.5	38.2	6.6	7.9	3.8	5.8	5.3	1.3	8.8
3.74	5.03	2.71	2.63	1.85	14.40	13.40	15.20	12.20	11.40	17.00	14.50
39.7	41.3	37.1	38.5	38.8	50.6	49.5	62.0	52.7	48.7	64.8	46.7
0.02	0.03	0.02	0.03	0.02	0.08	0.07	0.14	0.13	0.08	0.14	0.09
0.01	0.02	0.01	0.01	0.01	0.14	0.08	0.69	1.02	0.21	0.73	0.22
3.31	3.84	2.50	0.31	0.01	9.41	11.30	3.21	4.32	8.71	4.90	7.64
0.208	0.268	0.173	0.181	0.130	0.967	0.850	0.648	1.700	2.290	0.621	1.130
0.27	0.33	0.24	0.28	0.23	0.01	0.01	0.02	0.01	0.01	0.01	0.01
0.15	0.16	0.16	0.19	0.14	0.25	0.22	0.09	0.20	0.28	0.15	0.24
9.23	10.50	8.54	7.65	7.55	13.50	13.50	6.97	17.20	19.90	5.23	15.10
8.70	8.05	13.60	11.70	12.20	2.40	2.15	2.40	4.10	0.55	1.80	2.55
98.9	98.8	98.7	99.0	99.2	100.5	100.6	99.7	99.5	100.2	100.2	99.7
0.23	0.35	0.35	0.41	0.31	3.69	2.91	14.66	9.23	3.59	16.92	4.60
0.76	1.09	1.00	1.10	0.89	9.50	8.01	31.49	21.40	9.82	36.43	11.16
0.13	0.19	0.16	0.17	0.14	1.31	1.19	3.62	2.91	1.42	4.31	1.73
0.89	1.17	0.91	0.86	0.75	6.78	6.44	15.61	14.34	7.96	16.35	9.06
0.40	0.50	0.32	0.28	0.28	2.24	2.11	3.26	4.52	2.76	2.92	2.81
0.16	0.20	0.13	0.09	0.09	0.83	0.72	1.20	1.32	1.00	0.90	1.02
0.61	0.80	0.45	0.49	0.39	2.95	2.74	3.10	5.11	3.68	2.62	3.53
0.12	0.14	0.09	0.08	0.07	0.49	0.46	0.39	0.85	0.64	0.35	0.61
0.79	1.01	0.65	0.59	0.45	3.36	3.31	2.14	5.73	4.46	2.21	4.31
0.17	0.22	0.13	0.13	0.11	0.75	0.71	0.41	1.22	0.95	0.41	0.89
0.52	0.68	0.38	0.38	0.34	2.26	2.18	1.18	3.66	2.97	1.21	2.68
0.07	0.10	0.06	0.06	0.05	0.33	0.32	0.18	0.56	0.42	0.18	0.41
0.51	0.68	0.36	0.34	0.32	2.23	2.01	1.17	3.63	2.70	1.15	2.69
0.07	0.09	0.06	0.06	0.04	0.32	0.30	0.15	0.53	0.42	0.17	0.40
5.4	7.2	5.1	5.0	4.2	37.0	33.4	78.6	75.0	42.8	86.1	45.9
0.4	0.5	0.7	0.9	0.7	1.1	0.9	2.9	1.3	0.8	3.7	1.1
1.0	1.0	1.0	1.2	1.0	1.1	1.1	2.2	1.2	1.1	1.9	1.1
0.3	0.4	0.7	0.9	0.7	1.2	1.0	9.0	1.8	1.0	10.6	1.2
3.87	6.45	0.07	1.55	0.81	16.16	14.07	29.79	59.62	5.33	19.67	18.74
22.70	20.27	14.75	14.89	11.33	53.90	58.84	18.92	48.71	66.61	9.81	41.23
123.3	113.7	77.1	66.3	55.7	320.0	394.2	131.0	588.6	916.4	109.4	320.5
0.64	2.04	1.02	-0.10	-0.14	1.81	0.66	22.31	31.74	3.92	19.98	3.54
6.52	9.89	29.10	2.64	1.54	109.93	102.11	155.68	145.59	87.05	310.94	123.80
5.52	5.46	3.30	3.45	2.94	21.14	18.62	12.87	31.94	26.70	11.26	23.16
10.08	12.32	6.72	9.14	6.75	53.76	48.16	106.40	115.36	68.32	125.18	70.56
0.66	0.37	0.49	0.51	0.50	3.09	2.63	3.65	4.39	2.89	5.39	3.22
3.24	1.54	2.30	0.82	0.76	45.71	23.11	148.22	150.45	33.59	188.39	26.50
0.28	0.35	0.15	0.30	0.25	0.88	0.97	2.10	1.58	1.15	3.51	1.93
0.62	0.31	10.04	0.26	0.37	0.63	0.95	1.29	2.46	0.76	3.94	4.76
0.06	0.06	0.07	0.08	0.05	0.30	0.31	1.60	0.48	0.29	2.55	0.34
0.37	0.09	0.08	0.11	0.63	0.10	0.15	0.44	0.15	0.20	0.74	0.39
0.26	0.17	0.20	0.20	0.16	0.08	0.11	0.11	0.05	0.08	0.15	0.07
2.87	1.06	1.40	1.24	1.61	0.84	0.90	0.25	0.48	0.81	0.32	0.70
25.2	24.6	21.0	32.6	24.1	24.0	22.8	32.6	25.5	24.8	42.9	25.1
0.70	0.70	0.47	1.07	0.89	0.39	0.46	0.64	0.35	0.42	1.20	0.69
2.4	0.9	1.3	1.2	1.5	0.8	0.8	0.3	0.5	0.8	0.3	0.7
1.2	1.1	0.9	1.3	1.0	1.0	0.9	1.0	1.0	1.0	1.2	1.0
1.2	1.1	0.7	1.5	1.4	1.1	1.0	1.1	1.0	1.1	1.2	1.0

Intermediate to felsic rocks are mainly confined to the central area (Figure 6-1). They consist dominantly of a variety of tuffs. Plagioclase, ranging from albite to sodic oligoclase, is the principal mineral, with quartz and lesser lithic fragments. Alteration minerals are mainly sericite and chlorite, with minor epidote and opaque minerals.

6-3. Geochemistry of komatiites and tholeiites

Concentrations of major and trace elements for komatiites and tholeiites from McArthur Township are listed in Table 6-1. Komatiites are characterized by high MgO (18-38%), Al_2O_3/TiO_2=18 to 21, and CaO/Al_2O_3=0.8 to 1.1, clearly showing the characteristics of Al-undepleted komatiites, similar to the Al-undepleted komatiites from Tisdale and Munro Townships (Figures 5-4 and 6-2) . There are a few exceptions, e.g., samples 93-249 and 93-250. Both spinifex textured and olivine cumulate zone komatiites have low REE contents ($\sum$REE=8-18 ppm), LREE depletion [$(La/Yb)_n$=0.3-0.7], flat HREE [$(Gd/Yb)_n$=0.9-1.2]. There are variable enrichments of HFSEs relative to REEs, where Nb/Nb* = 0.9-2.1, Zr/Zr* = 1.0-1.4, and Hf/Hf* = 1.0-1.5 (Table 6-1; Figures 6-3, 6-4). These relationships are also similar to Munro type komatiites (see Chapter 5).

Spatially associated tholeiites feature MgO=5-9%, high Ti (TiO_2=0.6-2.3%) and Fe (Fe_2O_3*=5-20%; Table 6-1 and Figure 6-2). The tholeiites have flat REE patterns [$\sum$REE=33-86 ppm; $(La/Yb)_n$=1.0-1.8], and zero HFSE/REE fractionations (Table 6-1; Figures 6-3 and 6-4), characteristics similar to Mg-tholeiites associated with komatiites from Tisdale and Munro Townships. Two felsic samples (93-40 and 93-264) have relatively lower MgO (3.8% and 1.3%, respectively), enriched LREE [$(La/Yb)_n$=10 and 9, respectively] and LILEs, and pronounced Nb and Ti depletions. These two felsic samples are likely the

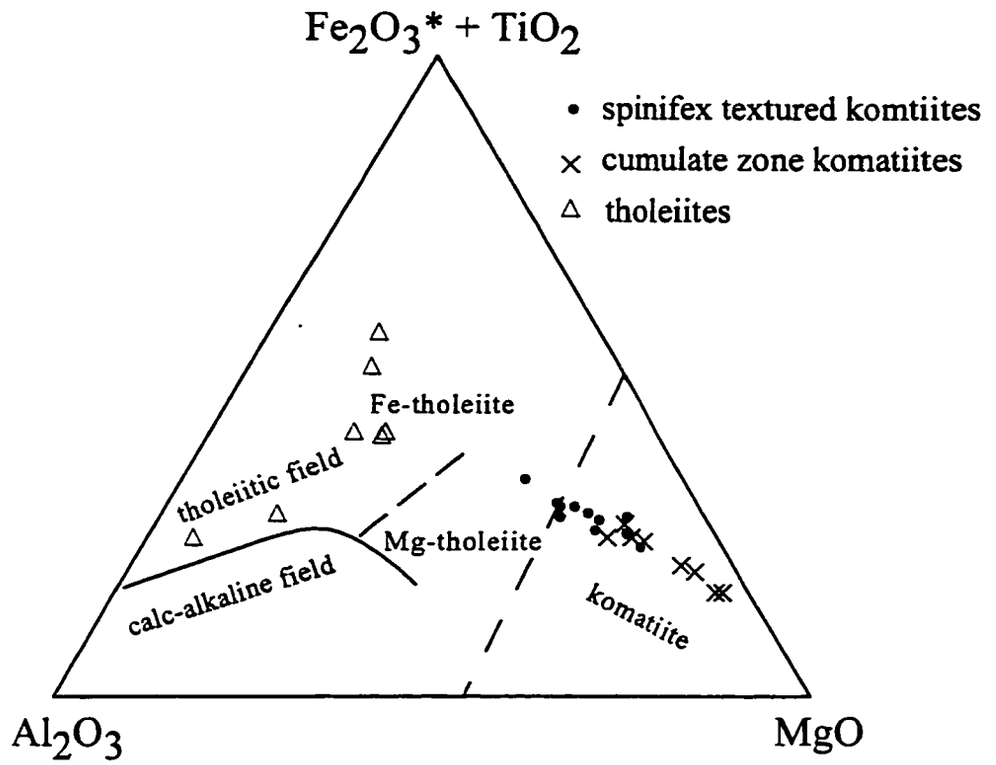

Figure 6-2. Cation triangular plot of komatiites and tholeiites from McArthur Township. Field of rock types from Jensen (1976)

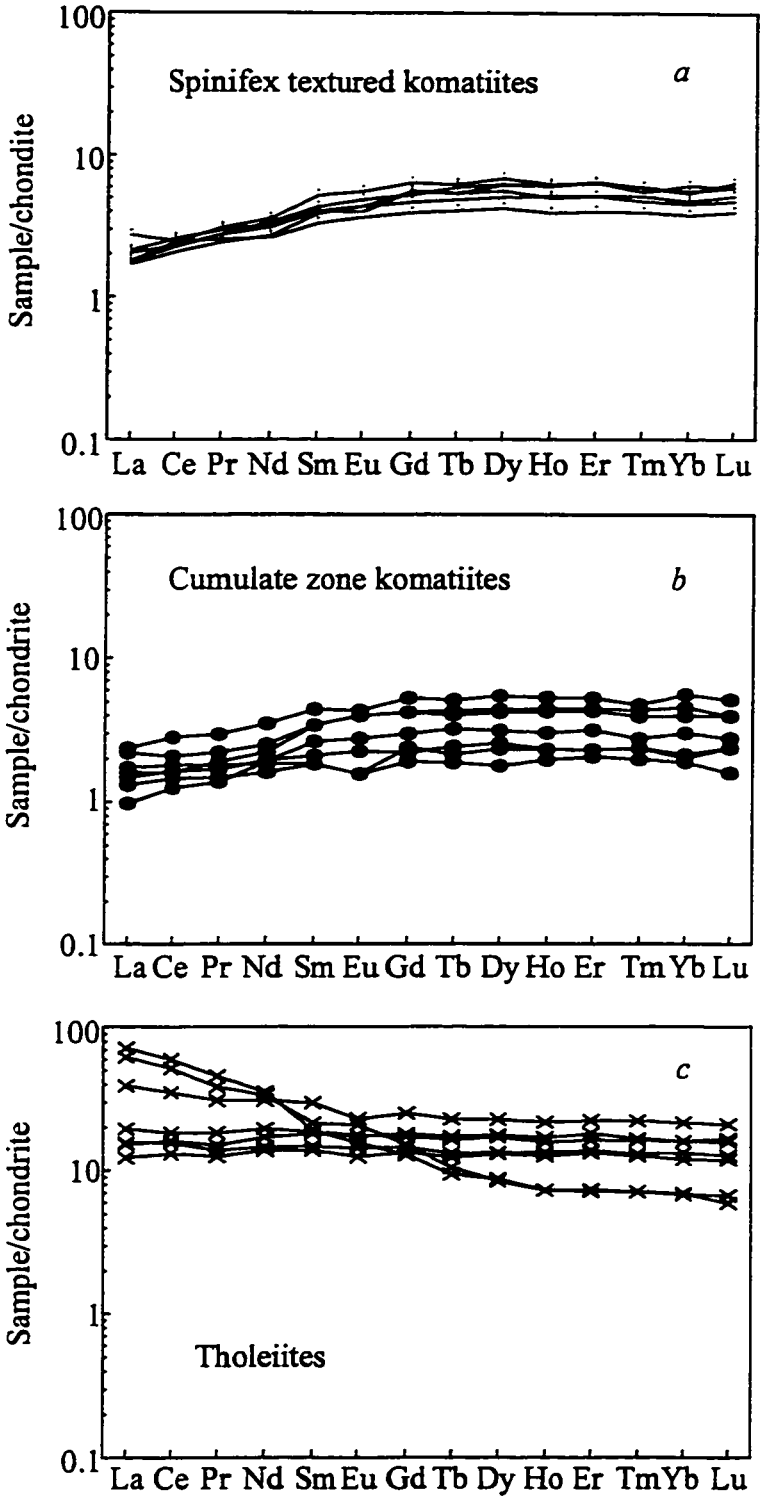

Figure 6-3. REE patterns for komatiites and tholeiites from McArthur Township

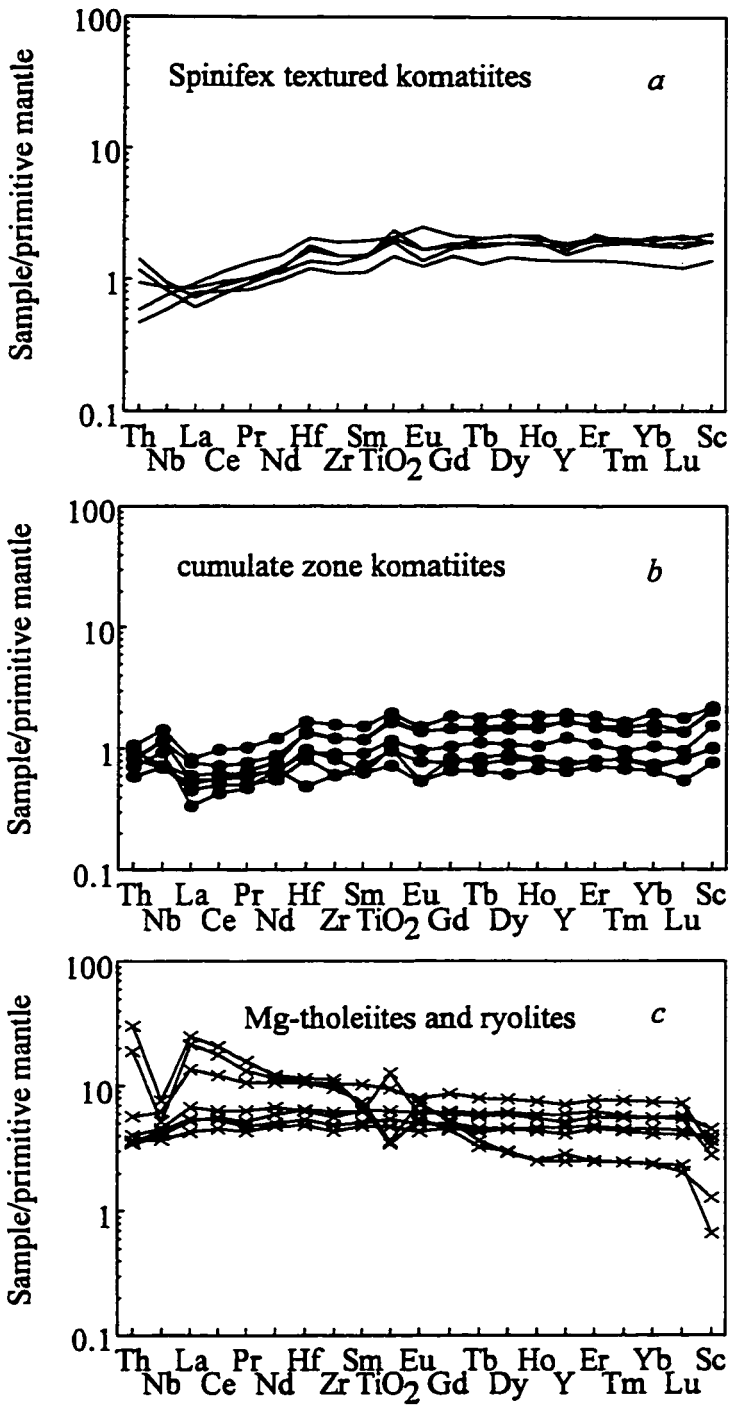

Figure 6-4. Primitive mantle normalized patterns of komatiites and tholeiites from McArthur Township

products of fractional crystallization of the primary tholeiitic magmas.

6-4. Discussion

In the following discussion, the possible effects of hydrothermal alteration, and olivine fractional crystallization on the geochemical characteristics of komatiites, particularly REE patterns and HFSE/REE interrelationships, are first examined. The mantle sources of McArthur komatiites and tholeiites, and comparison with the three other komatiite-tholeiite sequences, are then discussed.

6-4-1. Mobility of trace elements during hydrothermal alteration

All volcanic rocks in Archean greenstone belts have undergone varied intensities of submarine hydrothermal alteration and regional metamorphism, which may modify primary igneous chemical compositions. Accordingly, geochemical data must first be evaluated for the possible effects of secondary mobility of elements, prior to interpreting primary geochemical characteristics. In general, large lithophile elements (LILEs; i.e., Cs, Rb, Sr, Pb and Ba etc) have been shown to be mobile during hydrothermal alteration, whereas REEs and HFSEs are considered relatively insensitive to alteration (Beswick, 1982; Ludden and Gelinas, 1982). However, in some cases where intensive alteration occurs, REEs and HFSEs may also be mobile, particularly during intensive carbonate alteration (Kerrich and Fryer, 1979; Hynes, 1980; Arndt et al., 1989; Feng and Kerrich, 1990a; Tourpin et al., 1991; Valsami and Cann, 1992; Kerrich and King, 1993; Lecuyer et al., 1994). For example, hydrothermal zircon and baddelyite have been found in some Archean lode gold deposits (Kerrich and King, 1994).

A general consensus exists for sets of criteria that may be applied in evaluating the alteration sensitivity, or mobility or immobility, of elements, or groups of elements, in volcanic rocks that have experienced submarine hydrothermal alteration and metamorphism. These criteria can be considered under field, petrographic, and geochemical contexts.

In the field:

(1) Preservation of primary volcanic features, such as zoning in komatiite flows, or pillows in basalts.

(2) Lack of deformation.

Petrographic:

(3) Preservation of primary igneous mineralogy or pseudomorphs indicative of minimal (e.g., olivine to serpentine+magnetite) as against major (e.g., olivine to magnetite+Cr muscovite) open system chemical behaviour.

(4) Absence of deformation at a microscopic scale.

Geochemical:

(5) Low H_2O and CO_2 contents.

(6) For komatiites, major elements and trace elements incompatible in olivine showing correlations with MgO content that plot on olivine control lines, reflecting magmatic fractionation or accumulation of olivine; e.g., MgO negatively correlated with SiO_2, Al_2O_3, TiO_2, but positively correlated with Ni.

(7) Uniformity of interelement ratios such as Al_2O_3/TiO_2, Ti/Zr, Ti/Sc (etc). Specifically, if the ratios of groups of elements that show systematic trends during igneous

processes but contrasting behaviour in secondary alteration, are uniform in a given volcanic lithology, then there is compelling evidence for isochemical behaviour. Examples include an incompatible HFSE and an LREE (Nb/La), moderately compatible HFSE and MREE (Zr, Hf/MREE), and a compatible HFSE and REE (Ti/Gd).

(8) Smooth REE patterns (excepting Ce and Eu).

(9) For komatiites, coherence of REE and primitive mantle normalized patterns for sets of spinifex and cumulate zone samples. A corollary to this is that cumulate zones, with relatively lower REE and HFSE contents, may show trace element mobility where alteration has occurred (Lecuyer et al., 1994).

Samples from McArthur Township were all collected from surface outcrop, with well preserved primary igneous textures, such as spinifex and olivine accumulate zones. The secondary minerals are mainly serpentine, chlorite, and minor carbonates.

Correlations between some major and trace elements and MgO, which is an index of olivine fractionation or accumulation, are clear in Figures 6-5, 6-6 and 6-7. CaO, Al_2O_3, REEs, and HFSEs all plot on the olivine control line, indicating that concentrations of these elements have not been significantly disturbed by secondary hydrothermal alteration. Plots of MgO and incompatible elements intercept on the MgO axis at about 49%, equivalent to liquidus olivine with Fo_{87}. This is in agreement with the average composition of liquidus olivine that crystallized in komatiitic liquids (Arndt, 1994). SiO_2, Rb, Sr and Pb, however, do not plot on the olivine control line, rather the data are scattered, suggesting that the primary contents of these elements have been modified by secondary alteration (Figures 6-5,

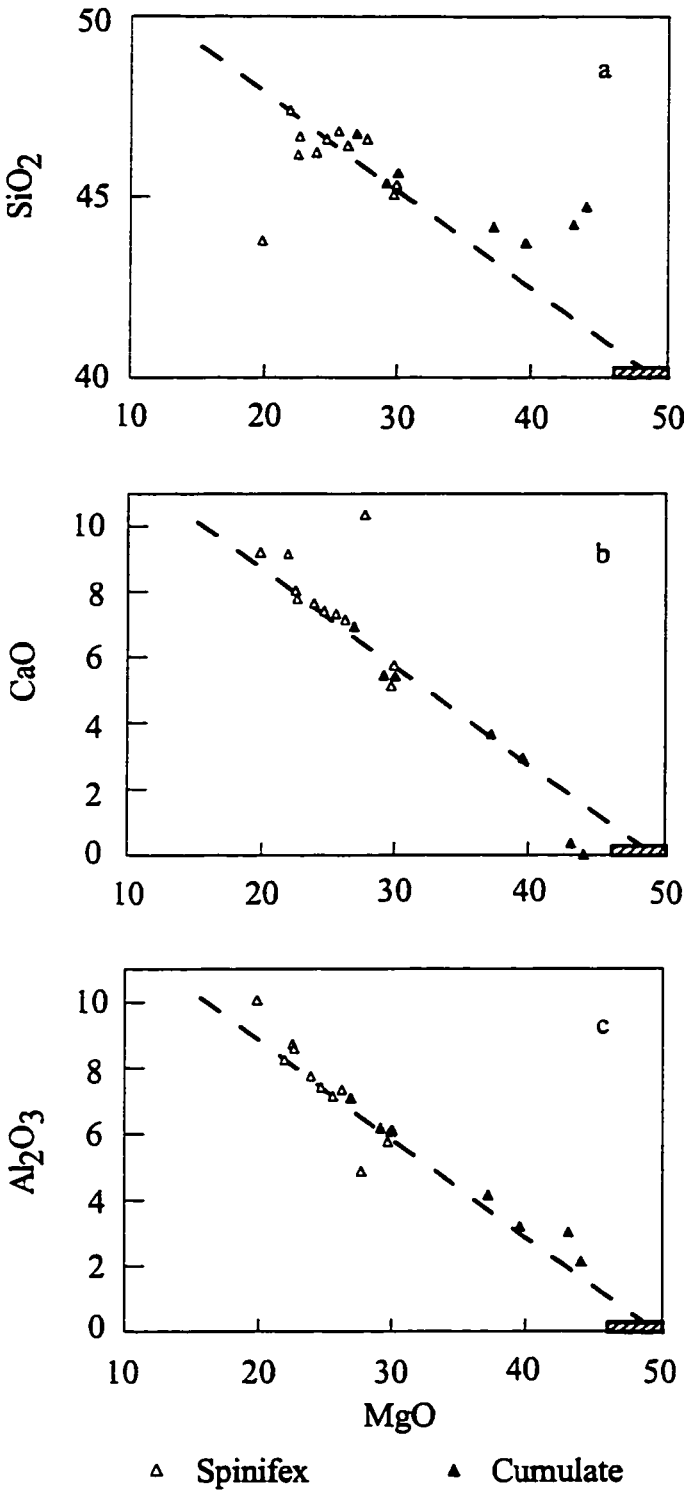

Figure 6-5. SiO_2, CaO, and Al_2O_3 vs MgO plots of komatiites from McArthur Township. Average composition of liquidus olivine in komatiitic liquid shown as hatched box is from Arndt (1995).

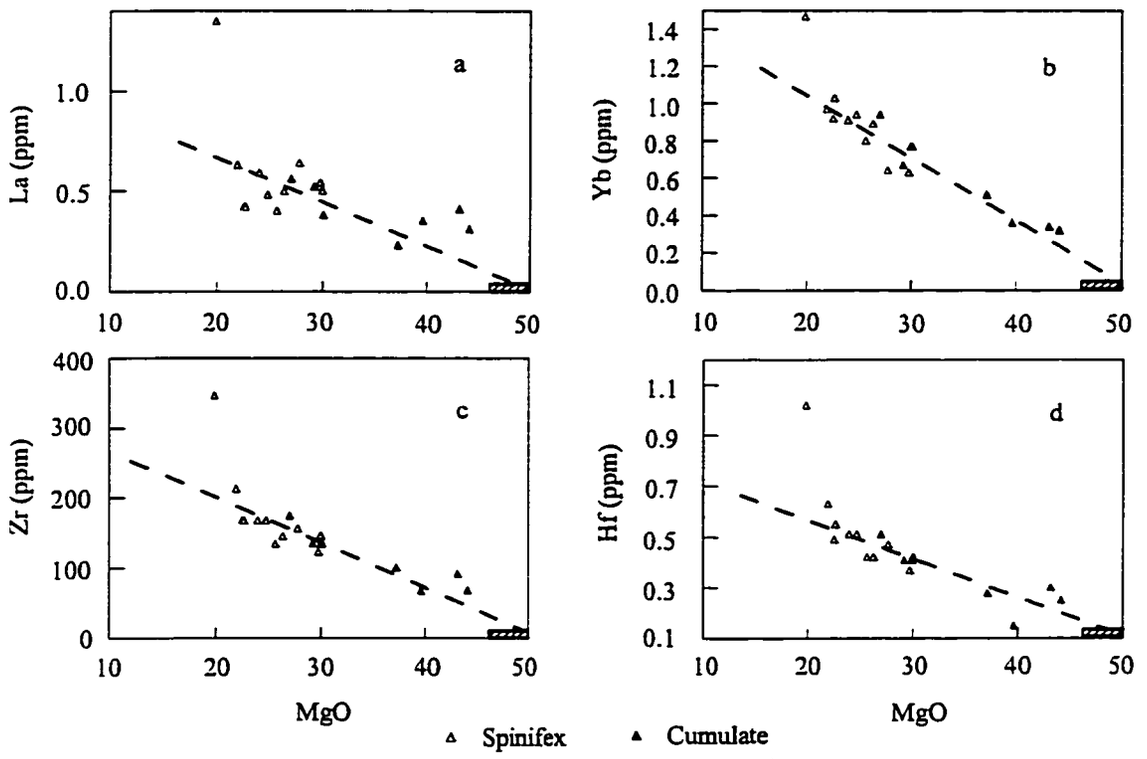

Figure 6-6. Plots of immobile trace elements vs MgO. Average liquidus olivine composion from Arndt (1995)

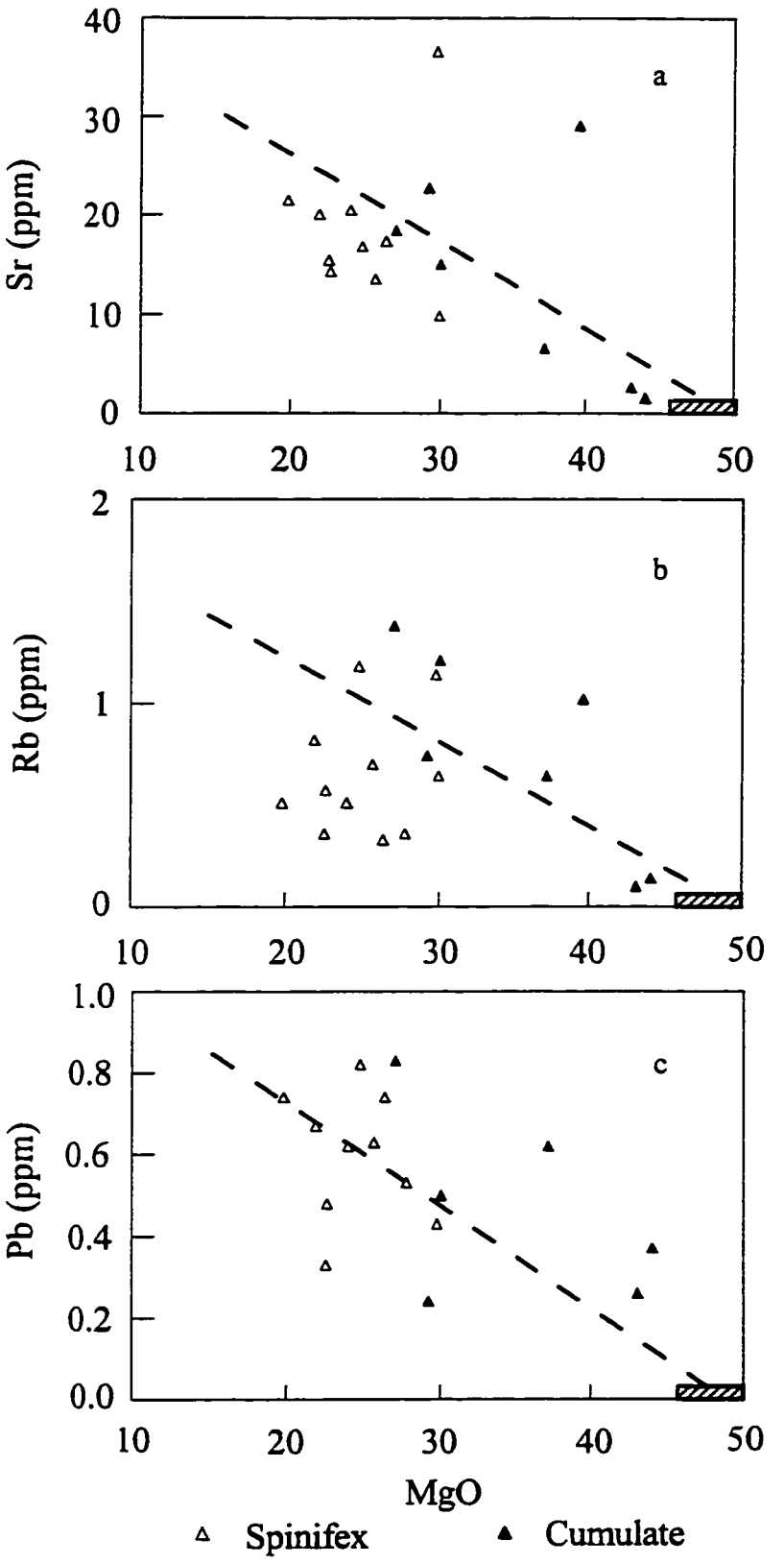

Figure 6-7. Mobile trace elements vs MgO

6-7).

These results suggest that Ca, Al, REEs and HFSEs were insensitive to any hydrothermal alteration, whereas most LILEs (i.e., K, Na, Rb, Sr, Pb etc.) were mobile during alteration. Both spinifex textured and olivine cumulate komatiites in this study share the same REE and primitive mantle normalized patterns, with variable enrichment of HFSEs relative to REEs, similar to the Al-undepleted komatiites from Munro Township (see discussion later).

In contrast, Lahaye et al. (1995) showed that olivine accumulate zones in komatiites from the Texmont mine have pronounced negative Zr and Hf anomalies, whereas spinifex textured komatiites do not have such anomalies (Figure 6-8). They attributed the negative Zr and Hf anomalies in the olivine accumulate zone to mobility of Zr and Hf during dolomitization (Lahaye et al., 1995). Moreover, their results show variably positive Ti anomalies in flows with variable Zr and Hf anomalies (TiO_2/Sm =0.4-0.9, Zr/Sm =1-22, Hf/Sm =0.05-0.75), an effect also evident in the data for altered komatiites (Kerrich and Fryer, 1979; Fan, 1995). In contrast, fresh komatiites do not show positive, or negative, Ti anomalies (Sun and Nesbitt, 1979; Arndt and Nesbitt, 1982; Xie et al., 1993; this study). The difference between the data of Lahaye et al. (1995) and data in this study is probably due to the fact that their samples are from a nickel deposit, which has been subject to intensive carbonate alteration and mineralization, whereas samples used in this study were selected to be least altered using the criteria described above. This underscores the importance of sampling strategies for the study of the primary source characteristics of mafic and ultramafic volcanic rocks. Given the intense carbonatization at Textmont, mobility of HFSEs in carbonic aqueous fluids is not unusual (Kerrich and Fryer, 1979; Hynes, 1980; Arndt et al.,

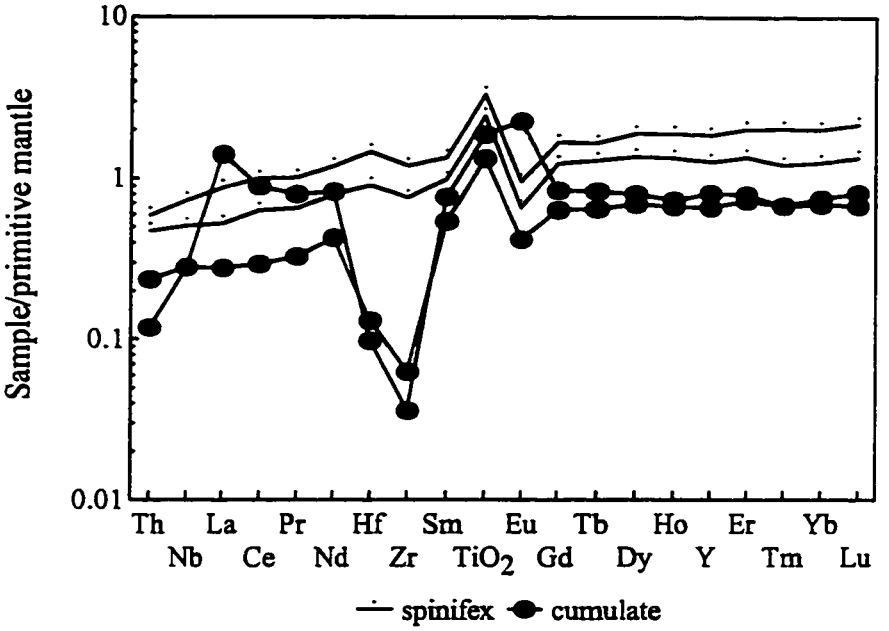

Figure 6-8. Lahaye et al.'s data for komatiites from Texmont nickel mine, which is in the same stratigraphic unit as komatiites from McArthur Township in this thesis. Note that the data show large Zr and Hf negative anomalies in cumulate komatiites, but not in spinifex textured komatiites.

1989; Tourpin et al., 1991; Valsami and Cann, 1992; Kerrich and King, 1993; Lecuyer et al., 1994).

6-4-2. Olivine fractional crystallization

In komatiitic liquids, the only principal liquidus mineral is olivine. Chromite also crystallizes, but in amounts so small that it influences only Cr concentration and has no significant effect on other elements (Arndt, 1986a, 1994). Elements incompatible to olivine, such as Al, REEs and HFSEs, increase with decreasing MgO, as shown in Figures 6-5 and 6-6, and hence ratios of incompatible elements [i.e., $(La/Sm)_n$, Nb/La and Zr/Sm] are not affected by olivine crystallization. However, Arndt and Lesher (1992) found that in some cases, incompatible element ratios vary significantly and correlate with MgO. An example was given in the Kambalda komatiites from Western Australia, in which incompatible element ratios [i.e., $(La/Sm)_n$ and $(Gd/Yb)_n$] vary significantly from the base to the top of a komatiitic flow, and positively correlate with MgO. On this basis, they suggested that HREE may be more compatible than LREE and MREE in olivine. Accordingly, it is necessary to assess the possible effects of olivine fractional crystallization on REE patterns and HFSE/REE interrelationships in komatiites, when these parameters are used as indicators of primary source characteristics.

The freshest komatiites from spinifex textured and olivine cumulate zones in McArthur Township share similar coherent REE patterns with depleted LREE, but unfractionated HREE, as their Munro counterparts (Figure 6-3). Figure 6-9 shows variation diagrams of $(La/Yb)_n$ and $(Gd/Yb)_n$ ratios with MgO. It is clear that $(La/Yb)_n$ and $(Gd/Yb)_n$ ratios remain essentially constant with increasing MgO, suggesting that olivine fractionation

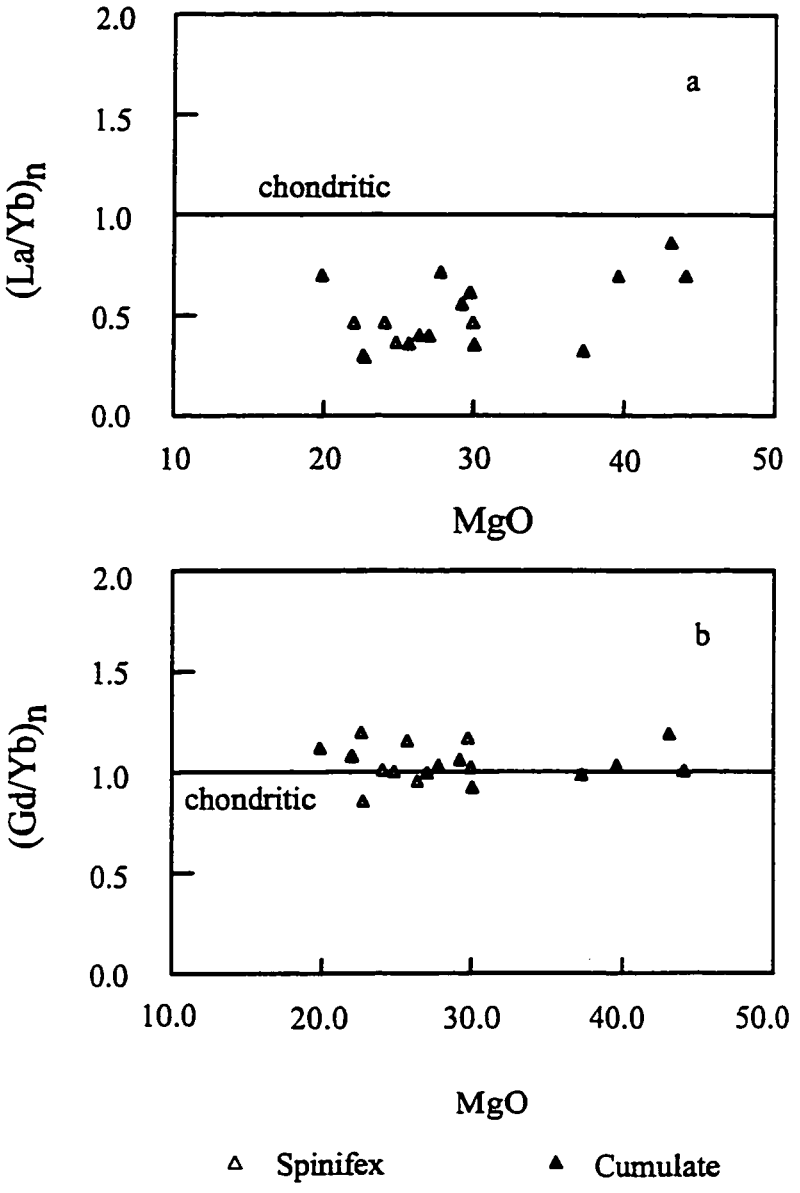

Figure 6-9. $(La/Yb)_n$ and $(Gd/Yb)_n$ vs MgO for komatiites from McArthur Township

does not change the REE patterns of komatiites. Similarly, variations of HFSE/REE versus MgO are shown in Figure 6-10. The interrelationship of HFSEs and REEs do not correlate with MgO contents. Therefore, REE patterns and HFSE/REE interrelationships of komatiites reflect the chemical characteristics of the primary komatiitic liquid, and hence it's mantle source.

6-4-3. HFSE/REE interrelationships in McArthur komatiites and comparison with Munro komatiites

To summarize the previous section, komatiites from McArthur Township are Al-undepleted, with LREE depletion (Figure 6-3), similar to Munro counterparts (Chapter 5). The two komatiite sequences also show similar HFSE/REE interrelationships with variable HFSE enrichment relative to REE, although the enrichment of Zr relative to Sm may not be as obvious as for the other HFSEs (Table 6-1; Figures 6-4 and 6-11).There is compelling evidence that these features are primary, and not an artifact of alteration. Consequently, HFSE enrichment relative to REE may be a global feature of Al-undepleted komatiites.

The enrichment of HFSEs relative to REEs in Munro komatiites was interpreted as a source characteristic, indicating an Mg-perovskite enriched source in the deep mantle (see Chapter 5). Accordingly, komatiites from McArthur Township could be derived from the same mantle sources as counterparts from Munro Township. Similarly, tholeiites in McArthur Township have flat REE patterns with zero HFSE/REE fractionation, comparable to Mg-tholeiites in Munro Township (Table 6-1, Figure 6-4). As discussed in Chapter 5, there is increasing evidence that Archean komatiites and spatially associated tholeiites have distinct mantle sources, with komatiites being generated from anomalously hot mantle

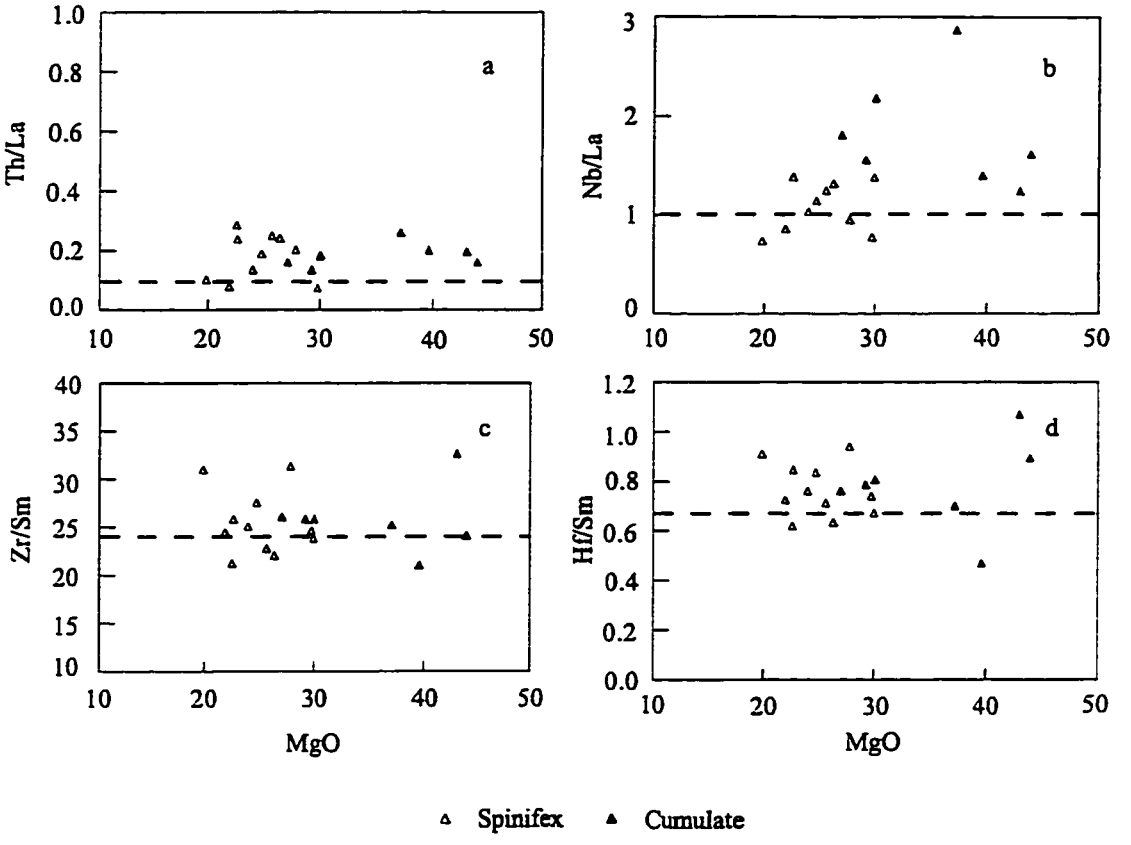

Figure 6-10. Plots of HFSE/REE vs MgO; showing no apparent correlation between HFSE/REE and MgO. Dashed line depicting correspondent primitive mantle values (from Sun and McDonough, 1989).

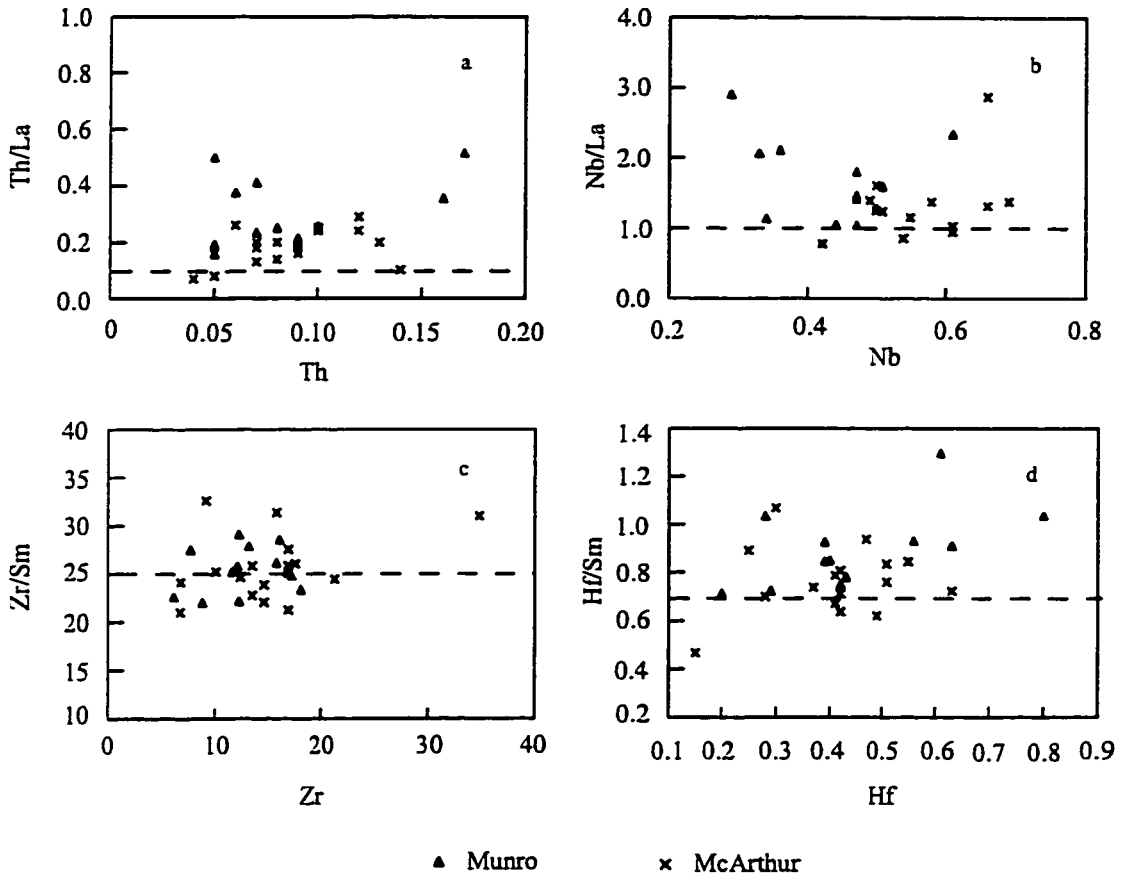

Figure 6-11. Comparison of Th/La vs Th (a), Nb/La vs Nb (b), Zr/Sm vs Zr (c), and Hf/Sm vs Hf (d) for komatiites from Munro and McArthur Townships. Dashed line depicting correspondent primitive mantle values (from Sun and McDonough, 1989).

plumes originating from the deep mantle, and spatially associated tholeiites representing upper mantle sources entrained in the komatiite plumes (Sun and Nesbitt, 1979; Arndt and Nesbitt, 1982; Campbell et al., 1989; Miller et al., 1991b; Herzberg, 1992a; Xie et al., 1993; Xie and Kerrich, 1994). By comparison with the Munro komatiite-tholeiite sequence, McArthur komatiites may also be interpreted as having been generated in a mantle plume originating from the deep mantle originally enriched in Mg-perovskite, whereas spatially associated tholeiites are undepleted upper mantle material entrained by the ascending komatiite plume.

6-5. Summary

The possible effects of hydrothermal alteration and fractional crystallization of olivine on the trace element systematics of komatiites have been examined, using samples from McArthur Township. REEs and HFSEs of komatiites show negative correlations with MgO contents that plot on olivine control lines, commensurate with REEs and HFSEs being insensitive to secondary hydrothermal alteration or regional metamorphism, whereas LILEs (K, Na, Rb, Sr and Pb) are mobile during secondary alteration. This is in general agreement with previous studies on trace element mobility during alteration of mafic and ultramafic volcanic rocks. Olivine is the only important liquidus mineral that crystallizes from komatiitic liquids. However, olivine fractional crystallization will not change the ratios of elements incompatible in olivine, such as $(La/Sm)_n$, Nb/La, Zr/Sm, and Hf/Sm, though it will result in an increase in the overall abundance of incompatible elements. Accordingly, REE and HFSE systematics of komatiites reflect chemical features of primary magmas.

Komatiites from McArthur Township in the central block of Abitibi SVZ are Al-

undepleted type, with LREE depletion and variable positive HFSE anomalies relative to REEs, whereas spatially associated tholeiites are Fe and Ti rich, with flat REE patterns and zero HFSE/REE fractionations. Such geochemical characteristics are similar to that of komatiites and tholeiites from Munro Township, north of the DPFZ. The komatiites in McArthur Township may also be interpreted as having been generated in a mantle plume originating from an Mg-perovskite enriched source in great depth, and tholeiites representing an upper mantle entrained by the ascending mantle plume, as the model invoked for Munro komatiite-tholeiite sequences.

It appears that komatiite-tholeiite sequences in McArthur Township may have been derived from the same mantle sources as in Munro Township. However, the plumes which may have produced Tisdale and Boston komatiite-tholeiite sequences were derived from different mantle sources at different depths.

CHAPTER 7 GEOCHEMISTRY OF VOLCANIC ROCKS FROM THE KINOJEVIS AND BLAKE RIVER GROUPS: IMPLICATIONS FOR PETROGENESIS AND TECTONIC SETTINGS

7-1. Introduction and scope

The Kinojevis (KJG) and Blake River (BRG) Groups are two neighbouring volcanic sequences with contrasting geochemical features in the Southern Volcanic Zone (SVZ) of the Archean Abitibi Greenstone Belt (Figure 2-3; Jensen and Langford, 1985; Ludden et al., 1986). The KJG consists mainly of tholeiitic basalt with minor tholeiitic andesite, dacite and rhyolite, whereas the BRG is predominantly calc-alkaline andesite with minor basalt and rhyolite (Jensen and Langford, 1985).The contrasting geochemical and aeromagnetic characteristics of the two groups have long been recognized (Smith, 1980; Capdevila et al., 1982; Ludden et al., 1982, 1986; Ujike and Goodwin, 1987; Lafleche et al., 1992a, b).

In previous studies, the geochemical differences of the two groups were interpreted to reflect either variable degrees of partial melting of a single mantle source, or differences in the extent of assimilation and fractional crystallization. Smith (1980) attributed the contrasting REE patterns of the mafic members of the KJG and BRG to the different residual mineral assemblages formed during partial melting of mantle lherzolite. Alternatively, Gelinas and Ludden (1984), and Ludden and Hubert (1986), suggested that the BRG calc-alkaline magmas differentiated from tholeiitic magmas through assimilation and fractional crystallization (AFC). In contrast, Capdevila et al. (1982) argued that the KJG tholeiitic

rocks were derived from a depleted mantle source similar to the sources of normal mid-ocean ridge basalts (N-MORB), whereas the BRG calc-alkaline rocks were generated from an enriched mantle source similar to the source of oceanic island-arc basalts (IAB). Fowler and Jensen (1985) further postulated that the KJG tholeiitic rocks came from partial melting of an undepleted mantle source with fractional crystallization in a shallow magma chamber, whereas the BRG calc-alkaline rocks were probably derived from partial melting of a mafic-ultramafic protolith (i.e., komatiites and tholeiites), followed by fractional crystallization with some assimilation of LREE-enriched crustal materials.

Recently, Lafleche et al. (1992a, b) studied the trace element geochemistry of BRG tholeiitic and calc-alkaline volcanic rocks in the Quebec sector of the SVZ (Figure 2-3). They divided the tholeiitic suite into three types from stratigraphically lower to upper sequences, and suggested that tholeiites from the lower sequence were produced by high degree partial melting of adiabatically rising mantle diapirs below rifted lithosphere, whereas tholeiites from the upper sequence were the products of magma mixing between asthenospheric tholeiites and subduction-related calc-alkaline andesites. They further compared calc-alkaline andesites of the BRG with modern oceanic island arc andesites derived from partial melting of subducted young and hot oceanic crust.

This chapter reports the trace element geochemistry of the KJG tholeiite suite and the BRG calc-alkaline suite in the Ontario sector of the SVZ, and discusses their contrasting characteristics (Figure 2-3). The geochemistry of the two groups are further compared with that of Mg- and Fe-tholeiites from Tisdale, Munro and Boston Townships presented in Chapter 5. Based on this and previous studies, it is attempted to provide further constraints on (1) the cause of the geochemical disparity between the KJG and BRG; (2) the tectonic

environments that the two groups may represent; and (3) implications for the tectonic evolution of the SVZ.

7-2. Regional geology and petrology

In the Kirkland Lake-Noranda area, the KJG and BRG are distributed in an east-west trending synclinorium (Figure 2-3). The KJG occurs on both limbs, whereas the BRG is in the core. The former consists mainly of alternating Mg- and Fe-tholeiitic basalts, with minor tholeiitic andesite, dacite and rhyolite at higher stratigraphic levels (Jensen, 1985). In the Timmins area, the KJG has been referred to as the middle formation of the Tisdale Group (Pyke, 1982; Jensen, 1985; for Mg- and Fe- tholeiites of the Tisdale Groups see Chapter 5). Primary mineral assemblages of the KJG tholeiites are plagioclase, clinopyroxene and Fe-Ti oxides with subordinate interstitial mesostasis. In felsic members, quartz becomes more abundant.

The BRG consists mainly of calc-alkaline andesite with minor basalt and rhyolite (Dimroth et al., 1982; Jensen and Langford, 1985). Volcanic rocks range from massive to pillowed flows with interlayered flow-breccias and pyroclastic units. The lavas are for the most part slightly porphyritic, containing small phenocrysts of clinopyroxene in a fine-grained groundmass of plagioclase, clinopyroxene and minor sulfide.

Originally, the structural and stratigraphic relationships between the two groups were interpreted as successive and conformable, with the BRG overlying the KJG (Dimroth et al., 1982; Jensen, 1985). Corfu et al. (1989; 1993), however, reported an U-Pb zircon age of 2701 ± 2 Ma for the KJG and of 2701 ± 3 Ma for the BRG, suggesting that the two groups do not represent successive volcanic sequences, but rather two separate volcanic suites

having similar ages that were tectonically juxtaposed. Recent aeromagnetic maps also indicate a sharp break between the two groups, with the KJG dominated by a highly variable 'striped' field and the BRG by a "flat" field (Jackson and Fyon, 1992; Jackson et al., 1994). These new lines of evidence suggest that the contacts between the KJG and BRG are structural, and accordingly that the two groups are unlikely to be related by the magmatic evolution of a single mantle liquid (Jackson and Fyon, 1992; Jackson et al., 1994).

Both the KJG and BRG are relatively undeformed and have well-preserved primary igneous textures, except in proximity to major shear zones, such as the PDFZ and KLFZ (Figure 2-3). The two groups experienced prehnite-pumpellyte facies metamorphism, excepting the BRG in the Rouyn-Noranda area where lower greenschist facies is developed (Jolly, 1978; Dimroth et al., 1983a). Upper greenschist and amphibolite facies occur only in aureoles of syn-, to post- kinematic plutons (Dimroth et al., 1983a). Alteration is pervasive in both groups. Dimroth (1983a) recognized two stages of alteration in the volcanic rocks of the two groups: low-temperature sea-floor weathering, and relatively high-temperature, but low intensity, hydrothermal alteration, although both stages predate regional metamorphism.

7-3. Samples and analytical methods

Twenty one samples were collected along two traverses, with sampling locations depicted on Figure 2-3. Major element contents were analysed by XRF at X-Ray Assay Labs Ltd., Ontario. Trace elements were determined by ICP-MS at the Department of Geological Sciences, University of Saskatchewan. Details of ICP-MS analysis were reported in Chapters 3 and 4.

7-4. Results

7-4-1. Magmatic series

Major and trace element contents of 21 samples from the KJG and BRG are listed in Table 7-1, along with some key interelement ratios. Samples from the KJG are mainly basalt with minor rhyolite. SiO_2 contents of the KJG basalts range from 45 wt% to 51 wt%. Iron and Ti enrichment trends are evident on AFM and Harker-type diagrams (Figures 7-1 and 7-2), a feature of the tholeiitic magma series. In contrast, the BRG samples are mainly andesite with minor basaltic andesite, with SiO_2 from 53 wt% to 66 wt%,. There is no Fe and Ti enrichment trend in the BRG samples, a feature of calc-alkaline magma series. These results are consistent with previous studies (Smith, 1980; Dimroth et al., 1983a; Gelinas et al., 1984; Jensen and Langford, 1985).

Trends of Al_2O_3, CaO, and SiQ vs. Mg number also show apparently different patterns for the two series (Figure 7-2). Samples of the KJG tholeiite show a positive correlation of Al_2O_3 and CaO with Mg number, whereas samples of the BRG calc-alkaline andesite show no correlations of Al_2O_3 or CaO with Mg number. These results suggest that plagioclase crystallization played an important role in early stages of magmatic differentiation of the KJG tholeiitic magmas as reflected by the presence of plagioclase phenocrysts in the KJG samples.

7-4-2. REE patterns

All samples of the KJG display flat REE patterns (Figure 7-3a). Normalized $(La/Yb)_n$ and $(Gd/Yb)_n$ ratios range from 0.8-1.6 and 0.9-1.3, respectively, signifying unfractionated LREE and HREE (Table 7-1 and Figure 7-3). Eu/Eu* is close to unity in most basaltic

Table 7-1. Major and trace element contents of volcanic rocks from the Kinojevis and Blake River Groups

	Kinojevis Group												Blake River Group								
Elements	Kj1	Kj2	Kj3	Kj4	Kj5	Kj6	Kj7	Kj8	Kj7a	a803.4	a804.6	a806.4	a784.0	a786.3	a797.9	a785.2	a791.1	a793.1	a794.1	a795.5	a797.2
SiO2	48.3	46.7	51.1	73.4	77.1	48.6	51.6	47.7	45.7	47.1	50.5	47.1	53.6	55.1	53.8	57.6	66.7	61.5	60.4	56.1	55.7
TiO2	1.55	1.81	2.43	0.279	0.23	2.57	2.02	0.95	1.78	1.65	2.35	0.936	0.827	0.945	1.04	0.885	0.7	0.67	0.636	0.951	1.13
Al2O3	13.4	12.3	12.8	12.1	11	11.7	13	14.9	13.8	13.5	11.6	15.6	14.8	14.9	16.8	15.9	13.7	15.5	14.8	14	17.1
Fe2O3#	15	15.2	15.9	4.6	4.6	17.5	15.3	13	17.1	14.7	15.7	11.8	7.25	7.34	9.25	8.15	5.57	7.56	7.12	9.44	8.89
MgO	6.73	5.3	4.79	0.81	0.64	5.77	4.84	7.41	6.14	4.15	3.38	7.64	5.22	4.81	5.25	5.26	3.06	2.92	5.34	6.43	4.88
CaO	9.41	7.46	6.7	0.8	0.52	7.2	7.09	10.6	10.4	7.59	7.67	12.3	7.64	6.09	7.99	5.76	2.67	5.56	3.19	8.16	6.75
Na2O	2.28	2.24	3.27	6.39	4.3	3.68	3.77	1.14	1.48	4.2	2.41	1.43	1.51	1.22	2.16	3.31	4.69	3.56	3.88	2.86	3.35
K2O	0.2	0.04	0.58	0.12	1.04	0.24	0.12	0.13	0.28	0.06	0.19	0.02	0.86	2	1	0.03	0.95	0.27	1.56	0.23	0.62
P2O5	0.13	0.11	0.22	0.06	0.04	0.28	0.18	0.06	0.16	0.15	0.28	0.08	0.11	0.16	0.14	0.12	0.14	0.12	0.09	0.15	0.15
MnO	0.22	0.18	0.21	0.09	0.03	0.28	0.2	0.21	0.29	0.18	0.29	0.17	0.18	0.16	0.16	0.13	0.08	0.14	0.12	0.15	0.17
LOI	2.77	8.77	2.39	0.93	0.93	2.23	2.23	4.08	3.16	5.62	6.23	2.77	7.54	7.54	1.93	2.08	2.08	2.77	2.93	1.54	1.85
SUM	100.1	100.2	100.5	100.1	100.6	100.1	100.4	100.3	100.4	100.5	100.7	99.6	99.6	100.3	99.6	99.3	100	101	100.2	100.1	100.7
Li	10.0	19.0	12.0	6.0	5.0	10.0	8.0	11.0	11.0	12.0	13.0	7.0	43.0	54.0	15.0	20.0	7.0	8.0	13.0	10.0	8.0
Be	0.30	0.50	0.30	2.80	2.00	0.40	0.30	0.10	0.50	0.50	0.30	0.30	0.70	0.90	0.30	0.80	0.20	0.50	0.40	0.60	0.40
Sc	41.6	41	43	5.1	2	43.8	41.6	43	36.2	43.9	42.8	37.7	16.1	18.7	27.9	17.4	15	15.5	15.6	20.3	27.8
V	403	410	463	1	0	508	422	342	394	435	463	277	164	156	232	153	106	105	150	166	252
Rb	5	3	12	2	19	4	4	3	4	2	3	0	24	88	57	1	19	6	50	8	26
Sr	96	116	101	35	32	59	51	108	118	136	159	146	111	62	167	261	125	205	170	82	159
Y	23.2	21.2	27.2	121.5	109.1	30.8	43.8	12.5	39.6	30.5	23.9	12.1	14.4	17.0	17.6	16.1	14.4	17.4	8.9	12.6	15.4
Zr	72	87	88	457	425	113	132	35	88	102	88	25	101	128	100	115	143	150	90	108	98
Nb	3.54	4.01	4.37	29.94	29.57	4.72	7.43	1.66	5.93	6.07	5.1	2.39	4.45	5.74	4.96	5.09	5.59	6.6	3.93	5.34	5
Cs	1.2	0.4	0.3	0	0.4	0.7	1	0.3	0.2	0.3	0.2	0.1	1.2	2.1	1.8	0.2	0.2	0.2	1	1.4	1.4
Ba	41	34.4	195	38.4	92.6	110	23.7	40.7	197	44.5	76	7.3	277	145	542	37.3	269	136	728	95.2	224
Hf	2.1	3.1	2.4	14.3	14.5	2.9	4	1.7	3.1	2.8	2.4	0.8	2.7	3.4	2.5	2.1	3	2.6	1.6	2.3	1.7
Ta	0.19	0.21	0.25	1.56	1.57	0.26	0.41	0.1	0.37	0.35	0.27	0.14	0.35	0.36	0.32	0.26	0.28	0.33	0.21	0.21	0.2
Pb	0.48	0.74	0.8	0.99	1.04	0.58	0.35	0.36	0.82	0.82	0.89	0.45	5.34	5.75	25.84	3.07	1.13	2.92	4.23	41.55	1.78
Th	0.68	0.92	0.84	3.85	4.01	0.88	1.25	0.46	1.08	0.97	0.58	0.29	2.17	1.96	1.35	2.42	2.26	2.43	1.65	1.14	1.02
U	0.09	0.11	0.11	0.81	0.71	0.11	0.2	0.03	0.16	0.21	0.08	0.03	0.44	0.39	0.28	0.58	0.49	0.59	0.44	0.28	0.29

(Table 7-1 continue)

Elements	Kj1	Kj2	Kj3	Kj4	Kj5	Kj6	Kj7	Kj8	Kj7a	a803.4	a804.6	a806.4	a784.0	a786.3	a797.9	a785.2	a791.1	a793.1	a794.1	a795.5	a797.2
La	4.03	4.48	5.21	40.83	26.78	4.75	7.24	1.69	6.53	7.41	4.08	2.11	8.66	12	9.7	12.26	10.5	15.8	7.92	8.5	10.83
Ce	11.07	11.93	13.75	105.4	71.89	13.25	20.72	4.84	18.42	18.55	11.4	5.88	18.41	26.13	22.4	25.3	24.4	33.2	17	20.32	24.42
Pr	1.8	1.87	2.16	15.67	11.02	2.21	3.32	0.82	2.99	2.76	1.77	0.93	2.28	3.25	2.95	3.11	3.12	4.09	2.12	2.64	3.12
Nd	9.77	10.13	11.71	78.72	55.84	12.32	17.84	4.34	16.38	13.97	9.59	5.08	10.2	13.9	12.99	13.61	13.1	16.7	8.83	11.83	13.6
Sm	2.94	2.92	3.6	20.51	16.06	4.06	5.56	1.48	5.01	3.9	3.1	1.58	2.39	3.08	3.01	2.99	2.89	3.47	2.04	2.64	2.92
Eu	1.08	0.98	1.4	3.76	3.38	1.44	1.64	0.56	1.63	1.33	1.53	0.72	0.81	1.02	0.9	0.84	0.64	0.92	0.51	0.76	0.92
Gd	3.96	4.15	4.91	23.88	19.36	5.27	7.4	2.04	6.64	5.12	4.09	2.14	2.85	3.31	3.35	2.92	2.68	3.25	1.76	2.4	2.91
Tb	0.68	0.6	0.8	3.68	3.12	0.87	1.26	0.35	1.09	0.81	0.68	0.34	0.41	0.48	0.52	0.52	0.47	0.58	0.33	0.45	0.52
Dy	4.74	4.25	5.58	25.37	21.52	6.23	8.8	2.58	7.68	5.67	4.61	2.31	2.81	3.19	3.37	3.4	3.04	3.67	1.98	2.94	3.31
Ho	0.98	0.89	1.17	5.29	4.49	1.29	1.83	0.54	1.58	1.2	0.98	0.47	0.57	0.66	0.68	0.68	0.59	0.74	0.39	0.56	0.69
Er	3.08	2.64	3.56	16.4	14.24	4.03	5.67	1.63	4.88	3.68	2.94	1.46	1.7	1.94	2.11	2.07	1.77	2.13	1.13	1.63	1.98
Tm	0.47	0.41	0.53	2.59	2.29	0.59	0.87	0.25	0.73	0.58	0.43	0.22	0.24	0.3	0.31	0.32	0.26	0.33	0.17	0.25	0.29
Yb	2.88	2.65	3.34	16.75	14.54	3.8	5.52	1.61	4.72	3.58	2.79	1.29	1.56	1.91	2.13	1.93	1.75	2.07	1.09	1.61	1.77
Lu	0.46	0.4	0.49	2.48	2.15	0.59	0.83	0.26	0.69	0.56	0.4	0.19	0.24	0.29	0.3	0.31	0.27	0.32	0.15	0.24	0.28
Eu/Eu*	0.98	0.87	1.03	0.52	0.59	0.97	0.79	0.99	0.86	0.91	1.31	1.20	0.95	0.97	0.86	0.86	0.69	0.83	0.80	0.91	0.96
(La/Yb)n	0.92	1.12	1.03	1.61	1.21	0.83	0.87	0.69	0.91	1.37	0.96	1.08	3.66	4.14	3.00	4.20	3.97	5.03	4.82	3.50	4.05
(La/Sm)n	0.84	0.94	0.89	1.22	1.02	0.72	0.80	0.70	0.80	1.17	0.81	0.82	2.23	2.39	1.98	2.52	2.24	2.80	2.38	1.98	2.28
(Gd/Yb)n	0.96	1.09	1.02	0.99	0.92	0.96	0.93	0.88	1.14	1.16	1.19	1.34	1.48	1.40	1.27	1.23	1.24	1.27	1.32	1.21	1.33
Total REE	48	48	58	359	265	60	88	23	79	69	48	25	53	71	65	70	65	87	45	57	68
(Th/La)n§	1.3	1.6	1.2	0.7	1.1	1.4	1.3	2.1	1.2	1.0	1.1	1.0	2.0	1.3	1.1	1.6	1.7	1.2	1.7	1.1	0.8
(U/La)n	0.7	0.7	0.6	0.6	0.8	0.7	0.8	0.5	0.7	0.9	0.6	0.4	1.7	1.1	0.9	1.5	1.5	1.2	1.8	1.1	0.9
(Nb/La)n	0.9	0.9	0.8	0.7	1.1	1.0	1.0	1.0	0.9	0.8	1.2	1.1	0.5	0.5	0.5	0.4	0.5	0.4	0.5	0.6	0.4
(Ta/La)n	0.8	0.8	0.8	0.7	1.0	1.0	1.0	1.0	1.0	0.8	1.2	1.2	0.7	0.5	0.6	0.4	0.4	0.3	0.4	0.4	0.3
(Zr/Sm)n	1.0	1.2	1.0	0.9	1.1	1.1	0.9	0.9	0.7	1.0	1.1	0.6	1.5	1.4	1.1	1.3	1.7	1.5	1.5	1.4	1.2
(Hf/Sm)n	1.0	1.5	1.0	1.0	1.3	1.0	1.0	1.7	0.9	1.0	1.1	0.7	1.4	1.4	1.0	0.9	1.3	0.9	1.0	1.1	0.7
(TiO2/Sm)n	1.1	1.3	1.4	0.0	0.0	1.4	0.8	1.4	0.8	0.9	1.6	1.3	0.7	0.7	0.7	0.6	0.5	0.4	0.7	0.8	0.8
(Th/Yb)n	1.2	1.8	1.3	1.2	1.4	1.2	1.2	1.5	1.2	1.4	1.1	1.1	8.1	6.0	3.7	7.3	7.5	6.8	8.8	4.1	3.3
(U/Yb)n	0.6	0.8	0.7	1.0	1.0	0.6	0.7	0.4	0.7	1.2	0.6	0.5	6.6	4.8	3.1	7.1	6.6	6.7	9.5	4.1	3.8
(Nb/Yb)n	0.8	1.0	0.9	1.2	1.4	0.8	0.9	0.7	0.8	1.1	1.2	1.2	2.0	2.1	1.6	1.8	2.2	2.2	2.5	2.3	2.0
(Zr/Yb)n	1.1	1.4	1.1	1.2	1.2	1.3	1.0	0.9	0.8	1.2	1.3	0.8	2.9	3.0	2.1	2.6	3.6	3.2	3.6	2.9	2.4
(Hf/Yb)n	1.1	1.8	1.1	1.3	1.5	1.2	1.1	1.6	1.0	1.2	1.3	1.0	2.8	2.8	1.9	1.7	2.7	2.0	2.3	2.3	1.5

Note: Major elements in wt%; trace elements in ppm; # Fe2O3=total Fe as Fe2O3; § (Th/La)n is ratio of primitive mantle normalized values.

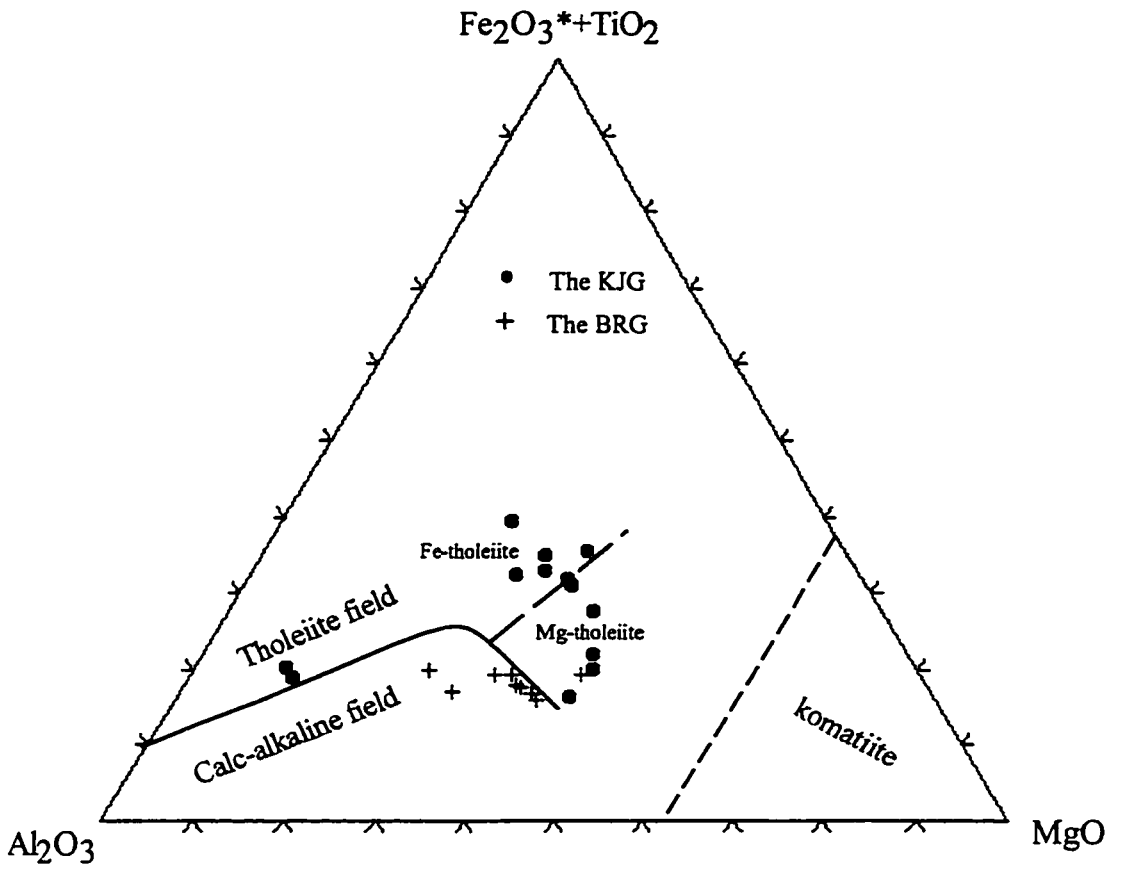

Figure 7-1. Triangular cation plot of basalts from the Kinojevis and Blake River Groups in the central Abitibi SVZ. Fields of rock types are from Jensen (1976).

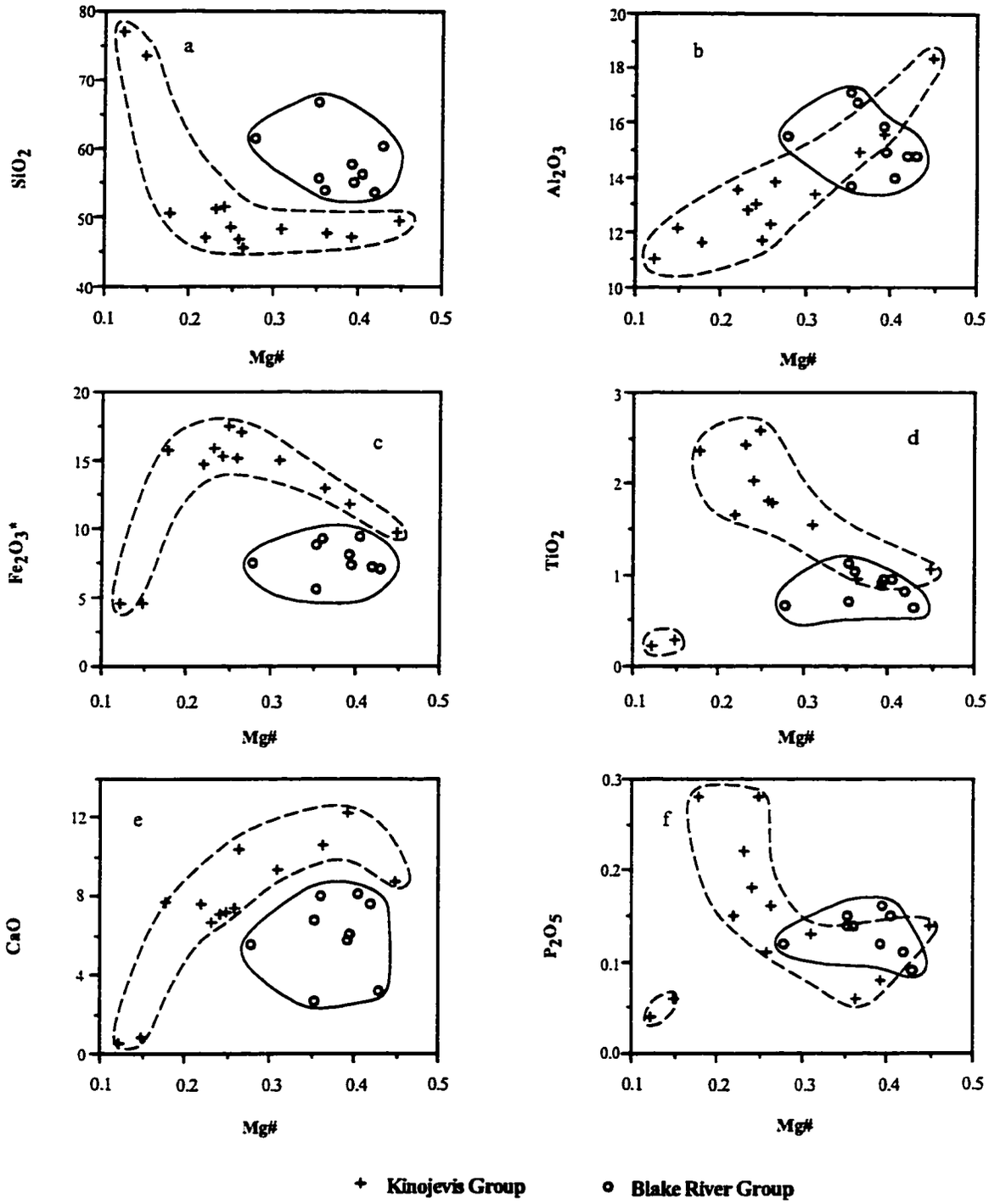

Figure 7-2. Variation of major elements versus magnesium number for the KJG and BRG, clearly showing two magma series, respectively tholeiitic and calc-alkaline.

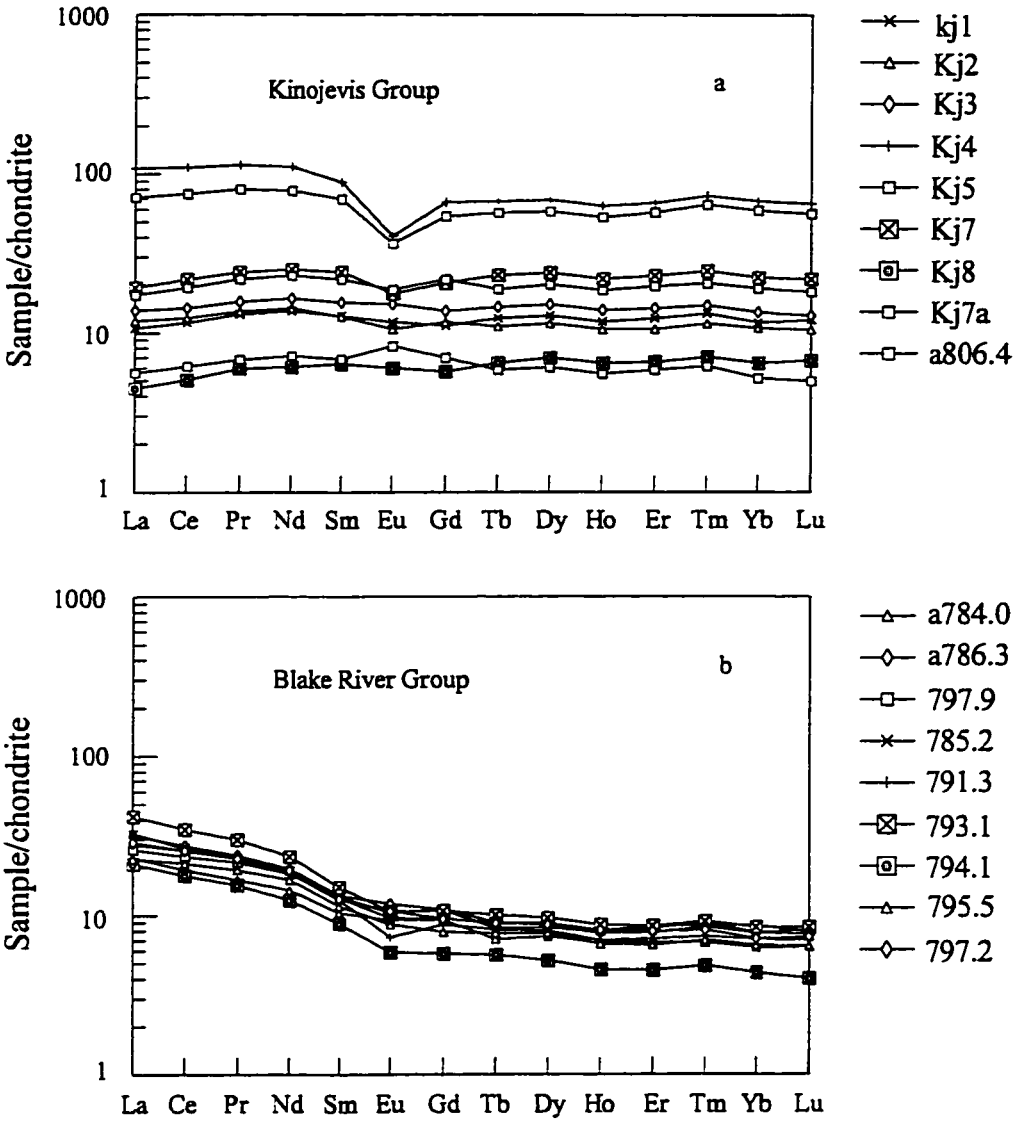

Figure 7-3. Representative REE patterns for volcanic rocks from the Kinojevis (a) and Blake River (b) Groups

samples, indicating no Eu anomaly, but significantly less than unity (0.52 and 0.59) in the two rhyolite samples which reflect the early fractional crystallization of plagioclase (Kj4 and Kj5; Table 7-1). REE contents are 6-20 times chondrite in basalts, but about 100 times chondrite in felsic endmembers.

The BRG samples show an LREE-enriched pattern (Figure 7-3b), with $(La/Yb)_n$=3 - 15 and $(Gd/Yb)_n$=1.2 - 1.5. There is no pronounced Eu anomaly, where Eu/Eu* = 0.82 - 0.96, excepting sample a791.1 in which Eu/Eu* = 0.69. In distinction from the KJG tholeiites, the BRG andesites are also depleted in HREE (Figure 7-3b), a feature which will be further discussed later in this chapter. The BRG andesites have REE contents ranging from 6 to 40 times chondrite.

7-4-3. HFSE and other trace element characteristics

Primitive mantle normalized patterns for the KJG and BRG are presented in Figure 7-4. The utility of such diagrams to present multiple element data for mafic and ultramafic rocks has been described in Chapter 5. Tholeiites from the KJG show flat parallel patterns, with minor positive to zero Ti anomalies, and absence of negative Nb and Ta anomalies. Two felsic endmembers, not shown on the diagram, are also characterized by flat patterns, but with higher absolute element contents (Figure 7-4a). The overall trace element patterns of the KJG are similar to that of Mg-tholeiites in Tisdale, Munro and McArthur Townships (Figures 5-8 and 6-5c), and to that of modern oceanic plateau basalts (Floyd, 1990).

Calc-alkaline andesites from the BRG have a fractionated pattern, with pronounced negative Nb and Ta anomalies relative to Th and La, and a negative Ti anomaly. There is, however, no Hf and Zr depletion relative to Nd and Sm in the BRG, contrasting with the

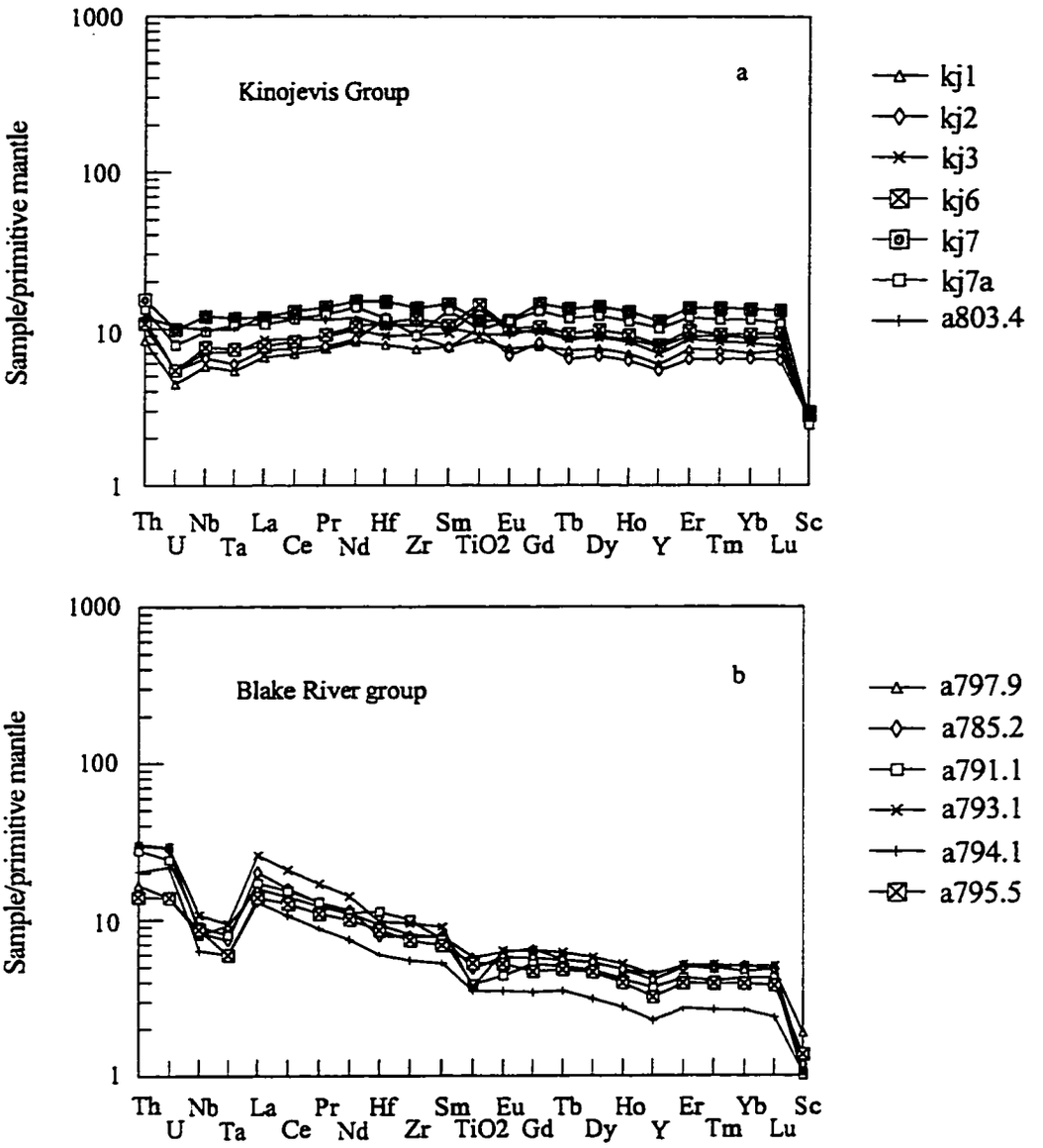

Figure 7-4. Primitive mantle normalized patterns for volcanic rocks from Kinojevis (a) and Blake River (b) groups. Primitive mantle values from Sun and McDonough (1989).

pronounced Hf and Zr depletions observed in Boston komatiites and coexisting Fe-tholeiites (Figure 5-8c). The trace element patterns of the BRG resemble, in general, that of modern ocean island arc volcanics (IAV) [Figure 7-12].

7-5. Discussion

7-5-1. General remarks on HFSE depletions in modern island arc volcanics

Depletions of HFSEs in modern IAV are generally depicted on two types of normalized diagrams: normalized to normal mid-ocean ridge basalts (N-MORB; Pearce, 1982) or normalized to primitive mantle (Hofmann, 1988; Sun and McDonough, 1989). The sequence of elements on the diagrams is based upon the compatibility/incompatibility of elements in the generation of N-MORB, involving the melting of a depleted spinel lherzolite mantle source at depths of 20-60 km. In melting of peridotite, and subsequent fractional crystallization in the upper mantle, the relative incompatibility of these elements should be consistent, that is the normalized diagram should appear as a smooth curve.

In contrast to N-MORB, IAV show a negative anomaly of HFSE, especially Nb, Ta and Ti, in these diagrams (Figure 7-12), although the magnitude of Nb (Ta) and Ti depletions are not necessarily coupled (Salters and Hart, 1991), and the ratios of Nb and Ta vs the adjacent elements Th, U and La, or Ti vs Sm and Gd, are correspondingly low relative to N-MORB. The HFSE depletions of IAV suggest that some process or processes have modified the N-MORB incompatibility of HFSEs in the magma generation of IAV.

Although the HFSE, particularly Nb, Ta and Ti, depletion in IAV has long been recognized, the mechanism, which induces the relative depletion, remains controversial (Green, 1981; Tatsumi et al., 1986; Foley and Wheller, 1990; Kelemen et al., 1990a;

Ringwood, 1990b; Hawkesworth et al., 1991, 1993; McCulloch and Gamble, 1991; Pearce and Peate, 1995).

Pearce and Peate (1995) summarized current models regarding magma generation in a subduction environment (Figure 7-5). They recognizing that volcanic arc magmas owe their compositions to many factors (e.g., fertility of the mantle wedge, compositions of subducted slab, transport of subduction component to the mantle wedge, processes occurring in the melting column, etc.). In an attempt to resolve the question of HFSE depletion, they divided the behaviour of elements in the subduction system into conservative and non-conservative. According to their definition, a conservative element is one for which there is no detectable slab contribution to the source of arc volcanism, whereas a non-conservative element is one for which there is a detectable slab contribution. An element may behave as conservative in a subduction system, due to a number of factors (Pearce and Peate, 1995, and references therein):

(1) Buffering by a high concentration in the mantle source. For example, Ca is certainly mobile in subduction-derived fluids, but is unable to generate detectable enrichment in IAV, because of high Ca content in the mantle wedge;

(2) Retention in the subducting slab, because of low solubility of its host minerals in slab-derived fluids. For example, HFSEs (Nb, Ta, Ti and Zr) tend to be concentrated in minor phases (zircon, apatite and rutile) with very low solubility in slab-derived fluids;

(3) Retention in the subducting slab, due to its high partitioning coefficients for the

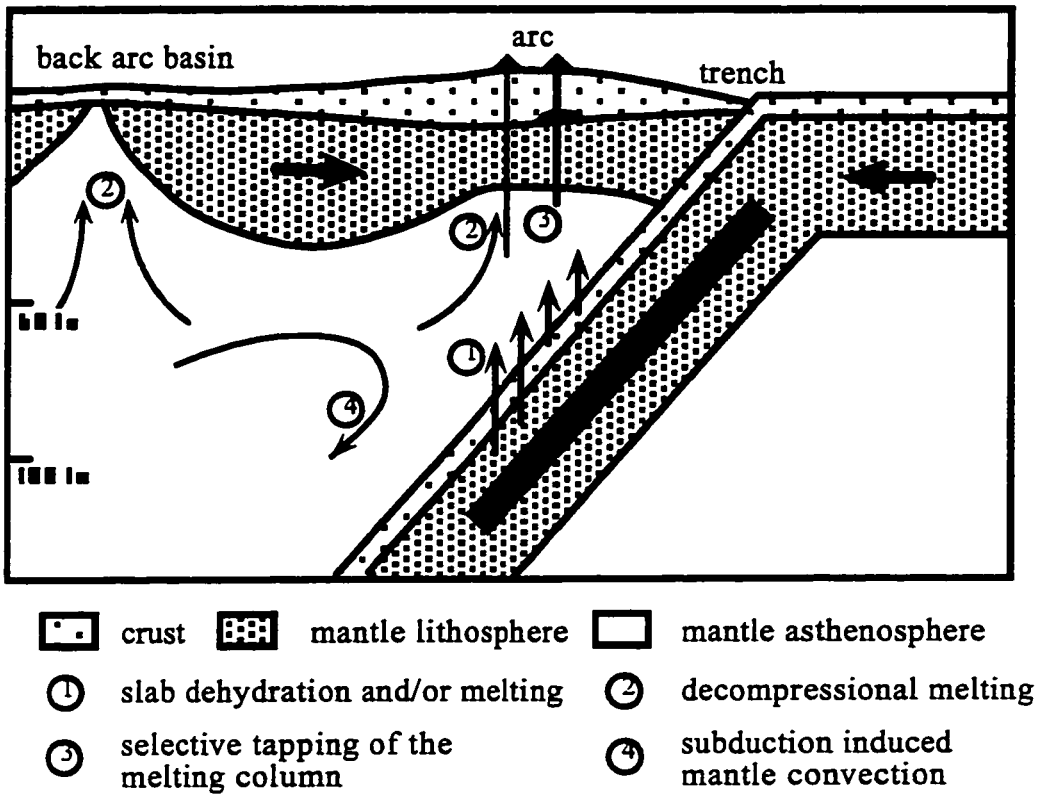

Figure 7-5. A schematic diagram summarizing the processes occurring in a subduction system (simplified from Pearce and Peate, 1995)

residual phases during slab melting. For example, yttrium and HREEs are likely to be conservative during slab melting with amphibole and garnet as residual phases;

(4) Retention in the mantle wedge, whereas non-conservative elements are stripped from the mantle by slab-derived fluids.

The behaviour of an element is also controlled by physical and chemical conditions of the subduction system. Figure 7-6 illustrates how behaviour of elements in slab-derived aqueous and in slab-derived siliceous melts changes. Note that Nb, Ta, Zr and Hf (but not Ti) change from conservative in hydrous fluids to nonconservative in siliceous melts, suggesting that slab dehydration may generate HFSE depletion in IAV, whereas slab-melting may not. The change of Nb, Ta, Zr and Hf from conservative during slab dehydration to nonconservative in slab melting is due to the fact that the mechanism which controls the behaviour of an element is different between the two processes. During slab dehydration, the behaviour of an element is governed by the bulk distribution coefficient (Ds) between slab and aqueous fluid. HFSEs generally have high slab/fluid Ds both because of their small ionic radius (Tatsumi, 1986), and tendency to reside in minor phases with low solubility (Ayers and Watson, 1991). In slab melting, however, the behaviour of an element is controlled by Ds between melt and residual phases. Partial melting of subducted slabs generally occur at depths where garnet and amphibole are in the residue (Defant and Drummond, 1990; Ringwood, 1990b). Garnet and amphibole have high Ds for Y and HREE, but low Ds for Nb, Ta, Zr, Hf and LREEs (Watson and Harrison, 1984). Accordingly, HFSEs and LREEs will behave nonconservatively in a subduction system where slab melting is involved.

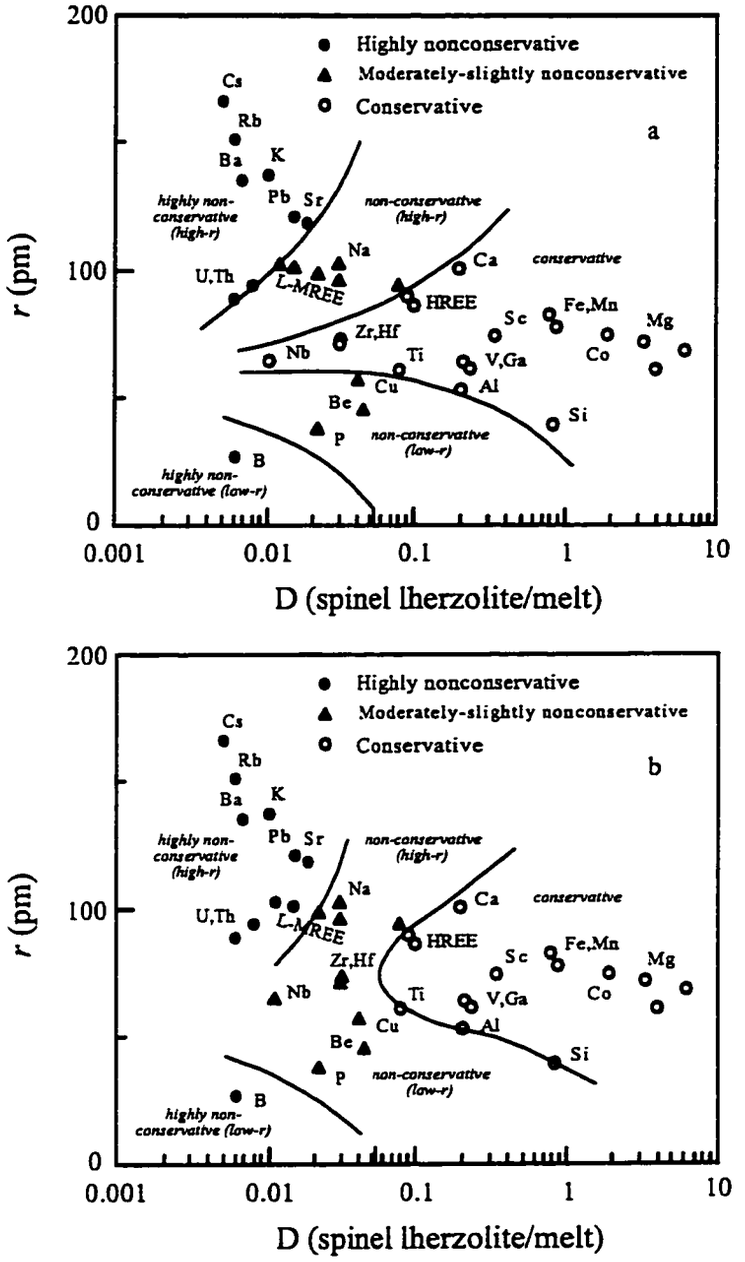

Figure 7-6. Element behaviour in the subduction system as a function of ionic radius (r) and bulk mantle-melt distribution coefficient (D) for (a) hydrous fluids and (b) siliceous melts (from Pearce and Peate, 1995).

Using such an approach, Pearce and Peate (1995) summarized four typical patterns of trace element characteristics for modern IAV (Figure 7-7). All IAV show strong enrichment of LILEs and LREEs, but depletion of HFSEs (particularly Nb and Ta) relative to U and LREEs, clearly suggesting that LILEs and LREEs are nonconservative, whereas HFSEs and HREEs are conservative in most subduction environments. In Figure 7-7, the bold lines linking conservative elements are the "baselines" of element compositions that the mantle source would have without input of subduction components, which basically define four types of mantle sources: (a) undepleted; (b) depleted; (c) enriched; and (d) highly depleted.

7-5-2. Implications of contrasting geochemistry between the KJG and BRG

From the discussion in section 7-4, it is clear that the major elements, LILE, REE and HFSE are distinct between the KJG and BRG. The KJG consists mainly of basalt (SiO_2=46-51 wt%), whereas samples from the BRG are dominantly andesite (SiO_2=53-66 wt%). Thus, the different geochemical characteristics between the two groups may stem from fractional crystallization, crustal contamination, or distinct mantle sources. These possibilities are discussed in turn below.

Fractional crystallization

Based on Figure 7-2, samples of the two groups apparently do not follow a simple fractional crystallization trend. Samples of the KJG show no pronounced increase of SiO_2, but a decrease of Al_2O_3 and CaO with decreasing Mg number. This may reflect the early crystallization of plagioclase, pyroxene and olivine. In contrast, samples of the BRG have

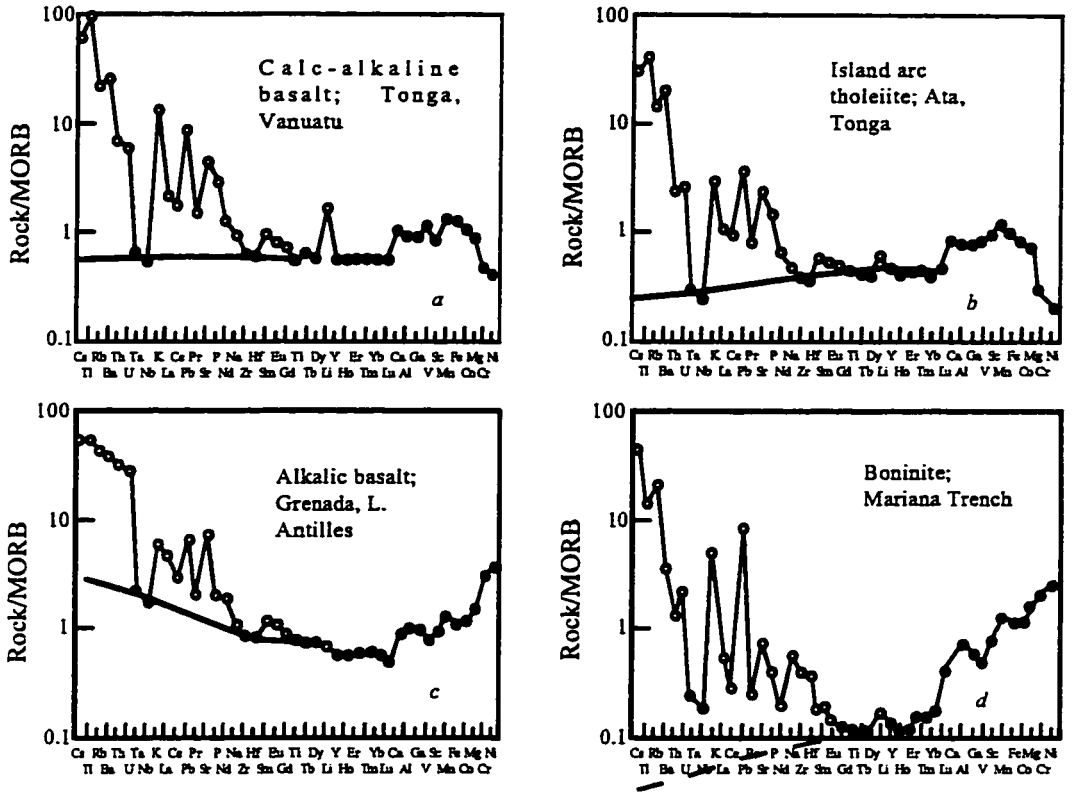

Figure 7-7. MORB-normalized patterns for a range of modern volcanic arc lavas. Solid circles refer to conservative elements, open circles to nonconservative elements. The bold lines are the "baselines" that link the compositions the elements would have had without subduction. The elements increase from right to left in incompatibility during spinel-lherzolite melting (from Pearce and Peate, 1995).

higher SiO_2 contents at comparable Mg numbers, and no Al_2O_3 and CaO decrease with magma differentiation. These trends indicate that plagioclase crystallization is not important at early stages of magma evolution in the BRG. Samples of the KJG have strong Fe and Ti enrichment trends as magmas differentiated (Figure 7-2c and 7-2d), a typical feature of the tholeiitic magma series, whereas samples of the BRG have no such enrichment.

Another systematic compositional difference between the two groups is the Nb, Ta and Ti anomalies. As illustrated in Figure 7-4, samples from the KJG have no HFSE anomalies relative to REEs, whereas samples from the BRG feature pronounced negative Nb, Ta and Ti anomalies. Variations of Nb/Nb* and Ti/Ti* with Mg number are shown in Figure 7-8 (see Chapter 5 for calculation of Nb/Nb* and Ti/Ti*). Nb/Nb* in the BRG is lower than in the KJG, and remains essentially constant with decreasing Mg number. Ti/Ti* is similar to Nb/Nb*, except for the two felsic endmembers of the KJG, which have much lower values of Ti/Ti*. The uniform Nb/Nb* and Ti/Ti* with respect to magma evolution in the KJG indicates that fractional crystallization does not generate Nb and Ti anomalies. Only when ilmenite and magnetite precipitate in mafic magmas does Ti content decrease sharply in the residual melt, the situation observed in the two felsic members of the KJG. From the evidence cited above, fractional crystallization is unlikely the cause for the chemical differences between the KJG and BRG.

Crustal contamination

Crustal contamination, one of the possibilities which may have induced chemical differences between the two groups, is common in magma evolution, especially for intracontinental basalts (Arndt, 1986b, 1994). It is possible that the BRG was derived from

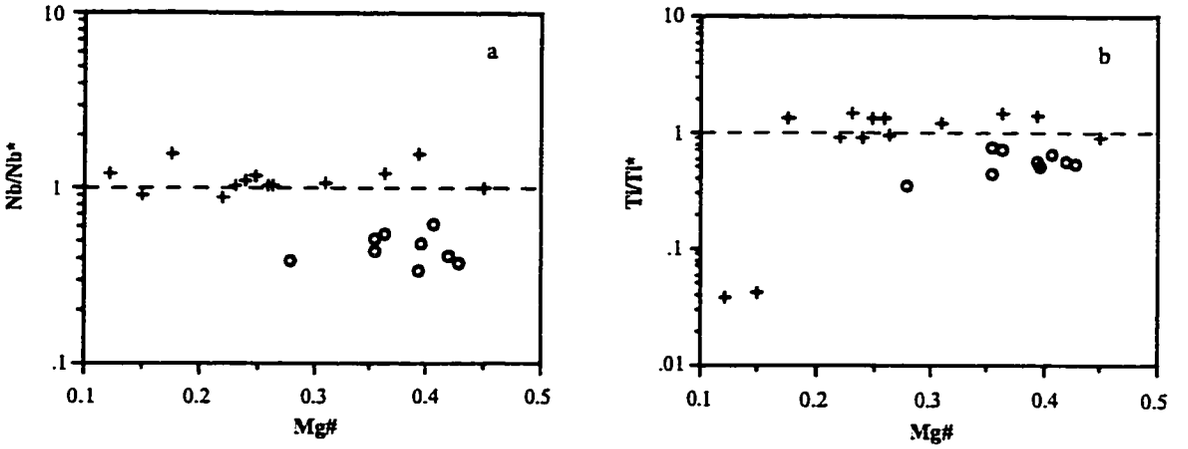

Figure 7-8. Nb/Nb* (a) and Ti/Ti* (b) versus Mg number. The differences between the BRG and the KJG cannot be accounted for by fractional crystallization of a common parental magma (see Chapter 5 for calculation of Nb/Nb* and Ti/Ti*).

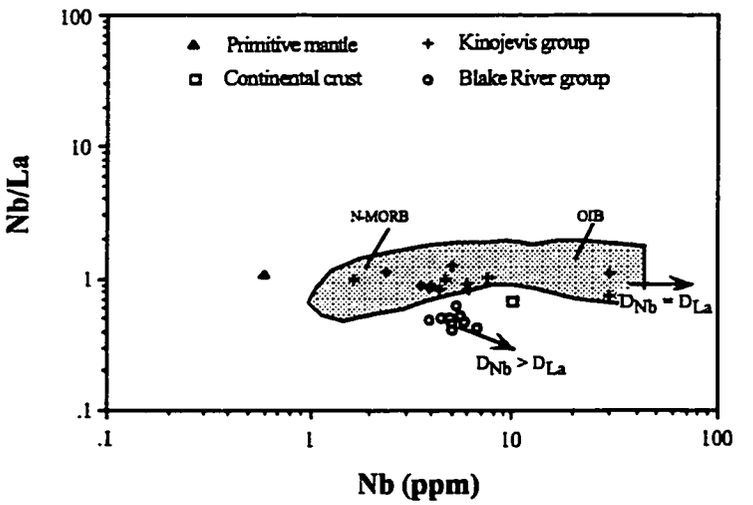

Figure 7-9. Variation of Nb/La ratios and Nb contents for the BRG and KJG. Note that samples from the BRG do not plot on the mixing line between the KJG and continental crust, suggesting that a parental magma with a composition of the KJG contaminated by crustal materials would not produce trace element signatures observed in the BRG. Data sources are as follows: primitive mantle, Sun and McDonough (1989); continental crust, Taylor and McLennan (1985); field of N-MORB and OIB, Jochum et al. (1990).

the same parental magma as that of the KJG by crustal contamination, as proposed by Gelinas and Ludden (1984) and Ludden and Hubert (1986). Based on the geochemical differences between the two groups, the most likely contaminant seems to be continental crust, as continental crust has high LILEs and LREEs, but low HFSE, HREEs and Y (Taylor and McLennan, 1985).

Detailed examination of the trace element geochemistry of the two groups, however, suggests that crustal contamination cannot account for the differences between the KJG and BRG. For example, relationships between Nb/La ratios and Nb contents of the two groups cannot be explained by crustal contamination (Figure 7-9). Samples of the KJG have Nb/La ratios similar to those of N-MORB and OIB, whereas samples of the BRG have much lower Nb/La ratios, which apparently do not plot along the mixing line between KJG and bulk continental crust. Similarly, Zr/Yb and Hf/Yb ratios of the BRG cannot be explained by mixing between the KJG and contaminants with continental crustal composition (Figure 7-11c and 7-11d), as suggested in some previous studies (Gelinas et al., 1984; Paradis et al., 1988).

Mantle sources

In summary, the distinct major and trace element characteristics of the KJG and BRG are interpreted to reflect distinct magma sources, given that fractional crystallization and crustal contamination have been ruled out. The two groups have distinct Nb/La and Ta/La ratios, but similar Zr/Sm and Hf/Sm ratios at comparable Mg numbers, suggesting depletion of Nb and Ta, but no Zr and Hf depletion in the BRG (Figure 7-10). Considering ratios of highly (Nb, Ta) and moderately (Zr and Hf) incompatible to compatible (Y and HREEs)

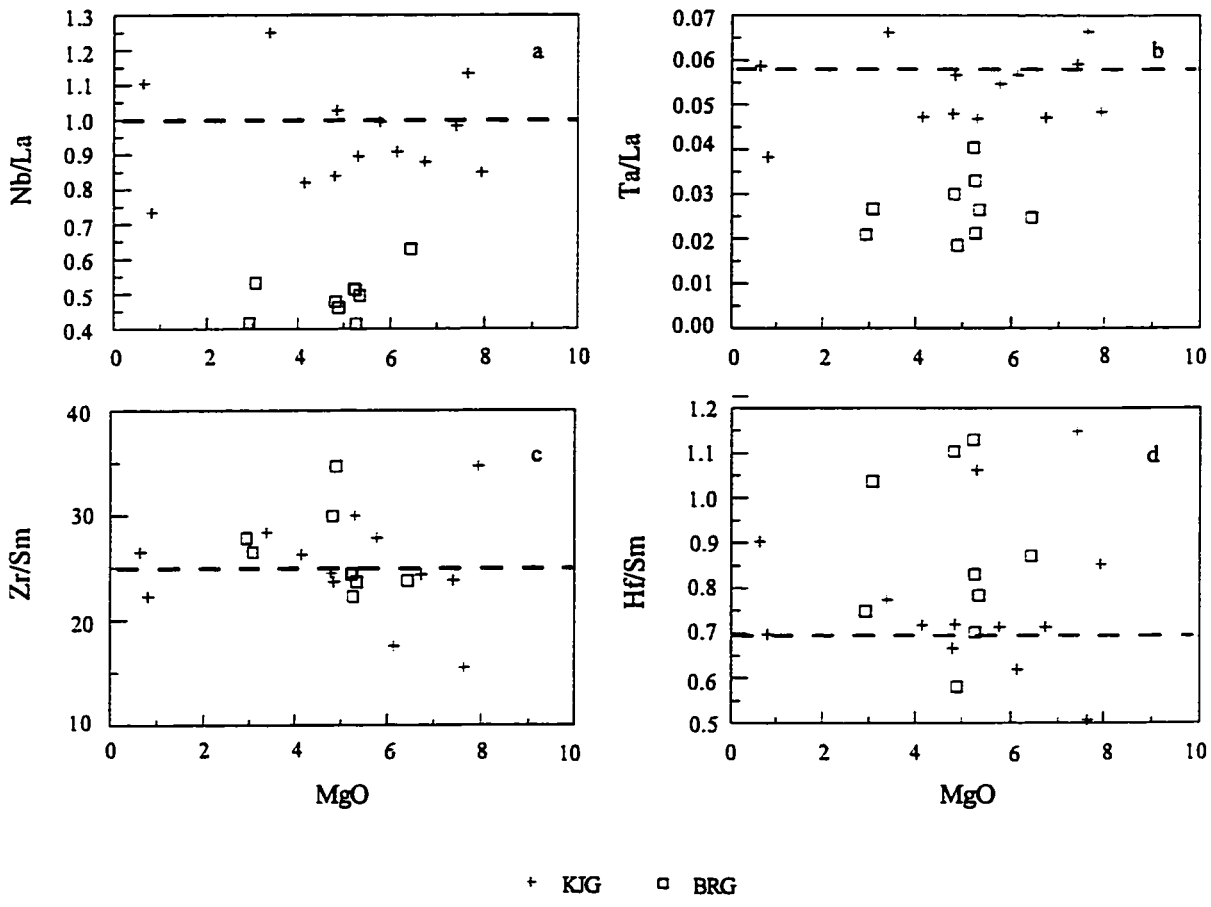

Figure 7-10. Variations of elemental ratios versus MgO for samples from the KJG and BRG, showing distinct Nb/La (a) and Ta/La (b) ratios between the two groups, but essentially indistinguishable Zr/Sm (c) and Hf/Sm (d) ratios. See text for discussion. Dashed lines depict correspondent primitive mantle values (Sun and McDonough, 1989).

elements, samples of the BRG have much higher Nb/Yb, Ta/Yb, Zr/Yb and Hf/Yb ratios than the KJG counterparts at similar absolute Nb, Ta, Zr and Hf abundances (Figure 7-11). These results indicate that HREEs and Y are depleted in the BRG, compared with the KJG samples (see Figures 7-3 and 7-4). The depletion of HREEs and Y in the BRG is further discussed in the following section.

7-5-3. Petrogenesis of the KJG and BRG: implications for the tectonic setting

In the tholeiitic suite of the KJG, both REE and primitive mantle normalized diagrams show a parallel patterns from mafic to more evolved lavas (Figures 7-3 and 7-4). These features suggest that fractional crystallization has changed absolute element contents, but not element ratios, such as $(La/Yb)_n$ and Nb/La, excepting the early accumulation of plagioclase, which produces an Eu anomaly. Accordingly, the parent magma of the tholeiites should have similar flat patterns of REE and trace elements, and element ratios. Flat REE and primitive mantle normalized patterns of the parent magma indicate that the tholeiitic magma is most likely derived from relatively large degree partial melting of an undepleted mantle source (Figure 7-12).

The KJG tholeiites have REE and HFSE characteristics similar to komatiites and Mg-tholeiites from Tisdale Township, as well as to Mg-tholeiites from Munro and Boston Townships (Figures 5-7 and 5-8). In Chapter 5, Tisdale komatiites and Mg-tholeiites are interpreted as having been generated in a mantle plume originating from an undepleted mantle source at shallow depth (<300 km). Similarly, Mg-tholeiites in Munro and Boston Townships are considered to have formed from undepleted upper mantle sources, either entrained in plumes originating from great depths which generated komatiites, or to have

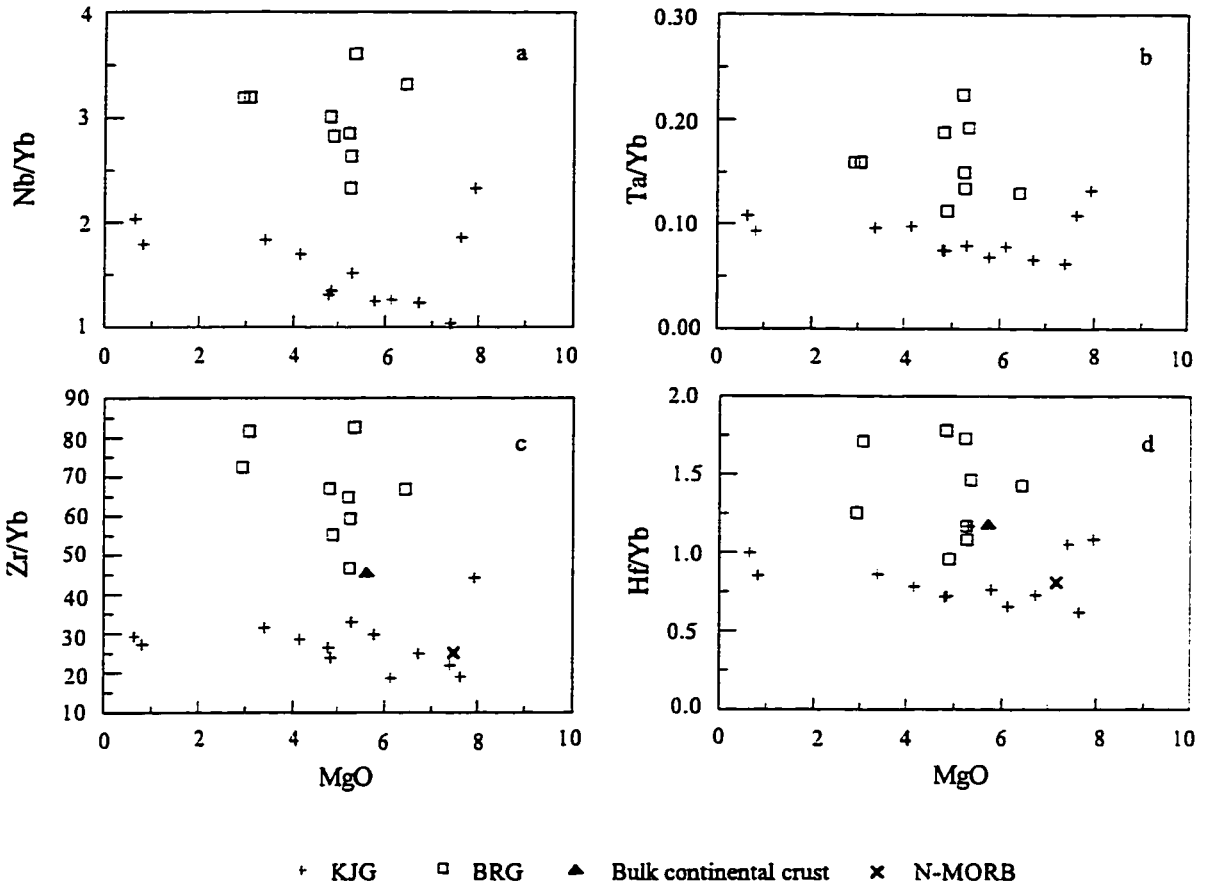

Figure 7-11. Variation of highly incompatible element/moderately incompatible element ratios versus MgO. Sampes of the BRG show clearly higher ratios than that of the KJG, due to enrichment of highly incompatible elements in the BRG (data for bulk continental crust from Taylor and McLennan, 1985; data for N-MORB from Hofmann, 1988).

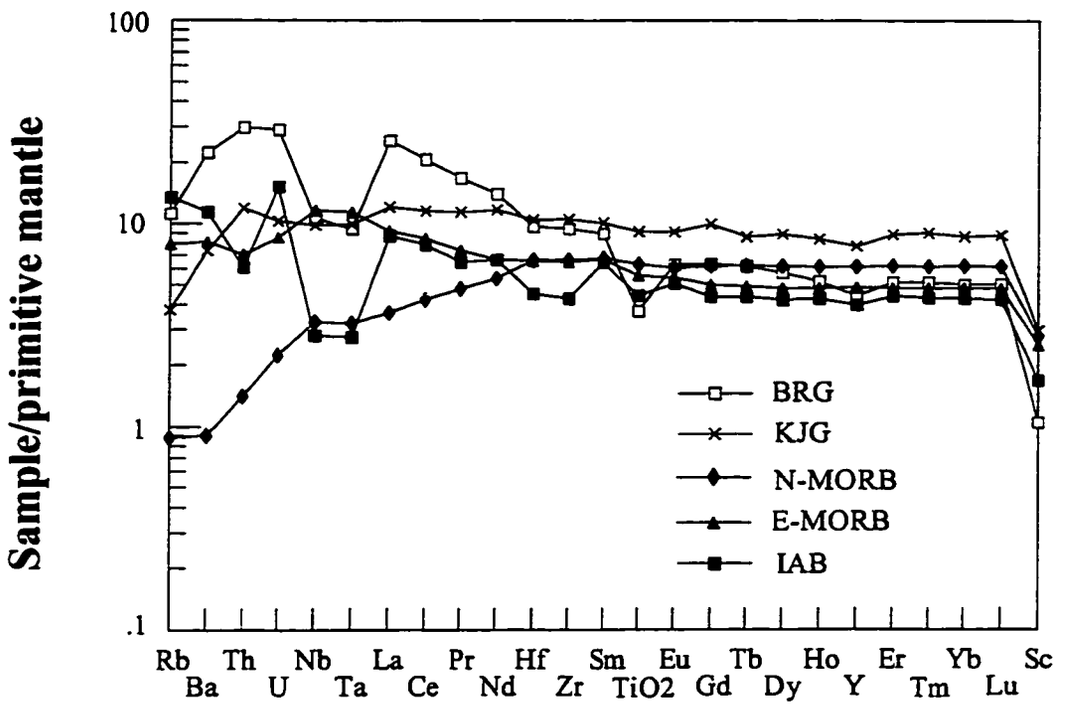

Figure 7-12. Primitive mantle normalized patterns of the BRG and KJG, compared with those of modern N-MORB, E-MORB and IAB. Data for primitive mantle, N-MORB and E-MORB are from Sun and McDonough(1989). Data for oceanic IAB (Type b of Figure 7-7) from Stolz et al. (1990) and Woodhead and Johnson (1993).

formed by separate plumes derived from undepleted mantle sources at shallow depths. The KJG tholeiites are also interpreted to have been generated in a mantle plume originating from an undepleted upper mantle source. Given that the KJG is about 20 Ma younger than the three komatiite-tholeiite sequences, and there are no komatiites associated with KJG tholeiites, there may may have been a transition from deeper plume activity to shallow plume activity in the SVZ.

The BRG calc-alkaline volcanic sequence is characterized by LILE and LREE enrichment, pronounced Nb, Ta and Ti depletion relative to REEs, and low HREE and Y contents. These geochemical characteristics overall resemble that of modern IAV (Figure 7-12). Detailed examination of trace element data, however, has revealed some differences between the BRG and typical modern oceanic IAV. Figure 7-12 presents primitive mantle normalized patterns for average BRG and KJG samples. Patterns for N-MORB, E-MORB and typical oceanic IAV are also depicted for comparison. It is clear that although the BRG show Nb and Ta depletion relative to Th and La, concentrations of Nb and Ta are higher than that of N-MORB. Thus, the BRG is in fact enriched in Nb and Ta, but depleted in HREEs, Y and Sc, compared with N-MORB. These characteristics are further illustrated in Figure 7-13, in which the BRG samples were normalized to N-MORB. Also shown on the diagram are patterns of two types of modern oceanic IAV. The IAV from New Britain, Papua New Guinea, and Sunda, Indonesia, have been interpreted as having formed by partial melting of mantle wedge enriched in LILEs and LREEs by fluids from dehydration of subducted slab (Type b of Figure 7-7; Stolz et al., 1990; Woodhead and Johnson, 1993), whereas IAB from Mt. Arayat, Philippines, has been considered to have been generated by partial melting of young and hot subducted oceanic crust (Type c of Figure 7-7; Defant et

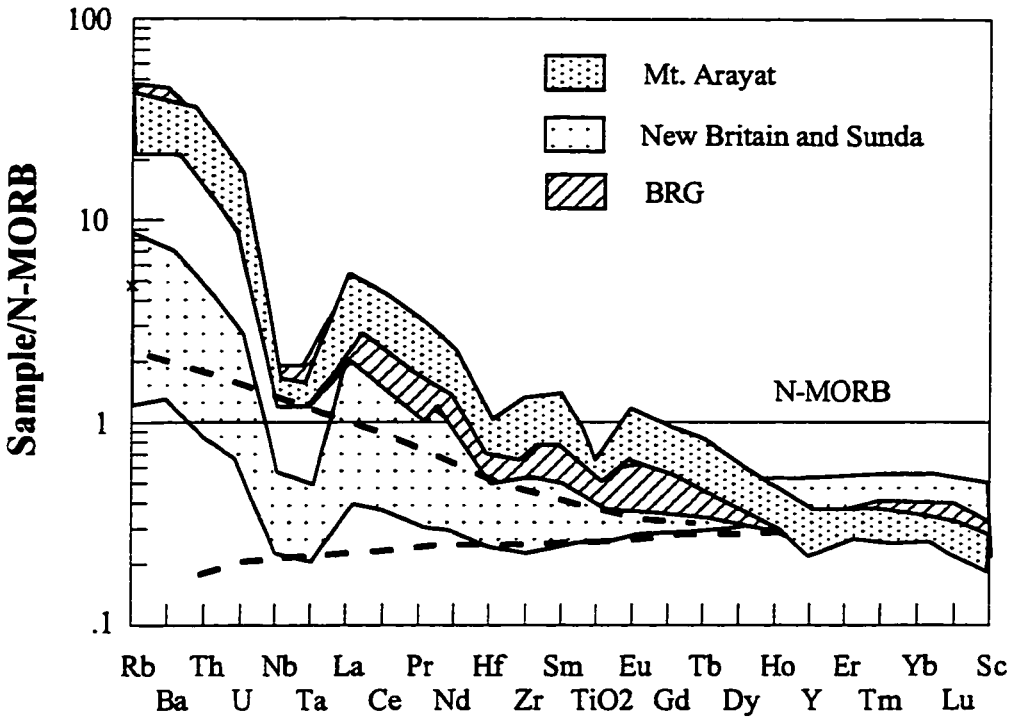

Figure 7-13. Comparison of BRG samples with modern oceanic arc basalts and andesites. Dashed lines linking conservative elements give the "baselines" of element compositions the mantle wedge would have without input from hydrous fluids derived from slab dehydration. There is strong evidence that the Mt. Arayat arc involved melting from young subducted slab, whereas the New Britain and Sunda arcs were derived from melting of mantle wedge enriched in LILE by fluids from slab dehydrathion. Note the overall similarity between BRG and Mt. Arayat (see section 7-5-3 for discussion). Data for Mt. Arayat are from Bau and Knittel (1993); Data for New Britain and Sunda are from Woodhead and Johnson (1993) and Stolz et al. (1990).

al., 1991; Bau and Knittel, 1993).

Following the approach of Pearce and Peate (1995), LILEs and LREEs behave as nonconservative elements, whereas HFSEs and HREEs as conservative elements during slab dehydration. Partial melting of an incompatible element depleted mantle wedge, metasomatized by fluids from slab dehydration, would lead to melt enriched in LILEs and LREEs, but depleted in HFSEs and HREEs, such as basalts in New Britain and Sunda arcs. During slab melting, however, Nb and Ta become nonconservative. Slab melting with garnet or amphibole in the residue would produce magma with high LILEs, LREEs and HFSEs, but low HREEs and Y. If mantle wedge is metasomatized by such melt, as well as slab-derived fluids, partial melting of such a mantle source would generate melt with high LILEs and LREEs, low HREEs and Y, Nb and Ta depletion relative to U and La, but higher Nb and Ta concentrations than N-MORB, characteristics similar to those observed in the Mt. Arayat arc (Figure 7-13; Gill, 1981; Defant and Drummond, 1990).

Modern oceanic island arc volcanics derived from partial melting of young, hot subducted oceanic lithosphere have been termed adakites (Defant and Drummond, 1990). Adakites were first documented in Adak Island, Alaska (Kay, 1978). They are volcanic or intrusive rocks in Cenozoic arcs associated with subduction of young ($\leq$ 25 Ma) and hot oceanic crust. Adakites are characterized by $\geq$ 56 wt% SiO_2, > 15 wt% Al_2O_3, usually < 3 wt% MgO (rarely above 8 wt%), and low Y and HREEs (Y$\leq$ 18 ppm and Yb < 1.9 ppm) relative to typical oceanic IAV that is generated by melting of mantle wedge induced by hydrous fluids from slab dehydration (Defant and Drummond, 1990). Figure 7-14 further describes the different geochemical characteristics between adakites (Mt. Arayat) and typical arc basalts (New Britain and Sunda), especially low Y and HREEs, but high HFSEs in

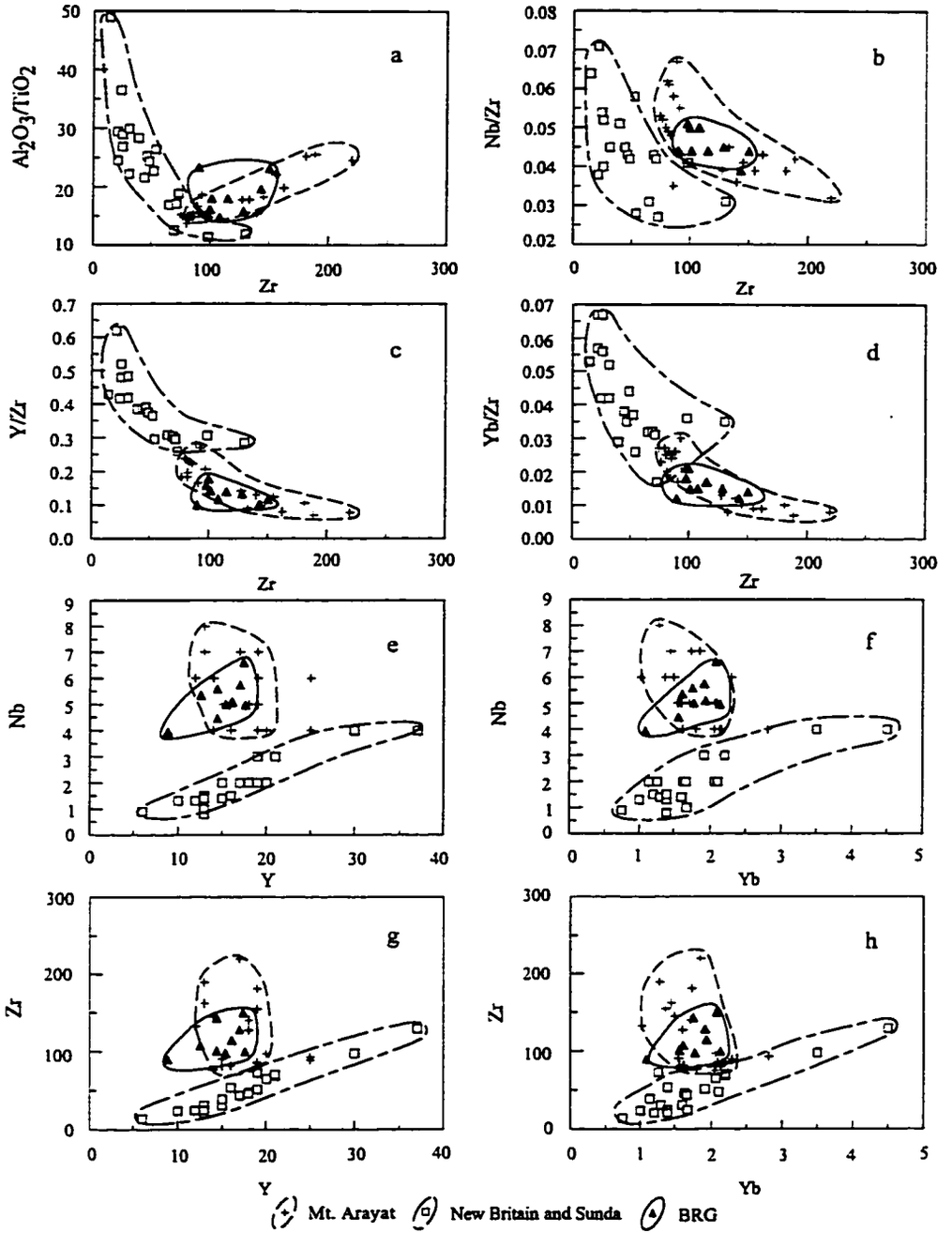

Figure 7-14. Trace elements variations of BRG basalts and andesites. Also shown are island arc basalts and andesites from Mt.Arayat, New Britain, and Sunda. The Mt. Arayat arc volcanic rocks are believed to involve melting of subducted young oceanic crust (Defant and Drummond, 1990; Bau and Knittel, 1993), whereas New Britain and Sunda arc volcanics were generated by melting of mantle wedge enriched in LILE by slab dehydration (Defant and Drummond, 1990; Stolz et al., 1990; Woodhead and Johnson, 1993).

adakites. The BRG have geochemical characteristics closely resembling that of modern adakites (Figures 7-13 and 7-14). Lafleche et al. (1992) have also pointed out the similarity between Archean calc-alkaline volcanic rocks and modern adakites. Accordingly, the BRG calc-alkaline basalts and andesites may have been generated in a subduction related environment involving melting and dehydration of subducted oceanic lithosphere. Melting of subducted oceanic lithosphere has long been recognized as an important fact in the generation of Archean tonalite-trondhjemite-granodiorite (TTG) suite, and shoshonitic lamprophyres (Arth, 1979; Wyman and Kerrich, 1989; Drummond and Defant, 1990; Feng and Kerrich, 1992, and references therein), but generally has not been considered significant in the petrogenesis of Archean calc-alkaline basalts and andesites (Jensen and Langford, 1985; Ludden et al., 1986; Paradis et al., 1988; Fowler and Jensen, 1989).

Experimental studies indicate that slab melting occurs only when young and hot oceanic crust is subducted (Defant and Drummond, 1990; Peacock et al., 1994). Specifically, Peacock et al. (1994) pointed out that substantial melting of the oceanic crust will only occur during subduction of very young (< 5 Ma) oceanic lithosphere, based on experimental results and numerical simulation. This conclusion is consistent with the observation that most modern adakites occur in volcanic arcs where oceanic crust younger than 25 Ma is being subducted (Defant and Drummond, 1990; Peacock et al., 1994). As discussed in Chapter 5, the widespread occurrence of mantle plume generated komatiites in Archean greenstone belts is consistent with a hotter Archean mantle (Bickle, 1978; Nisbet et al., 1993). The hotter mantle and higher thermal gradients in the Archean probably led to rapid production and subduction of young hot oceanic crust (Martin, 1986; Bickle, 1990; Drummond and Defant, 1990). Partial melting of young and hot subducted oceanic crust may have been a dominant

process in the production of calc-alkaline basalts and andesites throughout Archean greenstone belts, whereas most modern oceanic IAV are generated by partial melting of mantle wedge metasomatized by slab-derived fluids. This is perhaps one of the reasons that Archean calc-alkaline volcanic rocks generally have geochemical characteristics somewhat different from that of typical modern IAV (Condie, 1989, 1990, 1994).

7-6. Summary and conclusions

Major and trace element studies of basalts from the KJG and BRG have revealed distinct geochemical characteristics between the two volcanic sequences. The KJG consists mainly of tholeiitic basalts, with flat REE and primitive mantle normalized patterns, and no normalized Nb, Ta and Ti anomalies relative to LILEs and LREEs. In contrast, the BRG is dominantly calc-alkaline andesite, enriched in LILEs and LREEs, depleted Nb, Ta and Ti relative to LILEs and LREEs, and depleted in HREEs and Y. The contrasting geochemical features of the two groups cannot be explained by fractional crystallization of a common parental magma, nor can they be explained by crustal contamination, but rather suggest that the KJG and BRG were derived from distinct mantle sources in different tectonic environments.

The KJG tholeiites are geochemically similar to Mg-tholeiites in the Tisdale Township, as well as Mg-tholeiites in the Munro and Boston Townships, suggesting their common features of magma generation, that is having formed in mantle plumes deriving from undepleted mantle sources with melt segregation at depths above the garnet stable field comparable to modern intraoceanic plateau basalts (<100 km). In contrast, the BRG calc-alkaline andesites have geochemical characteristics closely resembling that of one type of

modern island arc volcanic rocks, namely adakite, where melting of subducted young (<25 Ma) oceanic crust is involved. Accordingly, the BRG calc-alkaline volcanic sequence may have been generated in a subduction related tectonic environment where young and hot Archean oceanic crust was subducted

The two volcanic sequences are similar in age, yet with contrasting geochemical features stemming from different tectonic settings. They may have been juxtaposed by late collisions within the Abitibi SVZ (Green et al., 1990; Jackson and Fyon, 1992). Unlike most modern oceanic island arc calc-alkaline volcanics which are generated by partial melting of mantle wedge metasomatized by fluids derived from slab dehydration, Archean calk-alkaline volcanic rocks may have been dominantly formed by partial melting of mantle wedge which was metasomatized by fluids deriving from both slab dehydration and melting, due to subduction of young and hot Archean oceanic crust. The different thermal structure of subducted ocean lithosphere during the late Archean may explain the geochemical differences between typical modern ocean island arc volcanics and Archean calc-alkaline volcanic rocks (Condie, 1989, 1990, 1994).

CHAPTER 8 SUMMARY AND IMPLICATIONS

In this chapter, the principal results of the thesis are first summarized. Implications of the results are then explored, in an attempt to provide new constraints on some of the questions outlined in Chapter 1. Specifically, implications for chemical evolution of the mantle are discussed, and models for Archean greenstone belt development are critically evaluated, based on the results of this study and a literature survey.

8-1. The principal results

The major results of this thesis are summarized as follows:

(1) Detailed experiments were designed to evaluate quantitatively potential difficulties in multiple trace element analysis of low abundance samples by ICP-MS, such as possible incomplete sample dissolution and solute instability, potential isobaric and polyatomic interferences, and memory effects. Analytical protocols were developed that either overcame such problems or demonstrated that the effects were negligible.

(2) New data for 28 trace elements, including all REEs and HFSEs, in low abundance international reference materials (including BIR-1, MRG-1 and BCR-1) have been obtained by ICP-MS using the new protocols. The new ICP-MS data for these international reference materials indicate that precise and accurate multiple trace element data can be obtained by ICP-MS for low abundance samples, such as Archean komatiites and basalts.

(3) Experiments were also conducted to optimize instrumental operating parameters (IOPs) for isotope ratio measurement by ICP-MS. These IOPs include rf power, dwell time, B lens settings, and nebulizer flow rate. The results suggest that an overall precision of 0.2 to 0.6 RSD% can be achieved for isotope ratio measurement using ICP-MS, under optimum IOPs. Isotope dilution ICP-MS analysis for Zr and Hf in low abundance international reference materials and komatiites has been carried out, and ID-ICP-MS data confirm the Zr and Hf data obtained by external calibration ICP-MS.

(4) Three komatiite-tholeiite sequences separated by major terrane boundaries from the late Archean (2.7 Ga) Abitibi Southern Volcanic Zone (SVZ) have been analysed by ICP-MS for major and trace elements. The three mafic-ultramafic volcanic sequences show distinct geochemical characteristics, particularly REE patterns and HFSE/REE interrelationships, that reflect undepleted, depleted, and possibly enriched mantle sources respectively. This is the first time that distinct HFSE/REE fractionations have been reported in Archean komatiites and tholeiites. Different geochemical characteristics of the three komatiite-tholeiite sequences support the hypothesis that Archean komatiites and spatially associated tholeiites were generated in mantle plumes originating from different sources at different depths, or melting at different depth intervals. HFSE/REE systematics of Munro and Boston komatiites are consistent with Mg-perovskite, and majorite signatures, respectively.

(5) A fourth komatiite-tholeiite sequence from the Central Block of the Abitibi SVZ, namely McArthur Township, has also been studied for comparison with the other three

komatiite-tholeiite sequences. Major elements, REE patterns and HFSE/REE interrelationships of McArthur komatiites resemble that of Munro komatiites, suggesting that they may have derived from similar mantle sources, although the two ultramafic volcanic suites are separated by major terrane boundaries.

(6) Further major and trace element studies have been carried out on tholeiitic volcanic rocks of the Kinojevis group (KJG) and calc-alkaline volcanic rocks of the Blake River group (BRG), both from the Central Block of the Abitibi SVZ, in an attempt to constrain the evolution of volcanism in the Abitibi SVZ. In terms of REE patterns and HFSE/REE interrelationships, the KJG tholeiites are similar to komatiites and Mg-tholeiites from Tisdale Township, as well as to Mg-tholeiites from Munro and Boston Townships, indicative of similar mantle sources and magma evolution. The geodynamic environment of the KJG is considered to have been an intraoceanic plateau. The BRG calc-alkaline andesites and basalts have geochemical characteristics closely resembling that of one type of modern island arc volcanics, namely adakite, and may have been generated in a subduction related tectonic environment, where young and hot Archean oceanic crust was subducted, melted and have fertilized subarc mantle lithosphere. The geodynamic setting of the BRG is interpreted as an intraoceanic arc.

Geochemistry of mafic-ultramafic volcanic rocks from the Archean Abitibi greenstone belt presented in this thesis have provided new constraints on issues such as chemical evolution of the mantle, and tectonic development of Archean greenstone belts.

8-2. Chemical evolution of the mantle

Geochemical studies of mantle derived rocks though time have greatly improved our understanding of mantle evolution (Fyfe, 1978; Sun, 1982; Hofmann, 1988; Hart and Zindler, 1989; Smith and Ludden, 1989; Armstrong, 1991; Bowring and Housh, 1995; Herzberg, 1995). As pointed out in Chapter 1, it is widely accepted that the initial composition of the primitive mantle resembles chondrites with Fe and siderophile element depletion after core formation (Jagoutz et al., 1979; Sun, 1982; Anderson, 1989a). Such a primitive mantle has been depleted in incompatible elements due to the extraction of Earth's crust. It is, however, the timing, amount, site(s) and rate of such mantle depletion that is still in debate.

Numerous models have been put forward to account for the chemical evolution of the mantle. For example, DePaolo (1988) postulated a three reservoir model, consisting of the continental crust, depleted upper mantle, and a primitive lower mantle. He suggested that the entire continental crust formed within the first 500 million years or so of Earth history, and subsequent evolution of the depleted upper mantle involves recycling of crustal materials and injection of primitive lower mantle.

A modified three reservoir model has recently been proposed by McCulloch and Bennett (1994). Instead of suggesting crustal recycling and lower mantle injection to explain the chemical evolution of the depleted upper mantle, these authors argued that the volume of the depleted upper mantle increases downwards in a stepwise manner which is linked to major episodes of rapid crustal formation. Alternatively, Hofmann (1988) suggested that the mantle underwent a two stage evolution, in which the crust was first extracted from domains of the mantle, and the mantle rehomogenized to an uniform Nb/U and Ce/Pb ratios, and

differentiated into the chemically and isotopically distinct sources of present MORB and OIB.

Most models for chemical evolution of the mantle argued that Archean komatiites are representative of Archean depleted upper mantle, based on the assumption of high degree partial melting at relatively shallow depths, just as modern N-MORB represents the present depleted upper mantle. Comparison between modern N-MORB and Archean komatiites is drawn, and the chemical and isotopic differences between modern N-MORB and Archean komatiites are interpreted as chemical evolution of the mantle (Depaolo, 1988; Hofmann, 1988; Smith and Ludden, 1989; McCulloch and Bennett, 1994). However, as pointed out in this study, as well as other recent studies, komatiites may have formed by low degree partial melting in mantle plumes originating from different sources at different depths, rather than reflecting an Archean counterpart of shallow high level melting of the modern N-MORB sources (Miller et al., 1991b; Arndt and Lesher, 1992; Herzberg, 1992a, 1995; Xie et al., 1993; Xie and Kerrich, 1994). If this interpretation about komatiite petrogenesis is correct, then the geochemistry of komatiites may not represent the Archean upper mantle; rather they may have sampled different parts of a heterogeneous mantle at different depths. Accordingly, geochemical and isotopic differences between Archean komatiites and modern MORB cannot be interpreted in terms of the secular evolution of the mantle.

The question then becomes which rocks in Archean greenstone belts may be the best samples of Archean upper mantle? The majority of Archean basalts do not show the LREE depleted character of modern N-MORB. As presented in Chapters 5 and 6, various komatiites from the Abitibi SVZ are spatially associated with Mg-tholeiites which are characterized by flat REE patterns and zero HFSE/REE fractionations, signifying undepleted

mantle sources and melt segregation at shallow depths. The volume of Mg-tholeiite is much larger than that of komatiite, suggesting that the former are far more abundant than various komatiites in the Abitibi SVZ. Such a relationship between Mg-tholeiites and komatiites is also a common feature of other Archean greenstone belts, such as the Uchi and Wabigoon belts of the Superior Province, Canada (Jackson and Fyon, 1992), Norseman-Wiluna belt of Western Australia (Morris, 1993), and Belingwe belt of Zimbabwe (Kusky and Kidd, 1992; Bickle et al., 1994).

Based on discussion in Chapters 5 and 6, Mg-tholeiites cannot be related to spatially associated komatiites either by different degrees of partial melting, or fractional crystallization; rather they may represent relatively undepleted mantle sources at shallow depths, which were either entrained by ascending komatiite plumes, or sampled by separate plumes originating from shallow depths. Accordingly, voluminous Mg-tholeiites in Archean greenstone belt may be better samples of Archean upper mantle.

Tisdale komatiites and tholeiites, as well as Mg-tholeiites from Munro, Boston and McArthur Townships, all share similar trace element characteristics, i.e., flat REE patterns and zero HFSE/REE fractionations, suggesting undepleted shallow mantle sources. If source of Mg-tholeiites was Archean upper mantle, then the conclusion may be drawn that upper mantle has progressively evolved from relatively undepleted in the Archean to the highly depleted modern N-MORB source.

This mantle scheme is, however, obviously oversimplified. There are at least two uncertainties. First, Archean ridge basalts may have been thicker, denser, and therefore more subductable than modern oceanic lithosphere, and consequently not preserved in the geological record (Bickle, 1990). Mg-tholeiites may then be equivalents to modern oceanic

plateau basalts. The spatial relationship of the mantle source of modern undepleted ocean plateau basalts and the N-MORB source is unconstrained. Second, the undepleted feature of the mantle sources of Archean Mg-tholeiites may not be a long term characteristic, that is the mantle sources of Mg-tholeiites could originally have been depleted in incompatible elements, but enriched prior to partial melting which generated Mg-tholeiites. If that is the case, then the Archean upper mantle may have been depleted in incompatible elements, just like the modern N-MORB source. Trace elements alone are not able to resolve this uncertainty. However, the likelihood of a depleted source being exactly balanced by an enriched source to produce the flat REE patterns of Archean Mg-tholeiites worldwide is remote.

Further isotope study is needed to determine the time-integrated depletion or enrichment in the mantle sources of Archean Mg-tholeiites. Preliminary Sm-Nd isotope results for the three komatiite-tholeiite sequences by the author, and existing isotope data in the literature for the Abitibi belt, suggest that in addition to distinct REE patterns and HFSE/REE fractionations, the three mafic-ultramafic volcanic suites also have different Sm-Nd isotope systematics, signifying long term heterogeneity in the mantle source of komatiites in the Archean Abitibi belt (Zindler, 1982; Machado et al., 1986; Smith and Ludden, 1989; Walker et al., 1991). Mg-tholeiites are spatially associated with komatiites which may have formed by melting of anomalously hot plumes originating from different deep mantle sources. Even those Mg-tholeiites not spatially associated with komatiites, such as in the Kinojevis group (Chapter 7), do not resemble modern N-MORB; rather their geochemical characteristics are closer to modern oceanic plateau basalts (Floyd, 1991). The Cretaceous Gorgona komatiites are associated with ocean plateau basalts having flat REE and therefore

an undepleted mantle source. Hence, there may be some feature of plumes in which komatiites are generated that entrains undepleted mantle.

Modern OIBs are generated in plumes that have long-term enriched mantle sources. Thus both Archean and Cretaceous komatiites involve plumes tapping mantle sources distinct from those of modern OIBs.

In summary, it appears that until Archean mid-ocean ridge basalts are positively identified, the exact composition of Archean upper mantle will remain undefined. Accordingly, any model for chemical evolution of the mantle, based on a comparison between modern MORB and Archean komatiites and tholeiites, may not be valid.

8-3. Tectonic evolution of Archean greenstone belts: evidence from the geochemistry of mafic-ultramafic volcanic rocks

Numerous models have been proposed for the tectonic evolution of Archean greenstone belts, including oceanic ridge, oceanic plateau, continental rift, arc-back arc, plume, or some combination. Storey et al. (1991) argued that the Cretaceous Gorgona komatiite-tholeiite sequences are part of oceanic plateaus, which formed during multistage melting of a plume or plumes from different mantle sources; the komatiites from a depleted source, and the tholeiites from an undepleted sources. They further suggested that some Archean komatiite-tholeiite sequences could also be remnants of plume-related Archean oceanic plateaus.

Hill et al. (1992) proposed a superplume model to account for the development of the Archean Yilgarn greenstone belt, Western Australia. In their model, a plume starting from the core-mantle boundary can have a head 2000 km in diameter beneath the lithosphere lid.

Partial melting in the bulk of a rising and spreading plume head resulted in an early period of basaltic volcanism, whereas melting of the much hotter materials that ascended in the axial conduit of the plume produced komatiites. Heat conduction from plume head to the base of older crust resulted in the production of crustally derived melts which generated granites and calc-alkaline volcanic rocks, over an elapsed time of 20 to 500 Ma. They suggested that this superplume model was generally applicable to Archean greenstone belt development, and Phanerozoic flood basalt provinces (e.g., the Siberian and Columbia River flood basalts).

Komatiites in some cratons (e.g., Belingwe, South Africa, and Yilgarn, Western Australia) were apparently erupted through continental crust, as evidenced by xenocrystic zircons, and the geochemical characteristics of crustally contaminated komatiites (Arndt and Jenner, 1986; Barley, 1986; Compston et al., 1986; Bickle, 1993; Bickle et al., 1994), whereas komatiites in other cratons (e.g., the Slave and Abitibi provinces, Canada, and Kaapvaal, South Africa) appear to have erupted in a within plate oceanic environment (Hoffman and Ranalli, 1988; de Wit et al., 1992; Kusky and Kidd, 1992). In the Abitibi belt, the absence of xenocrystic zircons, and lack of geochemical signatures of crustal contamination in komatiite-tholeiite sequences (see Chapters 5 and 6), strongly argue against eruption through continental lithosphere (Thurston and Chivers, 1990; Jackson and Fyon, 1992; Jackson et al., 1994).

As discussed in Chapters 1 and 5, there is increasing evidence that komatiites formed in anomalously hot mantle plumes, and that mantle plumes played an important role in development of Archean greenstone belts. However, there are many difficulties if the superplume model proposed by Hill et al. (1992) is used to explain the whole geological evolution of Archean greenstone belts. Considering the Abitibi SVZ as an example, the three

komatiite-tholeiite sequences presented in Chapter 5 have distinct geochemical characteristics, particularly REE patterns and HFSE/REE interrelationships, which require at least three different plumes originating from different mantle sources at various depths. In addition, voluminous Mg-tholeiites in Munro and Boston Townships have geochemical characteristics differing from komatiites. According to the superplume model, tholeiites represent partial melting of plume head, whereas komatiites formed by melting of hot axis of the plume. Yet there is no mixing trend between the geochemical composition of Mg-tholeiites and komatiites (see Chapters 5, 6 and 7). These geochemical differences of mafic and ultramafic volcanic rocks also argue for different plumes from different mantle sources for Mg-tholeiites.

It is also difficult to account for calc-alkaline volcanism in the Abitibi SVZ, using the single superplume model. As pointed out in Chapter 7, BRG calc-alkaline andesites and basalts may have formed in an intraoceanic subduction-related environment, involving partial melting and dehydration of subducted oceanic crust. Numerous synvolcanic and syntectonic granites also have subduction signatures (Feng and Kerrich, 1992). These volcanic and plutonic rocks require some form of plate tectonic activity operating in the Abitibi SVZ.

Perhaps the most difficult aspect of the single superplume model is to explain the linear distribution of the greenstone belts, the major strike-slip and thrust faults within the belts, and the geochronological constraints on diachronous accretion of the Superior Province (Figures 2-1, 2-2; Thurston et al., 1991). Recent seismic investigations in the Abitibi SVZ have revealed several major strike-slip and thrust faults within the Abitibi SVZ, which accommodated large crustal shortening (Green et al., 1990; Calvert et al., 1995). Such structures are common features in convergent margins of modern plate tectonics, such as

arc-continental collision (i.e., Northwest Pacific and Cordillera), and continental-continental collision (i.e., Alpine and Himalaya) [Condie, 1989b].

As outlined in Chapter 2, the Abitibi SVZ consists of komatiite-tholeiite sequences (i.e., Tisdale, Munro, and Boston), tholeiitic sequences (i.e., Kinojevis group), and calc-alkaline volcanic sequences (i.e., Blake River group) [Figures 2-3 and 2-4]. Various komatiite-tholeiite sequences have ages ~ 2720 Ma, whereas the Kinojevis tholeiites and Blake River calc-alkaline volcanics are dated as ~ 2700 Ma (Figure 2-4; Corfu, 1993). Four distinct granitic magma series have also been recognized in the Abitibi SVZ; they are synvolcanic tonalite-trondjemite-granodiorite (TTG series; ~ 2700 Ma); syntectonic tonalitic granodiorite-granite and quartz monzonite (TGGM series; ~ 2690 Ma); late-tectonic quartz syenite-quartz monzonite-granite (SMG series; ~ 2681-2676 Ma); and late- to post-tectonic alkali feldspar syenite-alkali feldspar quartz syenite (SS series; ~ 2680-2670 Ma) [Feng and Kerrich, 1992]. The geochemistry of the four granitic magma series suggests that they all have subduction signatures, and evolved from melting of subducted oceanic crust (TTG and TGGM series) to melting of mantle wedge metasomatized by dehydration of subducting oceanic crust (SMG series; Feng and Kerrich, 1992). The late granitic magmatism (SS series) was accompanied by shoshonitic lamprophyre dikes (~ 2670 Ma), which are prevalent along major translithospheric faults zones (e.g., DPFZ and KLFZ; Figure 2-2) and have geochemical characteristics similar to Phanerozoic lamprophyres that occur in accretional tectonic regimes (Wyman and Kerrich, 1993).

The temporal and spatial relationships of magmatism in the Abitibi SVZ outlined above are difficult to reconcile with the single superplume model, inasmuch as the superplume model fails to provide a mechanism for the transition from a divergent tectonic regime to a

convergent tectonic regime, in order to account for the evolution of magmatism. It is likely that the Abitibi SVZ represents a composite of different plumes and oceanic island arc terranes, which were tectonically juxtaposed during terminal accretion of the belt (Kerrich and Feng, 1991; Desrochers et al., 1993; Wyman and Kerrich, 1993; Xie and Kerrich, 1993). The belt evolved from multiple plume activity in an oceanic setting at ~ 2720-2700 Ma, which generated various komatiites and tholeiites, through arc volcanism and plutonism at ~ 2700 Ma, to S-type granites and shoshonitic magmatism at ~ 2680-2670 Ma coeval with thrusting of the composite collage of diverse terranes onto older continental crust of the Pontiac Subprovince in the south (Figure 2-3; Feng and Kerrich, 1992).

REFERENCES

Abe, Y. and Matsui, T. 1986. Early evolution of the Earth: accretion, atmosphere formation, and thermal history. Proceding of Lunar and Planetary Science Conference, **17th**:E291-E302.

Agee, C.B. 1990. A new look at differentiation of the Earth from melting experiments on the Allende meteorite. Nature, **346**:834-837.

Agee, C.B. and Walker, D. 1988. Mass balance and phase desity constraints on early differentiation of chondritic mantle. Earth Planet. Sci. Lett., **90**:144-156.

Agee, C.B. and Walker, D. 1989. Comments on "Constraints on element partition coefficients between MgSiO3 perovskite and liquid dertermined by direct measurements" by T. Kato, A.E. Ringwood, and T. Irifune. Earth Planet. Sci. Lett., **94**:160-161.

Ahrens, T.J., 1990. Earth accretion. In: Newsom, H.E. and Jones, J.H., Origin of the Earth.211-227.

Anderson, D.L. 1979. Chemical stratification of the mantle. J. Geophys. Res., **84**:6297-6298.

Anderson, D.L. 1989a. Composition of the Earth. Science, **243**:367-370.

Anderson, D.L., 1989b. Theory of the Earth. Blackwell Scientific Publications, 366p.

Armstrong, R.L. 1991. The persistent myth of crustal growth. Australian. J. Earth Sci., **38**:613-630.

Arndt, N.T. 1977a. Thick, layered peridotite-gabbro lava flows in Munro Township, Ontario. Can. J. Earth Sci., **14**:2620-2637.

Arndt, N.T. 1977b. Ultrabasic magmas and high-degree melting of the mantle. Contrib. Mineral. Petrol., **64**:205-221.

Arndt, N.T. 1986a. Differentiation of komatiite flows. J. Petrol., **27**:279-301.

Arndt, N.T. 1986b. Komatiites:a dirty window to the Archean mantle. Terra Cognita Acta, **6**:59-66.

Arndt, N.T., 1994. Archean komatiites. In: Condie, K.C., Archean Crustal Evolution. Developments in Precambrian Geology, b11:11-44.

Arndt, N.T. and Jenner, G.A. 1986. Crustally contaminated komatiites and basalts from Kambalda, Western Australia. Chem. Geol., **56**:229-255.

Arndt, N.T. and Lesher, C.M. 1992. Fractionation of REEs by olivine and the origin of Kambalda komatiites, Western Australia. Geochim. Cosmochim. Acta, **56**:4191-4204.

Arndt, N.T. and Nesbitt, R.W., 1982. Geochemistry of Munro Township basalts. In: Arndt, N.T. and Nisbet, E.G., Komatiites.309-329.

Arndt, N.T. and Nisbet, E.G., 1982. What is komatiite? In: Arndt, N.T. and Nisbet, E.G., Komatiites.19-27.

Arndt, N.T., Naldrett, A.J., and Pyke, D.R. 1977. Komatiitic lavas of Munro Township: their field, petrographic and chemical characteristics. J. Petrol., **18**:319-369.

Arndt, N.T., Teixeira, N.A., and White, W.M. 1989. Bizarre geochemistry of komatiites from the Crixas greenstone belt, Brazil. Contrib. Mineral. Petrol., **101**:187-197.

Arth, J.G., 1979. Some trace elements in trondhjemites: their implications to magma genesis and paleotectonic setting. In: Barker, F., Trondhjemites, dacites, and related rocks.123-137.

Ayers, J.C. and Watson, E.B. 1991. Solubility of apatite, monazite, zircon and rutile in supercritical aqueous fluids with implications for subduction zone geochemistry. Phil. Trans. R. Soc. Lond., **335**:365-375.

Ayres, L.D. and Thurston, P.C., 1985. Archean supracrustal sequences in the Canadian shield: a review. In: Ayres, L.D., Thurston, P.C., Card, K.D., and Weber, W., Evolution of Archean upracrustal sequences. Geological Association of Canada, Special paper, b28:343-380.

Barley, M.E. 1986. Incompatible element enrichment in Archean basalts: a consequence of contamination by older sialic crust rather than mantle heterogeneity. Geology, **14**:947-950.

Barley, M.E. and Kerrich, R. 1995. Trace elements fingerprint multiple sources and melting depths for Yilgarn komatiite-tholeiite associations: HFSE/REE evidence for the transition from mantle plumes to accretionary tectonics in the Late Archean., :(in preparation).

Barnes, S.J. 1985. The petrography and geochemistry of komatiite flows from the Abitibi Greenstone belt and a model for their formation. Lithos, **18**:241-270.

Barnes, S.J., Naldrett, A.J., and Gorton, M.P. 1985. The origin of the fractionation of platinum group elements in terrestial magmas. Chem. Geol., **53**:303-323.

Barnes, S.J., Hill, R.E.T., and Gole, M.J. 1988. The perseverence ultramafic complex,

Western Australia: the product of a komatiite lava river. J. Petrol., **29**:305-323.

Barrie, C.T. and Davis, D.W. 1990. Timing of magmatism and deformation in the kamiskotia-Kidd Creek area, western Abitibi Subprovince, Canada. Precamb. Res., **46**:217-240.

Bau, M. and Knittel, U. 1993. Significance of slab-derived partial melts and aqueous fluids for the genesis of tholeiitic and calc-alkaline island-arc basalts: evidence from Mt. Arayat, Philippines. Chem. Geol., **105**:233-251.

Beattie, P., Ford, C., and Russell, D. 1991. Partiton coefficients for olivine-melt and orthopyroxene-melt systems. Contrib. Mineral. Petrol., **109**:212-224.

Beattie, P., Drake, M., Jones, J., Leeman, W., Longhi, J., McKay, G., Nielsen, R., Palme, H., Shaw, D., Takahashi, E., and Watson, B. 1993. Terminology for trace-element partitioning. Geochim. Cosmochim. Acta, **57**:1605-1606.

Begley, I.S. and Sharp, B.L. 1994. Occurrence and reduction of noise in inductively coupled plasma mass spectrometry for enhanced precision in isotope ratio measurement. J. Anal. At. Spectrom., **9**:171-176.

Bennett, V.C., Nutman, A.P., and McCulloch, M.T. 1993. Nd isotopic evidence for transient, highly depleted mantle reservoirs in the early history of the Earth. Earth Planet. Sci. Lett., **119**:299-317.

Beswick, A.E., 1982. Some geochemical aspects of alteration, and genetic relations in komatiitic suites. In: Arndt, N.T. and Nisbet, E.G., Komatiites.281-308.

Bickle, M.J. 1978. Heat loss from the Earth: constraint on Archean tectonics from the relationships between geothermal gradients and the ate of plate production. Earth Planet. Sci. Lett., **40**:301-315.

Bickle, M.J., 1982. The magnesian contents of komatiitic liquids. In: Arndt, N.T. and Nisbet, E.G., Komatiites.479-494.

Bickle, M.J., 1990. Mantle evolution. In: Hall, R.P. and Hughes, D.J., Early Precambrian basic magmatism.111-135.

Bickle, M. 1993. Plume origin for komatiites. Nature, **365**:390-391.

Bickle, M.J., Nisbet, E.G., and Martin, A. 1994. Archean Greenstone belts are not oceanic crust. J. Geol., **102**:121-138.

Blichert-Toft, J. and Albarede, F. 1994. Short-lived chemical heterogeneities in the Archean mantle with implications for mantle convection. Nature, **263**:1593-1596.

Blusztajn, J. and Shimizu, N. 1994. The trace-element variations in clinopyroxenes from spinel peridotite xenoliths from southwest Poland. Chem. Geol., **111**:227-243.

Boer, R.H., Beukes, G.J., Meyer, F.M., and Smith, C.B. 1993. Fluoride precipitates in silicate wet-chemistry:implications on REE fractionation. Chem. Geol., **104**:93-98.

Bowring, S.A. and Housh, T. 1995. The Earth's early evolution. Science, **269**:1535-1540.

Brooks, C. and Hart, S.R. 1972. An extrusive basaltic komatiite from a Canadian metavolcanic belt. Can. J. Earth Sci., **9**:1250-1253.

Calvert, A.J., Sawyer, E.W., Davis, W.J., and Ludden, J.N. 1995. Archean subduction inferred from seismic images of a mantle suture in the Superior Province. Nature, **375**:670-674.

Campbell, I.H., Griffiths, R.W., and Hill, R.I. 1989. Melting in an Archean mantle plume:Heads it's basalts, tails it's komatiites. Nature, **339**:697-699.

Campbell, M.J., Vandecasteele, C., and Dams, R., 1991. The appication of isotope dilution, techniques to the accurate and precise determination of lead in reference materials by ICP-MS. In: Holland, G. and Eaton, A., Applications of Plasma Source Mass Spectrometry.130-138.

Capdevila, R., Goodwin, A.M., Ujike, O., and Gorton, M.P. 1982. Trace-element geochemistry of Archean volcanic rocks and crustal growth on southwestern Abitibi Belt, Canada. Geology, **10**:418-422.

Card, K.D. 1990. A review of the Superior province of the Canadian shield: a product of Archean accretion. Precamb. Res., :.

Cattell, A.C. 1987. Enriched komatiitic basalts from Newton Township, Ontario:their genesis by crustal contamination of komatiite magma. Geol. Mag., **124**:303-309.

Cattell, A.C. and Arndt, N.T. 1987. Low- and high-alumina komatiites from a late-Archean sequence, Newton Township, Ontario. Contrib. Mineral. Petrol., **97**:218-227.

Cattell, A.C. and Taylor, R.N., 1990. Archean basic magmas. In: Hall, R.P. and Hughes, D.J., Early Precambrian Basic Magmatisam.11-39.

Claoue-Long, J.C., King, R.W., and Kerrich, R. 1990. Archean hydrothermal zircon in the Abitibi greenstone belt: constraints on the timing of gold mineralization. Earth Planet. Sci. Lett., **98**:109-128.

Colvine, A.C., Fyon, J.A., Heather, K.B., Marmont, S., Smith, P.M., and Troop, D.G. 1988. Archean lode gold deposits in Ontario. Ontario Geol. Surv. Misc. Pap., **139**:1-136.

Compston, W., Williams, I.S., Campbell, I.H., and Gresham, J.J. 1986. Zircon xenocrysts from the Kambalda volcanics: age constraints and direct evidence for older continental crust below the Kambalda-Norseman greenstones. Earth Planet. Sci. Lett., **76**:299-311.

Condie, K.C. 1989a. Geochemical changes in basalts and andesites across the Archean-Proterozoic boundary: identification and significance. Lithos, **23**:1-18.

Condie, K.C., 1989b. Plate Tectonics and Crustal Evolution. Pergamon (Third edition), p.

Condie, K.C., 1990. Geochemical characteristics of Precambrian basaltic greenstones. In: Hall, rp and Hughes, dj, Early Precambrian basic magmatism.40-55.

Condie, K.C., 1994. Greenstone through time. In: Condie, K.C., Archean crustal evolution.85-120.

Corfu, F. 1993. The evolution of the Southern Abitibi greenstone belt in light of precise U-Pb geochronology. Econ. Geol., **88**:1323-1340.

Corfu, F., Krogh, T.E., Kowk, Y.Y., and Jensen, L.S. 1989a. U-Pb zircon geochronlogy in the southwestern Abitibi greenstone belt, Superior Province. Can. J. Earth Sci., **26**:1747-1763.

Corfu, F., Krogh, T.E., Kwok, Y.Y., and Jensen, L.S. 1989b. U-Pb zircon geochronology in the southwestern abitibi greenstone belt, Superior province. Can. J. Earth Sci., **26**:1747-1763.

Corfu, F., Jackson, S.L., and Sutcliffe, R.H. 1991. U-Pb ages and tectonic significance of late Archean alkaline magmatism and nonmarine sedimentation: Timiskaming Group, southern Abitibi belt, Ontario. Can. J. Earth Sci., **28**:489-503.

Defant, M.J. and Drummond, M.S. 1990. Derivation of some modern arc magmas by melting of young subducted lithosphere. Nature, **347**:662-665.

Defant, M.J., Maury, R.C., Ripley, E.M., Feigenson, M.D., and Jacques, D. 1991. An example of island-arc petrogenesis: geochemistry and petrology of the Southern Luzon arc, Philippines. J. Petrol., **32**:455-500.

De Laeter, J.R., Heumann, K.G., and Rosman, K.J.R. 1991. Isotopic compositions of the elements 1989. J. Phys. Chem. Ref. Data, **20**:1327-1337.

DePaolo, D.J., 1988. Neodymium Isotope Chemistry: An Introduction. Springer, p.

Desrochers, J.P., Hubert, C., Ludden, J., and Pilote, P. 1993. Accretion of Archean oceanic plateau fragmants in the Abitibi greenstone belt, Canada. Geology, **21**:451-454.

de Wit, M.J., Roering, C., Hart, R.J., Armstrong, R.A., de Ronde, C.E.J., Green, R.W.E., Tredoux, M., Peberdy, E., and Hart, R.A. 1992. Formation of an Archean continent. Nature, **357**:553-562.

Dimroth, E., Imreh, L., Rocheleau, M., and Goulet, N. 1982. Evolution of south-central part of the Archean Abitibi belt, Quebec, Part I: stratigraphy and paleogeographic model. Can. J. Earth Sci., **19**:1729-1759.

Dimroth, E., Imreh, L., Rocheleau, M., and Goulet, N. 1983a. Evolution of the south-central segment of the Archean Abitibi Belt, Quebec, Part II: Tectonic evolution and geomechanical model. Can. J. Earth Sci., **20**:1355-1373.

Dimroth, E., Imreh, L., Rocheleau, M., and Goulet, N. 1983b. Evolution of the south-central segment of the Archean Abitibi belt, Quebec, Part III: Plutonic and metamorphic evolution and geotectonic model. Can. J. Earth Sci., **20**:1374-1388.

Drake, M.J., McFarlane, E.A., Gasparik, T., and Rubie, D.C. 1993. Mg-perovskite/silicate melt and majorite garnet/silicate melt partition coefficients in the system caO-MgO-SiO2 at high temperatures and pressures. J. Geophys. Res., **98**:5427-5431.

Drummond, M.S. and Defant, M.J. 1990. A model for tronhjemite-tonalite-dacite genesis and crustal growth via slab melting: Archean to modern compositions. J. Geophys. Res., **95**:21503-21521.

Dupuy, C., Liotard, J.M., and Dostal, J. 1992. Zr/Hf fractionation in intraplate basaltic rocks: Carbonate metasomatism in the mantle source. Geochim. Cosmochim. Acta, **56**:2417-2423.

Echeverria, L.M., 1982. Komatiites from Gorgona Island, Colombia. In: Arndt, N.T. and Nisbet, E.G., Komatiites.199-210.

Ewart, A. and Hawkesworth, C.T. 1987. The Pleistocene-recent Tonga-Kermadec arc lavas:Interpretation of new isotopic and rare earth data in terms of a depleted mantle source model. J. Petrol., **28**:495-530.

Farges, F. 1991. Structural environment aroud Th+4 in silicate glasses: implications for geochemistry of incompatible Me4+ elements. Geochim. Cosmochim. Acta, **55**:3303-3319.

Fassett, J.D. and Paulsen, P.J. 1989. Isotope dilution mass spectrometry for accurate elemental analysis. Anal. Chem., **61**:643A-649A.

Fedorowich, J.S., Richards, J.P., Jain, J.C., Kerrich, R., and Fan, J. 1993. A rapid method for REE and trace element analysis using laser sampling ICP-MS on direct fusion whole-rock glasses. Chem. Geol., **106**:229-249.

Feng, R. and Kerrich, R. 1990a. Geobarometry, differential block movements, and crustal structure of the southeastern Abitibi greenstone belts, Canada. Geology, **18**:870-873.

Feng, R. and Kerrich, R. 1990b. Geochemistry of fine-grained clasic sediments in the Archean Abitibi greenstone belt, Canada: implication for provenance and tectonic setting. Geochim. Cosmochim. Acta, **54**:1061-1081.

Feng, R. and Kerrich, R. 1991. Single zircon age constraints on the tectonic juxtaposition of the Archean Abitibi Southern Volcanic Zone and the Pontiac Subprovince. Geochim. Cosmochim. Acta, **55**:3437-3441.

Feng, R. and Kerrich, R. 1992. Geochemical evolution of granitoid from the Archean Abitibi Southern Volcanic Zone and the Pontiac Subprovince, Superior Province, Canada:Implications for tectonic history and Source regions. Chem. Geol., **98**:23-70.

Feng, R., Kerrich, R., and Mass, R. 1993a. Geochemical, oxygen, and neodymium isotope compositions of metasediments from the Abitibi greenstone belt and Pontiac Subprovince, Canada: Evidence for ancient crust and Archean terrane juxtaposition. Geochim. Cosmochim. Acta, **57**:641-658.

Feng, R., Kerrich, R., McBride, S., and Farrar, E. 1993b. 40Ar/39Ar age constraints on the thermal history of the Archean Abitibi greenstone belt and the Pontiac Subprovince: implications for terrane collision, differential uplift, and overprinting of gold deposits. Can. J. Earth Sci., **29**:1389-1411.

Floyd, P.A., 1991. Oceanic islands and seamounts. In: Floyd, P.A., Oceanic basalts.174-218.

Foley, S.F. and Wheller, G.E. 1990. Parallels in the origin of the geochemical signatures of island arc volcanics and continental potassic igneous rocks: the role of residual titanates. Chem. Geol., **85**:1-18.

Fowler, A.D. and Jensen, L.S. 1989. Quantitative trace-element modelling of the crystallization history of the Kinojevis and Blake river groups, Abitibi greenstone belt, Ontario. Can. J. Earth Sci., **26**:1356-1367.

Frarey, M.J. and Krogh, T.E., 1986. U-Pb zircon ages of late internal plutons of the Abitibi and eastern Wawa subprovinces Ontario and Quebec. Geological Survey of Canada, Paper 86-1A, pp.43-48.

Fyfe, W.S. 1978. The evolution of the earth's crust: modern plate tectonics to ancient hot spot tectonics? Chem. Geol., **23**:89-114.

Galer, S.J.G., Goldstein, S.L., and O'Nions, R.K. 1989. Limits on chemical and convective isolation in the earth's interior. Chem. Geol., **75**:257-290.

Gelinas, L., Trudel, P., and Hubert, C. 1984. Chemostratigraphic division of the Blake River Group, Rouyn-Noranda area, Abitibi, Quebec. Can. J. Earth Sci., **21**:220-231.

Gill, J.B., 1981. Orogenic andesites and plate tectonics. Springer-Verlag (1st edition), p.

Goldschmidt, V.M. 1937. The principle of distribution of chemical elements in minerals and rocks. J. Chem. Soc., :655-672.

Goodwin, A.M., 1977. Archean volcanism in Superior province, Canadian shield. In: Baragar, wra, Coleman, lc, and Hall, jm, Volcanic Regimes in Canada. Geological Association of Canada, Special paper,205-241.

Goodwin, A.M. and Ridler, R.H., 1970. The Abitibi orogenic belt. In: Baer, A.J., Basins and geosynclines of the Canadian shield. Geological Survey of Canada, Paper, b70-40:1-30.

Govindaraju, K. 1989. 1989 compilation of working values and sample description for 272 geostandards. Geostand. Newslett., **13**:1-113.

Green, A.G., Milkereit, B., Mayrand, L.J., Ludden, J.N., Hubert, C., Jackson, S.L., Sutcliffe, R.H., West, G.F., Verpaelst, P., and Simard, A. 1990. Deep structure of an Archean greenstone terrane. Nature, **344**:327-330.

Green, D.H. 1975. Genesis of Archean peridotitic magmas and constraints on Archean geothermal gradients and tectonics. Geology, **3**:15-18.

Green, T.H. 1981. Experimental evidence for the role of accessory phases in magma genesis. J. Volcanol. Geotherm. Res., **10**:405-422.

Griffiths, R.W. and Campbell, I.H. 1990. Stirring and structure in mantle starting plumes. Earth Planet. Sci. Lett., **99**:66-78.

Gruau, G., Tourpin, S., Jahn, B.-M., and Anhaeusser, C.R. 1988. New geochemical and isotopic data for komatiites from the Onverwacht Group, southern Africa. Chem. Geol., **70**:144-156.

Gruau, G., Chauvel, C., Arndt, N.T., and Cornichet, J. 1990a. Aluminum depletion in komatiites and garnet fractionation in the early Archean mantle: Hafnium isotopic constraints. Geochim. Cosmochim. Acta, **54**:3095-3101.

Gruau, G., Chauvel, C., and Jahn, B.M. 1990b. Anomalous Sm-Nd ages for the early Archean Onverwacht Group Volcanics. Contrib. Mineral. Petrol., **104**:27-34.

Hall, G.E.M. and Pelchat, J.C. 1990a. Analysis of standard reference materials for Zr, Nb, Hf and Ta by ICP-MS after lithium metaborate fusion and cupferron seperation.

Geostand. Newslett., **14**:197-206.

Hall, G.E.M. and Pelchat, J.C. 1990b. Determination of Zirconium, Niobium, Hafnium and Tantalum at low levels in geological materials by inductively coupled plasma mass spectrometry. J. Anal. At. Spectrom., **5**:339-349.

Hall, G.E.M. and Plant, J.A. 1990. Are your REE results total? Explore, **68**:18-20.

Hall, G.E.M. and Plant, J.A. 1992. Analytical errors in the determination of high field strength elements and their implications in tectonic interpretation studies. Chem. Geol., **95**:141-156.

Harper, C.L. and Jacobsen, S.B. 1992. Evidence from coupled ^{147}Sm-^{143}nd and ^{146} Sm-^{142}Nd systematics for very early (4.5-Gyr) differentiation of the Earth's mantle. Nature, **360**:728-732.

Hart, S.R. and Dunn, T. 1993. Experimental Cpx/melt partitioning of 24 trace elements. Contrib. Mineral. Petrol., **113**:1-8.

Hart, S. and Zindler, A., 1989. Constraints on the nature and Development of chemical heterogeneities in the mantle. In: Peltier, W.R., Mantle convection: plate tectonics and global dynamics. The fluid mechanics of astrophysics and geophysics, b4:261-873.

Hart, S.R., Hauri, E.H., Oschmann, L.A., and Whitehead, J.A. 1992. Mantle plumes and entrainment:isotopic evidence. Science, **256**:517-520.

Hawkesworth, C.J., Hergt, J.M., McDermott, F., and Ellam, R.M. 1991. Destructive margin magmatism and the contributions from the mantle wedge and subducted crust. Australian. J. Earth Sci., **38**:577-594.

Hawkesworth, C.J., Gallagher, K., Hergt, J.M., and McDermott, F. 1993. Trace element fractionation processes in the generation of island arc basalts. Phil. Trans. R. Soc. Lond., **A342**:179-191.

Hemley, R.J. and Cohen, R.E. 1992. Silicate perovskite. Annu. Rev. Earth Planet. Sci., **20**:553-600.

Herzberg, C.T. 1984. Chemical stratification in the silicate Earth. Earth Planet. Sci. Lett., **67**:249-260.

Herzberg, C.T. 1992a. Depth and degree of melting of komatiites. J. Geophys. Res., **97**:4521-4540.

Herzberg, C.T., 1992b. Phase equilibria and trace element partitioning in a magma ocean to

200 kilobars. Workshop on the physics and chemistry of magma oceans from 1 bar to 4 mbar (abstract). LPI technical report. 92-03. p. 22-23.

Herzberg, C.T. 1995. Generation of plume magmas through time: an experimental perspective. Chem. Geol., **(in press)**:.

Herzberg, C.T. and Forsythe, R.D. 1983. Destabilization of a 650 km chemical boundary layer and its bearing on the evolution of the continental crust. Phys. Earth Planet. Inter., **32**:352-360.

Herzberg, C.T. and Gasparik, T. 1991. Garnet and pyroxene in the mantle: a test of the majorite fractionation hypothesis. J. Geophys. Res., **96**:16263-16274.

Herzberg, C.T. and O'Hara, M.J. 1985. Origin of mantle peridotite and komatiite by partial melting. Geophys. Res. Lett., **12**:541-544.

Herzberg, C.T. and Ohtani, E. 1988. origin of komatiite at high pressures. Earth Planet. Sci. Lett., **88**:321-329.

Herzberg, C.T., Feigenson, M., Skuba, C., and Ohtani, E. 1988. Majorite fractionation recorded in the geochemistry of peridotites from South Africa. Nature, **332**:823-826.

Herzberg, C.T., Gasparik, T., and Sawamoto, H. 1990. Origin of mantle peridotite: constraints from melting experiments to 16.5 GPa. J. Geophys. Res., **95**:15,779-803.

Heuzen, A.A.van, Hoekstra, T., and Wingerden, B.van 1989. Precision and accuracy attainable with isotope dilution analysis applied to inductively coupled plasma mass spectrometry: Theory and experiments. J. Anal. At. Spectrom., **4**:483-489.

Hill, R.I., Campbell, I.H., Davies, G.F., and Griffiths, R.W. 1992. Mantle plumes and continental tectonics. Science, **256**:186-193.

Hodgson, C.J. and Hamilton, J.V., 1989. Gold mineralization in the Abitibi greenstone belt: end stage result of Archean collisional tectonics? Economic Geology, Monograph 6, p.86-100.

Hoffman, P.F. and Ranalli, G. 1988. Archean oceanic flake tectonics. Geophys. Res. Lett., **15**:1077-1080.

Hofmann, A.W. 1988. Chemical differentiation of the earth:the relationship between mantle, continental crust, and oceanic crust. Earth Planet. Sci. Lett., **90**:297-314.

Horlick, G., Tan, S.H., Vaughan, M.A., and Rose, C.A. 1985. The effect of plasma operating parameters on analyte signals in inductively coupled plasma mass spectrometry. Spectrochimica Acta, **40B**:1555-1572.

Hynes, A. 1980. Carbonatization and mobility of Ti, Y, and Zr in Ascot Formation metabasalts, SE Quebec. Contrib. Mineral. Petrol., **75**:79-87.

Ito, E. and Takahashi, E. 1987. Melting of peridotite at uppermost lower-mantle conditions. Nature, **328**:514-517.

Jackson, S.L. and Fyon, J.A., 1992. The western Abitibi subprovince in Ontario. In: Thurston, P.C., Williams, H.R., Sutcliffe, R.H., and Stott, G.M., Geology of Ontario. Ontario Geological Survey Special Volume, b4:405-482.

Jackson, S.L., Fyon, J.A., and Corfu, F. 1994. Review of Archean supracrustal assemblages of the Southern Abitibi greenstone bel in Ontario, Canada: products of microplate interaction within a large-scale plate-tectonic setting. Precamb. Res., **65**:183-205.

Jagoutz, E., Palme, H., Baddenhausen, H., Blum, K., Cendales, M., Dreibus, G., Spettel, B., Lorenz, V., and Wanke, H. 1979. The abundances of major, minor and trace elements in the earth's mantle as derived from primitive ultramafic nodules. Proceding of Lunar and Planetary Science Conference, 10th, :2031-2050.

Jahn, B.-M., Auvray, B., Blais, S., Capdevila, R., Cornichet, J., Vidal, P., and Hameurt, J. 1980. Trace element geochemistry and petrogenesis of Finnish greenstone belts. J. Petrol., **21**:201-244.

Jahn, B.M., Gruau, G., and Glikson, A.Y. 1982. Komatiites of the Onverwacht Group, s. Africa: REE geochemistry, Sm/Nd age and mantle evolution. Contrib. Mineral. Petrol., **80**:25-40.

Janghorbani, M. and Ting, B.T.G., 1989. Stable Isotope Tracer Applications of ICP-MS. In: Date, A.R. and Gray, A.L., Applications of Inductively Coupled Plasma Mass Spectrometry.115-140.

Jarvis, K.E. 1990. A critical evaluation of two sample preparation techniques for low-level determination of some geologically incompattible elements by inductively coupled plasma-mass spectrometry. Chem. Geol., **83**:89-103.

Jarvis, K.E., Gray, A.L., and Houk, R.S., 1992. Handbook of Inductively Coupled Plasma Mass Spectrometry. Blackie, 376p.

Jeanloz, R. and Knittle, E. 1989. Density and composition of the mantle. Phil. Trans. R. Soc. Lond., **A328**:377-389.

Jenner, G.A., Longerich, H.P., Jackson, S.E., and Fryer, B.J. 1990. ICP-MS--- A powerful tool for high-precision trace-element analysis in Earth sciences: Evidence from analysis of selected U.S.G.S. reference samples. Chem. Geol., **83,**:133-148.

Jensen, L.S., 1976. A new method of classifying subalkalic volcanic rocks. Ontario Division of Mines, Misceneous Paper No. 66.

Jensen, L.S., 1985. Stratigraphy and petrogenesis of Archean metavolcanic sequences, southwestern Abitibi subprovince, Ontario. In: Ayres, L.D., Thurston, P.C., Card, K.D., and Weber, w, Evolution of Archean Supeacrustal sequences.

Jensen, L.S. and Langford, F.F., 1985. Geology and Petrogenesis of the Archean Abitibi belt in the Kirkland Lake area, Ontario. Ontario Geological Survey, p.

Jochum, K.P., Seufert, H.M., Midinet-Best, S., Rettmann, E., Schonberger, K., and Zimmer, M. 1988. Multi-element analysis by isotope dilution-spark source mass spectrometry (ID-SSMS). Fresenius Z. Anal. Chem., **331**:104-110.

Jochum, K.P., McDonough, W.F., Palme, H., and Spettel, B. 1989. Compositional constraints on the continental lithospheric mantle from trace elements in spinel peridotite xenoliths. Nature, **340**:548-550.

Jochum, K.P., Seufert, H.M., and Thirlwall, M.F. 1990a. High-sensitivity Nb analysis by spark-source mass spectrometry(SSMS) and calibration of XRF Nb and Zr. Chem. Geol., **81**:1-16.

Jochum, K.P., Seufert, H.M., and Thirlwall, M.F. 1990b. Multi-element analysis of 15 international standard rocks by isotope-dilution spark source mass spectrometry. Geostand. Newslett., **14**:469-473.

Jochum, K.P., Arndt, N.T., and Hofmann, A.W. 1991. Nb-Th-La in komatiites and basalts: constraints on komatiite petrogenesis and mantle evolution. Earth Planet. Sci. Lett., **107**:272-289.

Jolly, W.T., 1978. Metamorphic history of the Archean Abitibi belt. In: Fraser, ja and Heywood, ww, Metamorphism in Canadian Shield.78-100.

Kato, T., Ringwood, A.E., and Irifune, T. 1988a. Constraints on element partition coefficients between MgSiO3 perovskite and liquid determined by direct measurements. Earth Planet. Sci. Lett., **90**:65-68.

Kato, T., Ringwood, A.E., and Irifune, T. 1988b. Experimental determination of element partitioning between silicate perovskites, garnets and liquids:constraints on early differentiation of the mantle. Earth Planet. Sci. Lett., **89**:123-145.

Kato, T., Ringwood, A.E., and Irifune, T. 1989. Constraints on element partition coefficients between MgSiO3 perovskite and liquid determined by direct mearsurements--reply to C.B. Agee and D. Walker. Earth Planet. Sci. Lett., **94**:162-164.

Kay, R.W. 1978. Aleutian magnesian andesites: melts from subducted Pacific ocean crust. J. Volcanol. Geotherm. Res., **4**:117-132.

Kelemen, P.B. 1990. Reaction between ultramafic rock and fractionaing basaltic magma, part I, phase relations, the origin of calc-alkaline magma series, and the formation of discordant dunite. J. Petrol., **31**:51-98.

Kelemen, P.B., Johnson, K.T.M., Kinzler, R.J., and Irving, A.J. 1990a. High-field-strength element depletions in arc basalts due to mantle-magma interaction. Nature, **345**:521-524.

Kelemen, P.B., Joyce, D.B., Webster, J.D., and Holloway, J.R. 1990b. Reaction between ultramafic rock and fractionating basaltic magma II. experimental investigation of reaction between olivine tholeiite and harzburgite at 1150-1050 C and 5 kb. J. Petrol., **31**:99-134.

Kelemen, P.B., Dick, H.J.B., and Quick, J.E. 1992. Formation of harzburgite by pervasive melt/rock reaction in the upper mantle. Nature, **358**:635-641.

Kennedy, A.K., Lofgren, G.E., and Wasserburg, G.J. 1993. An experimental study of trace element partitioning between olivine, orthopyroxene and melt in chondrules: equilibrium values and kinetic effects. Earth Planet. Sci. Lett., **115**:177-195.

Kerrich, R., 1989. Geodynamic setting and hydraulic regimes: shear zone hosted mesothermal gold deposits. In:, . Mineralogy Association of Canada, short course notes, b6:89-128.

Kerrich, R., 1991. Radiogenic isotope systems applied to mineral deposits. In: Heaman, L. and Ludden, J., Application of radiogenic isotope systems to problems in geology. Mineralogy Association of Canada, Short Course Notes, b19:365-421.

Kerrich, R. and Feng, R. 1991. Archean geodynamics and the Abitibi-Pontiac collision:implication for advection of fluids at transpressive collisional boundaries and the origin of giant quartz vein systems. Earth Sci. Rev., **32**:33-60.

Kerrich, R. and Feng, R. 1992. Archean geodynamics and the Abitibi-pontiac collision: implications for advection of fluids at tranpressive collisional boundaries and the origin of giant quartz vein. Earth Sci. Rev., **32**:33-60.

Kerrich, R. and Fryer, B.J. 1979. Archean precious-metal hydrothermal systems, Downe mine, Abitibi Greenstone Belt, II: REE and oxygen isotope relations. Can. J. Earth Sci., **16**:440-458.

Kerrich, R. and King, R. 1993. Hydrothermal zircon and baddeleyite in Val-d'Or Archean mesothermal gold deposits:characteristics, compositions, and fluid-inclusion

properties, with implications for timing of primary gold mineralization. Can. J. Earth Sci., **30**:2334-2351.

Kerrich, R. and Wyman, D.A. 1994. The mesothermal gold-lamprophyre association: significance for an accretionary geodynamic setting, supercontinent cycles, and metallogenic processes. Mineral. Petrol., **51**:147-172.

Kesson, S.E., Sinclair, W.J., and Ringwood, A.E. 1983. Solid solution limits in synroc zirconolite. Nucl. Chem. Waste Man., **4**:259-265.

Kishida, A. and Kerrich, R. 1987. Hydrothermal alteration zoning and gold concentration at the Kerr-Addison Archean lode gold deposit, Kirkland Lake, Ontario. Econ. Geol., **82**:649-690.

Knittle, E. and Jeanloz, R. 1989. melting curve of (Mg, Fe)SiO3 perovskite to 96 GPa: evidence for a structural transition in lower mantle melts. Geophys. Res. Lett., **16**:421-424.

Kusky, T.M. and Kidd, W.S.F. 1992. Remnants of an Archean oceanic plateau, Belingwe greenstone belt, Zimbabwe. Geology, **20**:43-46.

Lafleche, M.R., Dupuy, C., and Bougault, H. 1992a. Geochemistry and petrogenesis of Archean mafic volcanic rocks of the Southern Abitibi belt, Quebec. Precamb. Res., **57**:207-241.

Lafleche, M.R., Dupuy, C., and Dostal, J. 1992b. Tholeiitic volcanic rocks of the late Archean Blake River Group, Southern Abitibi greenstone belt: origin and geodynamic implications. Can. J. Earth Sci., **29**:1448-1458.

Lahaye, Y., Arndt, N.T., Byerly, G., Chauvel, C., Fourcade, S., and Gruau, G. 1995. The influence of alteration on the trace-element and Nd isotope compositions of komatiites. Chem. Geol., :(in press).

Lajoie, J. and Ludden, J. 1984. Petrology of the Archean Pontiac and kewagama sediments and implication for the stratigraphy of the southern Abitibi belt. Can. J. Earth Sci., **21**:1305-1314.

Lecuyer, C., Gruau, G., Anhaeusser, C.R., and Fourcade, S. 1994. The origin of fluids and effects of metamorphism on the primary chemical compositions of Barberton komatiites:new evidence from geochemical (REE) and isotopic (Nd, O, H, 39Ar/40Ar) data. Geochim. Cosmochim. Acta, **58**:969-984.

Lesher, C.M., Phillips, G.N., Groves, D.I., and Campbell, I.H., 1991. Immobility of REE and most high field-strength elements and first transition of metabasalts at the Hunt mine, Western Australia. Brazil Gold'91, edited E.A. Ladeira. Balkema, Rotterdam. p. 327-

334.

Lichte, F.E., Meier, A.L., and Crock, J.G. 1987. Determination of the rare earth elements in geological materials by inductively coupled plasma mass spectrometry. Anal. Chem., **59**:1150-1157.

Longerich, H.P. 1989. The application of isotope dilution to inductively coupled plasma-mass spectrometry. Atomic Spectroscopy, **10**:112-115.

Longerich, H.P., Fryer, B.J., and Strong, D.F. 1987a. Determination of lead isotope ratios by inductively coupled plasma-mass spectrometry (ICP-MS). Spectrochimica Acta, **42B**:39-48.

Longerich, H.P., Fryer, B.J., Strong, D.F., and Kantipuly, C.J. 1987b. Effects of operating conditions on the determination of the rare earth elements by inductively coupled plasma-mass spectrometry(ICP-MS). Spectrochimica Acta, **42B**:75-92.

Longerich, H.P., Jenner, G.A., Fryer, B.J., and Jackson, S.E. 1990. Inductively coupled plasma-mass spectrometric analysis of geological samples: A critical evaluation based on case studies. Chem. Geol., **83**:105-118.

Ludden, J.N. and Gelinas, L., 1982. Trace element characteristics of komatiites and komatiitic basalts from the Abitibi metavolcanic belt of Quebec. In: Arndt, N.T. and Nisbet, E.G., Komatiites.331-346.

Ludden, J., Gèlinas, L., and Trudel, P. 1982. Archean metavolcanics from the Rouyn-Noranda district, Abitibi greenstone belt, Quebec. 2. mobility of trace elements and petrogenetic constraints. Can. J. Earth Sci., **19**:2276-2287.

Ludden, J.N., Hubert, C., and Gariepy, C. 1986. The tectonic evolution of the Abitibi greenstone belt of Canada. Geol. Mag., **123**:153-166.

Machado, N., Brooks, C., and Hart, S.R. 1986. Determination of initial $^{87}Sr/^{86}Sr$ and $^{143}Nd/^{144}Nd$ in primary minerals from mafic and ultramafic rocks: Experimental procedure and implications for the isotopic characteristics of the Archean mantle under the Abitibi greenstone belt, Canada. Geochim. Cosmochim. Acta, **50**:2335-2348.

Martin, H. 1986. Effect of steeper Archean geothermal gradient on geochemistry of subduction-zone magmas. Geology, **14**:753-756.

Matsui, T. and Abe, Y. 1986. Formation of a "magma ocean" on the terrestrial planets due to the blanketing effect of an impact-induced atmosphere. Earth Moon Planets, **34**:223-230.

McCallum, I.S. and Charette, M.P. 1978. Zr and Nb partition coefficients: implications for the genesis of Mare basalts, Kreep, and sea floor basalts. Geochim. Cosmochim. Acta, **42**:859-869.

McCuaig, T.C., Kerrich, R., and Xie, Q. 1994. Phosphorus and high field strength element anomalies in Archean high-magnesian magmas as possible indicators of source mineralogy and depth. Earth Planet. Sci. Lett., **124**:221-239.

McCulloch, M.T. and Bennett, V.C. 1994. Progressive growth of the Earth's continental crust and depleted mantle: geochemical constraints. Geochim. Cosmochim. Acta, **58**:4717-4738.

McCulloch, M.T. and Gamble, J.A. 1991. Geochemical and geodynamical constraints on subduction zone magmatism. Earth Planet. Sci. Lett., **102**:358-374.

McDonough, W.F. and Ireland, T.R. 1993. Intraplate origin of komatiites inferred from trace elements in glass inclusions. Nature, **365**:432-434.

McDonough, W.F., Stosch, H.G., and Ware, N.G. 1992. Distribution of titanum and the rare earth elements between peridotitic minerals. Contrib. Mineral. Petrol., **110**:321-328.

McFarlane, E.A. and Drake, M.J., 1990. Element partitioning and the early thermal history of the Earth. In: Newsom, H. and Jones, J.H., Origin of the Earth.135-150.

McKay, G.A., 1989. Partitioning of rare earth elements between major silicate minerals and basaltic melts. In: Lipin, B.R. and McKay, G.A., Geochemistry and Mineralogy of Rare Earth Elements. Reviews in Mineralogy, b21:45-77.

McKenzie, D. 1985. The extraction of magma from the crust and mantle. Earth Planet. Sci. Lett., **74**:81-91.

McKenzie, D. and Bickle, M.J. 1988. The volume and composition of melt generated by extension of lithosphere. J. Petrol., **29**:625-679.

McKenzie, D. and O'Nions, R.K. 1991. Partial melt distributions from inversion of rare earth element concentrations. J. Petrol., **32**:1021-1091.

Melosh, H.J., 1990. Giant impacts and the thermal state of the early Earth. In: Newsom, H.E. and Jones, J.H., Origin of the Earth.69-84.

Miller, G.H., Stolper, E.M., and Ahrens, T.J. 1991a. The equation of state of a molten komatiite 1. shock wave compression to 36 GPa. J. Geophys. Res., **96**:11,831-48.

Miller, G.H., Stolper, E.M., and Ahrens, T.J. 1991b. The equation of state of a molten komatiite 2. application to komatiite petrogenesis and the Haden mantle. J. Geophys.

Res., **96**:11,849-64.

Morris, P.A., 1993. Geochemistry and volcanology of mafic and ultramafic volcanics in the Norseman-Menzies and adjacent areas, Eastern Yilgarn craton. Gological Survey of Western Australia, Report 36.

Mortensen, J.K. 1993a. U-Pb geochronology of the eastern Abitibi Subprovince. Part 2: Noranda-Kirkland Lake area. Can. J. Earth Sci., **30**:29-41.

Mortensen, J.K. 1993b. U-Pb geochronology of the Lapparent Massif, northeastern Abitibi belt: basement or synvolcanic pluton? Can. J. Earth Sci., **30**:42-47.

Mortensen, J.K. 1993c. U-Pb geochronology og eastern Abitibi Subprovince. Part 1: Chibougamau-Matagami-Joutel region. Can. J. Earth Sci., **30**:11-28.

Mukherji, J.K., 1970. Analytical Chemistry of Zirconium and Hafnium. Pergamon Press, 300p.

Murthy, V.R. 1991. early differentiation of the Earth and the Problem of mantle siderophile elements: a new approach. Science, **253**:303-306.

Naldrett, A.J. and Turner, A.R. 1977. The geology and petrogenesis of a greenstone belt and related nickle sulphide mineralization at Yakabindie, Western Australia. Precamb. Res., **5**:43-103.

Nesbitt, R.W. and Sun, S.S. 1976. Geochemistry of Archean spinifex-tectured peridotites and magnesian and low magnesian tholeiites. Earth Planet. Sci. Lett., **31**:433-453.

Nesbitt, R.W., Sun, S.S., and Purvis, A.C. 1979. Komatiites: geochemistry and genesis. Can. Mineral., **17**:165-186.

Nesbitt, R.W., Jahn, B.-M., and Purvis, A.C. 1982. Komatiites: an early Precambrian phenomenon. J. Volcanol. Geotherm. Res., **14**:31-45.

Nisbet, E.G., 1982. The tectonic setting and petrogenesis of komatiites. In: Arndt, N.T. and Nisbet, E.G., Komatiites.501-522.

Nisbet, E.G. and Walker, D. 1982. komatiites and the structure of the Archean mantle. Earth Planet. Sci. Lett., **60**:105-113.

Nisbet, E.G., Bickle, M.J., and Martin, A. 1977. The mafic and ultramafic lavas of the Belingwe greenstone belt, Rhodesia. J. Petrol., **4**:521-566.

Nisbet, E.G., Cheadle, M.J., Arndt, N.T., and Bickle, M.J. 1993. Constraining the potential temperature of the Archean mantle: a review of the evidence from komatiites. Lithos,

30:291-307.

Nunes, P.D. and Pyke, D. 1981. Time-stratigraphic correlation of the Kidd Creek orebody with volcanic rocks south of Timmins, Ontario, as inferred from zircon U-Pb ages. Econ. Geol., **76**:944-951.

Ohtani, E. 1984. Generation of komatiite magma and gravitational differentiation in the deep upper mantle. Earth Planet. Sci. Lett., **67**:261-272.

Ohtani, E. 1985. The primordial terrestrial magma ocean and its implications for stratification of the mantle. Phys. Earth Planet. Inter., **38**:70-80.

Ohtani, E. 1988. Chemical stratification of the mantle formed by melting in the early stage of the terrestrial evolution. Tectonophysics, **154**:201-210.

Ohtani, E. and Sawamoto, H. 1987. Melting experiment on a model chondritic mantle composition at 25 Gpa. Geophys. Res. Lett., **14**:733-736.

Ohtani, E., Kawabe, I., Moriyama, J., and Nagata, Y. 1989. Partitioning of elements between majorite garnet and melt and implications for petrogenesis of komatiite. Contrib. Mineral. Petrol., **103**:263-269.

Owen, L.B. and Faure, G. 1974. Simultaneous determination of Hafnium and Zirconium in silicate rocks by isotope dilution. Anal. Chem., **46**:1323-1326.

Paradis, S., Ludden, J., and Gelinas, L. 1988. Evidence for contrasting compositional spectra in comagmatic intrusive and extrusive rocks of the late Archean Blake River Group, Abitibi, Quebec. Can. J. Earth Sci., **25**:134-144.

Patchett, P.J. and Tatsumoto, M. 1980. A routine high-precision method for Lu-Hf isotope geochemistry and chronology. Contrib. Mineral. Petrol., **75**:263-267.

Peacock, S.M., Rushmer, T., and Thompson, A.B. 1994. Partial melting of subducting oceanic crust. Earth Planet. Sci. Lett., **121**:227-244.

Pearce, J.A., 1982. Trace element characteristics of lavas from destructive plate boundaries. In: Thorpe, R.S., Andesites: Orogenic Andesites and Related Rocks.525-548.

Pearce, J.A. and Cann, J.R. 1973. Tectonic setting of basic volcanic rocks using trace element analyses. Earth Planet. Sci. Lett., **19**:290-300.

Pearce, J.A. and Peate, D.W. 1995. Tectonic implications of the composition of volcanic arc magmas. Annu. Rev. Earth Planet. Sci., **23**:251-285.

Potts, P.J., 1987. A handbook of silicate rock analysis. Blackie, 622p.

Potts, P.J., Webb, P.C., and Watson, J.S. 1990. Zirconium determination by ED-XRF: a critical evaluation of silicate reference materials as calibration standards. Geostand. Newslett., **14**:127-136.

Potts, P.J., Tindle, A.G., and Webb, P.C., 1992. Geochemical reference material compositions. Whittles Publishing, 313p.

Pyke, D.R., 1978. Geology of the Redstone River area, District of Timiskaming. Ontario Division of Mines, Ministry of Natural Resources, 278p.

Pyke, D.R., 1982. Geology of the Timmins area, district of Cochrane. Ontario geological Survey, 456p.

Pyke, D.R., Naldrett, A.J., and Ecstrand, O.R. 1973. Archean ultramafic flows in Munro Township, Ontario. Geol. Soc. Am. Bull., **84**:955-978.

Rampone, E., Bottazzi, P., and Ottolini, L. 1991. Complementary Ti and Zr anomalies in orthopyrone and clinopyroene from mantle peridotites. Nature, **354**:518-520.

Renner, R., Nisbet, E.G., Cheadle, M.J., Arndt, N.T., Bickle, M.J., and Cameron, W.E. 1994. Komatiite flows from the Reliance Formation, Belingwe belt, Zimbabwe:I--petrography and mineralogy. J. Petrol., :(in press).

Ringwood, A.E., 1990a. Earliest history of the Earth-Moon system. In: Newsom, H.E. and Jones, J.H., Origin of the Earth.101-134.

Ringwood, A.E. 1990b. Slab-mantle interactions 3, Petrogenesis of intraplate magmas and structure of the upper mantle. Chem. Geol., **82**:187-207.

Ringwood, A.E. 1991. Phase transitions and their bearing on the constitution and dynamics of the mantle. Geochim. Cosmochim. Acta, **55**:2083-2110.

Russ III, G.P., 1989. Isotope ratio measurements using ICP-MS. In: Date, A.R. and Gray, A.L., Applications of Inductively Coupled Plasma Mass Spectrometry.90-114.

Russ III, G.P. and Bazan, J.M. 1987. Isotope ratio measurements with an inductively coupled plasma source mass spectrometer. Spectrochimica Acta, **42B**:49-62.

Salters, V.J.M. and Hart, S.R. 1991. The mantle sources of ocean ridge, islands and arc: the Hf-isotope connection. Earth Planet. Sci. Lett., **104**:364-380.

Salters, V.J.M. and Shimizu, N. 1988. World-wide occurrence of HFSE-depleted mantle. Geochim. Cosmochim. Acta, **52**:2177-2182.

Salters, V.J.M. and Zindler, A. 1995. Extreme $^{176}Hf/^{177}Hf$ in the sub-oceanic mantle. Earth

Planet. Sci. Lett., **129**:13-30.

Sautter, V., Haggerty, S.E., and Field, S. 1991. Ultradeep (>300 Kilometers) ultramafic xenoliths: petrological evidence from the transition zone. Science, **252**:827-830.

Schonberg, C.D.G. 1993. Simultaneous determination of thirty-seven trace elements in twenty-eight international rock standards by ICP-MS. Geostand. Newslett., **17**:81-97.

Shirey, S.B. and Hanson, G.N. 1986. Mantle heterogeneity and crustal recycling in Archean granite-greenstone belts: evidence from Nd isotopes and trace elements in the Rainy Lake area, Superior Province, Ontario, Canada. Geochim. Cosmochim. Acta, **50**:2631-2651.

Smith, A.D. and Ludden, J.N. 1989. Nd isotopic evolution of the Precambrian mantle. Earth Planet. Sci. Lett., **93**:14-32.

Smith, H.S. and Erlank, A.J., 1982. Geochemistry and petrogenesis of komatiites from the barberton greenstone belt, South Africa. In: Arndt, N.T. and Nisbet, E.G., Komatiites.347-397.

Smith, I.E.M. 1980. Geochemical evolution in the Blake River Group, Abitibi greenstone belt, Superior Province. Can. J. Earth Sci., **17**:1292-1299.

Solomah, A.G., Richardson, P.G., and McFlovain, A.K. 1987. Phase identification, microstructural characterization, phase microanalyses and leaching performance evaluation of SYN-ROC-FA crystalline ceramic waste form. J. Nucl. Mat., **148**:157-165.

Stein, M. and Hofmann, A.W. 1994. Mantle plumes and episodic crustal growth. Nature, **372**:63-68.

Stolz, A.J., Varne, R., Davies, G.R., Wheller, G.E., and Foden, J.D. 1990. Magma source components in an arc-continental collision zone: the Flores-Lembata sector, Sunda arc, Indonesia. Contrib. Mineral. Petrol., **105**:585-601.

Stone, W.E., Jensen, L.S., and Church, W.R. 1987. Petrography and geochemistry of an unusual Fe-rich basaltic komatiite from Boston Township, northeastern Ontario. Can. J. Earth Sci., **24**:2537-2550.

Stone, W.E., Crocket, J.H., and Fleet, M.E. 1992. Field guides to platinum-metal mineralization in the Archean Boston Creek flow, Abitibi belt, Ontario:significance to exploration in mafic/ultramafic rock terrains., :.

Storey, M., Mahoney, J.J., Kroenke, L.W., and Saunders, A.D. 1991. Are oceanic Plateaus

site of komatiite formation? Geology, **19**:376-379.

Stott, G.M., Sanborn-Barrie, M., and Corfu, F., 1987. Major transpression events recorded across Archean subprovince boundaries in northwestern Ontario. Geological Association of Canada, Summer Field Meeting, Yellowknife, N.W.T., August 1987, Program with Abstracts, p.24.

Sun, S.S. 1982. Chemical composition and origin of the earth's primitive mantle. Geochim. Cosmochim. Acta, **46**:179-192.

Sun, S.S. and McDonough, W.F., 1989. Chemical and isotopic systematics of oceanic basalts: implications for mantle composition and processes. In: Saunders, ad and Norry, mj, Magmatism in the ocean basins. Geological Society of London, Special Publication,313-345.

Sun, S.S. and Nesbitt, R.W. 1978. Petrogenesis of Archean ultrabasic and basic volcanic rocks:evidence from rare earth elements. Contrib. Mineral. Petrol., **65**:301-325.

Sun, S.S. and Nesbitt, R.W. 1979. Petrogenesis of Archean ultrabasic and basic volcanics: evidence from rare earth elements. Contrib. Mineral. Petrol., **65**:301-325.

Sun, X.F., Ting, B.T.G., Zeisel, S.H., and Janghorbani, M. 1987. Accurate measurement of stable isotope of lithium by inductively coupled plasma mass spectrometry. Analyst, **112**:1223-1228.

Takahashi, E. 1986. Melting of a dry peridote KLB-1 up to 14 GPa: Implications on the origin of peridotitic upper mantle. J. Geophys. Res., **91**:9367-9382.

Takahashi, E. and Scarfe, C.M. 1985. Melting of peridotite to 14 GPa and the genesis of komatiite. Nature, **315**:566-568.

Tatsumi, Y., Hamilton, D.L., and Nesbitt, R.W. 1986. Chemical characteristics of fluid phase released from a subducted lithosphere and origin of arc magmas: evidence from high-pressure experiments and natural rocks. J. Volcanol. Geotherm. Res., **29**:293-309.

Taylor, S.R. and McLennan, S.M., 1985. The continental crust: Its composition and evolution. Blackwell, 312p.

Thurston, P.C., 1990. Early Precambrian basic rocks of the Canadian Shield. In: Hall, R.P. and Hughes, D.J., Early Precambrian basic magmatism.221-247.

Thurston, P.C. and Chivers, K.M. 1990. Secular variation in greenstone sequence development emphasizing Superior Province, Canada. Precamb. Res., **46**:21-58.

Thurston, P.C., Osmani, I.A., and Stone, D., 1992. Northwestern Superior Province: Review

and terrane analysis. In: Thurston, P.C., Williams, H.R., Sutcliffe, R.H., and Stott, G.M., Geology of Ontario. Ontario Geological Survey Special Volume, b4:81-144.

Ting, B.T.G. and Janghorbani, M. 1988. Optimisation of instrumental parameters for the precise measurement of isotope ratios with inductively coupled plasma mass spectrometry. J. Anal. At. Spectrom., **3**:325-336.

Tourpin, S., Gruau, G., Blais, S., and Fourcade, S. 1991. Resetting of REE, and Nd and Sr isotopes during carbonitization of a komatiite flow from Finland. Chem. Geol., **90**:15-29.

Ujike, O. and Goodwin, A.M. 1987. Geochemistry and origin of Archean felsic metavolcanic rocks, Central area, Quebec, Canada. Can. J. Earth Sci., **24**:2551-2567.

Valsami, E. and Cann, J.R., 1992. Mobility of rare earth elements in zones of intense hydrothermal alteration in the Pindos ophiolite, Greece. In: Parson, L.M., Murton, B.J., and Browning, P., Ophiolites and their modern oceanic analogues. Geological society of London, Special Publication, bNo. 60:219-232.

Viljoen, R.P. and Viljoen, M.J. 1969. Evidence for the composition of the primitive mantle and its products of partial melting from a study of the mafic and ultramafic rocks of the Barberton Mountain Land. Sp. Publ. Geol. Soc. S. Afr., **2**:275-295.

Walder, A.J., Platzner, I., and Freedman, P.A. 1993. Isotope Ratio Measurement of Lead, Neodymium and Neodymium-Samarium Mixtures, Hafnium and Hafnium-Lutetium Mixtures with a Double Focusing Multiple Colletor Inductively Coupled Plasma Mass Spectrometer. J. Anal. At. Spectrom., **8**:19-23.

Walker, R.J., Shirey, S.B., and Stecher, O. 1988. Comparative Re-Os, Sm-Nd and Rb-Sr isotope and trace element systematics for Archean komatiite flows from Munro Township, Abitibi Belt, Ontario. Earth Planet. Sci. Lett., **87**:1-12.

Walker, R.J., Echeverria, L.M., Shirey, S.B., and Horan, M.F. 1991. Re-Os isotopic constraints on the origin of volcanic rocks, Gorgona Island, Colombia: Os isotopic evidence for ancient heterogeneities in the mantle. Contrib. Mineral. Petrol., **107**:150-162.

Watson, E.B. and Harrison, T.M. 1984. Accessary minerals and the geochemical evolution of crustal magmatic systems: a summary and prospectus of experimental approaches. Phys. Earth Planet. Inter., **35**:19-30.

Weaver, B.L. and Tarney, J. 1979. Thermal aspects of komatiite generation and greenstone beltmodels. Nature, **79**:689-692.

Wei, K., Tronnes, R.G., and Scarfe, C.M. 1990. Phase relations of aluminum-undepleted and

aluminum-depleted komatiites at pressures of 4-12 Gpa. J. Geophys. Res., **95**:15817-15827.

White, W.M. and Patchett, J. 1984. Hf-Nd-Sr isotopes and incompatible element abundances in island arcs: implications for magma origins and crust-mantle evolution. Earth Planet. Sci. Lett., **67**:167-185.

Woodhead, J. and Johnson, R.W. 1993. Isotopic and trace-element profiles across the New Britain island arc, Papua New Guinea. Contrib. Mineral. Petrol., **113**:479-491.

Wyman, D. and Kerrich, R. 1988. Alkaline magmatism, major structures, and gold deposits: implications for greenstone belt gold metallogeny. Econ. Geol., **83**:454-461.

Wyman, D.A. and Kerrich, R. 1989. Archean lamprophyre dikes of the Superior Province, Canada:distribution, petrology, and geochemical characteristics. J. Geophys. Res., **94**:4667-4696.

Wyman, D.A. and Kerrich, R. 1993. Archean shoshonitic lamprophyres of the Abitibi Subprovince, Canada: petrogenesis, age, and tectonic setting. J. Petrol., **34**:1067-1109.

Xie, Q. and Kerrich, R., 1993. Volcanic evolution of the Abitibi Southern volcanic zone: compared with Gorgona and the Caribbean plate (abstract). GAC/MAC, Edmonton '93, A-112.

Xie, Q. and Kerrich, R. 1994. Silicate-perovskite and majorite signature komatiites from Archean Abitibi Belt: implications for early mantle diffrentiation and stratification. J. Geophys. Res., **99**:15,799-15,812.

Xie, Q. and Kerrich, R. 1995a. Application of isotope dilution for precise measurement of Zr and Hf in low abundance samples and international reference materials by inductively coupled plasma mass spectrometry. Chem. Geol., **123**:17-27.

Xie, Q. and Kerrich, R. 1995b. Optimization of operating conditions for improved precision of Zr and Hf isotope ratio measurement by inductively coupled plasma mass spectrometry (ICP-MS). J. Anal. At. Spectrom., **10**:99-103.

Xie, Q., Kerrich, R., and Fan, J. 1993. HFSE/REE fractionations recorded in three komatiite-basalt sequences, Archean Abitibi belt: implications for multiple plume sources and depths. Geochim. Cosmochim. Acta, **57**:4111-4118.

Xie, Q., Jain, J., Sun, M., Kerrich, R., and Fan, J. 1994. Multi-element analysis of low abundance international reference material BIR-1: results by ICP-MS. Geostand. Newslett., **18**:53-63.

Xie, Q., McCuaig, T.C., and Kerrich, R. 1995. Secular trends in the melting depths of mantle plumes: evidence from HFSE/REE systematics of Archean high-Mg lavas and modern oceanic basalts. Chem. Geol., **(in press)**:.

Yurimoto, H. and Ohtani, E. 1992. Element partitioning between majorite and liquid: a secondary ion mass spectrometric study. Geophys. Res. Lett., **19**:17-20.

Zhang, J. and Herzberg, C.T. 1994. Melting experiments on anhydrous peridotite KLB-1 from 5.0 to 22.5. J. Geophys. Res., **99**:17,729-17,742.

Zindler, A., 1982. Nd and Sr isotope studies of komatiites and related rocks. In: Arndt, N.T. and Nisbet, E.G., Komatiites.399-420.

Zindler, A. and Hart, S. 1986. Chemical geodynamics. Annu. Rev. Earth Planet. Sci., **14**:493-571.